

WestminsterResearch

<http://www.westminster.ac.uk/westminsterresearch>

Novel Inhibitors for Isocitrate Lyase as a Potent Antitubercular Agent for Mycobacterium Tuberculosis

Gaspar Quinonez, C.

A PhD thesis awarded by the University of Westminster.

© Dr Camila Gaspar Quinonez, 2021.

The WestminsterResearch online digital archive at the University of Westminster aims to make the research output of the University available to a wider audience. Copyright and Moral Rights remain with the authors and/or copyright owners.

**NOVEL INHIBITORS FOR ISOCITRATE LYASE AS A POTENT
ANTITUBERCULAR AGENT FOR MYCOBACTERIUM TUBERCULOSIS**

CAMILA GASPAR QUINONEZ

A thesis submitted in partial fulfilment of the
requirements of the University of Westminster
for the degree of Doctor of Philosophy

November 2021

Abstract

Introduction: *Mycobacterium tuberculosis* (Mtb) is the causative agent of tuberculosis (TB). TB claimed 1.4 million lives in 2019. It is estimated that one-quarter of the world's population is infected with latent TB. Current first- and second-line drugs used to treat TB require adherence to an extended period of therapy (at least six months) and do not target latent TB. It has been shown that the enzyme isocitrate lyase (ICL) is essential for the survival and persistence of Mtb in latent TB. ICL plays an important role in two metabolic pathways required during TB latency, the glyoxylate and methylcitrate cycle. ICL is absent in humans, and therefore, it is considered a promising drug target. Herein, is reported a novel family of ICL inhibitors that is effective *in vitro* against both the enzyme and Mtb.

Methods: The His-tagged ICL1 enzyme was expressed using *E. coli* as a host and purified by Ni-NTA chromatography. The recombinant enzyme was used to set up crystallisation trials and *in vitro* enzymatic assay was performed on ICL1 inhibitors. The synthesis of D/L-*threo*-2-methylisocitrate and the methylation of five other drug candidates were described. Both co-crystallisation and soaking techniques were performed to obtain an ICL1:CL-54-04 complex crystal, whose structure was solved. The CL-54 drug family was tested against Mtb. A checkerboard assay was utilised to test the combinatory effect of CL-54-04 with rifampicin or bedaquiline in both glycerol and propionate media. To investigate the role of acetate metabolism in drug tolerance, $\Delta pckA$, ICL knock-down and $\Delta prpD$ Mtb mutants were assessed.

Results: Seven new conditions to crystallise ICL1 were identified, and eleven drugs were tested against the isolated enzyme. A promising new family of drugs have been identified as the most potent ICL1 inhibitors reported to date. One of the analogues, CL-54-04, had a bacteriostatic effect at 10 μM and a bactericidal effect at 100 μM against Mtb *in vitro*. A drug combination screening of CL-54-04 with rifampicin or bedaquiline led to an additive effect in the checkerboard assay and a significant impact in the colony-forming unit assay. The role of fatty acid metabolism in drug tolerance was investigated by testing three central carbon metabolism mutant strains against isoniazid.

Discussion: From the three CL-54 analogues tested, only CL-54-04 caused a bactericidal effect against Mtb. A solved ICL1:CL-54-04 complex crystal structure showed that the catalytic loop had a distinctive move of 13.8 Å, suggesting that the binding of ICL with CL-54-04 leads to a close conformation of the active site. A superimposition of the solved ICL1:CL-54-04 complex and the ICL1 structure alignment with 3-nitropropionate demonstrates that CL-54-04 inhibitor binds and causes the same conformational changes as 3-nitropropionate. Using metabolomics analysis, the combination of rifampicin and CL-54-04 causes an accumulation of the methylcitrate cycle metabolites in propionate media, suggesting that the ICL has been inhibited. Fatty acid as a sole carbon source showed to increase the drug tolerance of all three Mtb mutants against isoniazid.

Conclusion: A new drug family has been identified as lead compounds against ICL. The estimated IC_{50} of CL-54-01 is approximately half of the 3-nitropropionamide, and it causes the exact conformational change to the enzyme as 3-nitropropionate (the analogue of 3-nitropropionamide). These findings suggest that this drug family are the most promising ICL1 inhibitors reported to date.

Acknowledgements

Behind every thesis, there is a person with many stories to tell. Four years of steep learning curve and a lot to be thankful for. I am only writing this acknowledgment and thesis thanks to my supervisors, Dr Saki Raheem and Dr Mark Odell. My interest in Tuberculosis started on my final year of undergraduate, when I wrote a review about the epidemiological aspects of multi-drug resistance tuberculosis. I found the topic to be both fascinating and challenging. Mark taught me everything about Biochemistry. His classes were dynamic, exciting and challenging. And when the opportunity for this project came up, I was thrilled to be working with Saki and Mark. I loved learning medicinal chemistry from Saki and setting up the crystal trials with Mark. I will fondly remember the hours in the lab until late at night. I will always cherish the chats about science and life, discussing experiments and results over a pint and wings.

During my second year of PhD, the opportunity to spend one year in L.A. in a BLS3 lab under the supervision of Dr Eoh turned out to be one of the richest experiences of my life, both professionally and personally. Dr Eoh and his lab welcomed me so kindly. I got training to work in the BSL3 and embarked on a learning curve of critical thinking and experimental design skills. Dr Eoh – thank you for challenging me and pushing me. It was a pleasure to learn from you. Special thanks to Joey (Dr Jae-Jin Lee), my BSL3 buddy, who gave me incredible support. On the days we spent 5-6 hours in the BSL3, his uplifting energy made the difference. Special thanks as well to all the friendships in the lab: Warisa, who at the time was finishing her master's degree, Juhyeon the lab manager, Anna, a visiting PhD student from Brazil that made me feel closer to home and Jill, who taught me the best BSL3 practices. Thank you all for the lovely chats and support! I cannot thank Aria enough because without the yeast project and the flow cytometry; I wouldn't have met my hike buddy and best friend in LA, Pedram. A special thanks to Chuck for welcoming me in his spare room on my first two weeks in LA and to my roommates – Jess (my garlic buddy), Courtney and Rachel and their four-legged buddies, Lola, Percy and Rylin - for making LA life wholesome.

They say that life without friends is like a garden without flowers. Following this analogy, I am fortunate to have the most beautiful and colourful flowers in my garden (and with a high biodiversity given that they are from all parts of the world!). To name a few: Nirvana, Gareth (for being a dear friend and a life-long mentor!), Matt, Claudio, Kyle, Reza, Zain, Livia, Egg, Henrique, Mary, Tachi, Lima and everyone in Brazil, London, LA (holla to Echo Park Boxing crew) and elsewhere in the world. I am lucky to be surrounded by amazing and inspiring friends.

Last but not least, I would like to thank the people who have always been the biggest supporters, sharing every moment and celebrating every win (big or small). That is, my mum, my brother, my sister-in-law, my uncle, and my true love, Leo. I hold dear every meal we shared, every Rummikub we played and every adventure we have been to. To my beloved family in Brazil: thank you for always cheering me even at 9,492 km away. I can't thank you all enough for all the support throughout the years. I must also acknowledge my furry family, Gururis and Ziba, for all the love and cuddles and Geleia, the most lively and playful kitten Leo and I adopted during the pandemic. They are a source of joyfulness immensely needed after long days in the lab!

I would like to thank my internal examiner Dr Paul Curley, who was also my lecturer when I was doing my undergraduate degree, for all the thoughtful feedback throughout the annual progress reviews and the follow-up discussions. The warmest thanks go to Amy, now Dr Maclatchy, for her endless kindness and support. I have fond memories of us in the 5.05 lab! Thanks to all the collaborators and colleagues who helped and were involved along the way: Professor David Warhurst, Dr Christopher Lawson, Professor Peter Moody, Dr Enrico Ferrari, Laura Slack-Boardman, Harry, Jack, Milva, Renald and Farzana. Lastly, I would like to thank Dr Tania Lupoli, my external examiner, for the insightful discussions on my VIVA, which I enjoyed thoroughly. It felt like the perfect ending to my PhD journey.

I'm grateful for the long hours, the tears, the worries, and even the stress, all leading to the feeling of accomplishment I share today. I am incredibly proud of myself for having contributed to the research and fight against TB. I will be forever a TB advocate, raising awareness about the seriousness of this disease. I feel privileged for the opportunity to dedicate four years of my life to this cause. And finally, I can only thank Quintin Hogg Foundation for the annual stipend and for covering the bench fees that made this research possible.

Table of contents

CHAPTER 1 – INTRODUCTION	1
1.1 HISTORY AND EPIDEMIOLOGY OF TUBERCULOSIS	1
1.2 THE EVOLUTION OF <i>MYCOBACTERIUM TUBERCULOSIS</i>	3
1.3 THE IMMUNOLOGY RESPONSE TO <i>MYCOBACTERIUM TUBERCULOSIS</i>	6
1.4 HISTORY OF ANTI-TB DRUGS AND MODE OF ACTION.....	9
1.5 THE RISE OF MULTI-DRUG (MDR) AND EXTENSIVE MULTI-DRUG RESISTANT (XDR) STRAINS.....	20
1.6 MYCOBACTERIUM TUBERCULOSIS AND ITS FOUR PHENOTYPES: DRUG-SUSCEPTIBLE, DRUG-TOLERANT, DRUG-RESISTANT AND PERSISTENT POPULATIONS	22
1.7 LATENT TB	23
1.8 ISOCITRATE LYASE.....	25
1.9 ICL1 INHIBITORS.....	31
1.10 AIM OF THIS RESEARCH.....	34
CHAPTER 2 – ISOCITRATE LYASE 1 EXPRESSION, PURIFICATION AND CRYSTALLISATION	35
INTRODUCTION	35
MATERIALS AND METHODS	39
RESULTS.....	42
DISCUSSION	48
CHAPTER 3 – SYNTHESIS OF ICL 1 INHIBITORS.....	52
INTRODUCTION	52
RESULTS.....	59
DISCUSSION	66
EXPERIMENTAL PROCEDURES.....	67
CHAPTER 4 – ISOCITRATE LYASE 1 <i>IN VITRO</i> ASSAY	72
INTRODUCTION	72
MATERIALS AND METHODS	73
RESULTS.....	75
DISCUSSION	84

CHAPTER 5 – ISOCITRATE LYASE 1 CO-CRYSTALLISATION WITH INHIBITORS.....	88
INTRODUCTION	88
MATERIALS AND METHODS	90
RESULTS.....	92
DISCUSSION	95
CHAPTER 6 – ASSESSING THE CL-54 DRUG FAMILY AGAINST <i>MYCOBACTERIUM TUBERCULOSIS</i>.....	98
INTRODUCTION	98
MATERIALS AND METHODS	101
RESULTS.....	103
DISCUSSION	115
CHAPTER 7 – INVESTIGATING THE ROLE OF FATTY ACIDS METABOLISM IN DRUG TOLERANCE IN <i>MYCOBACTERIUM TUBERCULOSIS</i>.....	121
INTRODUCTION	121
MATERIALS AND METHODS	123
RESULTS.....	125
DISCUSSION	137
CHAPTER 8 – DISCUSSION AND FUTURE DIRECTIONS.....	140
CHAPTER 9 – CONCLUSION.....	148
REFERENCES	149
APPENDIX A – LITERATURE DATA.....	172
APPENDIX B – RAW DATA.....	174

List of Figures

- Figure 1-1:** Top 10 causes of death and death by an infectious agent. **A)** Top 10 causes of death worldwide in 2016 (WHO, 2018). Deaths from TB among HIV-positive patients are shown in grey. **B)** Top 10 causes of death by an infectious agent. Data shown is the average disease death per day worldwide for endemic pathogens and average disease death per number of outbreaks for pandemic pathogens (Data taken from WHO, 2018 and Furin *et al.*, 2019)..... 2
- Figure 1-2:** List of 30 countries with high TB, multi-drug resistance (MDR-TB) and TB/HIV burden based on the incidence cases per 100,000 population per year (WHO, 2019). 3
- Figure 1-3:** Phylogenetic tree of mycobacteria. Highlighted in yellow are *M. abscessus* (top left) as an unusual example of a fast-growing and virulent species, *M. smegmatis* (top centre) and *M. phlei* (top right) as an example of fast-growing and non-virulent species, and *M. leprae*, *Mtb*, *M. bovis* (bottom centre) and *M. avium* (bottom left) as examples of slow-growing and virulent species. Adapted from Bachmann *et al.* (2020). 5
- Figure 1-4:** Overview of *Mtb* colonising the host's immune system. Created with BioRender.com. Adapted from Ndlovu and Marakalala (2016). 7
- Figure 1-5:** Timeline of the anti-TB drug discovery and the development of first-line regimens. Adapted from Ma *et al.* (2010). 12
- Figure 1-6:** Estimated incidences of MDR-TB in 2018 for countries with at least 1000 incident cases. White dots represent islands. Adapted from WHO (2019). 21
- Figure 1-7:** Diagrammatic representation of the differences between resistant, susceptible and persister *Mtb* cells upon antibiotic exposure. Susceptible cells are rapidly killed by antibiotics. Resistant cells have a gene mutation that allows them to be immune to the antibiotics, whereas persisters cells are genetically identical to the susceptible population but can temporarily survive in minimal inhibitory concentrations of antibiotics due to metabolic changes. 22
- Figure 1-8:** Diagrammatic representation of the metabolic change of *Mtb* inside the host's macrophages. The lack of glucose and oxygen inactivates glycolysis (shown as dot arrows), and lipids become the main carbon source, activating the glyoxylate and methylcitrate cycles. The glyoxylate cycle by-passes three TCA cycle reactions (shown as dot arrows). Full names: GLU for Glucose; PYR for Pyruvate; ACCOA for Acetyl-CoA; CIT for Citrate; ICIT for Isocitrate; α -KG for alpha-ketoglutarate; SUCCOA for Succinyl-CoA; SUCC for Succinate; FUM for Fumarate; MAL for Malate; OAA for Oxaloacetate; ICL for Isocitrate Lyase; GLX for Glyoxylate; PCOA for Propionyl-CoA; MCIT for Methylcitrate and MICIT for Methylisocitrate. No by-product, co-factors or enzymes (besides ICL) are shown. Adapted from Muñoz-Elías *et al.* (2006). 26
- Figure 1-9:** Sequence alignment of ICL1 and ICL2. **A)** Alignment sequence of ICL1 (ACEA1) amino acids 157-216 and ICL2 (ACEA2) amino acids 181-240. The conserved active site motif 'KKCGH' is highlighted. **B)** Superimposition of ICL1 (brown, 1F61) and ICL2 (blue, 6EE1) with a zoom in the active site highlighting the amino acids motif. 28
- Figure 1-10:** Catalytic mechanism of ICL1 with isocitric acid to form glyoxylate and succinate. B refers to a general base. Adapted from Pham *et al.* (2017) and created with BioRender.com. 29
- Figure 1-11:** The structure of ICL1. **A)** Ribbon representation of the ICL1 homotetramer (Shukla *et al.*, 2017). **B)** Amino acid sequence of Mycobacterium tuberculosis isocitrate lyase. The orange box highlights the amino acids responsible for the active site (Moynihan and Murkin, 2014). The dark blue box around the 18 residues is a loop that acts as a lid to the

catalytic site, opening when the enzyme is active and closing when the enzyme binds with the substrate (Shukla <i>et al.</i> , 2015). The two lysine residues in green are part of a regulatory mechanism of ICL1 by acetylation (Bi <i>et al.</i> , 2017). The sequence was obtained from the UniProt (2018) database.	30
Figure 1-12: Structure of ICL substrates (isocitrate and 2-methylisocitrate) and the three ICL1 inhibitors: itaconate, 3-bromopyruvate and 3-nitropropionate (McFadden and Purohit, 1977; Schloss and Cleland, 1982; Ko and McFadden, 1990).	31
Figure 1-13: A timeline of the ICL1 inhibitors developed to date (1977-2016).	33
Figure 2-1: Representation of the plasmid, pET28a, with the antibiotic resistance marker (kanamycin) and the gene coding for isocitrate lyase (ICL1). Created with BioRender.com.	35
Figure 2-2: Overview of the two methodologies for crystallisation trial: hanging drop and sitting drop. Created with BioRender.com.	36
Figure 2-3: Solubility curve for crystal formation. Image adapted from Chayen and Saridakis (2008).	37
Figure 2-4: An example of the SDS-PAGE for ICL purification.	43
Figure 2-5: ICL1 yield obtained in the five protein expression methods tested. Method 1, protein expression induced at OD ₅₉₅ 0.5; Method 2, protein expression induced at OD ₅₉₅ 0.8; Method 3, protein expression induced at OD ₅₉₅ 1.2; Method 4, protein expression induced at OD ₅₉₅ 0.5 after diluting from OD ₅₉₅ 1.2; Method 5, protein expression induced at OD ₅₉₅ 0.8 after diluting from OD ₅₉₅ 1.2.	44
Figure 2-6: Pictures of crystal drops containing ICL1 crystals viewed with a compound light microscope at 10x magnification. ICL1 crystals obtained with a solution of 0.1 M sodium cacodylate pH 6.5 and 27% (w/v) PEG _{mme} 2000, sitting against 500 µL of 27% (w/v) PEG _{mme} 2000 in the reservoir. In this trial, ICL1 concentration was 4.11 mg/mL. A) A 1:0.5 volume ratio of protein with the solution. B) A 2:1 volume ratio of protein with the solution.	45
Figure 2-7: Pictures of crystal drops containing ICL1 crystals viewed with a compound light microscope at 10x magnification. Crystals were obtained with a solution of 0.1 M sodium cacodylate pH 6.5 and 27% (w/v) PEG _{mme} 2000, sitting against 500 µL of 27% (w/v) PEG _{mme} 2000 in the reservoir. In this trial, ICL1 concentration was 3.8 mg/mL, and a volume ratio of 2:1 protein with the solution.	46
Figure 2-8: Picture of a crystal drop containing ICL1 crystals viewed with a compound light microscope at 10x magnification. ICL1 crystals were obtained with a solution of 0.2 M imidazole malate pH 6.0, 20% (w/v) PEG 4000 sitting against 500 µL of 20% (w/v) PEG 4000 in the reservoir. In this trial, ICL1 concentration was 4.11 mg/mL and a volume ratio of 1:1 protein with the solution.	46
Figure 2-9: X-Ray diffraction pattern of ICL1 crystal obtained 'in-house' with a resolution of 6.28 Å. The crystal used to diffract was obtained with the condition 0.2 M imidazole malate pH 6.0 and 20% (w/v) PEG4000. The ICL1 concentration was 4.11 mg/mL.	47
Figure 2-10: Pictures of four drops containing ICL1 crystals with new conditions (viewed with a compound light microscope at 10x magnification). A) 0.2 M imidazole malate pH 7.0 and 25% (w/v) PEG 4000, B) 0.1 M sodium HEPES pH 7.5 and 20% (w/v) PEG 10000, C) 0.1 M sodium cacodylate pH 6.5 and 27% (w/v) PEG 4000, D) 0.2 M imidazole malate pH 6.0 and 20% (w/v) PEG 4000. Images are a courtesy from Laura Boardman-Slack from Odell's Lab at University of Lincoln.	47
Figure 3-1: Structure of three ICL inhibitors.	52
Figure 3-2: Structure of IMBI-3 and the proposed docking structure of IMBI-3 with Mtb ICL1 (1F8I). Green dots represent hydrogen bond; Purple represents van der Waals force (Liu <i>et al.</i> , 2016).	53
Figure 3-3: Reaction scheme. Reagents and conditions a) SOCl ₂ , CaCl ₂ 110 °C, 3 h.	54

Figure 3-4: Reaction scheme. Reagents and conditions a) HNO ₃ , CH ₃ COOH, 40 °C and b) Fe, H ₂ O, CH ₃ COOH, 135 °C.....	55
Figure 3-5: Reaction scheme. Reagents and conditions a) TEA, ether, RT, 1 h.	55
Figure 3-6: Reaction scheme. Reagents and conditions a) P ₄ S ₁₀ , pyridine, 115 °C, HCl, CHCl ₃ , 4 h.	55
Figure 3-7: Reaction scheme. Reagents and conditions a) K ₂ CO ₃ , DMSO, 90 °C, 8 h; b) Red-Al, 0 °C, dry THF, 3 h; c) 11, CH ₂ Cl ₂ , Et ₃ N, RT.....	56
Figure 3-8: Reaction scheme. Reagents and conditions a) Ph ₃ P=CHCOOC ₂ H ₅ ; b) NH ₂ NH ₂ .H ₂ O, PTSA; c) 4-Bromo-1-bromomethyl-2-fluorobenzene, NaOH; d) C ₂ H ₅ OH, H ₂ SO ₄ ; e) NH ₂ NH ₂ .H ₂ O; f) Various aldehydes and ketones.	57
Figure 3-9: Reaction scheme. Reagents and conditions a) H ₂ SO ₄ , C ₂ H ₅ OH; b) NH ₂ NH ₂ .H ₂ O; c) CH ₃ COOH.....	58
Figure 3-10: Structure of the 23a nitrofuranyl derivative.....	59
Figure 3-11: Structure of isocitrate lyase substrate, isocitric acid, and the structure of 2-methylisocitrate, a proposed ICL inhibitor.....	59
Figure 3-12: Reaction scheme. Reagents and conditions a) H ₂ O, Na ₂ WO ₄ ·2H ₂ O, NaOH 0 °C - 65 °C.....	60
Figure 3-13: Reaction scheme. Reagents and conditions a) SO ₂ Cl ₂ , MeOH, 0 °C – RT, 8 h.	61
Figure 3-14: Reaction scheme. Reagents and conditions a) Na/MeOH, CH ₂ (CO ₂ CH ₃) ₂ , RT, 3 days.	61
Figure 3-15: Reaction scheme. Reagents and conditions a) 6 N HCl, reflux, 0- 60 °C, 3 h; b) NaOH/H ₂ O, 80 °C for 2 h.	62
Figure 3-16: ¹ HNMR of 29 in D ₂ O.	62
Figure 4-1: Representation of the ICL1 enzyme assay mechanism, where the substrate, isocitric acid, is converted into two products, glyoxylate and succinate, by ICL1. Glyoxylate reacts with phenylhydrazine, forming phenylhydrazone that can be detected at 324 nm.....	72
Figure 4-2: ICL1 assay optimisation with different enzyme, salt and substrate concentrations over a period of 5 minutes at 37 °C at 324 nm. A) Three concentrations of ICL1 were screened for assay optimisation with 1 mM of the substrate, isocitric acid. B) Different concentration of sodium chloride (5-100 mM), with 0.127 μM ICL1 and 1 mM substrate. C) Different concentrations of isocitric acid (0-10 mM) with 0.127 μM ICL1. Data represented is three biological replicates, and error bars are standard deviations.....	75
Figure 4-3: Characterisation of ICL1. A) The effect of 5-minute incubation of 0.127 μM ICL1 with 1 mM EDTA (+) or without EDTA (-). B) The effect of re-freezing to -80 °C and thawing, once or twice, in the ICL activity. All assays were measured at 324 nm over 5 minutes at 37 °C. Data represented is three biological replicates, and error bars are standard deviations.	76
Figure 4-4: Structure of the substrate, isocitric acid, and two candidates as ICL1 inhibitors, DL-threo-2-methylisocitrate and Garcinia acid. DL-threo-2-methylisocitrate is a derivative of the substrate, 2-methylisocitrate of the methylcitrate cycle, and it was synthesised in-house (see Chapter 3), and Garcinia acid was purchased from Sigma, UK.	77
Figure 4-5: Garcinia and 2-methylisocitrate effect upon ICL1 activity. A) Effect of 10 and 50 mM of Garcinia acid on ICL1 activity. B) Effect of 5, 10 and 20 mM of 2-methylisocitrate on ICL1 activity. Values shown are one measurement and it was normalised in respect to 0 mM value, which is assigned as 100% enzyme activity.	77
Figure 4-6: Structure of the drugs screened in the ICL1 activity assay. CL-54 drug family structures are confidential (R represents identical structure) and only the functional groups are depicted. These three analogues were chemically synthesised by Dr Lawson as an anti-malaria drug and were repurposed as part of a collaboration. See Table 3 in Materials and Methods section for more details of the drugs.	78

Figure 4-7: ICL1 activity assay in the presence of 5% (v/v) DMSO over 5 minutes at 324 nm at 37 °C. A) Activity of ICL1 with MOPS buffer (50 mM MOPS pH 7.0, 5 mM MgCl ₂) or 5% (v/v) DMSO and B) activity of ICL1 after incubated with MOPS buffer or 5% (v/v) DMSO for 10 minutes and buffer exchanged using a MicroSpin PD-10 chromatography column.....	79
Figure 4-8: Schematic representation of the method to assess coloured inhibitors in the ICL1 activity assay. The chromatography column is equilibrated with 50 mM MOPS pH 7.0, 5 mM MgCl ₂ buffer and kept on ice before adding the enzyme. A) After incubating the enzyme with the drug on ice for 10 minutes, the mixture was added to the chromatography column and centrifuged for 2 minutes at 800 x g. B) Representation of the chromatography column after centrifugation. The unbound drug is filtered by the column, and the enzyme (bound or not to the drug) is harvested and added immediately to the enzyme assay mixture for spectrophotometer analysis.....	80
Figure 4-9: Drug effect on ICL1 activity after employing the chromatography column methodology at 324 nm for 3 minutes at 37 °C. A) ICL1 activity in MOPS buffer and in DMSO as positive controls, and in the initial presence of 1 mM itaconate (as a positive control) and the candidate 7-methoxy-4-oxo-1,4-dihydroquinoline-2-carboxylic acid (labelled as '7-methoxy'). B) Effect on ICL1 activity in the presence of two drugs at 1 mM (initial) 3,4-dihydroxycinnamic acid and 3-(4-methoxybenzoyl)acrylic acid. Data represents an average of three biological replicates.	81
Figure 4-10: Drug effect on ICL1 activity after employing the chromatography column methodology at 324 nm for 3 minutes at 37 °C with DMSO as a negative control. A) Effect of 2-(3-bromophenyl)-1-(2,4,6-trihydroxyphenyl)ethanone, shown as 'bromophenyl' and 3,4-dimethoxycinnamic acid. B) Effect of the CL-54 drug family. Data represent an average of two biological replicates. Values represent an average of three biological replicates of one independent experiment.....	82
Figure 4-11: Effect of different concentrations of CL-54-01 on ICL1 activity assay. Values represent one individual reading.....	83
Figure 5-1: Diagrammatic representation of co-crystallisation and soaking; the two methods used in this research to obtain a crystal of ICL1 bound to the inhibitor. In the co-crystallisation method, the protein is pre-incubated with the ligand/inhibitor before the crystal trial is set up, whilst in soaking, the crystal is first obtained, and the ligand is then added to the drop prior to X-ray diffraction. Created with BioRender.com.....	89
Figure 5-2: Soaking method of ICL crystals with CL-54-01. ICL1 crystals crystallised using 0.2 M imidazole malate pH 6.0 and 20% (w/v) PEG 4,000, and 1 mM (final concentration) of CL-54-01 was added to the drop. The drug, whose colouration is yellow, can be seen faded in the drop. Pictures are courtesy of Laura Boardman-Slack from Dr Odell's lab at the University of Lincoln.....	92
Figure 5-3: Comparison of sequence and structural alignment of CL-54-01 bound ICL with ICL1 and ICL2. The structure of ICL1 (red, PDB ID 1F61), ICL2 (blue and cyan, PDB ID 6EE1) and ICL1 bound to CL-54-01 (pink). The white arrows point at the catalytic loops containing the KKCGH motif. In the sequence alignment, ACEA1 refers to ICL1, and ACEA2 refers to ICL2.	93
Figure 5-4: Magnified view of the catalytic loop of ICL1, ICL2 and ICL1 bound to CL-54-01, showing relative movement of the α-carbon of the active site cysteine.....	94
Figure 5-5: Structural alignment of ICL1 active site complexed with CL-54-01 (green) and 3-nitropropionate (yellow, PDB ID 6C4A), and their chemical structure. The green sphere is the positive magnesium ion needed for catalytic activity. For confidentiality, only the functional group of CL-54-01 is displayed, and R represents the common backbone structure that is the same for all three analogues.	95

Figure 6-1: Structure of CL-54 family compounds. Only functional groups are shown as the full structure is confidential (this drug family has been synthesised by Dr Christopher Lawson at the University of Glasgow originally as anti-malaria drug but were repurposed as part of a collaboration). R represents the common backbone structure that is the same for all three analogues. Molecular weight: CL-54-01 (356.37 g/mol), CL-54-02 (340.38 g/mol), CL-54-04 (354.40 g/mol). 98

Figure 6-2: Diagrammatic representation of the checkerboard assay. A series of dilutions of Drug A is pipetted along the abscissa (the first row is drug A only to serve as a control), whilst Drug B is pipetted along the ordinate (the first column is drug B only to serve as control). Red to yellow represents the drug concentration, where red is the most concentrated and yellow the least. C stands for control, in which the mycobacteria are grown without any drug. BL stands for blank as it is only media without mycobacteria to ensure there is no contamination. 99

Figure 6-3: Effect of CL-54-01 in the growth of Mtb Erdman wild type in both glycerol and propionate media for 9 days. Data represent an average of three biological replicates. 104

Figure 6-4: Effect of CL-54-02 and CL-54-04 in the growth of Mtb Erdman strain in both glycerol and propionate as sole carbon sources. Data represents an average of three biological replicates, and error bars are standard deviations. ***P<0.001 by two-way ANOVA. 105

Figure 6-5: Effect of 100 µM CL-54-02 and CL-54-04 in the growth of Mtb Erdman in glycerol and propionate media. Time points were 0, 4 and 9 days. Data represent an average of three biological replicates, and error bars are standard deviations. Ns, not significant by two-way ANOVA. 106

Figure 6-6: Colony-forming unit of Mtb Erdman challenged with different concentrations (1, 10 and 100 µM) of CL-54-04 in both glycerol and propionate media. Data represent an average of three biological replicates, and error bars are standard deviations. ***P<0.001; Ns, not significant by two-way ANOVA. 107

Figure 6-7: Drug combination effect of CL-54-04 with bedaquiline (BDQ) and rifampicin (RIF) against Mtb Erdman strain in 0.2% (v/v) glycerol M7H10 media. Drug concentrations were based on the FIC index: 0.3 µg/mL bedaquiline with 15.6 µM CL-54-04 and 0.0625 µg/mL rifampicin with 15.6 µM CL-54-04. Data represent an average of three biological replicates, and error bars are standard deviations. *P<0.01 by two-way ANOVA. 112

Figure 6-8: The inhibition of ICL in Erdman wild type by CL-54-04 leads to an increase in methylcitrate cycle (MCC) intermediates in propionate media. In glycerol (0.2% v/v) condition, the drug combination used was 15.62 µM CL-54-04 and 0.3 µg/mL bedaquiline. In propionate (0.1% w/v) condition, the drug combination was 7.81 µM CL-54-04 and 0.0052 µg/mL bedaquiline. Values depicted are ion count/mg and are an average of three biological replicates. BDQ, bedaquiline; 04, CL-54-04. MCC, 2-methyl-cis-aconitate and 2-methyl-isocitrate. 113

Figure 6-9: The combination of rifampicin and CL-54-04 leads to an increase in MCC metabolites in Erdman wild type in propionate media. In glycerol (0.2% v/v) condition, the drug combination used was 15.62 µM CL-54-04 and 0.0625 µg/mL rifampicin. In propionate (0.1% w/v) condition, the drug combination was 7.81 µM CL-54-04 and 0.03125 µg/mL rifampicin. Values depicted are ion count/mg and are an average of three biological replicates. RIF, rifampicin; 04, CL-54-04. MCC, 2-methyl-cis-aconitate and 2-methyl-isocitrate. 114

Figure 7-1: Growth curve of Erdman wild type (WT ●), Erdman $\Delta pckA$ ($\Delta pckA$ ■), and Erdman *pckA* complementary (COM ▲) strains in glycerol and acetate media. The OD₅₉₅ was measured over a 21-day period. Data represent an average of three biological replicates. 126

Figure 7-2: Metabolomics analysis of Erdman wild type (WT) in acetate (A) media and $\Delta pckA$ in glycerol (G) and acetate (A) media. **A)** Semi-untargeted metabolomics analysis of 231

metabolites. **B)** 3D principal component analysis (PCA). **C)** Volcano plot of up-regulated $\Delta pckA$ metabolites in acetate (A) media (green box) against up-regulated metabolites of WT in acetate (red box). **D)** TCA cycle metabolites of WT in acetate media and $\Delta pckA$ in both glycerol and acetate media. $\Delta pckA$ in acetate is depicted in green; $\Delta pckA$ in glycerol in blue; WT in acetate in red. Data represent an average of three biological replicates, and error bars are standard deviations. Cit, citrate ($p=0.001$); Pyr, pyruvate ($p=0.0001$); α -KG, α -ketoglutarate ($p=0.0159$); Succ, succinate ($p=0.001$); Fum, fumarate ($p=0.0038$); Mal, malate ($p=0.001$); MCC, 2-methyl-cis-aconitate and 2-methyl-isocitrate ($p=0.0005$); Asp, aspartate ($p=0.0001$). *** $P < 0.001$, ** $P < 0.01$, * $P < 0.05$ by two-way ANOVA. 127

Figure 7-3: Decreased mRNA expression levels (\log_{10} CT values) of the TCA cycle and MCC genes in $\Delta pckA$ strain in 0.2% (v/v) acetate (A) media compared to 0.2% glycerol (G) and Erdman wild type (WT) in both carbon sources. The diagram represents a pathway map of each gene tested and the deletion of *pckA*. Data represent an average of three biological replicates. 129

Figure 7-4: Accumulation of the TCA cycle and MCC metabolites in $\Delta pckA$ strain in 0.2% (v/v) acetate media compared to 0.2% (v/v) glycerol. Data represent an average of three biological replicates, and error bars are standard deviations. α -KG, α -ketoglutarate; Cit, Citrate; COM, complementary strain, Succ, Succinate; Fum, Fumarate; Mal, Malate; MCC, 2-methyl-cis-aconitate and 2-methyl-isocitrate, WT, wild type. 129

Figure 7-5: Targeted metabolomic analysis of phosphoenolpyruvate (PEP) with uniformly 0.2% (v/v) ^{13}C labelled ([U- ^{13}C]) acetate in wild type (WT), $\Delta pckA$ and complementary (COM) strains. The diagram represents the central carbon metabolism and the *pckA* deletion. Data represent an average of three biological replicates, and error bars are standard deviations. 130

Figure 7-6: Phenotypic changes in Erdman $\Delta pckA$ ($\Delta pckA$ ■) mutant compared to Erdman wild-type (WT ●) and *pckA* complementary (COM ▲) strains in carbon-dependent media. Viable count (CFU/mL) and optical density (OD₅₉₅) were used to measure the growth effect following treatment with 100 $\mu\text{g/mL}$ DCS in glycerol media and acetate media. The assay was done according to Keren *et al.* (2011). Data represent an average of three biological replicates, and error bars are standard deviations. *** $P < 0.001$, ns, not significant by two-way ANOVA. Differences of WT and $\Delta pckA$ growth in glycerol media is not statistically significant, whereas in acetate is extremely significant (***). 131

Figure 7-7: Drug tolerance against 0.3 $\mu\text{g/mL}$ isoniazid (INH) of Erdman wild type (WT ●), $\Delta pckA$ (■) and *pckA* complementary (COM ▲) strains in 0.2% (v/v) glycerol and 0.2% (v/v) acetate. Data represent an average of three biological replicates, and error bars are standard deviations. 132

Figure 7-8: Accumulation of the TCA cycle and MCC metabolites in $\Delta pckA$ upon isoniazid treatment in acetate media. WT, $\Delta pckA$ and COM strains were cultured in 0.2% (v/v) glycerol (blue scheme) or 0.2% (v/v) acetate media (black scheme) in the presence of 3 $\mu\text{g/mL}$ isoniazid (INH). Values represent ion count/mg and are an average of three biological replicates. Asp, Aspartate; Pyr, Pyruvate; Cit, Citrate; α -KG, α -ketoglutarate; Succ, Succinate; Fum, Fumarate; Mal, Malate; MCC, 2-methyl-cis-aconitate and 2-methyl-isocitrate. 133

Figure 7-9: Growth curve of Erdman WT (□), ICL KD (■), CDC 1551 (⊙) and $\Delta prpD$ (⊗) in 0.2% (v/v) glycerol and 0.1% (w/v) propionate over 21 days. 134

Figure 7-10: Accumulation of the MCC metabolites in ICL KD strain in 0.1% (w/v) propionate media compared to Erdmand (Erd) WT, ICL KD, CDC 1551 and $\Delta prpD$ and in 0.2% (v/v) glycerol media. Asp, Aspartate; Cit, Citrate; α -KG, α -ketoglutarate; Succ, Succinate; Mal, Malate; MCC, 2-methyl-cis-aconitate and 2-methyl-isocitrate. 135

Figure 7-11: The effect of 0.3 $\mu\text{g/mL}$ isoniazid in the survival of Erdman WT, ICL KD, CDC 1551, $\Delta prpD$ in 0.2% (v/v) glycerol (Gly) and 0.1 (w/v) propionate (Prop) media after 5 days.

Data represent an average of three biological replicates, and error bars show the standard deviation. ***P < 0.001, **P < 0.01, ns, not significant by two-way ANOVA. The statistical analysis highlighted in propionate media are comparing ICL KD and $\Delta prpD$ (**), Erd WT and CDC 1551 (ns), Erd WT and ICL KD (**), and CDC 1551 and $\Delta prpD$ (***). 136

Figure 7-12: Comparison of colony formation of Erdman WT against **A)** 100 $\mu\text{g/mL}$ DCS ($p = 0.0011$) and **B)** 0.3 $\mu\text{g/mL}$ INH ($p = 0.0002$) in 0.2% (v/v) glycerol and 0.2% (v/v) acetate media. Data shown is the average of three biological replicates. ***P < 0.001, **P < 0.01 by two-way ANOVA. 136

Figure 8-1: Comparison of the ICL enzymatic assay used in this study and an alternative assay. Both assays are incubated at 37 °C. Created with BioRender.com. 142

Figure 8-2: Proposed ICL inhibitors based on CL-54-04 structure. R represents the identical core structure of all CL-54 family members. 144

Figure 8-3: Sequence alignment of ICL active site (motif KKCGH, highlighted in yellow) for different organisms. ACEA2_MYCBO refers to Mycobacterium bovis, A0A0H3JR68_ECO57 refers to Escherichia coli O157:H7 strain, ACEA1_MYCTO refers to Mycobacterium tuberculosis, Q73SW2_MYCPA refers to Mycobacterium avium paratuberculosis, ACEA_BRANA refers to Brassica napus, ACEA_ARATH refers to Arabidopsis thaliana, ACEA_CANGA refers to Candida glabrata, ACEA_CANAX refers to Candida albicans, ACEA_LEPMC refers to Leptosphaeria maculans, and C1G3G7_PARDBD refers to Paracoccidioides brasiliensis. All sequences were obtained from the UniProt database. 146

Figure 8-4: Superimposition of *C. albicans* ICL (Q9P8Q7) and Mtb ICL1 (P9WKK6). **A)** Surface model of both *C. albicans* and Mtb ICL superimposed with the active site highlighted. The faded structure refers to *C. albicans* ICL (550 amino acids), and the solid structure is Mtb ICL (428 amino acids). **B)** Ribbon representation of both ICL superimposition with a zoom in the active site. The catalytic residues ('KKCGH') are depicted, where Lys192-His196 belongs to Mtb ICL and Lys214-His218 to *C. albicans* ICL. Sequences were obtained from the UniProt database. 147

List of Tables

Table 1: Overview of current first- and second-line drugs, their adverse effects, their mechanism of action and the genes involved in resistance. Adapted from Njire <i>et al.</i> (2015) and Zhang and Yew (2015).	15
Table 2: Overview of seven TB drugs, from new chemical classes, that are currently in clinical trials.....	18
Table 3: Summary of the drugs tested in the ICL1 activity assay.....	74
Table 4: Estimated IC ₅₀ of the ICL inhibitors screened in this study.....	84
Table 5: Categories of Fractional Inhibitory Concentration (FIC) index	100
Table 6: FIC index for the combination of itaconate and bedaquiline against mc ² 6206 with glycerol as a sole carbon source.....	108
Table 7: FIC index for the combination of itaconate and bedaquiline against mc ² 6206 with propionate as a sole carbon source.	108
Table 8: FIC index for the combination of itaconate and rifampicin against mc ² 6206 with glycerol as a sole carbon source.....	109
Table 9: FIC index for the combination of itaconate and rifampicin against mc ² 6206 with propionate as a sole carbon source.	109
Table 10: FIC index for the combination of bedaquiline and CL-54-04 against mc ² 6206 with glycerol as a sole carbon source.....	110
Table 11: FIC index for the combination of bedaquiline and CL-54-04 against mc ² 6206 with propionate as a sole carbon source.	110
Table 12: FIC index for the combination of rifampicin and CL-54-04 against mc ² 6206 with glycerol as a sole carbon source.....	111
Table 13: FIC index for the combination of rifampicin and CL-54-04 against mc ² 6206 with propionate as a sole carbon source.	111

Abbreviations, acronyms, symbols and nomenclature

Å	Ångström
α KG	α -ketoglutarate
°C	Degrees Celsius
Δ	Knockout
μ g	Microgram
μ L	Microlitre
μ M	Micromolar
ACCOA	Acetyl-CoA
AIDS	Acquired immune deficiency syndrome
Alr	Alanine race-mase
AOT	Diocylsulfosuccinate sodium
Asp	Aspartate
ATP	Adenosine triphosphate
B.C	Before Christ
BCG	Bacillus Calmette-Guerin
BDQ	Bedaquiline
BL	Blank
BSA	Bovine serum albumin
BSL2	Biosafety level 2
BSL3	Biosafety level 3
CaCl ₂	Calcium chloride
CDC	Central for Disease Control
CDCl ₃	Deuterated chloroform
CD ₃ OD	Deuterated methanol
CFU	Colony forming unit
CH ₂ Cl ₂	Dichloromethane
CHCl ₃	Chloroform
CH ₂ (CO ₂ CH ₃) ₂	Dimethyl malonate

CH ₃ COOH	Acetic acid
C ₇ H ₁₀ O ₇	Homocitric acid
C ₂ H ₅ OH	Ethanol
Cit	Citrate
CoA	Coenzyme A
COM	Complementary strain
Cys	Cysteine
DCM	Dichloromethane
DCS	D-cycloserine
Ddl	D-Ala:D-Ala ligase
DMS	Dimethyl sulphide
DMSO	Dimethyl sulphoxide
DNA	Deoxyribonucleic acid
DosR-DosS	Dormancy survival regulator system
EDTA	Ethylenediaminetetraacetic acid
EMB	Ethambutanol
ERD	Erdman strain
ETC	Electron transport chain
ETH	Ethionamide
Et ₃ N	Triethylamine
Fe	Iron
FIC	Fractional inhibitory concentration
Fum	Fumarate
GABA	Gamma-aminobutyric acid
Gln	Glutamine
Glu	Glutamate / Glutamic acid
GLX	Glyoxylate
HCl	Hydrochloric acid
HEPES	4-(2-hydroxyethyl)-1-piperazineethanesulfonic acid
His	Histidine
HIV	Human immunodeficiency viruses

^1H NMR	Proton nuclear magnetic resonance
HNO_3	Nitric acid
H_2O	Water
H_2O_2	Hydrogen peroxide
H_2SO_4	Sulfuric acid
HTS	High-throughput screening
Hz	Hertz
IC_{50}	Half maximal inhibitory concentration
ICIT	Isocitrate
ICL1	Isocitrate lyase 1
ICL2	Isocitrate lyase 2
ICL KD	Isocitrate lyase knock-down
IFN- γ	Interferon gamma
INH	Isoniazid
IPTG	Isopropyl β -D-1-thiogalactopyranoside
ITC	Isothermal titration calorimetry
J	Joules
K_2CO_3	Potassium carbonate
KD	Knock-down
kDa	Kilodaltons
KO	Knock-out
LB	Lysogeny broth
LC-MS	Liquid chromatography-mass spectrometry
LDH	Lactate dehydrogenase
Lys	Lysine
M	Molar
MAC	<i>Mycobacterium avium</i> complex
Mal	Malate
ManLAM	Mannosylated lipoarabinomannan
MCC	Methylcitrate cycle

MCIT	Methylcitrate
MDK ₉₉	Minimum length of time for killing 99%
MDR	Multi-drug resistance
MeOH	Methanol
Mg	Magnesium
mg/mL	milligram per millilitre
M7H9	Middlebrook 7H9 broth
M7H10	Middlebrook 7H10 agar base
MIC	Minimal inhibitory concentrations
MICIT	Methylisocitrate
mol	Mole
mmol	Millimole
mM	Millimolar
MOPS	(3-(N-morpholino)propanesulfonic acid)
Mtb	<i>Mycobacterium tuberculosis</i>
MTC	<i>Mycobacterium tuberculosis</i> complex
MTT	3-(4,5-dimethylthiazol-2-yl)-2,5-diphenyl-2H-tetrazolium bromide
NAD ⁺	Nicotinamide adenine dinucleotide
NADH	Nicotinamide adenine dinucleotide + hydrogen
NaOH	Sodium hydroxide
Na ₂ WO ₄ ·2H ₂ O	Sodium tungstate
NH ₂ NH ₂ ·H ₂ O	Hydrazine hydrate
nm	Nanometre
NMR	Nuclear magnetic resonance
Ns	Not significant
NTM	Non-tuberculous mycobacterial
OAA	Oxaloacetate
OD	Optical density
PAS	para-aminosalicylic acid
PCA	Principle component analysis

PCOA	Propionyl-CoA
PDB	Protein Data Bank
PDIM	<i>phthiocerol dimycocerosates</i>
PEG	Polyethylene glycol
PEP	Phosphoenolpyruvate
PEPCK	Phosphoenolpyruvate carboxykinase
$\text{Ph}_3\text{P}=\text{CHCOOC}_2\text{H}_5$	Ethoxycarbonyl methylene triphenyl phosphorane
PknG	Serine/threonine-protein kinase
ppm	Parts per million
<i>PrpD</i>	2-methylcitrate dehydratase
P_4S_{10}	Phosphorus pentasulphide
PTSA	p-Toluenesulphonic acid
Pyr	Pyruvate
PZA	Pyrazinamide
R_f	Retention factor
RIF	Rifampicin
RNA	Ribonucleic acid
rpm	Rotations per minute
RT	Room temperature
SDS-PAGE	Sodium dodecyl sulfate polyacrylamide gel electrophoresis
SOCl_2	Thionyl chloride
SO_2Cl_2	Sulphuryl chloride
Succ	Succinate
SUCCOA	Succinyl-CoA
TB	Tuberculosis
TCA	Tricarboxylic acid cycle
TDM	Trehalose dimycolate
TEA	Triethylamine
TFA	Trifluoroacetic acid
TGN	TRIS.HCl, glycerol, NaCl and imidazole buffer

Th1	T helper 1
THF	Tetrahydrofuran
TLC	Thin Layer Chromatography
TLR2	Toll-like receptor 2
TMM	Trehalose monomycolate
TNF	Tumour necrosis factor
Treg	Regulatory CD4 ⁺ T cells
UV	Ultraviolet
v/v	Volume to volume ratio
w/v	Weight to volume ratio
WHO	World Health Organisation
WT	Wild type
XDR	Extensive multi-drug resistant
x g	Times gravity

Chapter 1 – Introduction

1.1 History and epidemiology of Tuberculosis

Tuberculosis (TB) has haunted humankind throughout history. Archaeologists have traced TB back to 9,000 years from the remains of a mother and a child buried in a city, Atlit-Yam, which is now under the Mediterranean Sea (Levy, 2012). The earliest written records about TB were in India 3,300 years ago, though the first evidence of TB was found in the Granville mummy's lung from 600 B.C. (Donoghue *et al.*, 2010). Throughout history, TB was referred to as '*phthisis*' in ancient Greece, '*tabes*' in ancient Rome as '*schachepheh*' in ancient Hebrew, and later called the 'consumption' or 'white plague' in the 1700s (CDC, 2018). All terms refer to a progressive, decaying and fatal disease. In 1882, *Mycobacterium tuberculosis* (Mtb) was first described by the German microbiologist and physicist Robert Koch (Sakula, 1982). Before antibiotics were introduced in 1944, surgery and isolation in sanatoriums were the measures taken to treat and prevent the spread of the disease. Nevertheless, the spread of the disease inevitably occurred in human history due to migration such as pilgrimage and traders as well as military routes (Liverani, 2015).

Although TB was never eradicated with the introduction of antibiotics, mortality rates have significantly dropped over the last decades. WHO (2018) reports that 60 million people have been documented as treated and cured since 2000; however, TB is still ranked as one of the top 10 causes of death worldwide (WHO, 2018) – Figure 1-1A, and the leading cause of death from a single infectious agent (WHO, 2018) – Figure 1-1B. In 2016, TB accounted for 1.7 million deaths, and it is estimated that 10 million people fall ill with TB every year (WHO, 2018). Humanity is now facing a health security threat with the rise of multi-drug resistance (MDR) strains of Mtb. Nearly 500 000 new cases of multi drug-resistant Mtb were reported in 2016 (WHO, 2018).

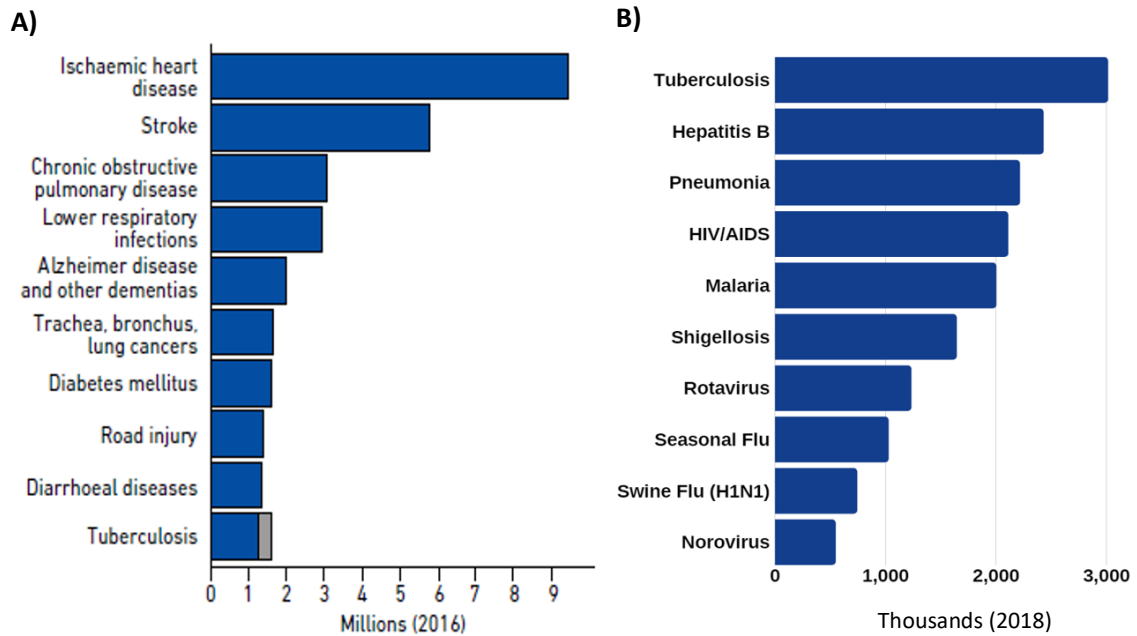


Figure 1-1: Top 10 causes of death and death by an infectious agent. **A)** Top 10 causes of death worldwide in 2016 (WHO, 2018). Deaths from TB among HIV-positive patients are shown in grey. **B)** Top 10 causes of death by an infectious agent. Data shown is the average disease death per day worldwide for endemic pathogens and average disease death per number of outbreaks for pandemic pathogens (Data taken from WHO, 2018 and Furin *et al.*, 2019).

TB has been a major international public health concern for many decades, but it is a burden in low- and medium-income countries, mainly African and Asian countries such as China, India, Myanmar, Indonesia, Nigeria, Ethiopia, Angola, Kenya, Mozambique, Zimbabwe and South Africa (Figure 1-2).

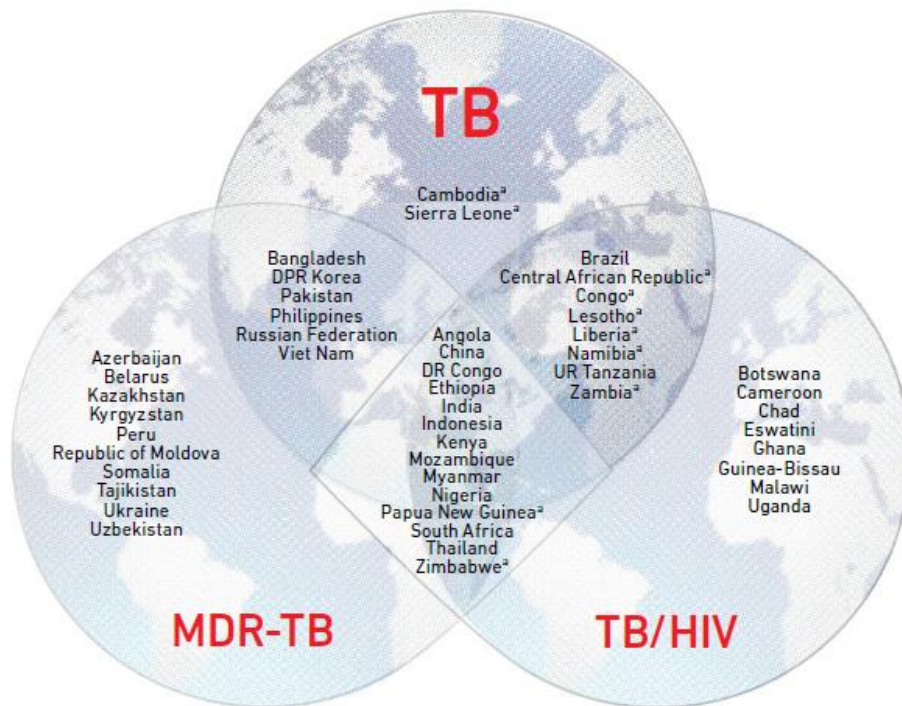


Figure 1-2: List of 30 countries with high TB, multi-drug resistance (MDR-TB) and TB/HIV burden based on the incidence cases per 100,000 population per year (WHO, 2019).

There are two key reasons for catastrophic TB epidemics in developing countries. The first one is the inadequate prevention and control measures as well as the lack of diagnostic tools and treatments available. Secondly, immune-compromised patients such as the ones carrying HIV, with diabetes or renal insufficiency, or with poor lifestyle factors such as drug or alcohol abuse, malnutrition and air pollution are more likely to fall ill with TB due to the weakened immune system (Aziz *et al.*, 2006; Glaziou *et al.*, 2018).

1.2 The evolution of *Mycobacterium tuberculosis*

Mycobacteria have been classified depending on their growth rate phenotype as either slow or fast growers. The former takes more than seven days to grow *in vitro*, and the latter within 2-7 days (Kim *et al.*, 2013), which is considered slow-growing compared to other bacteria. Most of the pathogenic *Mycobacterium* strains responsible for causing diseases in humans and animals, such as *M. tuberculosis*, *M. leprae* and *M. bovis*, are slow-growers (Wee *et al.*, 2017). A limited number of

opportunistic pathogen mycobacterial species can be fast-growers (Phillee and Griffith, 2015), such as *M. abscessus* that is a non-tuberculous, multi-drug resistant mycobacteria commonly found in soil and water. Although this mycobacterium is distantly related to the slow-growing Mtb, it can cause lung disease (Wee *et al.*, 2017) and is known to be present in healthcare settings through medical device contamination (Lee *et al.*, 2015).

There are more than 170 species in the Mycobacterium genus. The majority are environmental organisms found in soil and water, such as *M. smegmatis* and *M. phlei* (Fedrizzi *et al.*, 2017). They are rapid-growing and non-pathogenic species (Phillee and Griffith, 2015). From phylogenetic analysis, it is believed that slow-growers have evolved from the rapid growers' mycobacteria (Devulder *et al.*, 2005). Wee *et al.* (2017) have demonstrated through a comparative genome analysis of 28 mycobacterial species that during the evolution, the slow-growers have gained 77 genes and lost 55 genes compared to the rapid growers. Among the 55 genes that were lost, there were genes involved in growth rate, such as access to extracellular nutrients. On the other hand, the rapid growers have gained 51 genes and lost only 8 genes (Wee *et al.*, 2017). Another study, comparing 157 mycobacterial genomes, identified that rapid-growing species have enriched genes related to amino acid transport and metabolism (31 genes in rapid growers vs 16 genes in slow growers) and transcription (26 genes in rapid growers vs 14 genes in slow growers) (Bachmann *et al.*, 2020). A phylogenetic tree containing 157 genomes of all well-characterised mycobacteria species is depicted in Figure 1-3. It shows five distinct sub-genera and indicates that slow-growing mycobacteria evolved from more ancestral fast-growing species (Bachmann *et al.*, 2020). These studies strengthen the view that rapid-growing mycobacteria led to slow growers species through gene losses responsible for growth rate. Moreover, the growth rate is also determined by a set of genes encoding several virulence determinants (Beste *et al.*, 2009). For instance, the *mce1* locus promotes bacteria uptake by nonphagocytic cells (Chitale *et al.*, 2001) with multiple roles during different periods of infection (Joshi *et al.*, 2006), which is a component of the switch to slow growth rate (Beste *et al.*, 2009). Thus, there was a trade-off between a fast growth rate and becoming a virulent strain that is consistent with the slow growth rate and virulence of Mtb (Beste *et al.*, 2009).

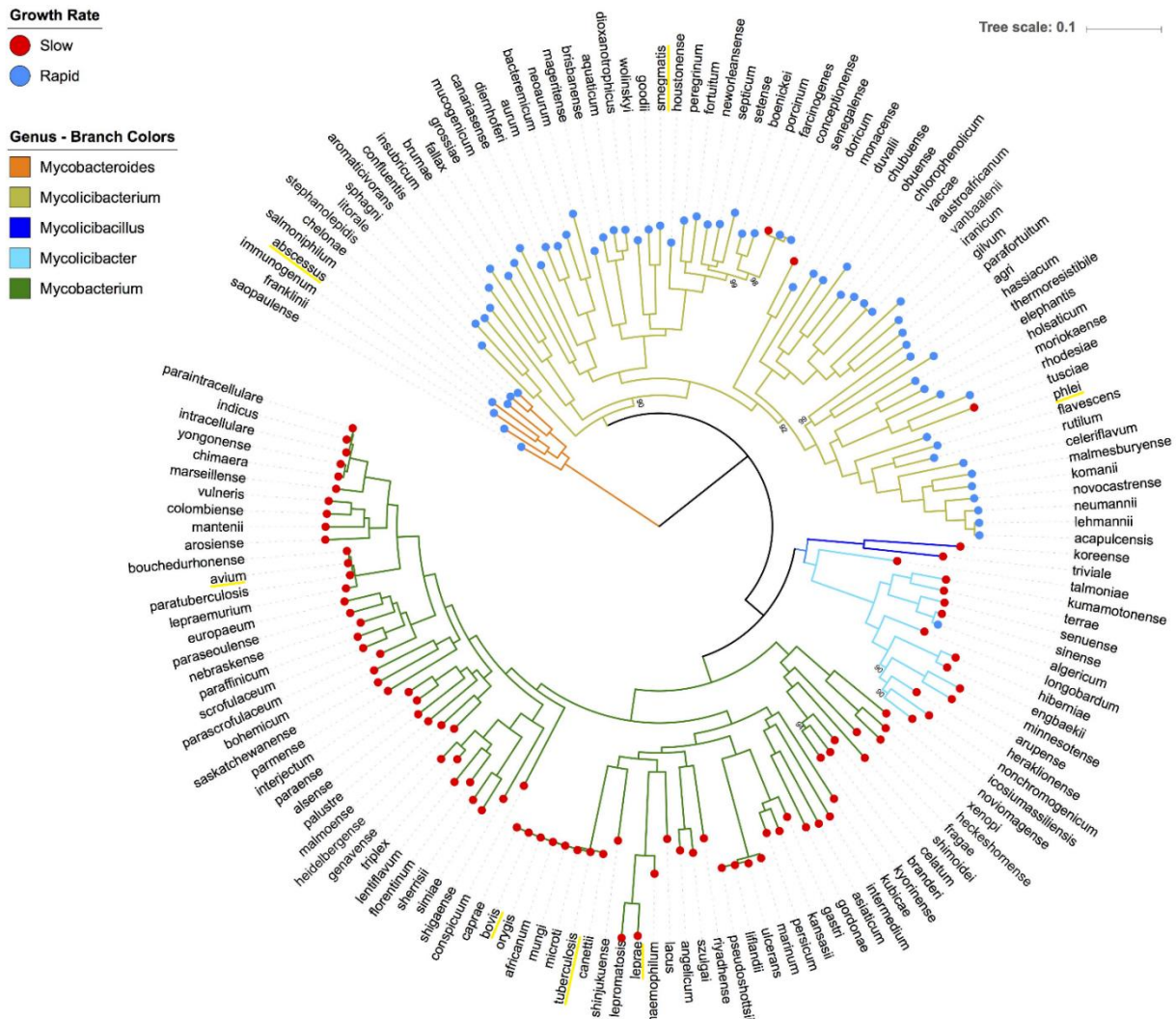


Figure 1-3: Phylogenetic tree of mycobacteria. Highlighted in yellow are *M. abscessus* (top left) as an unusual example of a fast-growing and virulent species, *M. smegmatis* (top centre) and *M. phlei* (top right) as an example of fast-growing and non-virulent species, and *M. leprae*, Mtb, *M. bovis* (bottom centre) and *M. avium* (bottom left) as examples of slow-growing and virulent species. Adapted from Bachmann *et al.* (2020).

There are multiple species and sub-species of Mtb that share 99.9% DNA sequence identity but differ in the mammalian host range and are referred to as *Mycobacterium tuberculosis* complex (MTC) (Brites and Gagneux, 2015). A possible event in the evolution of these environmental organisms to becoming host pathogens was the ability to exploit an intracellular niche, such as surviving in free-living protozoa that feed on environmental bacteria (Jang *et al.*, 2008), by acquiring new genes through horizontal gene transfer (Behr, 2013). In the process of becoming obligatory pathogens, the early form of MTC had four major adaptations. First, it lost the ability to replicate outside a host. Secondly, it evolved the ability to transmit between hosts

(such as humans and animals); thirdly, the ability to go into dormancy state to avoid extinction in small populations (Brites and Gagneux, 2012) and finally, it developed strategies to overcome and hide from the host's immune system (discussed further in section 1.3). The trajectory towards host-specialisation has allowed the MTC ancestor to spread all over the world, becoming one of the most successful human pathogens (Brites and Gagneux, 2015). The human-adapted MTC co-existed with its host causes pulmonary disease as a means of transmission between individuals (Brites and Gagneux, 2012), eventually flaring into active disease when a person is weakened by hunger (Levy, 2012). Genetic analysis of Mtb strains suggests that tuberculosis has evolved among our ancestors in Africa and spread as the human population increased (Levy, 2012).

1.3 The immunology response to *Mycobacterium tuberculosis*

Tuberculosis is predominantly an infection in the airways and lung parenchyma (Wolf *et al.*, 2007). Still, it can also infect other parts of the body (such as eyes, bones, kidneys, brain and spine), known as extrapulmonary TB (CDC, 2012), accounting for 22.4% of TB incidence (Kulchavenya, 2014). Symptoms of pulmonary TB include a persistent cough, usually with phlegm and blood that lasts more than three weeks, weight loss, night sweats, fever, tiredness and fatigue, loss of appetite and swelling in the neck (NHS, 2019).

There are three outcomes when Mtb encounters the host's immune system: immune response resulting in latent infection (discussed in section 1.7), tubercular disease or the complete clearance of the pathogen (Trauner *et al.*, 2012). Looking at the tubercular disease, the Mtb triggers both innate and adaptive immune responses (de Martino *et al.*, 2019). By inhaling aerosol droplets carrying a small number of bacteria (Kaufmann, 2001), the bacteria travels until it reaches the host's lungs (Figure 1-4).

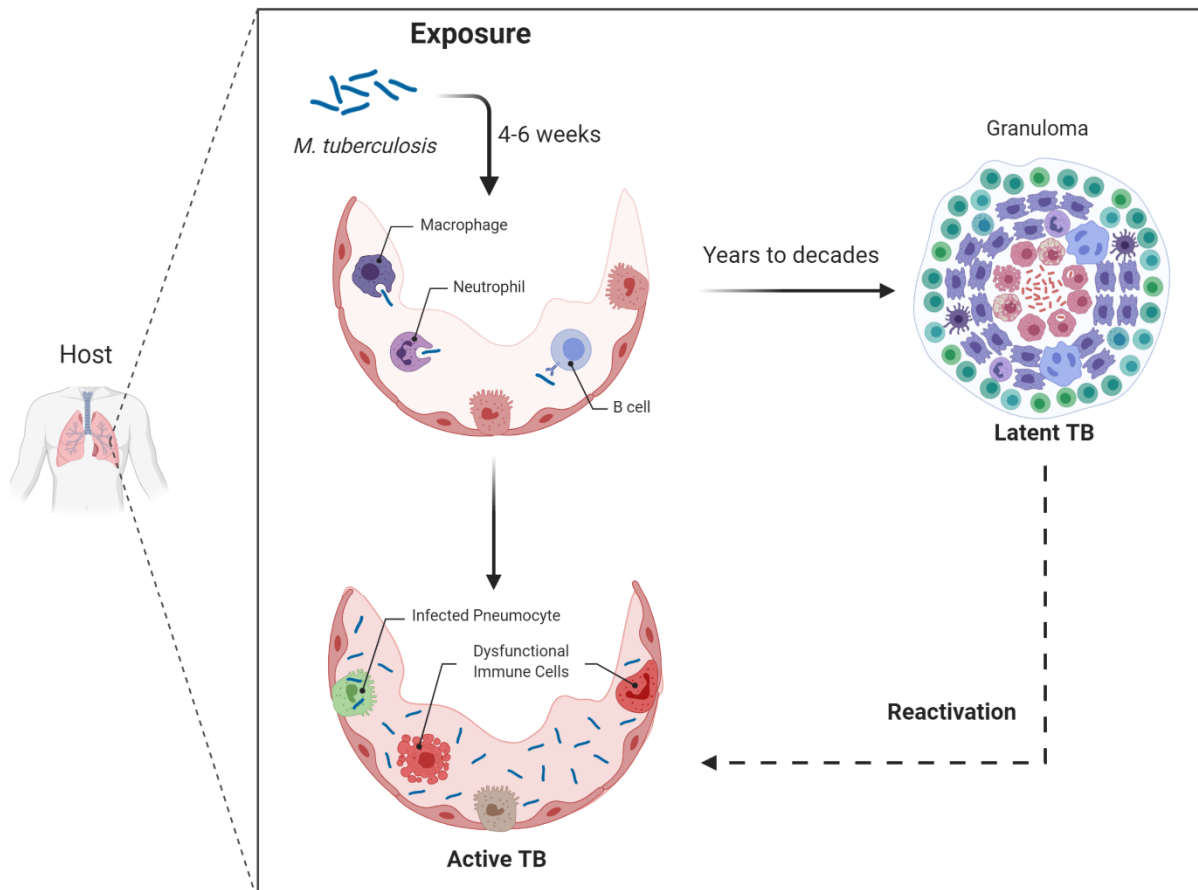


Figure 1-4: Overview of Mtb colonising the host's immune system. Created with BioRender.com. Adapted from Ndlovu and Marakalala (2016).

The airway epithelial cells are the first physical barrier that comes in contact with Mtb, but it can also detect the bacteria's presence through pattern recognition receptors (de Martino *et al.*, 2019). The recognition triggers a modulation in the composition of the airways surface liquid, production of inflammatory cytokines and activation of mucosal-associated invariant T cells stimulating IFN- γ and tumour necrosis factor (TNF)- α production (Li *et al.*, 2012; Harriff *et al.*, 2014). The first line of defence is the macrophages, and when in abundance and immediately recruited, the infection can be cleared (Queval *et al.*, 2017). Mtb is phagocytosed by the alveolar macrophages (Wolf *et al.*, 2007; Eum *et al.*, 2010). The innate immune is then triggered and begins to recruit mature macrophages surrounded by fibroblasts as well as neutrophils, dendritic cells and natural killer cells, forming a granuloma (de Martino *et al.*, 2019). Natural killer cells have been of particular interest recently, as it has been shown that these cells can interact with both macrophages and Mtb directly and play an important role in triggering the adaptive immune response. It has multiple receptors that allow it

to recognise Mtb upon entry into the lung tissue through toll-like receptor 2 (TLR2) (Marcenaro *et al.*, 2008), as well as recognise and lyse Mtb-infected macrophages via NKG2D and NKp46 receptors (Garg *et al.*, 2006).

Initially, as an effort of the immune system to contain and fight against the mycobacteria (Malani, 2012), the granuloma can also be exploited by Mtb to subvert the immune response, replicate and spread (Queval *et al.*, 2017). Moreover, the recruited cells do not leave the granuloma, preventing antigen presentation both locally and in lymph nodes, which delays the adaptive immune response (Silva Miranda *et al.*, 2012). Whilst necrosis with cell lysis begins to occur, allowing the Mtb to propagate locally and increasing the pathogen load, other cells undergo apoptosis that maintains the cellular membrane as a defence mechanism, favouring mycobacterial containment (Hinchey *et al.*, 2007; Behar *et al.*, 2011). The granuloma is a very dynamic and complex environment originally as a host-preventive structure by the accumulation of macrophages and other immune cells.

The adaptive immune responses are delayed in the early granuloma for several reasons. They rely on the presentation of a specific antigen by dendritic cells (under control and help by natural killer T cells) (Moretta, 2002; Vivier *et al.*, 2011), and it is only triggered by the apoptosis of Mtb-infected neutrophils (Blomgran *et al.*, 2012) and by the presence of infected-dendritic cells in the lymph node due to bacterial persistence in alveoli and lung tissues (Gallegos *et al.*, 2008; Wolf *et al.*, 2008). Therefore, the adaptive immune response slowly builds upon the initial innate response as an attempt in containing Mtb replication. The response begins in the lymph nodes, where regulatory CD4⁺ T cells (Treg), T helper 1 (Th1) CD8⁺ T lymphocytes migrate to the affected tissue (Shafiani *et al.*, 2010), crucial for the killing of Mtb, but also responsible for the failure in eradicating Mtb in the long run – as Kursar *et al.* (2007) demonstrated in mice model. Furthermore, the chronic antigenic load leads to the destruction of the lung tissue and the formation of cavities, which only increases the transmission potential of the mycobacteria (Ernst, 2012).

During the infection, different stages of the granulomas coexist, creating a range of microenvironments to which Mtb has to adapt to assure survival. This leads to a range of subpopulations of Mtb employing dormant-metabolism remodelling to cope with these drastic environmental changes in the granuloma such as nutrient limitation and

low oxygen levels (Gengenbacher and Kaufmann, 2012). These changes include cell wall remodelling and virulence factor production to counteract the macrophages' efforts in suppressing the pathogen, such as acidification, reactive oxygen and nitrogen species, hydrolytic enzymes (Liu *et al.*, 2017) and heavy metal poisoning (Botella *et al.*, 2011). For instance, PDIM (phthiocerol *dimycocerosates*), a cell wall lipid component produced by all virulent clinical isolates (Jackson, 2014) and known to be crucial for Mtb survival in mice (Cox *et al.*, 1999), allows Mtb to go unnoticed by the innate immune system because it masks the pathogen-associated molecular patterns that are recognised by toll-like receptors (TLRs) during pathogen infection (Cambier *et al.*, 2014). Moreover, it was later discovered that PDIM is also responsible for escaping the phagosome, inducing host cell necrosis and macroautophagy (Quigley *et al.*, 2017). Other mechanisms, such as the neutralisation of reactive oxygen and nitrogen species and acidification, are also used by Mtb to persist infection (Chen *et al.*, 2015; Lerner *et al.*, 2015).

1.4 History of anti-TB drugs and mode of action

Current drugs are classified as first-line and second-line drugs (Table 1) based on their efficacy and safety for treatment (Nath and Ryoo, 2013). These are antimicrobial molecules that usually target active replicating bacteria by inhibiting the cell wall formation or chromosomal replication (Evangelopoulos *et al.*, 2015). Only 18 anti-TB drugs have been discovered since the 1940s – Figure 1-5. The first TB drug, para-aminosalicylic acid (PAS), was found in 1940 by Frederick Bernheim (Ryan, 1992) and was administered to a patient in October 1944 (Lehmann, 1964). It is a pro-drug whose mechanism of action is not fully understood, but evidence shows that it may inhibit the folate pathway (Zheng *et al.*, 2013). From 1939 to 1944, a microbiologist found a series of effective but toxic compounds, which later led to the discovery of a less toxic and just as effective compound, streptomycin (Schatz *et al.*, 1944), and it was first injected into humans in November 1944 (Rawlins, 2012). This drug disrupts the initiation and elongation step in protein synthesis by binding to the 30S ribosomal subunit (Moazed and Noller, 1987; Ruiz *et al.*, 2002). Resistance to streptomycin quickly emerged *in vitro* with mutations occurring in the *rspL* gene, which codes for the ribosomal protein S12 (Funatsu and Wittmann, 1972), and in the *rrs* gene that codes for 16S rRNA

(Moazed and Noller, 1987). However, some streptomycin-resistant Mtb clinical isolates did not have a mutation on either of these genes (Honore and Cole, 1994). This indicates other possible mechanisms of resistance, such as modifications of other ribosomal components, or more likely, changes in cell membrane permeability, which decreases the drug uptake as observed in *M. avium* (Honore and Cole, 1994).

Although synthesised in 1912, the antitubercular properties of isonicotinic hydrazide (later renamed isoniazid) was only discovered in the 1950s simultaneously by three independent pharmaceutical companies (McDermott, 1969). The structure of isoniazid (INH) had already been published by a chemist, so it could not have been patented (Daniel, 1997). INH became the most commonly used medication to treat TB because of its potency and specificity to mycobacteria (Chakraborty and Rhee, 2015). The regimen of combining PAS, streptomycin and isoniazid for six months was quickly established to delay the development of resistance (Fox *et al.*, 1999). It was used as a 9-month monotherapy for latent infections (Ma *et al.*, 2010). Isoniazid is a pro-drug that enters the cell by passive diffusion (Bardou *et al.*, 1998) and is activated by the catalase-peroxidase, KatG. Active-INH targets InhA, an NADH-dependent enoyl acyl carrier reductase protein involved in the synthesis of mycolic acid (Vilchèze *et al.*, 2006), a highly-abundant component of the Mtb cell wall membrane (Rozwarski *et al.*, 1998). A major site for INH resistance is the *katG* gene (Zhang *et al.*, 1992; Zhang *et al.*, 1996; Slayden and Barry, 2000), in which mutations result in a partially active protein that can both maintain bacterial survival and reduce INH toxicity (Rouse *et al.*, 1995; Marttila *et al.*, 1998; Ramaswamy and Musser, 1998). On the downside, INH can cause acute clinically liver injury that can be severe and even fatal (National Institute of Diabetes and Digestive and Kidney Diseases, 2018).

Between 1952 and 1961, five more drugs were discovered: pyrazinamide, d-cycloserine, kanamycin, ethionamide and ethambutol. Unlike other antibiotics, pyrazinamide has no activity against actively growing Mtb (Zhang *et al.*, 2002; Hu *et al.*, 2006). Also a pro-drug, pyrazinamide (PZA), is converted to pyrazinoic acid by pyrazinamidase enzyme (Zhang *et al.*, 2008). Once active, it inhibits multiple targets such as ATP production and the coenzyme A pathway in non-growing bacteria (Zhang *et al.*, 2002; Hu *et al.*, 2006). Interestingly, PZA has been shown to only be active *in vitro* at acidic pH (Zhang *et al.*, 2014). Pyrazinamide is used in combination with INH and rifampicin to shorten the chemotherapy from 9-12 months to 6 months (British

Thoracic Association, 1976, 1982; Fox *et al.*, 1999). Discovered in the 1950s, D-cycloserine (DCS) is a second-line drug to treat multi and extensive drug resistance Mtb (WHO, 2018). DCS inhibits two enzymes, alanine race-mase (Alr) and D-Ala:D-Ala ligase (Ddl), in the peptidoglycan biosynthesis (Walsh, 1989; Helt and Rubin, 2008). Although the bactericidal effect comes from the inhibition of Ddl (Prosser and de Carvalho, 2013a, 2013b), the dual-target causes the low frequency of resistance in clinical isolates (Silver, 2007) as the emergence of DCS-resistance mutants provides no-fitness phenotypes that can propagate during infection (Evangelopoulos *et al.*, 2019). Given the associated neurological toxicity, DCS is limitedly used for treating multi-drug resistance TB patients (Caminero *et al.*, 2010).

Kanamycin, a second-line drug, also inhibits polypeptide synthesis by binding to 30S subunit of the bacterial ribosome, resulting in a misread that causes the wrong amino acid to be placed into the peptide (Moazed and Noller, 1987). It eventually leads to the breakdown of polysomes and detachment of mRNA (Oizumi *et al.*, 1974). This injectable agent is used to treat multidrug resistance (WHO, 2010). Ethionamide is structurally similar to isoniazid, and therefore, it has a similar mode of action by inhibiting InhA (Grumbach *et al.*, 1956). However, it is one of the less tolerable anti-TB drugs due to its strong side effects such as frequent gastric adverse events (Chan *et al.*, 2004; Nathanson *et al.*, 2004); thus, it is only used to treat multi-drug resistance TB (WHO, 2010). Another anti-TB agent to be administered to treat multi-drug resistant TB is ethambutol (Thomas *et al.*, 1961; Shepherd *et al.*, 1966). Its primary role is to curtail the resistance, but it also has strong side effects usually associated with increased light sensitivity, eye movement pain, blurred vision and even temporary vision loss (Bennett *et al.*, 2015). Its mode of action is not fully known but thought to target the early step of a mycobacterial cell wall component by inhibiting arabinosyl transferase (Goude *et al.*, 2009). This enzyme converts arabinose to arabinan, which is further catalysed into the arabinogalactan, a cell wall constituent. Mutations in this enzyme (*emB* gene) were observed in ethambutol treated TB patients (Bennett *et al.*, 2015).

Rifampicin was discovered in 1957 from a soil sample in Italy, and it was the last first-line TB drug until 2007 (Sensi, 1983). Rifampicin binds to the β -subunit of the RNA polymerase, inhibiting the elongation of mRNA (Wehrli, 1983; Palomino and Martin, 2014). It is also used to treat other bacterial infections such as meningitis (Lee *et al.*, 2017) but is most frequently prescribed to treat TB as a first-line drug. In 2012, a new class of drugs was discovered. Bedaquiline is the first ATP synthase inhibitor and is used to treat active multi-drug resistant strains as a second-line drug (Goel, 2014; Worley and Estrada, 2014). It kills Mtb by interacting with the hydrophobic region of subunit c, as well as with subunit ϵ of the F_1F_0 -ATP synthase (Biuković *et al.*, 2013). Inhibition of C-ring rotation due to disruption in the C-ring: ϵ subunit interaction results in inhibition of ATP production and subsequent cell death (Cholo *et al.*, 2017). Bedaquiline inhibition was initially thought to not cross-react with the human ATP synthase complex (Haagsma *et al.*, 2009); however, recent evidence shows that this drug can inhibit the human mitochondrial ATP synthase (Luo *et al.*, 2020). Common

side effects include nausea, joint pain, headache and chest pain and potentially causing fatal heart arrhythmia (CDC, 2014; Guglielmetti *et al.*, 2017; Luo *et al.*, 2020). An overview of the first- and second-line drugs and their side effects, mode of action, genes involved in resistance and mutation frequency are shown in Table 1.

Table 1: Overview of current first- and second-line drugs, their adverse effects, their mechanism of action and the genes involved in resistance. Adapted from Njire *et al.* (2015) and Zhang and Yew (2015).

Drug	Drug class	Adverse effects	Mechanism of action	Gene(s) involved in resistance	Mutation frequency in clinical isolates	General comments
Isoniazid (INH)	First-line drug	Numbness and tingling, hepatitis, nausea and vomiting, upset stomach, fever and rash.	Inhibition of mycolic acid synthesis.	<i>katG</i> S315 <i>inhA</i>	50-95% 8-43%	Active against growing Mtb. <i>inhA</i> mutation leads to cross-resistance to ethionamide drug.
Pyrazinamide (PZA)	First-line drug	Nausea, upset stomach, vomiting, loss of appetite, mild muscle and joint pain and fatigue.	Depletion of membrane energy inhibition of translation, pantothenate and CoA synthesis.	<i>pncA</i> <i>rpsA</i> <i>panD</i>	72-99%	It has to be converted into an active form by <i>pncA</i> coding enzyme. It kills non-growing bacteria. Analog structure to nicotinamide (Vitamin B3). It is used in combination with INH and RIF to shorten the treatment period.
Rifampicin (RIF)	First-line drug	Upset stomach, heartburn, nausea, menstrual changes, headache, drowsiness and dizziness.	Inhibition of RNA synthesis.	<i>rpoB</i>	95%	Induces hydroxyl formation.
Ethambutanol (EMB)	First-line drug	Blurred vision or trouble focusing, loss of vision in one eye that lasts an hour or longer, photosensitivity, loss of colour vision, pain with eye movement and pain behind your eyes.	Inhibition of arabinogalactan synthesis.	<i>embB</i>	47-65%	Mutation in <i>ubiA</i> linked with a high level of EMB resistance.
Amikacin/ kanamycin, Streptomycin, Capreomycin	Second-line drug	Changes in your hearing, spinning sensation, problems with balance, ringing or roaring sound in your ears, numbness or tingling of your skin, muscle twitching, seizure and urinating less than usual or not at all.	Inhibition of protein synthesis.	<i>rrs</i> , <i>eis</i> , <i>whiB7</i> <i>rpsL</i> S12, <i>rrs</i> 16S <i>tlyA</i>	76% 50%, 20% 85%	Mutations in <i>gidB</i> may be involved in Streptomycin drug resistance.

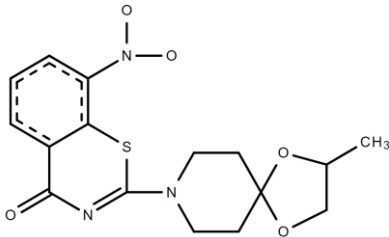
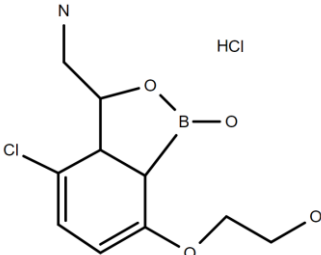
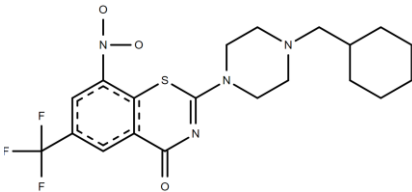
Quinolones (Levofloxacin, Moxifloxacin, Gatifloxacin)	Second- line drug	Nausea, diarrhoea, headache, vomiting, dizziness, nervousness, agitation and nightmares.	Inhibition of DNA synthesis.	<i>gyrA</i> <i>gyrB</i>	75-94%	It seems to become more resistant to quinolone when administrated with RMP.
D-cycloserine (DCS)	Second- line drug	Seizure, confusion, depressed mood, unusual thoughts or behaviour, severe drowsiness, severe dizziness or spinning sensation, swelling, rapid weight gain, overactive reflexes, tremors or shaking, trouble speaking and muscle weakness.	Dual inhibition of D- Ala-D-Ala branch of peptidoglycan biosynthesis.	N/A	N/A	Inhibition of Ddl is responsible for killing Mtb, but the co-inhibition of Alr makes resistance unfeasible. It is used to treat MDR-TB.
Ethionamide (ETH)	Second- line drug	Nausea, vomiting, diarrhoea; stomach pain, loss of appetite, increased salivation, metallic taste in your mouth, blisters or ulcers in your mouth, red or swollen gums, trouble swallowing, headache, dizziness, drowsiness, depressed mood and restless feeling.	Inhibition of mycolic acid synthesis.	<i>etaA/ethA</i> <i>ethR</i> <i>inhA</i>	37-56%	Inhibits the same target as INH.
Para- aminosalicylic acid (PAS)	Second- line drug	Persistent nausea, vomiting, diarrhoea, fatigue. May cause hepatitis.	Inhibition of folic acid and thymine nucleotide metabolism.	<i>thyA, dfrA,</i> <i>folC, ribD</i>	37%	Mutations causing PAS resistance is not fully understood.
Bedaquiline	Second- line drug	Nausea, joint and chest pain, and headache. Increased risk of death and arrhythmias.	Inhibits ATP synthase, leading to depletion of energy.	<i>atpE subunit</i> <i>C, rv0678,</i> <i>rv2535c</i>	Not yet determined	Active against both growing and non-growing bacteria. Evidence of efficiency against MDR-TB strains <i>in vitro</i> and mice. Promising effects when combined with PZA.

The treatment duration (between 6-9 months) and complexity of drug regimens affect adherence. Thus, the search for better regimens with effective, non-toxic drugs that can shorten the treatment duration is urgently needed (WHO, 2019). Besides bedaquiline, two other drugs (delamanid and pretomanid) have received regulatory approval to treat multi-drug resistance TB (WHO, 2019). Delamanid is a dihydro-nitroimidazooxazole derivative that inhibits methoxy mycolic acid and ketomycolic acid synthesis – important cell wall components. This pro-drug is activated by the deazaflavin dependent nitroreductase (Rv3547) enzyme (Xavier and Lakshmanan, 2014). Although the incidence of QT interval prolongation was higher in delamanid-based treatment, this drug has not been associated with arrhythmia (Blair and Scott, 2015). Reported side effects so far are gastrointestinal adverse events and insomnia.

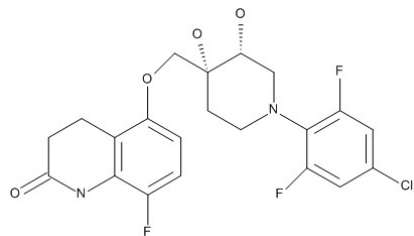
Pretomanid is a novel nitroimidazooxazine drug that is effective against both replicating and non-replicating Mtb through different mechanisms. Against actively replicating Mtb, this drug works by inhibiting mycolic acid biosynthesis, whilst against non-replicating Mtb, pretomanid works by inhibiting protein synthesis (Keam, 2019). Unlike bedaquiline and delamanid, pretomanid does not cause serious adverse events such as QT prolongation (Keam, 2019).

There are 20 drugs currently in Phase I, II or III clinical trials. Thirteen are new compounds, of which 7 of them belong to a new chemical class (BTZ-043, GSK-3036656, macozinone, OPC-167832, Q203, SPR720 and TBA-7371) – Table 2. The remaining 7 are repurposed drugs that are undergoing further testing (WHO, 2019).

Table 2: Overview of seven TB drugs, from new chemical classes, that are currently in clinical trials.

Drug name	Structure	Chemical class	Mechanism of action	Clinical trial stage
BTZ-043		Benzothiazinone	Mtb cell wall synthesis by blocking the decaprenyl-phosphoribose-2'-epimerase (DprE1), necessary for the synthesis of D-Arabinofuranose, a component of arabinogalactan and arabinomannan (Makarov <i>et al.</i> , 2009).	Started Phase 2a in South Africa (November 2020).
GSK-3036656 (GSK 656, GSK 070)		Oxaborole	cytoplasmic protein synthesis inhibition; highly specific for the Mtb LeuRS leucyl-tRNA synthetase enzyme (Palencia <i>et al.</i> , 2016; Li <i>et al.</i> , 2019; Tenero <i>et al.</i> , 2019).	Started Phase 2a (March 2019).
Macozinone (PBTZ-169, MCZ)		Benzothiazinone	Covalently inhibits DprE1, an enzyme essential for the biosynthesis of key cell wall components. It has synergic effects with bedaquiline and clofazimine in preclinical models (Makarov <i>et al.</i> , 2015).	Started Phase 1 trial in EU (December 2017). Started Phase 2A trial in Russia and Belarus (2017).

OPC-167832

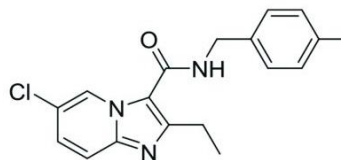


3,4-dihydrocarbostyryl derivative

Inhibiting decaprenylphosphoryl- β -D-ribose 2'-oxidase (DprE1), an essential enzyme for cell wall biosynthesis of Mtb (Hariguchi *et al.*, 2021).

Started Phase 1 (2018).

Q203
(Telacebec,
IAP6, CAS No.
1334719-95-7)

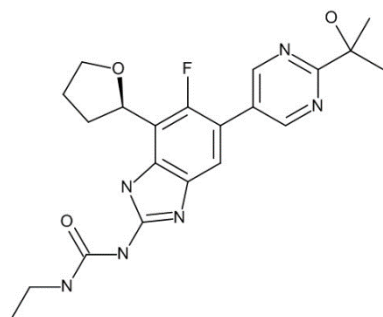


Imidazopyridine amide

Targeting the respiratory cytochrome bc1 complex - a critical component of the electron transport chain (Pethe *et al.*, 2013).

Started Phase 2 in South Africa (July 2018).

SPR720

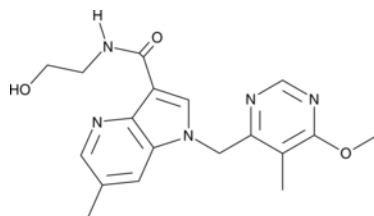


Ethyl urea benzimidazole

Inhibitor of DNA gyrase B/ParE with broad spectrum antibacterial activity. Developed for the treatment of rare non-tuberculous mycobacterial (NTM) infections (Stokes *et al.*, 2020).

Started Phase 2a for the treatment of patients with Mycobacterium Avium Complex (MAC) pulmonary disease (November 2020).

TBA-7371



Azaindole

Non-covalent inhibitor of decaprenylphosphoryl- β -D-ribose 2'-epimerase (DprE1), an essential enzyme for cell wall biosynthesis of Mtb. It also inhibits human PDE6 – a protein in the photoreceptor cells of the eye (Gawad and Bonde, 2018).

Completed Phase 1 (July 2018).

1.5 The rise of multi-drug (MDR) and extensive multi-drug resistant (XDR) strains

Mtb that is resistant to first-line drugs (mainly isoniazid and rifampicin), is considered as MDR-TB (Njire *et al.*, 2015; Zhang and Yew, 2015). Mycobacteria can naturally become resistant to antibiotics through a series of mechanisms such as horizontal gene transfer and spontaneous mutations in genes coding for drug targets (Read and Woods, 2014). The latter is the most common mechanism of resistance in Mtb (Musser, 1995), though there is also evidence of mutations in bacterial efflux pumps that upregulates its activity, resulting in a decrease of the intracellular drug concentrations, which overall reduces the susceptibility to several drug groups (Louw *et al.*, 2009; Miotto *et al.*, 2012).

Nonetheless, inadequate overuse and misuse of antibiotics create a natural selection pressure (Aziz *et al.*, 2006; Glaziou *et al.*, 2018), and so, they also drive the evolution of resistance (Read and Woods, 2014). Overall, the misuse and overuse happen as antibiotics are overprescribed worldwide, and in some countries without antibiotics regulation, as they are available over the counter without a prescription ('The antibiotic alarm.', 2013). It is also possible to buy them online, including in countries where antibiotics are regulated (Michael *et al.*, 2014). Moreover, the severe side effects coupled with the long treatment period can lead patients to discontinue the treatment, preventing Mtb to be eradicated from the host and allowing it to persist (TB Alliance, 2020). In developing countries, patients often cannot complete the treatment due to unavailability of drugs (Frieden, 2013), or the drugs available are either expired or of low quality, leading to a sub-dose of the antibiotic that makes it more favourable for the bacteria to become resistant (Chokshi *et al.*, 2019). It has been shown that resistance rates are increased by 2-6 fold when using expired medication compared to unexpired drugs (Chokshi *et al.*, 2019).

Another aggravating factor is the cross-war with the HIV pandemic. HIV-positive patients are 20 times more likely to become ill with TB than those that are HIV-negative (WHO, 2019). Treatment of this co-infection is further complicated due to drug-drug interaction between anti-TB drugs and antiretroviral therapies (Fry *et al.*, 2019). This causes an accumulation of drug toxicities, which may often lead to a lower likelihood of TB treatment completion (Chen *et al.*, 2003; Orenstein *et al.*, 2009).

Multi-drug resistant Mtb can become further resistant to second-line drugs (fluoroquinolones, streptomycin, aminoglycosides amikacin and kanamycin), and this is referred to as extensively multi-drug resistant (XDR) (Glaziou *et al.*, 2018). Treatment of MDR-TB with second-line drugs increases fourfold the risk for developing XDR-TB, and the treatment period increases to 18-20 months (Zhang and Yew, 2015). The treatment success rate for drug-susceptible TB is 85%, and only 56% for MDR-TB and 39% for XDR-TB (WHO, 2019), resulting in insufficient control of resistant Mtb (Scardigli *et al.*, 2016). Another concern is the cost of treating MDR and XDR-TB. In the US, it costs \$164,000 and \$526,000 per MDR and XDR case, respectively, as it consists of over 14,000 pills and daily injections for at least six months (Frieden, 2013). The complexity and cost of MDR and XDR treatment mean that few patients will receive proper treatment, aggravating the TB-health crisis. The countries with the highest MDR-TB burden are China, India and the Russian Federation, accounting for 47% of the global total (WHO, 2019) – Figure 1-6.



Figure 1-6: Estimated incidences of MDR-TB in 2018 for countries with at least 1000 incident cases. White dots represent islands. Adapted from WHO (2019).

With 500,000 new cases of drug resistance TB every year (WHO, 2019), there is an urgent need to find new, effective TB drugs to treat multi-drug resistant strains.

1.6 Mycobacterium tuberculosis and its four phenotypes: drug-susceptible, drug-tolerant, drug-resistant and persister populations

Mycobacterium tuberculosis is a rod shape bacterium of 1-5 microns in diameter. It is classified as neither a Gram-positive nor Gram-negative as its cell wall contains characteristics of both (Fu and Fu-Liu, 2002). Its cell membrane is rich in mycolic acids with chain variations, as well as other lipids such as trehalose monomycolate and dimycolate (TMM and TDM), phthiocerol dimycocerosate (PDIM) and mannose-capped lipoarabinomannan (ManLAM) (Jackson, 2014). The bacterium's cell wall is one of the major issues in drug penetration (Chiaradia *et al.*, 2017), drug resistance as well as in hiding from the host's immune system (Jackson, 2014). Mtb has the ability to adapt physiologically to a range of environments encountered in the host (Warner, 2015), which leads to a mixed population of Mtb with multiple metabolic phenotypes, drug-resistant, drug-tolerant, drug-susceptible and persisters (Figure 1-7). This mixed population with diverse metabolic states complicates drug treatment (Baer *et al.*, 2015).

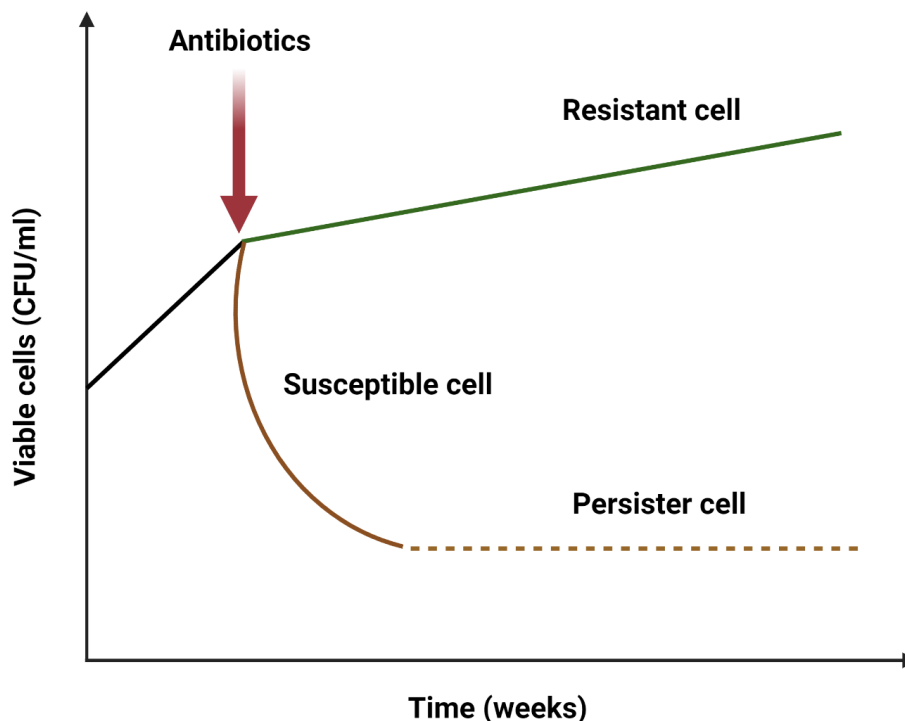


Figure 1-7: Diagrammatic representation of the differences between resistant, susceptible and persister Mtb cells upon antibiotic exposure. Susceptible cells are rapidly killed by antibiotics. Resistant cells have a gene mutation that allows them to be immune to the antibiotics, whereas persisters cells are genetically identical to the susceptible population but can temporarily survive in minimal inhibitory concentrations of antibiotics due to metabolic changes.

Drug-susceptible Mtb is the cell population that lack adaptive response, such as gene mutation or metabolic changes and are rapidly killed by the antibiotics (Blair *et al.*, 2015). Drug resistance is a result of a gene mutation encoding either the target of the drug or the enzyme which activates the pro-drug that leads to a decrease in the effectiveness of the drug (Koch *et al.*, 2018). Drug tolerance can be achieved through slow growth and a range of metabolic states that allow survival upon lethal concentrations of antibiotics (Brauner *et al.*, 2016). Phenotypically drug-tolerant populations have similar minimal inhibitory concentrations (MIC) to susceptible cells, but the minimum length of time for killing 99% of the bacteria (MDK₉₉) is much higher (Koch *et al.*, 2018). Persisters are similar to the drug-tolerant population, in which they can also transiently survive in the presence of an inhibitory concentration of antibiotics, but only 0.0001% of a population displays this phenotype. This is because the persisters are genetically identical to the susceptible population but are metabolic different, and therefore, they are killed much more slowly upon antibiotics (Koch *et al.*, 2018).

This surviving mechanism to the hostile environment has been seen by all bacterial species studied to date, but much of what is known is based on *E. coli* (Torrey *et al.*, 2016). In Mtb, there were five times more downregulated genes in persisters than upregulated ones (1,408 vs 282); of those downregulated, the majority are related to energy-metabolism pathways (Keren *et al.*, 2011). Thus, the persister population are specialised survivor cells that go into dormancy and become highly tolerant to antibiotics (Lewis, 2010). Although a 14-day treatment of isoniazid is enough to kill the susceptible Mtb population, TB regimens are 6-9 months long to avoid the regrow of the persisters that are the likely causes of recurrence TB (Jindani *et al.*, 2003; Torrey *et al.*, 2016). It has been proposed that the ability of Mtb to form persisters is the root of latent TB (Torrey *et al.*, 2016).

1.7 Latent TB

Latent TB is when Mtb has infected the host, but no symptoms are shown because the mycobacteria are in a dormant stage where the disease is not yet active (Sharma *et al.*, 2000). The latent, asymptomatic carrier can develop acute disease months or years after infection (Lillebaek *et al.*, 2002). It is estimated that one-quarter of the

global population harbours latent TB and that there is a 5-15% annual risk of the Mtb becoming active and the host falling ill with TB (WHO, 2019).

As the host's immune response fails to eliminate the pathogen, Mtb has evolved multiple strategies that manipulate the host cells as well as their own cell remodelling that allows them to persist (Ahmad, 2011). A large part of the Mtb genome has been devoted to functions that promote its intracellular survival in mammalian cells, including macrophages (Ahmad, 2011), giving the ability to adapt to distinct metabolic states (Liu *et al.*, 2016). Mtb activates a bacterial regulon, DosR-DosS signal transduction system when in the presence of hypoxia, carbon monoxide or nitric oxide – stimuli that are present inside the macrophage (Park *et al.*, 2003). This leads to an expression of genes that allows the use of alternative energy sources (Bozzano *et al.*, 2014), such as cholesterol and fatty acids, as the energy source to maintain its bacteriostatic state (Sharma *et al.*, 2000). Latent TB becomes highly dependent on purine, amino acid and pantothenate biosynthesis, iron acquisition, glyoxylate shunt, β -oxidation of fatty acids and gluconeogenesis, rather than the primary energy source pathway, glycolysis (Liu *et al.*, 2016). The glyoxylate shunt is upregulated to allow anaplerotic maintenance of the tricarboxylic acid cycle (TCA) and assimilation of carbon via gluconeogenesis. It means Mtb has the ability to intake multiple carbon sources (de Carvalho *et al.*, 2010). Moreover, when investigating the effect of the macrophage's environment (low oxygen and lack of glucose) on dormant Mtb, the non-replicating nutrient-starved mycobacteria is extremely drug-tolerant. Both models of nutrient-starved and hypoxic conditions of mycobacteria have shown 5-fold less ATP in these conditions (from $3.39 \pm 0.21 \times 10^{-18}$ to $0.59 \pm 0.10 \times 10^{-18}$ mol c.f.u.⁻¹) (Rao *et al.*, 2008; Gengenbacher *et al.*, 2010). These results suggest that Mtb undergoes a series of transcriptional and metabolic changes depending upon its environment that are crucial for adaptation to quiescent survival.

Reactivation of latent TB requires Mtb cells to exit dormancy. This is one of the most obscure areas in our understanding, as factors underlying the transition from latency to TB infection are only partially understood with a lack of precise mechanisms that induce the reactivation (Bozzano *et al.*, 2014). There are several factors involving both the mycobacteria and the host that could trigger the reactivation into acute infection, such as the weakening of the immune system (Ahmad, 2011). For instance, the co-infection with HIV, which causes the depletion of CD4⁺ T cells, and functional

abnormalities of CD4⁺ and CD8⁺ T cells that are crucial in protecting against active TB (Wells *et al.*, 2007). Further, Mtb infection accelerates the progression of asymptomatic HIV infection, leading to acquired immunodeficiency syndrome (AIDS), and eventually, death (Ahmad, 2011). Interestingly, Mtb has 30 functional toxin-antitoxin gene pair systems involved in either maintaining latency or progress to virulence depending on regulation (Ramage *et al.*, 2009). The toxin-antitoxin system is involved in the depletion of CD4⁺ T cells or impairment of TNF- α signalling that allows the mycobacteria to infect (Bozzano *et al.*, 2014).

Although during latent TB, the bacterium is not transmissible, being able to diagnose and treat this efficiently before it becomes active would decrease the morbidity and mortality numbers (WHO, 2019). Latent TB is indirectly diagnosed by evaluating the immunological response to both *in vivo* and *in vitro* stimulation by mycobacterial antigens through the tuberculin skin test and interferon-gamma release assay (WHO, 2019). None of the anti-TB drugs is specifically effective to treat latent TB, but the current regimen options are a 6-month monotherapy of isoniazid or a 3-month combination of rifampicin and isoniazid (Hamada *et al.*, 2018). Recently, it has been proposed that ICL1 is an attractive target to treat tuberculosis as it is an essential enzyme for latent Mtb, and it is absent in mammals (Liu *et al.*, 2016).

1.8 Isocitrate Lyase

Isocitrate lyase (ICL, types 1 and 2) plays an important role in Mtb metabolism during the dormancy stage. ICL is a key enzyme in two pathways, the glyoxylate and methylcitrate cycle (Gould *et al.*, 2006). Both pathways are activated in latent TB due to the depletion of glucose and oxygen, which is the environment inside of the macrophage (Shukla *et al.*, 2015). These conditions deactivate the enzymes in the TCA cycle and upregulate the enzymes responsible for the glyoxylate and methylcitrate cycles to continue to generate energy from a different carbon source, such as lipids (Bentrup *et al.*, 1999). The glyoxylate pathway resembles the tricarboxylic acid cycle, which operates as an anaplerotic route to replenish the TCA cycle during Mtb's growth on fatty acid substrates, where the first two reactions in both cycles are the same, followed by the catalysis of isocitrate to form succinate and glyoxylate by ICL (Sharma *et al.*, 2000) – Figure 1-8. In the methylcitrate cycle, ICL

participates in the last enzymatic step of the propionate degradation route, a by-product of the β -oxidation of odd fatty acids chains, where pyruvate and succinate are formed from 2-methylisocitrate (Bentrup *et al.*, 1999; Gould *et al.*, 2006). The purpose of the methylcitrate cycle is to remove a toxic by-product, propionyl-CoA, which results from β -oxidation of odd chains fatty acids (Eoh and Rhee, 2014).

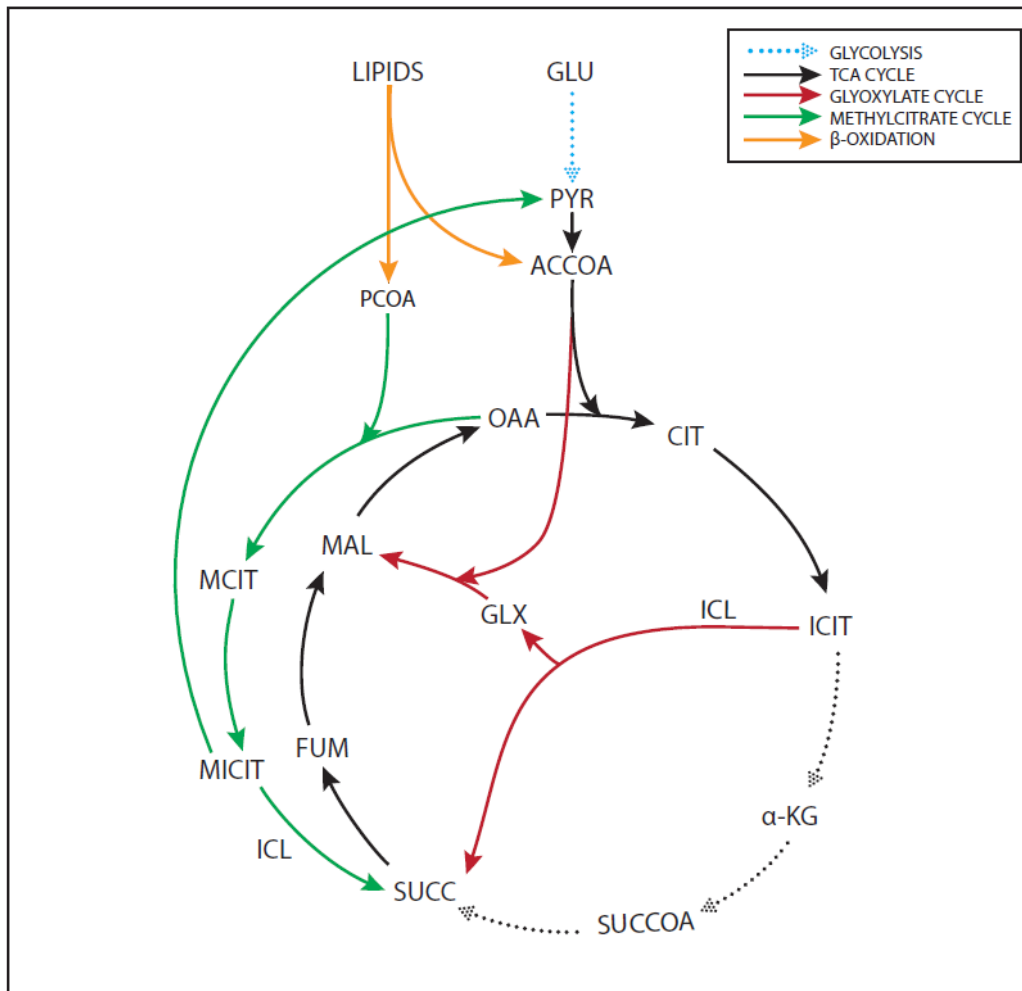


Figure 1-8: Diagrammatic representation of the metabolic change of Mtb inside the host's macrophages. The lack of glucose and oxygen inactivates glycolysis (shown as dot arrows), and lipids become the main carbon source, activating the glyoxylate and methylcitrate cycles. The glyoxylate cycle by-passes three TCA cycle reactions (shown as dot arrows). Full names: GLU for Glucose; PYR for Pyruvate; ACCOA for Acetyl-CoA; CIT for Citrate; ICIT for Isocitrate; α -KG for alpha-ketoglutarate; SUCCO for Succinyl-CoA; SUCC for Succinate; FUM for Fumarate; MAL for Malate; OAA for Oxaloacetate; ICL for Isocitrate Lyase; GLX for Glyoxylate; PCOA for Propionyl-CoA; MCIT for Methylcitrate and MICIT for Methylisocitrate. No by-product, co-factors or enzymes (besides ICL) are shown. Adapted from Muñoz-Elías *et al.* (2006).

Hence, inhibiting ICL will result in both starvation and the intoxication of the mycobacteria (Eoh and Rhee, 2014). Previous studies have demonstrated that the

disruption of the ICL gene attenuates the persistence of Mtb in mice and inflammatory macrophages in mice (McKinney *et al.*, 2000; Sharma *et al.*, 2000). Moreover, Gengenbacher *et al.* (2010) have concluded that ICL is key to non-replicating Mtb survival and regulation of intracellular ATP levels in a nutrient-depleted environment, such as the one in macrophages. There is also recent evidence that ICL plays an important role in antibiotic resistance (Nandakumar *et al.*, 2014; Zhou *et al.*, 2017). When the wild-type Mtb was exposed to a sub-lethal dose of anti-TB drugs, the activation of ICL and induction of oxidative stress response genes were observed, whilst in ICL mutant strain ($\Delta icl1/2$), the expression of oxidative stress response genes were basal levels. The ICL knock-out (KO) strain was also 100-fold more sensitive to anti-TB drugs than the wild-type (Nandakumar *et al.*, 2014). Another study investigated the succinylation of specific ICL1 residues, as at least three succinylated lysine residues (K189, K322, and K334) have been reported in Mtb ICL1 (Zhou *et al.*, 2017). These authors found that a mutant strain of ICL1-K189E was more sensitive to rifampicin and streptomycin than the wild-type, suggesting that regulation of K189 succinylation aids in antibiotic resistance (Zhou *et al.*, 2017). These results show that Mtb can fine-tune ICL at a metabolic and translational level to achieve bacterial resistance.

Both enzymes (ICL1 and ICL2) are essential for *in vivo* growth and virulence (Muñoz-Elías and McKinney, 2005). ICL1 (428 amino acids) is encoded by the *icl1* gene, whilst ICL2 (766 amino acids) is encoded by the *aceA* gene (McKinney *et al.*, 2000; Muñoz-Elías and McKinney, 2005; Gould *et al.*, 2006). Most studies have focused on ICL1 as the Mtb enzyme structure was solved in 2000 by Sharma *et al.*, and only recently the structure of Mtb ICL2 was solved (Bhusal *et al.*, 2019). Both enzymes are essential for *in vivo* growth and virulence (McKinney *et al.*, 2000; Muñoz-Elías and McKinney, 2005). The ICL2 N-terminal domain contains the α/β -barrel core common to all ICLs and is folded similarly to ICL1 (Sharma *et al.*, 2000). Its active site contains the conserved catalytic motif 'KKCGH' – Figure 1-9. One could conclude that an ICL inhibitor would inhibit both ICL1 and 2.

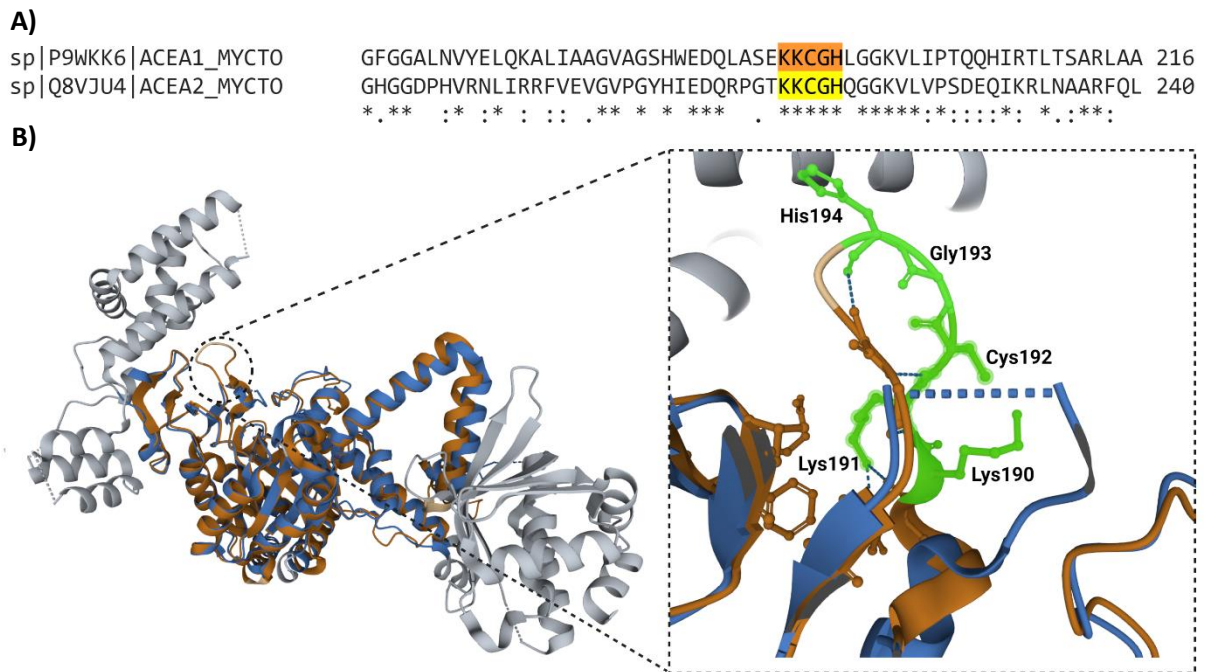


Figure 1-9: Sequence alignment of ICL1 and ICL2. **A)** Alignment sequence of ICL1 (ACEA1) amino acids 157-216 and ICL2 (ACEA2) amino acids 181-240. The conserved active site motif 'KKCGH' is highlighted. **B)** Superimposition of ICL1 (brown, 1F61) and ICL2 (blue, 6EE1) with a zoom in the active site highlighting the amino acids motif.

It is worth pointing out that ICL2 possess an additional helical structure in the N-terminal domain that is not present in ICL1 (helices α_{10} – α_{16} ; residues 278–427) (Bhusal *et al.*, 2019). The role of this isoform is not fully known, but recent evidence shows that it may act as a gate-keeping enzyme that regulates both glyoxylate shunt and the methylcitrate cycle by allosteric activation upon acetyl-CoA binding (Bhusal *et al.*, 2019).

ICL1 requires magnesium (Mg) ions for activity (Kumar and Bhakuni, 2008). The catalytic mechanism has been suggested by Pham *et al.* (2017) based on the crystal structure and kinetic analysis - Figure 1-10. In a two-step reaction, the substrate coordinates an active-site Mg ion and undergoes a base-catalysed retro-aldol reaction to form glyoxylate and the aci-anion of succinate, then Cys191 protonates C-2 of aci-anion of succinate to afford succinate (Pham *et al.*, 2017).

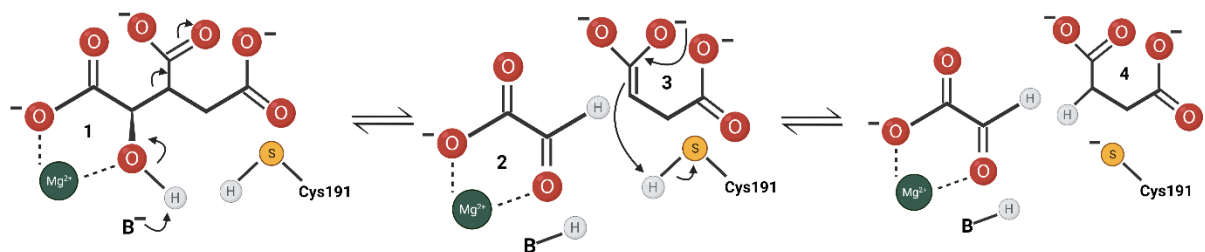


Figure 1-10: Catalytic mechanism of ICL1 with isocitric acid to form glyoxylate and succinate. B refers to a general base. Adapted from Pham *et al.* (2017) and created with BioRender.com.

ICL1 is composed of a homotetramer (Figure 1-11A), and both bioinformatics and mutagenesis analysis suggests that the motif 'KKCGH' (residues 189-193) is highly conserved and crucial for catalytic activity (Moynihan and Murkin, 2014) – Figure 1-11B, orange box. The interaction between glutamic acid (Glu423) and glutamic acid (Glu424) with lysine (Lys189) and lysine (Lys190), respectively, are important to keep the enzyme in its catalytically active conformation (Shukla *et al.*, 2015). Disrupting these interactions can lead to a reduction in the enzyme's catalytic activity – Figure 1-11B, blue boxes. Moreover, two lysine residues (K322 and K392) were found to play a role in the regulatory function in ICL1 by acetylation in response to changes of carbon sources (Bi *et al.*, 2017) – Figure 1-11B, green boxes.

A)

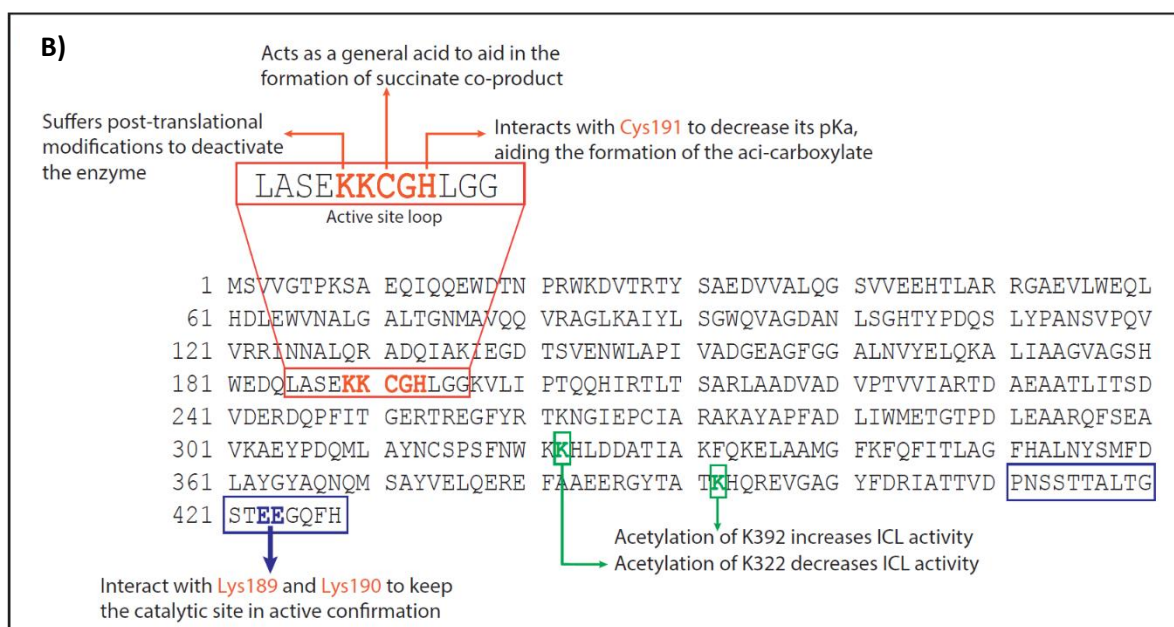
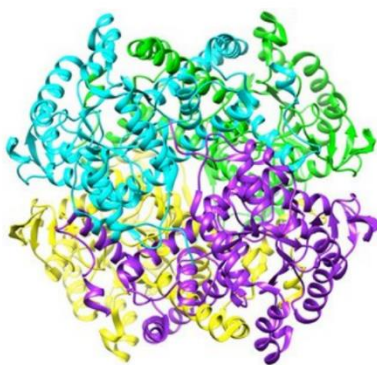


Figure 1-11: The structure of ICL1. **A)** Ribbon representation of the ICL1 homotetramer (Shukla *et al.*, 2017). **B)** Amino acid sequence of *Mycobacterium tuberculosis* isocitrate lyase. The orange box highlights the amino acids responsible for the active site (Moynihan and Murkin, 2014). The dark blue box around the 18 residues is a loop that acts as a lid to the catalytic site, opening when the enzyme is active and closing when the enzyme binds with the substrate (Shukla *et al.*, 2015). The two lysine residues in green are part of a regulatory mechanism of ICL1 by acetylation (Bi *et al.*, 2017). The sequence was obtained from the UniProt (2018) database.

A strategy for the development of enzyme inhibitors was synthesising compounds that form covalent bonds with cysteine residues in or near the active site (Sharma *et al.*, 2000; Singh *et al.*, 2011). This was a good strategy for ICL1 as there is a conserved catalytic cysteine (Cys₁₉₁) in the active site that is less prone to mutation (Pham *et al.*, 2017). ICL1 inhibitors can be used to treat latent TB as well as active TB in synergy with current first-line drugs to reduce the duration of the chemotherapy (Sharma *et al.*,

2000). ICL1 is present in many organisms such as plants, fungi, nematodes, protists and bacteria, but is absent in mammals (McKinney, 2005; Kondrashov *et al.*, 2006; Lee *et al.*, 2015). This means that ICL1 inhibitors could be candidates for the treatment of other pathogens that show persistent infections, including *Pseudomonas* (Rao and McFadden, 1965) and *Salmonella* (Wilson and Maloy, 1987).

1.9 ICL1 inhibitors

There have been previous attempts to inhibit Mtb's ICL1. The rationale was to design inhibitors that are similar to the substrate, in which the important properties such as polarity and size would match with the active site-specificity. Three inhibitors were developed: itaconic acid/ itaconate (McFadden and Purohit, 1977), 3-nitropropionate (Schloss and Cleland, 1982) and 3-bromopyruvate (Ko and McFadden, 1990) – Figure 1-12.

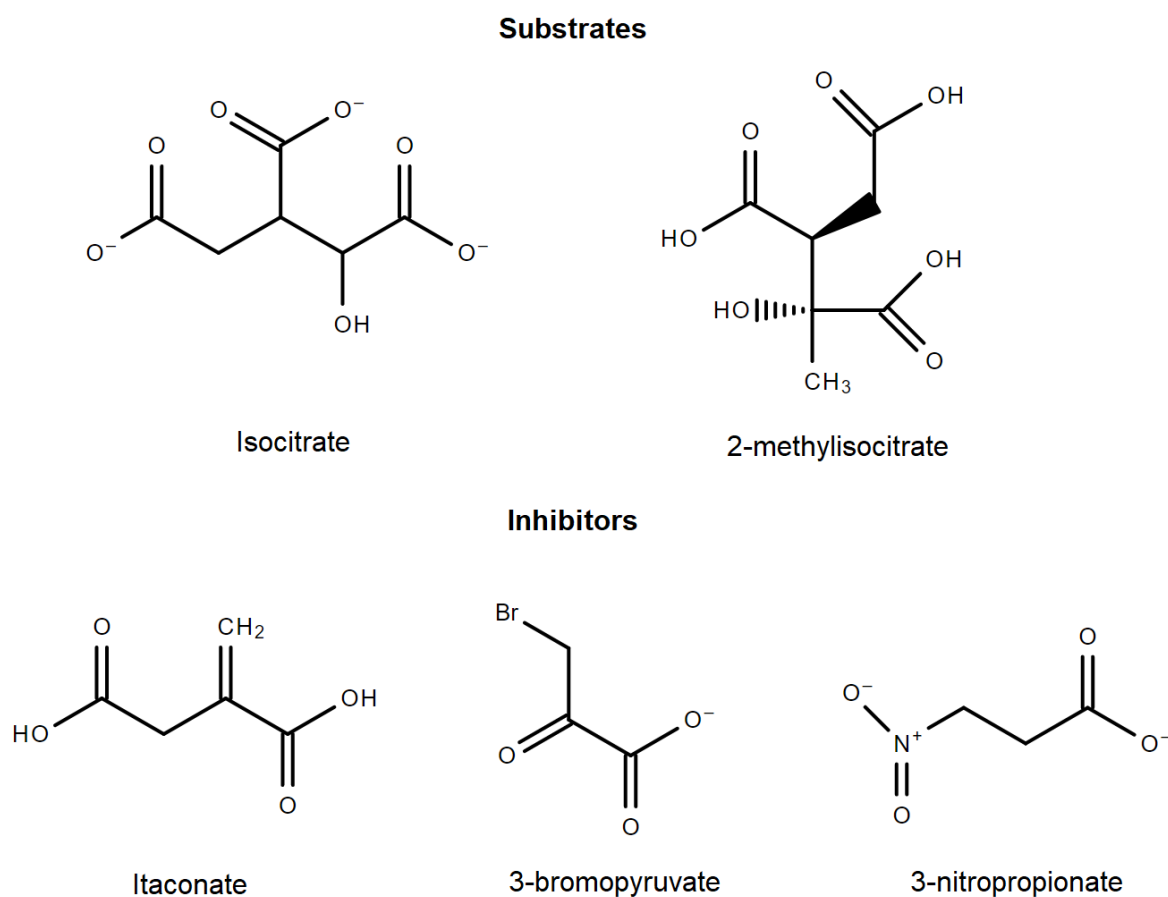


Figure 1-12: Structure of ICL substrates (isocitrate and 2-methylisocitrate) and the three ICL1 inhibitors: itaconate, 3-bromopyruvate and 3-nitropropionate (McFadden and Purohit, 1977; Schloss and Cleland, 1982; Ko and McFadden, 1990).

Itaconate is an ICL1 competitive inhibitor that has been shown to cause hypertonicity of blood pressure when administered to cats (Finkelstein *et al.*, 1947) and growth impairment in rats (Booth *et al.*, 1952). Itaconate is not suited to be a drug, but it has been a point of interest in immunology since it was reported to be biosynthesised by mammalian macrophages as an anti-microbial response during infection (Sugimoto *et al.*, 2011). Itaconate was detected in the lung tissue of Mtb-infected mice, and Michelucci *et al.* (2013) demonstrated that macrophages produce it as an attempt to inhibit the pathogen's growth by inhibiting the glyoxylate shunt. Although 3-nitropropionate binds 65,000 times more tightly to ICL1 than succinate (Schloss and Cleland, 1982), this compound extracted from the *Indigofera* can bind to succinate dehydrogenase, a key enzyme in the Krebs cycle and electron transport chain (Alston *et al.*, 1977). Greene *et al.* (1998) demonstrated that 3-nitropropionate leads to neuronal death in rats, and thus, it is not safe for clinical trials. 3-bromopyruvate was also identified as an ICL1 inhibitor because of its affinity to the enzyme (Ko *et al.*, 2004). The crystal structure of Mtb ICL1 treated with 3-bromopyruvate revealed cysteine 191 had been S-pyruvoylated (Sharma *et al.*, 2000). This is the residue thought to be involved in the protonation of C-2 to afford succinate, as seen in Figure 1-11. 3-bromopyruvate is not a safe drug either because it also inhibits ATP production (Ko *et al.*, 2004). Thus, the search for a compound that shows a high affinity to ICL1 with low toxicity remains.

Despite of many high-throughput screenings in the past 18 years, with more than 1,000,000 compounds being screened for activity against ICL1, no inhibitors have been successfully moved to clinical trials due to their high toxicity (Bhusal *et al.*, 2017) – Figure 1-13 shows a timeline of the ICL1 inhibitors developed to date. This is likely because most inhibitors are substrate-analogues and could be binding with other enzymes that use isocitrate or succinate as substrates, such as isocitrate dehydrogenase and succinate dehydrogenase (Bhusal *et al.*, 2017). The review of Lee *et al.* (2015) discusses in depth the attempts to design inhibitors for Mtb ICL1. A table with all published ICL1 inhibitors and their half-maximal inhibitory concentration (IC₅₀) can be found in Appendix A, Table A1.

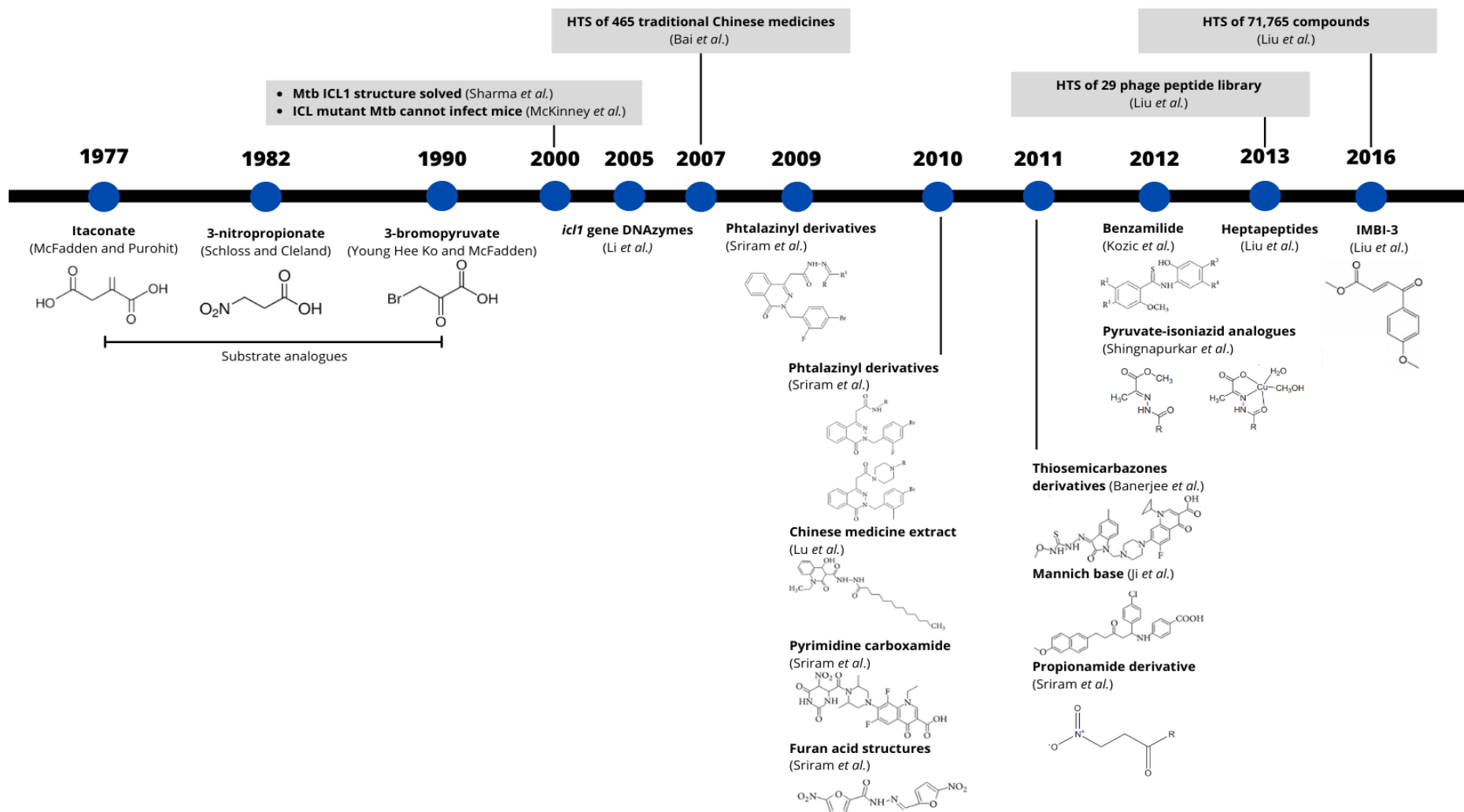


Figure 1-13: A timeline of the ICL1 inhibitors developed to date (1977-2016).

An ideal candidate would be a drug to be taken with current first- and second-line drugs, and that also shortens the long treatment period as this would lead to more people completing the course of the antibiotics and overall increasing treatment efficiency (WHO, 2019).

1.10 Aim of this research

The ultimate goal was to identify a potent ICL1 inhibitor that can inhibit the isolated enzyme and the bacteria *in vitro*.

This was achieved by:

1. Optimisation of ICL1 expression and purification.
2. Synthesising of a series of ICL1 inhibitors.
3. Testing the inhibitory effect of potential compounds against the isolated enzyme.
4. X-ray crystallography of the lead compound bound to the isolated enzyme to confirm the inhibitor's affinity to the active site and visualise the modifications caused to the enzyme.
5. Testing the inhibitor's efficiency against *Mycobacterium tuberculosis* and establishing if they are bactericidal or bacteriostatic, and performing metabolomics analysis to understand the impact of the drug on the metabolome.
6. Combining ICL1 inhibitor with current anti-TB drugs, such as rifampicin and bedaquiline, in an *ex vivo* assay to assess whether it can decrease the treatment period.

Chapter 2 – Isocitrate lyase 1 expression, purification and crystallisation

Introduction

Isocitrate lyase 1 (ICL1) is an important enzyme for *Mycobacterium tuberculosis* (Mtb) during persistent infection (Schnappinger *et al.*, 2003). For crystallography and *in vitro* assay purposes, this enzyme will be expressed and purified. To achieve that, the *icl1* gene containing a polyhistidine-tag was inserted into a pET-28a plasmid (Figure 2-1) provided by Professor Eoh's laboratory (University of Southern California, USA) – under kanamycin selection. The overexpression of the ICL1 protein was achieved in *Escherichia coli* Rosetta gami DE3 pLysS where the desired protein was induced by the lactose analogue, IPTG (isopropyl β -D-1-thiogalactopyranoside). The total cells protein is then used to purify the protein of interest by nickel-affinity chromatography.

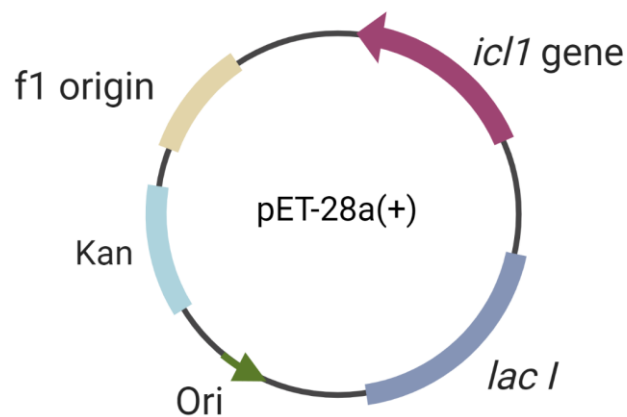


Figure 2-1: Representation of the plasmid, pET28a, with the antibiotic resistance marker (kanamycin) and the gene coding for isocitrate lyase (ICL1). Created with BioRender.com.

The purified enzyme was used for X-ray crystallisation. This technique is used by applying a beam of X-rays in a protein crystal that creates a diffraction pattern of the electron density, which can be used to reconstruct a three-dimensional shape of proteins (Hauptman, 1990) by measuring the angles and intensity of these diffracted

beams (Ryu, 2017). The data must be interpreted using semi-automatic computational methodologies (Khanna *et al.*, 2019).

Obtaining good quality protein crystals is desirable for high-resolution structural determination of the proteins using crystallography, and getting such crystals has long been a bottleneck (Hassell *et al.*, 2006). The crystal quality is affected by the growth environment and growth methods, such as pH, salt and protein concentration, temperature (Schmit and Dill, 2012; McPherson and Gavira, 2014). There are a number of methodologies for crystallisation trials, which involves the screening step (the identification of a crystallisation agent that can crystallise the targeted protein) (Luft *et al.*, 2003; McPherson and Gavira, 2014) and the optimisation step (the conditions for crystallisation are optimised to obtain diffracting protein crystals) (Brzozowski and Walton, 2001). Two vapour diffusion methods are generally employed: hanging drop and sitting drop (Figure 2-2).

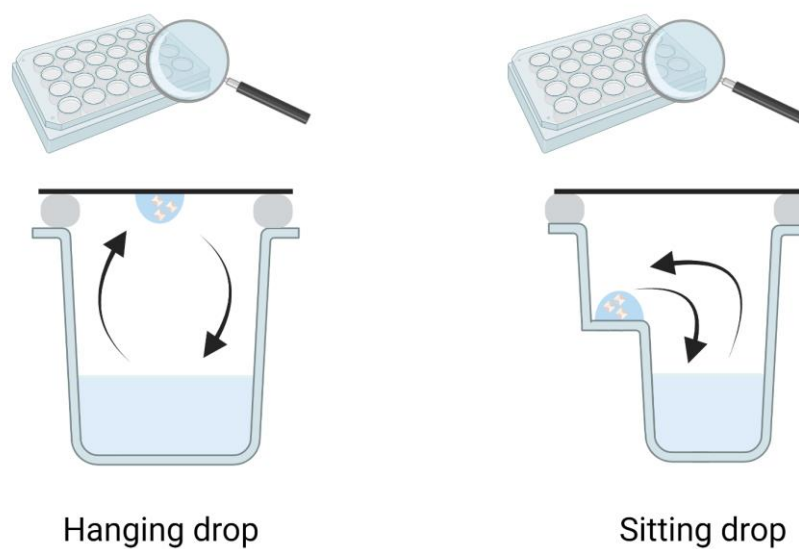


Figure 2-2: Overview of the two methodologies for crystallisation trial: hanging drop and sitting drop. Created with BioRender.com.

In vapour diffusion, a drop containing a mixture of precipitant and protein solutions is sealed in a chamber with pure precipitant. The water vapour then diffuses out of the drop until the osmolarity of both the drop and the precipitant are equal, reaching an equilibrium (McPherson and Gavira, 2014; Hou *et al.*, 2019). In hanging drop vapour diffusion, the protein mixed with the precipitant drop is suspended in siliconised glass

coverslips, whilst sitting drop is located in an elevated reservoir that is different from the precipitant reservoir. There are five outcomes when setting up a crystallisation trial, 1) obtaining no crystals; precipitation may occur or not, 2) obtaining a shower of small crystals that are not suitable for diffraction, 3) obtaining large crystals that do not diffract, 4) obtaining reasonable crystals that require improvement and 5) obtaining good crystals that are suitable to diffract but are often difficult to reproduce (Govada and Chayen, 2019). The growth of a diffraction-quality crystal is one of the major obstacles in X-ray crystallography (Wienczek, 1999; Kierzek and Zielenkiewicz, 2001; McPherson and Gavira, 2014).

Crystal formation happens when the protein solution is under-saturated to start with and attains super-saturation upon equilibrium with the precipitant in the reservoir over the course of the trial (Hou *et al.*, 2019) – Figure 2-3. The concentration of the protein is an important factor, as it must be the highest concentration possible without leading to aggregation or precipitation, and thus, finding the protein concentration range is often a challenge. Introducing a precipitating agent can promote either protein aggregation or the nucleation of protein crystals that can result in large three-dimensional crystals (Hou *et al.*, 2019).

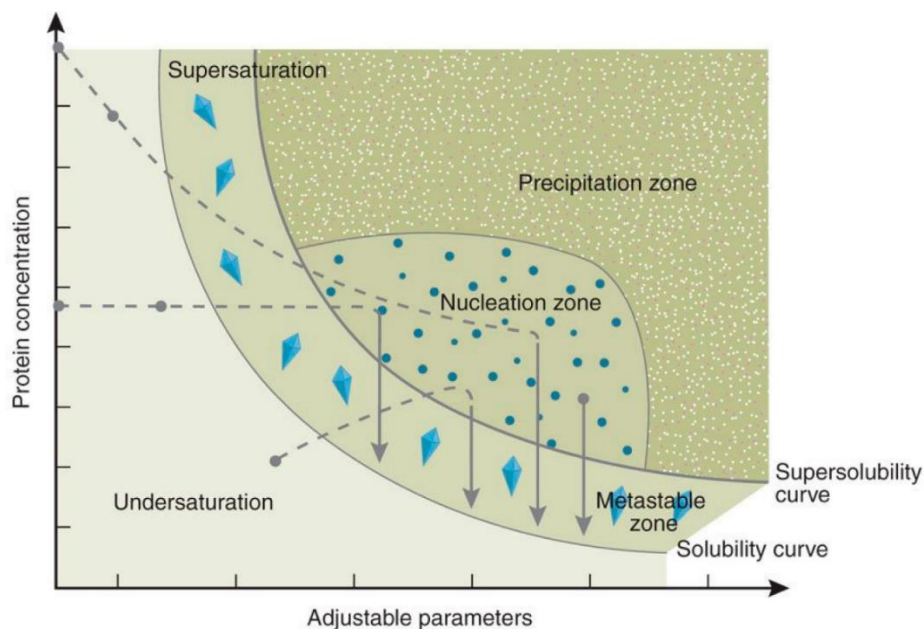


Figure 2-3: Solubility curve for crystal formation. Image adapted from Chayen and Saridakis (2008).

Isocitrate lyase crystallisation efforts

To date, ten solved Mtb ICL1 structures are available at Protein Data Bank (PDB). Three of them were solved by Sharma *et al.* (2000) using the *icl1* gene sequence from Mtb H37Rv strain. The first structure is the enzyme alone with magnesium ions at 2.00 Å resolution (PDB 1F61), the second one is with an inhibitor, 3-bromopyruvate of 1.80 Å (PDB 1F8M), and the final one was solved with succinic acid and glyoxylic acid as ligands which formed an ICL1:nitropropionate:glyoxylate complex of 2.25 Å resolution (PDB 1F8I). The technique employed was the vapour diffusion method and 100 mM HEPES pH 7.5, 1.4 M sodium citrate as the precipitation buffer or 0.1 M Tris.HCl (pH 8.0), 0.2 M sodium acetate, 20–30% (w/v) PEG 4000 (Sharma *et al.*, 2000).

In another three entries available at PDB, the authors solved a crystal of ICL1 from Mtb Erdman (ATCC 35801). The first group solved the ICL1 structure with the ligand 4-hydroxy-2-oxobutanoic acid, creating a Michael substrate, 2-vinyl glyoxylate (PDB 5DQL) (Pham *et al.*, 2017). The second group solved two crystals, one with pyruvate and 3-nitropropionate of 1.80 Å resolution (PDB 6C4A), and the second one was ICL1 with glyoxylate and pyruvate of 2.20 Å resolution (PDB 6C4C) (Ray *et al.*, 2018).

The last four entries were recently added to the PDB. The first solved structure of ICL1 with itaconate of 1.55 Å (PDB 6XPP) was reported by Kwai *et al.* (2021). Two structures of cis-2,3-Epoxy-succinic acid bound to ICL1 were solved; one at 1.75 Å resolution (PDB 6WSI) and the other as a covalent adduct at 1.88 Å resolution (PDB 6VB9) (Pham *et al.*, 2021). Finally, an ICL1 complex with succinate and itaconate was solved at 2.58 Å resolution (PDB 7CP1) (Kwon *et al.*, 2021). The structures of ICL1 has been solved for other organisms, for example, *Aspergillus* species such as *nidulans* (Britton *et al.*, 2000), *Fusarium graminearum*, *Magnaporthe oryzae* (Park *et al.*, 2016) and *E. coli* (Britton *et al.*, 2001).

The Mtb ICL2 was only solved recently by Bhusal *et al.* (2019), which until then was an isoform poorly understood. The authors obtained ligand-free ICL1 crystals in the apo form at 1.80 Å resolution (PDB 6EDW) and co-crystals with acetyl-CoA complex at 2.67 Å and 2.36 Å resolution (PDB 6EDZ and 6EE1) using sitting drop vapour diffusion (Bhusal *et al.*, 2019). Further, a known ICL1 inhibitor, 3-nitropropionate, was

added to the drops containing ICL2:Acetyl-CoA complex crystals, and the solved crystal was 2.36 Å resolution (Bhusal *et al.*, 2019).

Both ICL1 and ICL2 active sites are conserved, and thus, the solved crystal structure of either isoform can give a better insight into the development of an isocitrate lyase inhibitor. In this study, two strategies are employed: crystallisation of ligand-free ICL1 so novel inhibitors can be added to the crystal-containing drops and co-crystallisation of ICL1 and novel inhibitors – which will be further discussed in Chapter 5. In this chapter, the attempts to crystallise ligand-free ICL1 will be addressed.

Materials and Methods

Strains and plasmid

Both *Escherichia coli* Rosetta gami DE3 pLysS and BL21 strains were used for transformations. The recombinant plasmid pET 28a-ICL1, which expresses the ICL1 protein with N-terminal His₆-tag was sent from our collaborators, the Eoh Lab, University of Southern California, USA. The plasmid was stored at -20 °C. Chemically competent *Escherichia coli* BL21 (ThermoFisher, UK) was transformed with pET 28a-ICL1 for plasmid stock purposes, where the plasmid was extracted using the Spin Miniprep kit (QIAGEN) following the manufacturer's instruction. In general, the pellet of an overnight culture of BL21 cells was resuspended in 250 µL buffer P1 and gently mixed with 250 µL buffer P2, followed by 350 µL buffer N3 and centrifuged for 10 minutes at 17,900 x g as per guidelines. Then, 800 µL of supernatant was washed with 0.75 mL buffer PE using QIAprep 2.0 Spin Column, and the DNA was eluded with 50 µL buffer EB. The plasmid was stored at -20 °C. *Escherichia coli* Rosetta gami DE3 pLysS (Sigma-Aldrich, UK) were transformed with pET28a-ICL1 for protein expression.

Bacterial Transformation

E. coli BL21 and Rosetta gami DE3 pLysS competent cells were thawed on ice for 10 minutes, and 1 µL of pET28a-ICL1 DNA was added, and the mixture was incubated on ice for 30 minutes. The cells were then heat shocked at 42 °C for 60 seconds and placed on ice for 2 minutes. 500 µL of SOC (2% tryptone, 0.5% yeast extract, 10 mM NaCl, 2.5 mM KCl, 10 mM MgCl₂, 10 mM MgSO₄, and 20 mM glucose) media was added and the cells were incubated at 37 °C for 1 hour, shaking at 250 rpm. The cells

were then transferred to 10 mL LB (10% tryptone, 10% NaCl, 5% yeast extract) media with kanamycin (50 µg/mL) and grown overnight at 37 °C at 250 rpm. The overnight culture was used to extract the plasmid from the BL21 host using the Spin Miniprep kit (QIAGEN), and to overexpress ICL1 in the Rosetta gami DE3 pLysS host.

ICL1 Expression and Purification

For overexpression, an overnight culture of *E. coli* Rosetta gami DE3 pLysS was diluted 1/1000 in a 400 mL LB with kanamycin (50 µg/mL) and grown until OD₅₉₅= 0.5-1.2 at 37 °C and 250 rpm. The cells were then incubated on ice for 30 minutes and the protein expression was induced with 0.4 mM IPTG and 2% (v/v) ethanol. The protein expression lasted for 20 hours at 18 °C at 250 rpm. The cells were then harvested by centrifugation at 4500 rpm (Megafuge 8, ThermoFischer™) for 1 hour, and resuspended in 10 mL of TGN (50 mM Tris.HCl pH 7.5, 10% (v/v) glycerol, 250 mM NaCl and 10 mM imidazole). The cells were lysed or frozen at -80 °C.

Cell lysis. 1 mg/mL final concentration of lysozyme (Sigma) was added to the cells from the protein expression step and incubated on ice for 30 minutes. 0.1% (v/v) final concentration Triton-X was added to the cells and incubated on ice for 30 minutes. The cells were then sonicated for 3 x 30 seconds on ice at 40% power (Status US 200, Philip Harris Scientific) with rest in between cycles. The soluble protein was then harvested by centrifugation at 24,700 x g at 4 °C for 1 hour. The soluble protein was frozen at -80 °C.

ICL1 Purification. The Ni-NTA (ThermoFisher, UK) was washed 4 times in TGN (50 mM Tris.HCl pH 7.5, 10% (v/v) glycerol, 250 mM NaCl and 10 mM imidazole) and harvested by centrifugation at 800 x g for 1 minute. 1 mL of the resuspended nickel resin was added to the soluble protein and gently shaken at 4 °C for 1 hour. The bound protein was harvested by centrifugation at 1500 rpm for 5 minutes at 4 °C. The supernatant (unbound protein) was stored at -80 °C. The pellet was resuspended in 5 mL TGN and transferred to the purification column. The column was washed with 50 mL of TGN, and an aliquot was taken in the first and last 1 mL of the wash. The protein was then eluted in five separate 1 mL fractions of buffer containing 50 mM Tris.HCl pH 7.5, 10% (v/v) glycerol, 100 mM NaCl and a gradient of imidazole (50 mM, 100 mM, 150 mM, 200 mM and 300 mM). The purified fractions with ICL1 were analysed

by SDS-PAGE, and the concentration was determined by the Bradford protein assay. The fractions were stored at -80 °C until required.

Sodium-dodecyl sulphate-polyacrylamide gel electrophoresis (SDS-PAGE)

To analyse whether ICL1 is present in the eluted fractions from purifications, the samples were run on an SDS-PAGE described by Laemmli (1970). Briefly, the resolving gel was set by adding ammonium persulphate and TEMED in a 5:1 volume ratio, roughly 10 µL of ammonium sulphate per mL of gel solution. Once set, the stacking gel was prepared by adding ammonium persulphate and TEMED in a 1:5 volume ratio and poured on top of the resolving gel. The gel was run in Tris.glycine buffer (250 mM Tris.HCl pH 7.5, 1.92 M glycine, 1% (w/v) SDS). The molecular marker and samples were mixed with 5X DTT dye (BioRad), heated at 95 °C for 5 minutes and loaded onto the gel. The gel was run for 30-45 minutes at 180 V then stained with Coomassie Blue (40% (v/v) methanol, 10% (v/v) acetic acid, 50% deionised water and 0.25% (w/v) Brilliant Blue R) for 30 minutes on shaker at 40 rpm and de-stained (40% (v/v) methanol, 10% (v/v) acetic acid and 50% deionised water) for 30 minutes.

Bradford Protein Assay with Bovine Serum Albumin (BSA)

The BSA standard curve was used to estimate ICL1's concentration in the elution samples from purification. 0.2 mg/mL of BSA was prepared and stored at 4 °C. The standard curve was prepared for 0-6 µg of BSA with dH₂O and Bradford assay dye (BioRad), mixed by inverting three times and incubated at room temperature for 5 minutes. 5 µL of the nickel column elution was mixed with dH₂O and Bradford assay dye and incubated at room temperature for 30 minutes. The absorbance was measured at OD₅₉₅. Based on the direct relationship between the BSA protein concentration, it was possible to estimate the concentration of the ICL1 preparation.

Desalting ICL1

HiTrap Desalting columns with Sephadex G-25 resin by GE Healthcare were used to desalt the Ni-NTA purified-recombinant ICL1. The desalting columns were equilibrated with 20 mM Tris.HCl pH 7.5, 100 mM NaCl as instructed in the manual. 25 µL of the recombinant ICL1 was combined with 80 µL of 20 mM Tris.HCl pH 7.5, 100 mM NaCl, applied to the G-25 column and harvested by centrifugation at 800 x g for 2 minutes. The concentration (mg/mL) was determined by the Beer-Lambert law where the

recombinant ICL1 coefficient of extinction used was 71975, and the absorbance was determined by Nanodrop at 280 nm. The desalted ICL1 was used to set crystal trials at the specified condition.

Crystal Trials of Recombinant ICL1

The hanging drop vapour diffusion crystallisation technique was used to produce ICL1 crystals. The CleneGlass™ Coverslips were siliconised by dipping sequentially into Repelcote VS water repellent (VWR Chemicals), 96.5% (v/v) ethanol and deionised water and air-dried. The 24-well crystallisation plate (Hampton Research) were greased with Dow Corning® High Vacuum Grease (Hampton Research). The solution (0.1 M sodium cacodylate pH 6.5, 27% (w/v) PEG_{mme} 2000) with 10% and 20% (v/v) glycerol was used as a cryoprotectant, and the crystals were flash-frozen in liquid nitrogen for X-ray data collection. ICL1 crystals were also obtained by using 0.5 mL of 20% (w/v) PEG 4,000 in the reservoir, a 1:1 ratio of protein with a solution of 0.2 M imidazole malate pH 6.0, 20% (w/v) PEG 4000 in the drop within an ICL1 concentration of 5.76 mg/mL and 4.11 mg/mL.

X-ray diffraction

The crystal was removed from the drop by 'fishing' using a nylon loop before being plunged sequentially into the precipitant solution supplemented with first 10% (v/v) and then 20% (v/v) glycerol. Prior to diffracting in-house (University of Lincoln) or using a synchrotron at Diamond Light Source (Oxford, UK), the crystal was then flash-frozen in liquid nitrogen and stored under liquid nitrogen until diffraction.

Results

The transformation of Rosetta gami DE3 pLysS with pET 28a-ICL1 plasmid was successful, and the transformants were grown overnight for protein expression. The protein expression was induced with IPTG at the mid-log phase, and the soluble protein was purified using nickel affinity chromatography. To assess whether the protein was produced and whether the purification was successful, the unbound protein after binding with the nickel beads and all the washes and elution from the purification process were analysed in the SDS-PAGE (Figure 2-4). The molecular weight of ICL with the histidine tag is estimated to be 49.5 kDa.

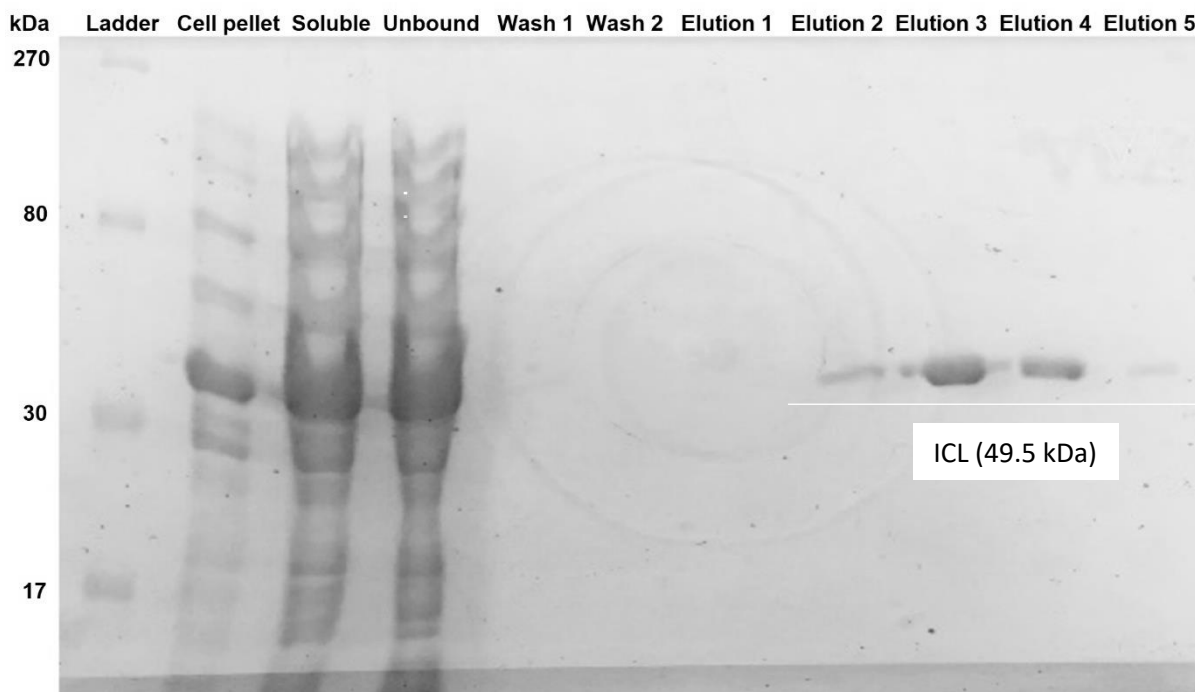


Figure 2-4: An example of the SDS-PAGE for ICL purification.

It was noticed that diluting a high-density bacterial culture to mid-logarithmic improved the protein yield. This observation was further explored, and five variables were tested to increase ICL1 yield. In methods 1 and 2, the protein expression was induced at the mid-log phase, at an OD_{595} of 0.5 and 0.8, respectively. Method 3 was diluted at the end of the log-phase transitioning to stationary phase, at an OD_{595} of 1.2. The final two methods have investigated whether diluting a bacterial population at an early stationary phase back to a mid-log phase would cause any effect in protein expression. Thus, the bacteria were grown to an OD_{595} of 1.2 and diluted to OD_{595} 0.5 and 0.8 using fresh, sterilised LB broth. All methods were induced with 0.4 mM IPTG and purified via Ni-NTA using an imidazole gradient. The results are shown in Figure 2-5.

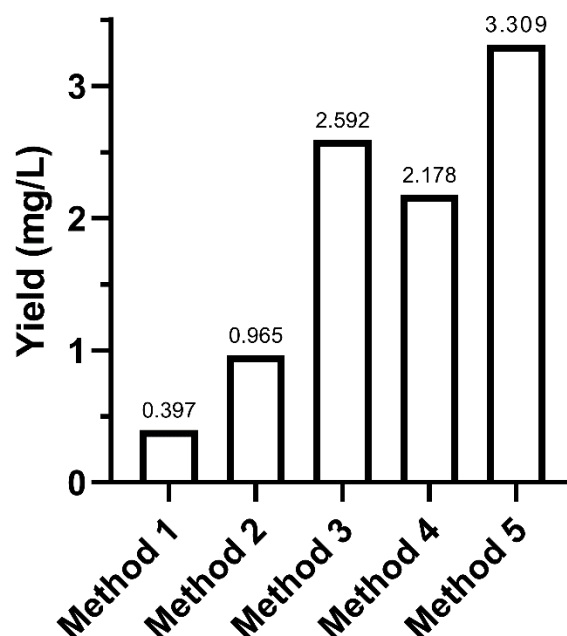


Figure 2-5: ICL1 yield obtained in the five protein expression methods tested. Method 1, protein expression induced at OD₅₉₅ 0.5; Method 2, protein expression induced at OD₅₉₅ 0.8; Method 3, protein expression induced at OD₅₉₅ 1.2; Method 4, protein expression induced at OD₅₉₅ 0.5 after diluting from OD₅₉₅ 1.2; Method 5, protein expression induced at OD₅₉₅ 0.8 after diluting from OD₅₉₅ 1.2.

Methods 1-3 serve as a reference for methods 4 and 5. There is a 3-fold increase between method 2 (OD₅₉₅ 0.8) and 5 (OD₅₉₅ 0.8 diluted from 1.2), whilst method 4 has a 5-fold increase compared to method 1. Although method 3 has a high yield that is similar to method 4, the highest protein yield was obtained in method 5.

Using the purified protein, more than 500 conditions were screened using a mosquito robot for crystallisation. The conditions that yielded crystals by the mosquito were reproduced and expanded by increasing the range of the condition's concentrations with drops of 100 nL protein in a 1:1 and 1:2 volume ratio with the precipitant by the hanging drop diffusion technique. In the first successful crystal trial (Figure 2-6), ICL1's concentration was 4.11 mg/mL, and it yielded crystals with different morphologies.

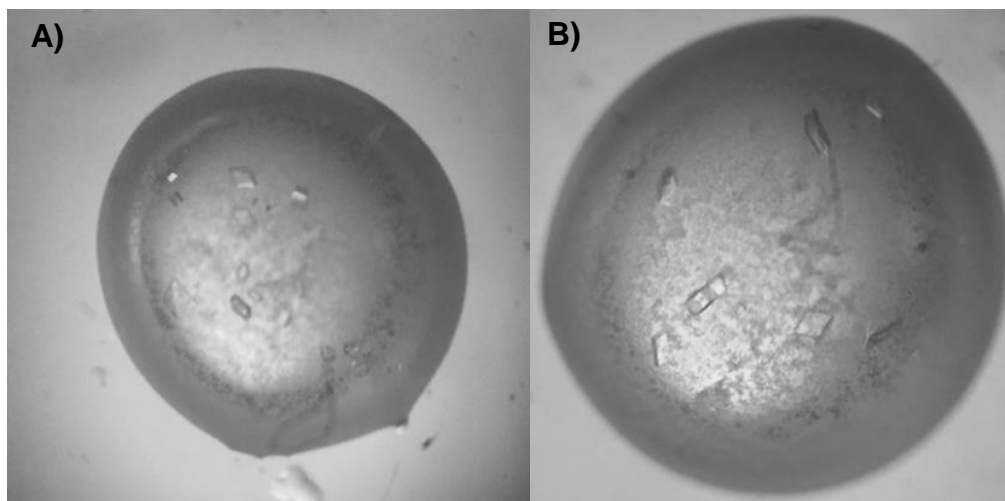


Figure 2-6: Pictures of crystal drops containing ICL1 crystals viewed with a compound light microscope at 10x magnification. ICL1 crystals obtained with a solution of 0.1 M sodium cacodylate pH 6.5 and 27% (w/v) PEG_{mme}2000, sitting against 500 μ L of 27% (w/v) PEG_{mme}2000 in the reservoir. In this trial, ICL1 concentration was 4.11 mg/mL. **A)** A 1:0.5 volume ratio of protein with the solution. **B)** A 2:1 volume ratio of protein with the solution.

ICL crystals were obtained by using 0.5 mL of 27% (w/v) PEG_{mme} 2000 in the reservoir, a 1:0.5 and 2:1 ratio of protein with a solution of 0.1 M sodium cacodylate pH 6.5, 27% (w/v) PEG_{mme} 2000 in the drop and the crystals appeared in 2 weeks after setting the 1.5 μ L, and 3 μ L drops against 500 μ L of 27% (w/v) PEG_{mme} 2000 in a closed reservoir at 16 °C. Samples of these crystals were flash-frozen with glycerol as a cryoprotectant (10% (v/v) in the precipitating buffer condition) in liquid nitrogen-cooled, air stream (approximately -100 °C) and diffracted. All thin diamond crystals from this trial failed to generate observable diffraction using an 'in-house' Bruker D8 Discover (Cu/Ma) diffractometer operating under cryo-cooled conditions, even under prolonged (10 minutes) exposure.

In the second successful crystal trial, there were more crystals formed using the same condition as the previous crystal trial but with a lower enzyme concentration - 3.8 mg/mL (Figure 2-7). The crystals seem to be square-shaped, however, it seemed that they lacked substantial depth in the third dimension, suggesting poor diffraction resolution. These crystals only took 3-5 days to form.

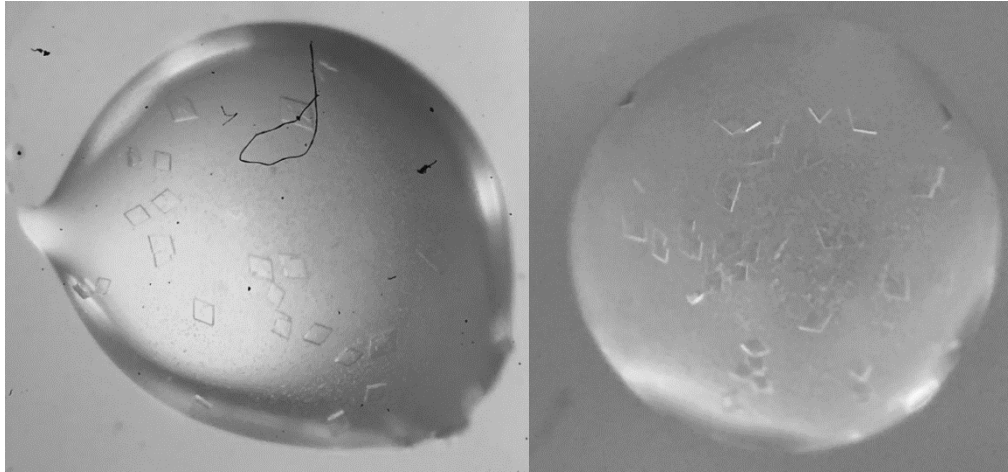


Figure 2-7: Pictures of crystal drops containing ICL1 crystals viewed with a compound light microscope at 10x magnification. Crystals were obtained with a solution of 0.1 M sodium cacodylate pH 6.5 and 27% (w/v) PEG_{mme}2000, sitting against 500 μ L of 27% (w/v) PEG_{mme}2000 in the reservoir. In this trial, ICL1 concentration was 3.8 mg/mL, and a volume ratio of 2:1 protein with the solution.

Further trials were initiated to find variants of the preliminary conditions that would facilitate growth in the third dimension to aid diffraction. The condition was different from the previous trial in that a higher concentration of ICL1 was used: 4.11 mg/mL. Apparently improved the crystals formed under 0.2 M imidazole malate pH 6.0, 20% (w/v) PEG 4000. These were rectangular with greater 3D uniformity (Figure 2-8).

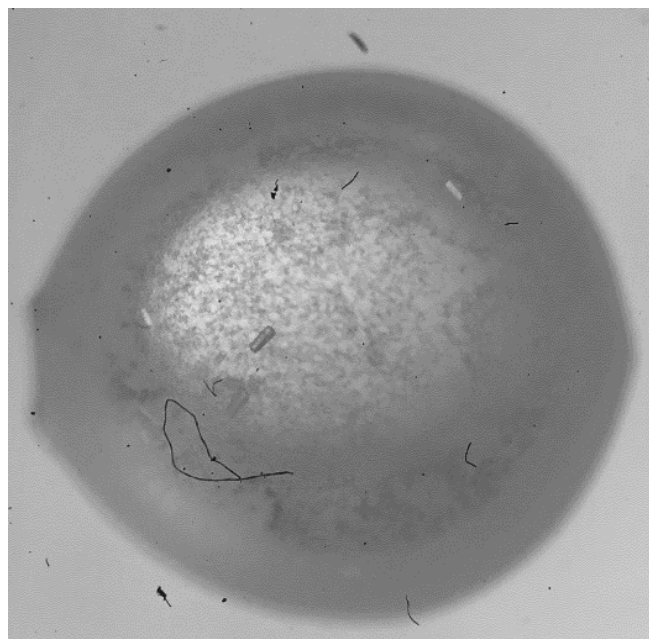


Figure 2-8: Picture of a crystal drop containing ICL1 crystals viewed with a compound light microscope at 10x magnification. ICL1 crystals were obtained with a solution of 0.2 M

imidazole malate pH 6.0, 20% (w/v) PEG 4000 sitting against 500 μ L of 20% (w/v) PEG 4000 in the reservoir. In this trial, ICL1 concentration was 4.11 mg/mL and a volume ratio of 1:1 protein with the solution.

The crystals in Figure 2.8 were flash-frozen as before and diffracted using an 'in-house' Bruker D8 Discover (Cu/Ma) diffractometer at the University of Lincoln. The resolution of this crystal was 6.8 Å (Figure 2-9).

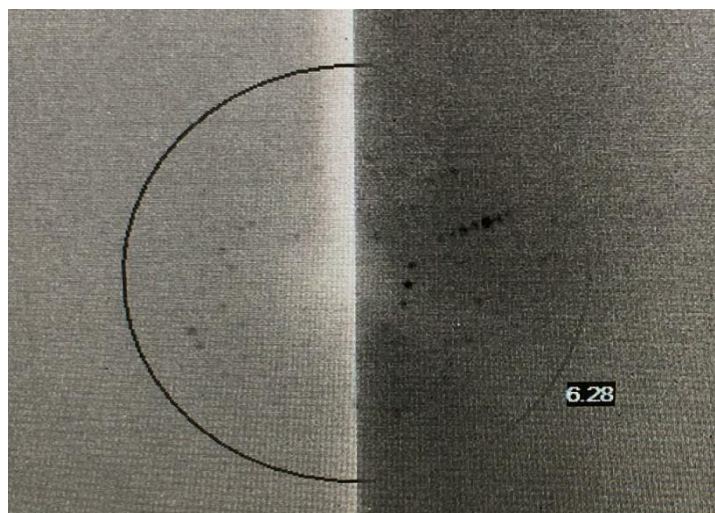


Figure 2-9: X-Ray diffraction pattern of ICL1 crystal obtained 'in-house' with a resolution of 6.28 Å. The crystal used to diffract was obtained with the condition 0.2 M imidazole malate pH 6.0 and 20% (w/v) PEG4000. The ICL1 concentration was 4.11 mg/mL.

A better diffraction resolution is desired, and therefore, the search for good diffraction-quality crystals remained. New crystal trials were set, and the new conditions yielded robust crystals with a great 3D depth (Figure 2-10). These crystals were used for soaking with CL-54-01 (Chapter 5).

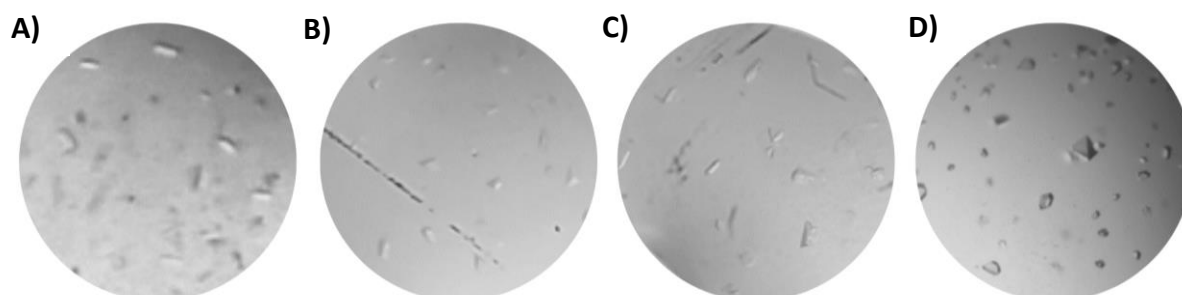


Figure 2-10: Pictures of four drops containing ICL1 crystals with new conditions (viewed with a compound light microscope at 10x magnification). A) 0.2 M imidazole malate pH 7.0 and 25% (w/v) PEG 4000, B) 0.1 M sodium HEPES pH 7.5 and 20% (w/v) PEG 10000, C) 0.1 M sodium calcodylate pH 6.5 and 27% (w/v) PEG 4000, D) 0.2 M imidazole malate pH 6.0 and

20% (w/v) PEG 4000. Images are a courtesy from Laura Boardman-Slack from Odell's Lab at University of Lincoln.

Discussion

The aim of this chapter was to express and purify ICL1 to use for crystallography and inhibition studies (Chapter 4). but also exploring different experimental conditions that would lead to a higher protein expression. Efforts to optimise protein expression experimentally focuses on bacterial population density (measured by optical density at 595 nm), IPTG concentration, growth temperature and duration of protein expression (Galloway *et al.*, 2003). Here, five variables (methods 1-5) were tested by varying the stage at which the protein expression was induced.

Protein expression can be induced anywhere from OD₅₉₅ 0.4 to 3.0, which represents the mid-logarithmic phase until the stationary phase of the *E. coli* growth curve (Malakar and Venkatesh, 2012; Boshtam *et al.*, 2018). Here, the aim was to improve the protein expression protocol and obtain high yields of ICL1. This was achieved by testing whether growing the bacterial cells to a late-logarithmic phase (OD₅₉₅ 1.2) then diluting them to a mid-logarithmic phase (OD₅₉₅ 0.5 or 0.8) would increase protein yield. The rationale behind this was to assess how the different metabolic stages have an impact on heterologous protein expression.

From the data, inducing protein expression at the later logarithmic phase is more beneficial (OD₅₉₅ 1.2 yielded 2.5 mg/mL of ICL1). It has been reported in the literature that IPTG induction with high-cell densities had greater protein yield than the low-cell-density counterparts (Sivashanmugam *et al.*, 2009). Interestingly, when the high-cell-density (OD₅₉₅ 1.2) was diluted to the mid-logarithmic phase (OD₅₉₅ 0.5) with fresh LB broth, the protein yield was similar to the high-cell-density (OD₅₉₅ 1.2). However, when another high-cell-density culture was diluted to OD₅₉₅ 0.8, the yield increased significantly when compared to its control (OD₅₉₅ 0.8) and still higher protein expression than just inducing at OD₅₉₅ 1.2. One reason for this behaviour is the re-introduction of fresh carbon sources, which replenishes nutrients and ions such as magnesium that are needed to maintain ribosome efficiency, which directly impacts protein yields (Lee *et al.*, 2019).

Protein production is of great interest in both the academic and industry settings to study specific proteins or to develop commercial goods (Rosano and Ceccarelli, 2014),

and consequently, improving protein yields is extremely important. The protocol of diluting high-cell-density to mid-logarithmic phase prior to IPTG induction was tested for another protein, PknG (serine/threonine-protein kinase) (Appendix B, Figure B1). Its molecular weight is 81.5 kDa, which is near twice the size of ICL1. This protein is also from Mtb and was expressed in *E. coli* BL21 following methods 1 and 4. As expected, PknG yield was higher in the diluted culture as compared to the control. Thus, this simple step can increase the yield of at least two different medium-size proteins in *E. coli*. It would be interesting to test whether this protocol also increases the yield of smaller proteins.

In our lab, other projects explored the role of diluting the cultures prior to protein expression. For instance, it was observed that diluting a high-density bacterial culture to a mid-logarithmic OD₅₉₅ with media from an already-grown culture of OD₅₉₅ 0.8 caused an even higher protein yield (data not shown). This suggests that autoinducer molecules secreted from the previous culture might have triggered a higher protein expression, a phenomenon that has been previously reported in the literature (Torres-Cerna *et al.*, 2019). To investigate this further, an in-depth literature search for autoinducers must be conducted to select a list of candidates. Afterwards, the media from a mid-logarithmic culture can be analysed (by HPLC or a biosensor system). The molecules can be characterised by mass spectrometry and tested individually in various concentrations during protein expression. Another future experiment would assess whether a complete re-introduction of nutrients would play a significant role in protein expression. This can be achieved by removing all previous media and diluting the culture with fresh LB to the desired OD₅₉₅. If this improves the yield as significantly as the autoinducers, it would be an easier alternative to implement in protein expression protocols.

Two conditions have been previously reported in the literature to crystallised ICL1 where the structure of the enzyme was solved: 100 mM HEPES pH 7.4 and 1.4 M sodium citrate by Sharma *et al.* (2000) and 0.1 M Tris.HCl pH 8, 0.2 M sodium citrate and 20-30% (v/v) PEG 4000 by Pham *et al.* (2017). In our lab, we previously crystallised ICL1 using 0.1 M HEPES pH 7.5, 20% isopropanol and 0.2 M sodium citrate. The first trials focused on expanding the grid screen by Pham *et al.* (2017) by varying the PEG 4,000 between 20-30%, then repeating the condition by Sharma *et al.* (2000) and setting up another grid screen by varying the isopropanol 16-26% in the

0.1 M HEPES pH 7.5, 20% Isopropanol and 0.2 M sodium citrate condition. No crystals were formed. Over 500 conditions were screened using the mosquito robot at the University of Lincoln (data not shown), and the successful conditions were tested using the hanging drop diffusion technique at the University of Westminster.

Two new conditions were found to crystallise ICL1: 0.1 M sodium cacodylate pH 6.5, 27% PEG_{mme} 2,000 and 0.2 M imidazole malate pH 6.0, 20% PEG 4,000. The first condition was tested with a range of ICL1 concentrations (4.17, 3.8, 2.8 mg/mL). Although crystals were obtained with all three ICL1 concentrations, the low ICL1 concentration yielded many crystals with shallow 3D robustness, whereas the high ICL1 concentration yielded fewer but bigger and more 3D robust crystals. When the drops were set at a 1:1 volume ratio, no crystals were formed. Crystals were only formed when the drop volume (μL) was 2:1 or 1:0.5 of protein to the precipitant. The lower volume yielded crystals quicker as the drop and the reservoir equilibrates faster. The impact of re-freezing ICL1 in its ability to crystallise was also investigated. The freezing and thawing process did not affect the ability to crystallise small and big crystals; however, it did impact the robustness of the crystals even at a high concentration of 4.17 mg/mL (data not shown).

The second new condition to crystallise ICL1 (0.2 M imidazole malate pH 6.0, 20% PEG 4,000) only formed crystals when the drop volume was 1:1 protein to precipitant. A grid screen varying the imidazole malate pH to 5.9-6.2 was tested with a variation of 16-26% PEG 4,000. Four of the variations yielded crystals (0.2 M imidazole malate pH 6.1, 20% PEG 4000; pH 6.1, 24% PEG 4000; pH 6.2 and 24% PEG 4000; pH 6.0 and 18% PEG 4000) but not as robust as the ones crystallised with 0.2 M imidazole malate pH 6.0 and 20% PEG 4,000. Two concentrations of ICL1 (5.76 mg/mL and 4.11 mg/mL) were tested with the grid screen. The higher concentration only crystallised with 0.2 M imidazole malate pH 6.0 and 20% PEG 4,000, and the other drops precipitated heavily. The lower concentration yielded crystals in the variations of the condition.

Overall, the crystals were only formed when sitting in PEG (20% PEG 4,000 or 27% PEG_{mme} 2,000) reservoir as opposed to 2.5 M sodium chloride or ammonium sulphate. A study by Wheeler *et al.* (2011) demonstrates that the relative humidity of 20% PEG 4,000 and 27% PEG 2,000 is 99.5%, whereas salt solutions such as sodium chloride

and ammonium sulphate the relative humidity are approximately 93.5 and 94.5%, respectively. This suggests that ICL1 crystallises in a very high humidity environment. The majority of crystals were formed within two weeks; the lower the protein concentration, the quicker the formation. For instance, at 2.8 mg/mL, crystals were formed within three days, but the morphology of the crystals was small and not 3D uniform, whereas 4.17 mg/mL formed crystals in approximately 12 days. Hence, it seems that better quality crystals grow more slowly.

Six attempts to diffract crystals were made at the University of Lincoln. Only one crystal diffracted with a low resolution of 6.28 Ångström. This could be improved by refining the crystals growth by finding new conditions that take longer to yield a robust crystal and tweak current conditions to optimise the crystal formation by varying the enzyme concentration subtly. In conclusion, six new conditions to crystallise ICL1 are reported in this chapter. This enzyme has been previously crystallised with other conditions, and so, ICL1 could be considered a relatively promiscuous enzyme regarding crystallisation. ICL1 crystallises in a high humidity environment, and the frozen-thawed enzyme can still form crystals, but the quality of the crystal was compromised.

Having identified a range of conditions, the production of multiple crystals was done. A range of drugs was added to the crystals-containing drops – a technique known as soaking, and diffraction of a ICL1:inhibitor bound complex was done (Chapter 5). Solving this structure allows investigating whether the drug binds effectively in the active site of the enzyme and will elucidate potential modifications that can be done to the derivatives in order to increase the binding affinity. Co-crystallisation of the drugs and the enzyme was simultaneously employed. The conditions are unlikely to be the same as the enzyme on its own, and therefore, new screening trials need to be done to determine the co-crystallisation condition. These trials were done using the sitting drop method with the mosquito robot at the University of Lincoln.

Chapter 3 – Synthesis of ICL 1 inhibitors

Introduction

Isocitrate lyase is an essential enzyme for *Mycobacterium tuberculosis* (Mtb) in latent tuberculosis (McKinney, 2005; Kumar and Bhakuni, 2008; Bhusal *et al.*, 2017). Moreover, ICL is absent in humans, making it an attractive drug target (McKinney, 2005; Kondrashov *et al.*, 2006). The best known ICL inhibitors are itaconate (McFadden and Purohit, 1977), 3-nitropropionate (Schloss and Cleland, 1982) and 3-bromopyruvate (Ko and McFadden, 1990) – Figure 3-1.

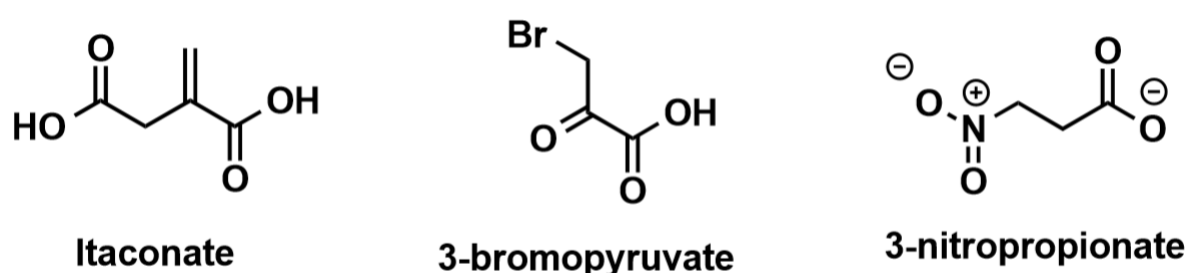


Figure 3-1: Structure of three ICL inhibitors.

However, due to the high toxicity effects of these compounds, they are not pharmacologically suitable, and the search for a new inhibitor remains. More than 1 million compounds have been screened against ICL1 (Lee *et al.*, 2015), and although many have shown activity against ICL, none has moved to clinical trials due to toxicity issues. For instance, Liu *et al.* (2016) screened the activity of 71,765 compounds against ICL1, and 14 compounds (named IMBI 1-14) showed activity, though IMBI-3 demonstrated the most significant inhibitory activity with IC_{50} of 30.9 mmol/L. It was potent against both Mtb and multi-drug resistant Mtb, and in combination with isoniazid, it decreased the colony-forming units of *M. marinum* in macrophages. However, this compound seems to have another unknown target, and it showed cytotoxicity in mouse liver and kidney (Liu *et al.*, 2016). The search for a potent ICL1 inhibitor with low toxicity remains.

The rationale behind the candidate drugs screened in this study is based on the structure and the docking model from Liu *et al.* (2016) – Figure 3-2. Even though it is only a computational model and the actual interaction still needs to be experimentally verified, it gives an understanding of the possible interaction between the key amino acids of ICL1 and the drug. Besides the conserved catalytic site with the KKCGH motif, it is also known that the amino acids Trp93, Thr347 and Leu348 are essential to the formation of the catalytic pocket (Sharma *et al.*, 2000). Two of these amino acids, Trp93 and Thr347, have formed hydrogen bonds with IMBI-3 in the docked model (Liu *et al.*, 2016). Five additional amino acids were suggested to interact with the drug: Ser191, Arg228, Asn313 and Ser315 through hydrogen bonds, and Ser317 through Van der Waals forces (Liu *et al.*, 2016).

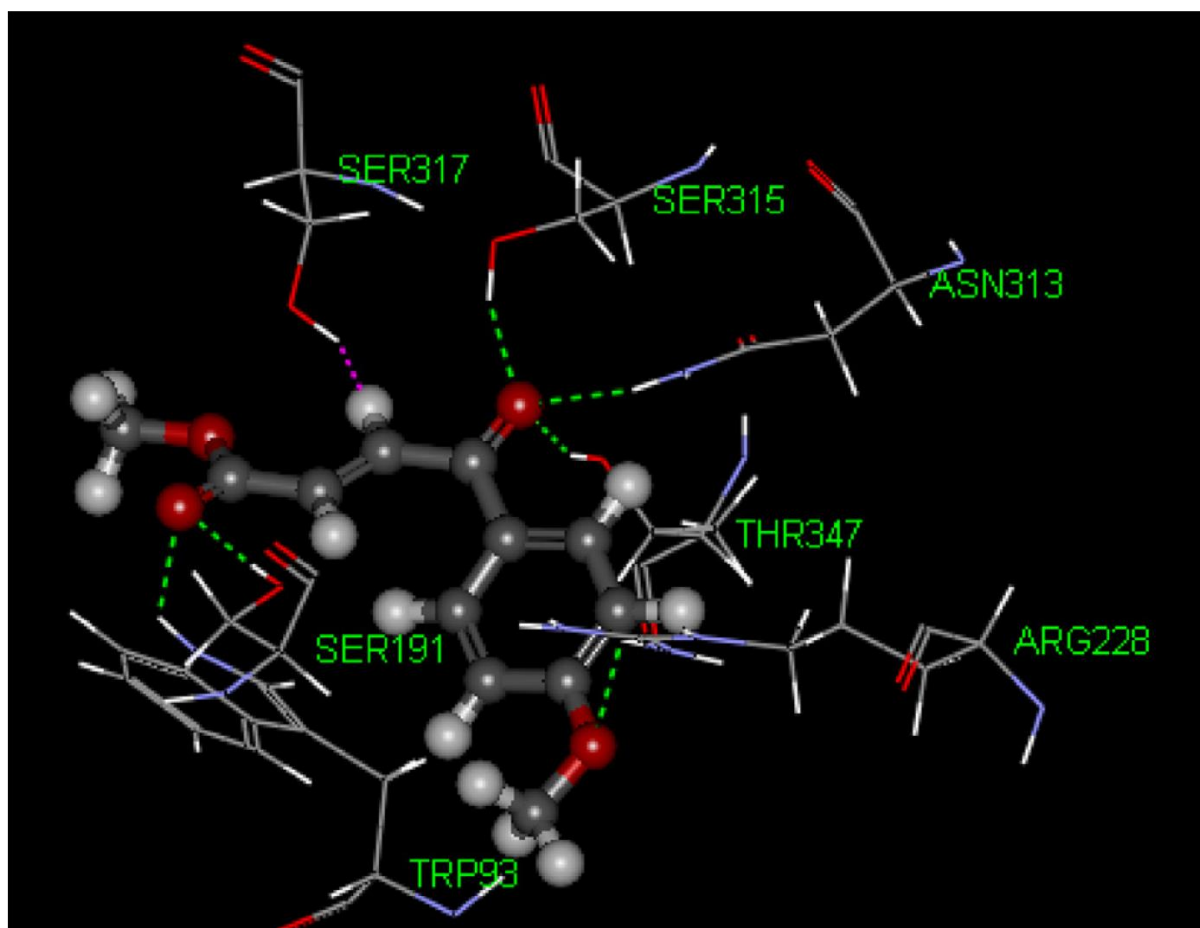


Figure 3-2: Structure of IMBI-3 and the proposed docking structure of IMBI-3 with Mtb ICL1 (1F8I). Green dots represent hydrogen bond; Purple represents van der Waals force (Liu *et al.*, 2016).

Compounds that share a structural resemblance to IMBI-3 have been proposed as ICL1 inhibitors. A series of known inhibitors have either an α,β -unsaturated carbonyl

moiety or an aromatic/heterocyclic functionality (or both), which might be responsible for occupying the ICL pocket. For this reason, all the compounds tested in this study contain these features, which includes: 3-(4-methoxybenzoyl)acrylic acid; 7-methoxy-4-oxo-1,4-dihydroquinoline-2-carboxylic acid; 3,4-dimethoxycinnamic acid; 3,4-dihydroxycinnamic acid and trans-4-hydroxy-3-methoxycinnamic acid (tested *in vitro* against the isolated enzyme in Chapter 4). Here, these compounds were methylated, generating methyl (2E)-4-(4-methoxyphenyl)-4-oxo-2-butenoate; methyl (2E)-3-(3,4-dimethoxyphenyl)acrylate; methyl 4-hydroxy-7-methoxy-2-quinolinecarboxylate; methyl (2E)-3-(3,4-dimethoxyphenyl)acrylate and methyl (2E)-3-(4-hydroxy-3-methoxyphenyl)acrylate.

The synthesis of four ICL1 inhibitors that have these functionality features from the literature will be outlined. For a timeline of the efforts to synthesise ICL1 inhibitors, see Chapter 1 (Figure 1-13).

Previous synthesis of ICL1 inhibitors

3.1 Synthesis of 2-methoxy-2'-hydroxybenzanilides

Kozic *et al.* (2012) reported the synthesis of 2-methoxy-2'-hydroxybenzanilide **1** derivatives and their thioxo **2** analogues. 2-methoxy-2'-hydroxybenzanilide derivatives were synthesized from commercially available 4/5-chloro-2-methoxybenzoic acid **3** and phenol **5**. Compound **4** was obtained by reacting 4/5-chloro-2-methoxybenzoic acid **3** with SOCl₂ and refluxed under a CaCl₂ drying tube for 3 h to afford 2-methoxybenzoyl chloride **4** (Figure 3-3).

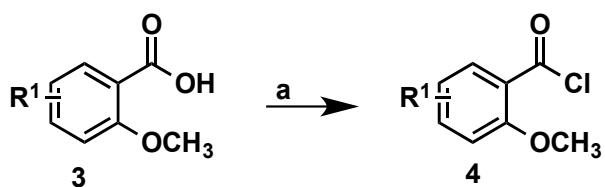


Figure 3-3: Reaction scheme. Reagents and conditions a) SOCl₂, CaCl₂ 110 °C, 3 h.

2-Aminophenols **7** was obtained in two steps using phenol **5** in glacial acetic acid at 40 °C for 15 min and at RT for 45 min to afford compound **7** (Figure 3-4).

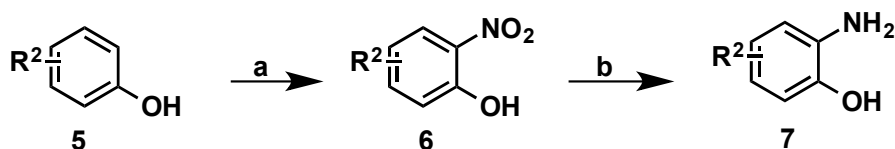


Figure 3-4: Reaction scheme. Reagents and conditions a) HNO_3 , CH_3COOH , 40°C and b) Fe , H_2O , CH_3COOH , 135°C .

In the final step of the synthesis, Kozic *et al.* (2012) employed the condensation reaction utilizing 2-methoxybenzoyl chloride **4**, TFA and 2-aminophenol **7** afforded the target compounds **1a** and **1b** (Figure 3-5).

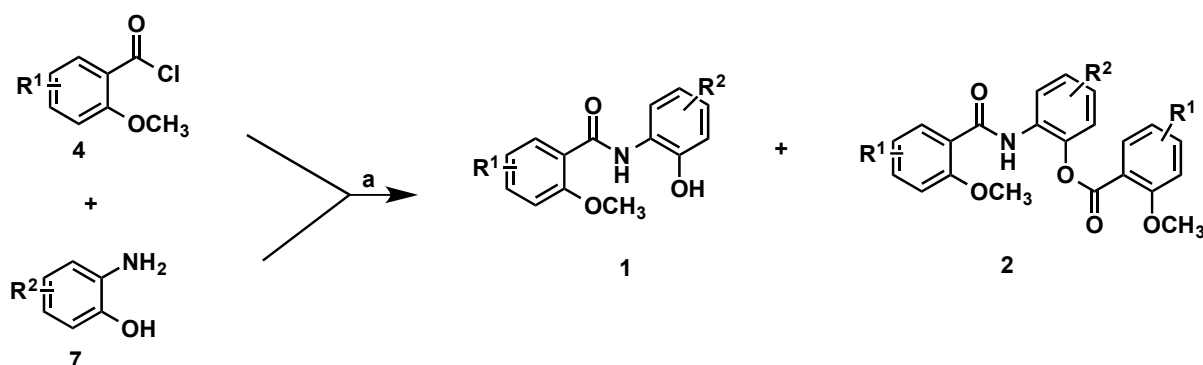


Figure 3-5: Reaction scheme. Reagents and conditions a) TEA, ether, RT, 1 h.

Thiomides **2** and **8** were obtained from reacting **1** with P_4S_{10} and pyridine in CHCl_3 under reflux for 4 h to afford **2** and **8** in excellent yield (Figure 3-6).

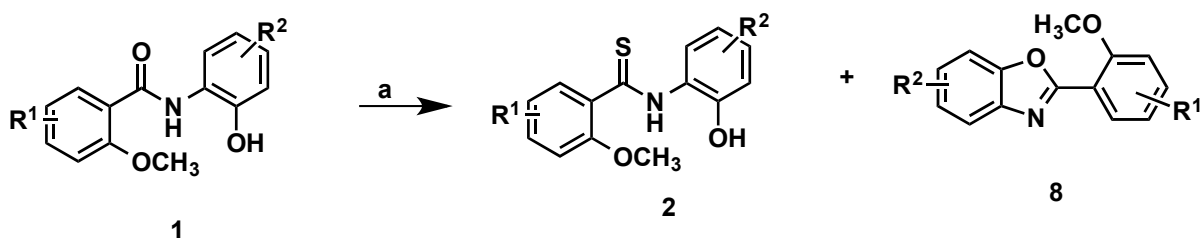


Figure 3-6: Reaction scheme. Reagents and conditions a) P_4S_{10} , pyridine, 115°C , HCl , CHCl_3 , 4 h.

3.2 Nitrofuranyl Amides

Tangallapally *et al.* (2005) reported the synthesis of nitrofuranyl amides, which showed activity against Mtb in both active and dormant states (Figure 3-7). This was achieved by nucleophilic aromatic substitution, where a cyano group was used as an electron-

withdrawing group to aid in the substitution reaction. The 3- or 4-fluoro benzonitrile (**8** or **9**) was substituted with a cyclic secondary amines in DMSO and K₂CO₃ at 90 °C, producing compounds **14a-h**, with yields ranging from 83% to 96%. Next, **14a-h** benzonitriles were subjected to reduction with Red-Al reagent to crude amines, and subsequently reacted immediately with 5-nitro-furan-2-carbonyl chloride to give benzyl amides **4a-h** in yields varying from 69% to 96%.

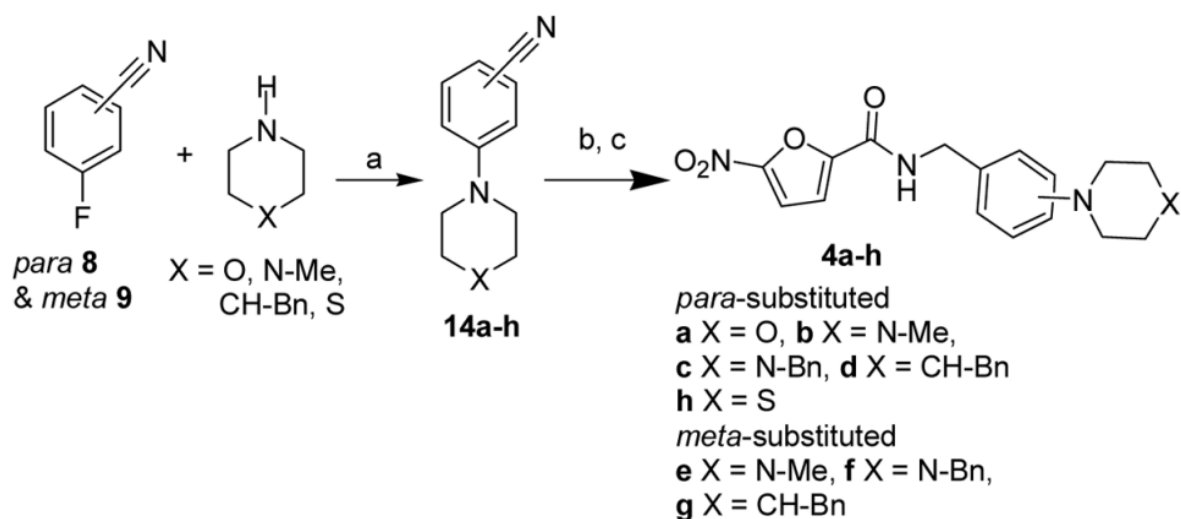


Figure 3-7: Reaction scheme. Reagents and conditions a) K₂CO₃, DMSO, 90 °C, 8 h; b) Red-Al, 0 °C, dry THF, 3 h; c) 11, CH₂Cl₂, Et₃N, RT.

The derivative benzyl-piperazine at *para*-position (**4c**) is the most active compound with a MIC value of 0.0125 µg/mL against Mtb H37Rv strain. Although **14a-h** are not specific to ICL, it served as a starting point for Sriram *et al.* (2010) to develop other ICL inhibitors, which is discussed in section 3.4.

3.3 Phthalazinyl Derivatives

Sriram *et al.* (2009) reported the synthesis of 2-[3-(4-bromo-2-fluorobenzyl)-4-oxo-3,4-dihydro-1-phthalazinyl]-acetic acid hydrazones. Treatment of phthalic anhydride **13** was reacted with ethyl 2-(1,1,1-triphenyl-5-phosphanylidene)acetate to give ethyl 2-(3-oxo-1,3-dihydro-1-isobenzofuranylidene) acetate **14**. Next, 1 mol equivalent of **14** was reacted with 0.8 mole equivalent of hydrazine hydrate in the presence of *p*-toluenesulphonic acid as a catalyst at room temperature to afford Ethyl 2-(4-oxo-3,4-dihydro-1-phthalazinyl)acetate **15** with 86% yield. To afford 2-[3-(4-bromo-

2-fluorobenzyl)-4-oxo-3,4-dihydro-1-phthalazinyl]acetic acid **16**, the N-alkylation of compound **15** with 4-bromo-1-bromomethyl-2-fluorobenzene in the presence of sodium hydroxide. The acid **16** was refluxed in absolute ethanol in the presence of sulphuric acid to give ethyl ester **17**. Treatment of **17** with hydrazine hydrate yielded 2-[3-(4-bromo-2-fluorobenzyl)-4-oxo-3,4-dihydro-1-phthalazinyl]ethanohydrazide **18**, which was then reacted with various carbonyl compounds in the presence of glacial acetic acid at pH 4-6 to yield compounds **19** and **19a** (Figure 3-8).

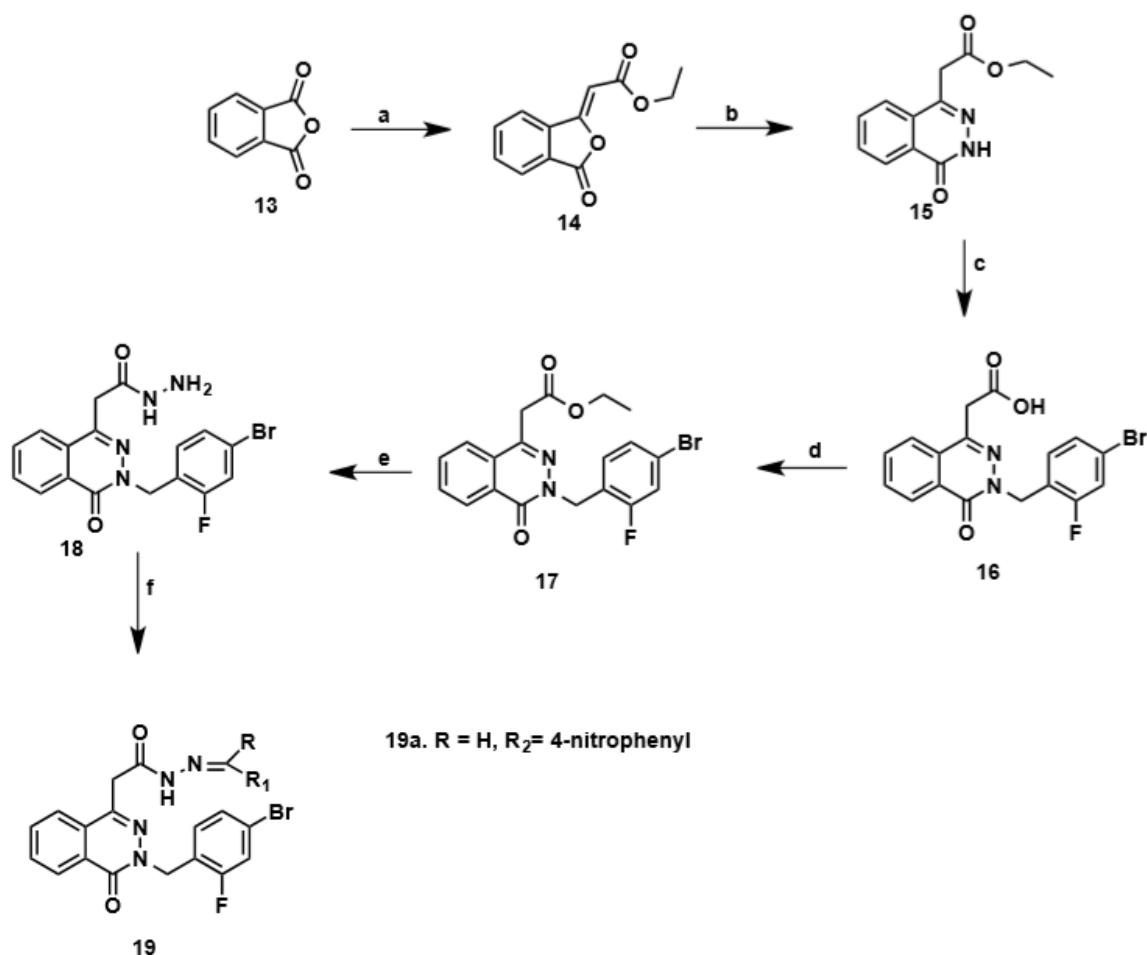


Figure 3-8: Reaction scheme. Reagents and conditions a) $\text{Ph}_3\text{P}=\text{CHCOOC}_2\text{H}_5$; b) $\text{NH}_2\text{NH}_2 \cdot \text{H}_2\text{O}$, PTSA; c) 4-Bromo-1-bromomethyl-2-fluorobenzene, NaOH; d) $\text{C}_2\text{H}_5\text{OH}$, H_2SO_4 ; e) $\text{NH}_2\text{NH}_2 \cdot \text{H}_2\text{O}$; f) Various aldehydes and ketones.

Among the 26 derivatives synthesised, N'-[(4-nitrophenyl)methylene]-2-[3-(4-bromo-2-fluorobenzyl)-4-oxo-1,2,3,4-tetrahydro-1-phthalazinyl]ethanohydrazide (**19a**) was found to be the most active compound *in vitro* with MIC of 0.18 μM against log-phase Mtb.

3.4 5-nitrofuranyl-2-acid hydrazones and their derivatives

In 2010, Sriram *et al.* also reported the synthesis of 5-nitrofuranyl-2-acid hydrazones (Figure 3-9).

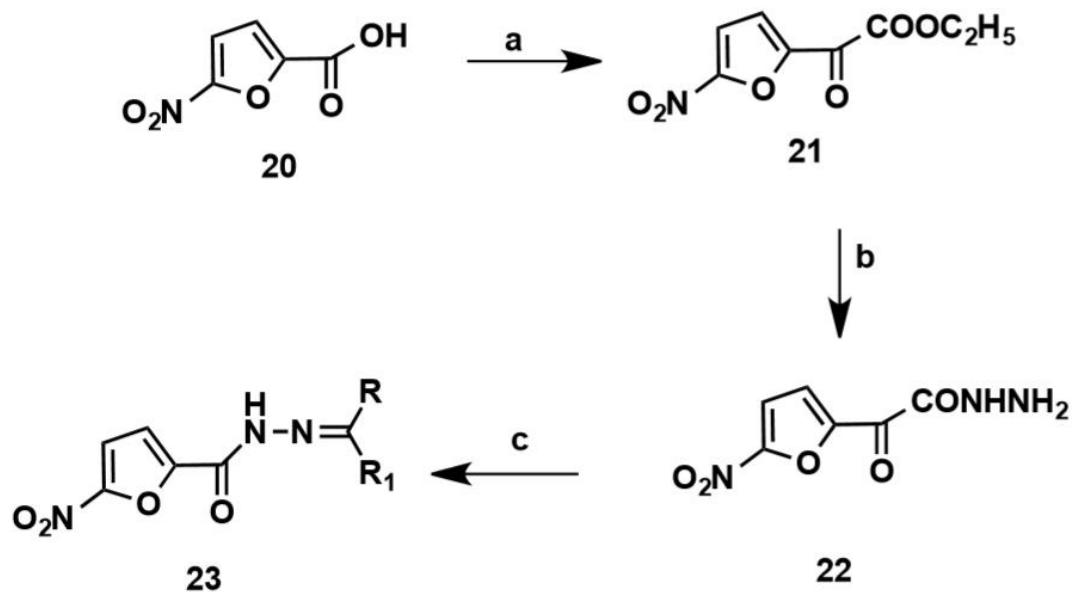


Figure 3-9: Reaction scheme. Reagents and conditions a) H_2SO_4 , $\text{C}_2\text{H}_5\text{OH}$; b) $\text{NH}_2\text{NH}_2 \cdot \text{H}_2\text{O}$; c) CH_3COOH .

5-Nitrofuroic acid **20** is converted to ethyl ester **21** by refluxing acid **20** in absolute ethanol and sulphuric acid. 1 mol of ethyl ester **21** on treatment with 2 mol hydrazine hydrate yielded acid hydrazide **22**. Next, hydrazide **22** was reacted with various carbonyl compounds by varying the glacial acetic acid at a pH 4–6 afforded derivatives **23a** derivatives in 52–89% yields (Figure 3-10).

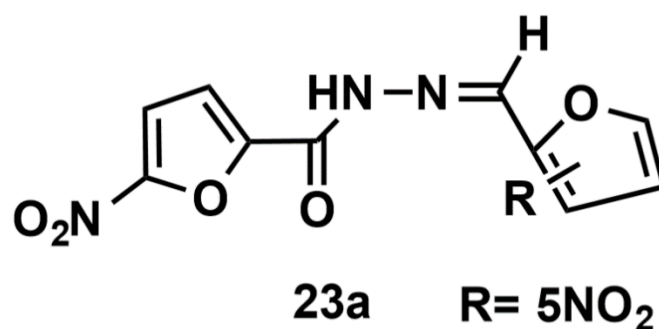


Figure 3-10: Structure of the **23a** nitrofuranyl derivative.

The yield of compound 5-nitro-N'-[(5-nitro-2-furyl)methylidene]-2-furohydrazide (**23a**) was 87%, and among the 22 derivatives, it was the most potent compound *in vitro* with MIC of 2.65 μ M against Mtb (Sriram *et al.*, 2010).

Results

Synthesis of *D/L*-threo-2-methylisocitrate (**29**)

The search for novel candidates to inhibit ICL commences with the synthesis of *D/L*-threo-2-methylisocitrate due to its resemblance with the substrate (Figure 3-11).

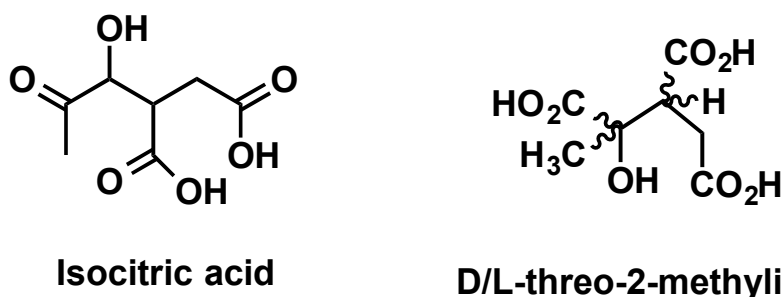


Figure 3-11: Structure of isocitrate lyase substrate, isocitric acid, and the structure of 2-methylisocitrate, a proposed ICL inhibitor.

The first step of the synthesis of *D/L*-threo-2-methylisocitrate involved the refluxing of mesaconate **24** in H₂O₂/ Na₂WO₄·2H₂O with NaOH at 0-65 °C for 8 h. Under these conditions, the desired product **25** was obtained in quantitative yield (Figure 3-12).

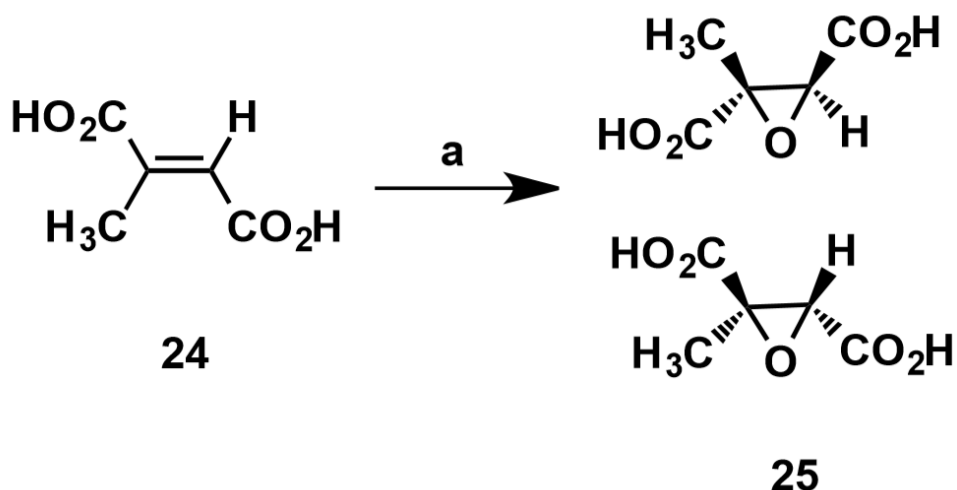


Figure 3-12: Reaction scheme. Reagents and conditions a) H₂O, Na₂WO₄·2H₂O, NaOH 0 °C - 65 °C.

The structure of *trans*-epoxymethylsuccinic acid **25** was confirmed by analysis of the ¹H NMR spectrum, which was found to be in close agreement with the literature data (Lee *et al.*, 2018). Further confirmation was provided by mass spectral analysis, which gave a signal at 147 Daltons, corresponding to the expected molar ion of [M+H]⁺ C₅H₆O₅.

O-methylation of carboxylic acid was achieved by treatment of *trans*-epoxymethylsuccinic acid **25** with SO₂Cl₂ in MeOH to afford dimethyl *trans*-epoxymethylsuccinate **26** in quantitative yield (Figure 3-13). The exact structure assignment was based on a literature study (Lee *et al.*, 2018). The ¹H NMR spectrum displayed the requisite resonances at δ 6.46 (d, *J* = 7.2 Hz, 1H), 6.09 (s, 1H), 4.94 (s, 1H), 4.62 (d, *J* = 7.2 Hz, 1H), 3.74 (s, 3H), 3.69 (s, 2H), 3.67 (d, *J* = 4.2 Hz, 5H), 1.71 (s, 3H), 1.44 (s, 3H).

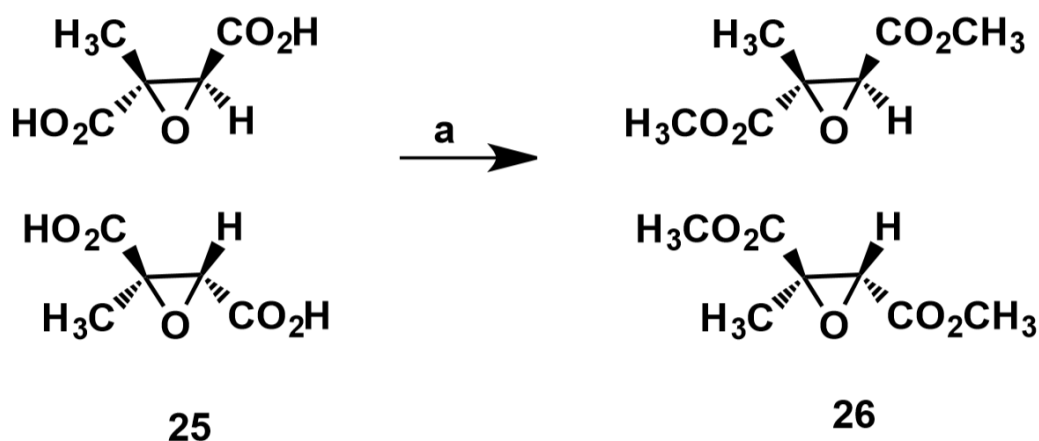


Figure 3-13: Reaction scheme. Reagents and conditions a) SO₂Cl₂, MeOH, 0 °C – RT, 8 h.

With dimethyl *trans*-epoxymethylsuccinate **26** in hand, the next step was the formation of the lactone ring. The cyclisation of **26** to the lactone **27** was achieved using sodium methoxide and dimethyl malonate in anhydrous MeOH at RT (Figure 3-14). These conditions afforded the desired product **27** in good yield and used without any further purification.

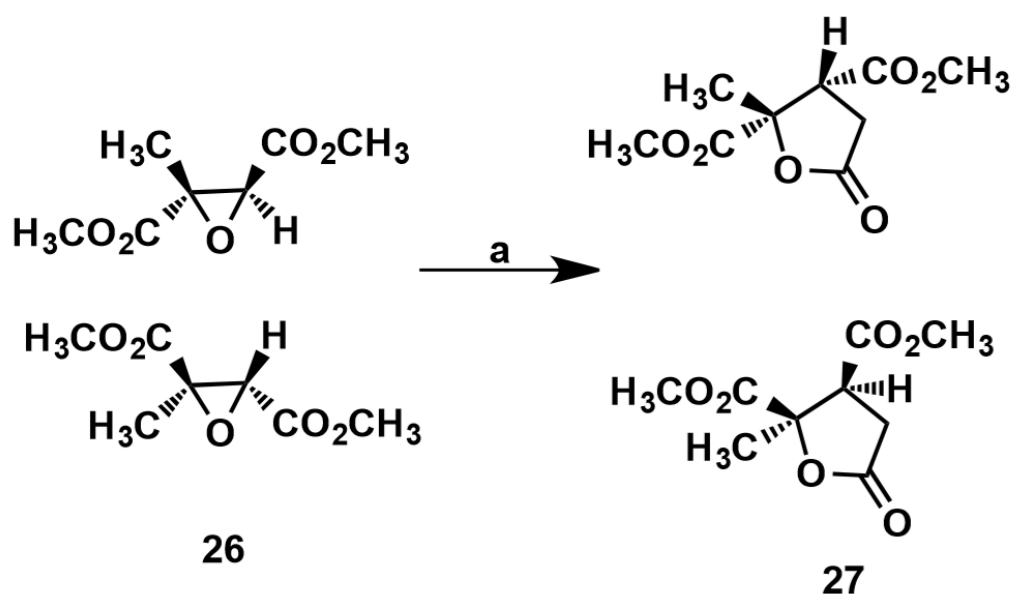


Figure 3-14: Reaction scheme. Reagents and conditions a) Na/MeOH, CH₂(CO₂CH₃)₂, RT, 3 days.

Global deprotection was accomplished with 6N HCl to afford **27**. Next came the crucial step involving the opening of the lactone ring. Using NaOH in H₂O at 80 °C for 12 h afforded the **29** in good (60%) yield (Figure 3-15).

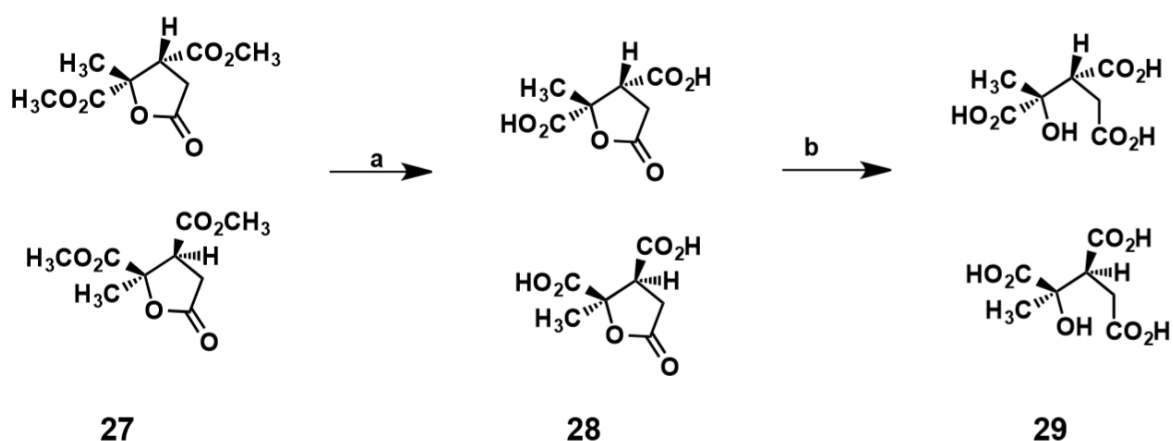


Figure 3-15: Reaction scheme. Reagents and conditions a) 6 N HCl, reflux, 0- 60 °C, 3 h; b) NaOH/H₂O, 80 °C for 2 h.

The structure of **29** was confirmed by ¹H NMR spectroscopy (Figure 3-16) and mass spectral analysis, which gave a signal at 205 Daltons, corresponding molar ion of [M+H] C₇H₁₀O₇.

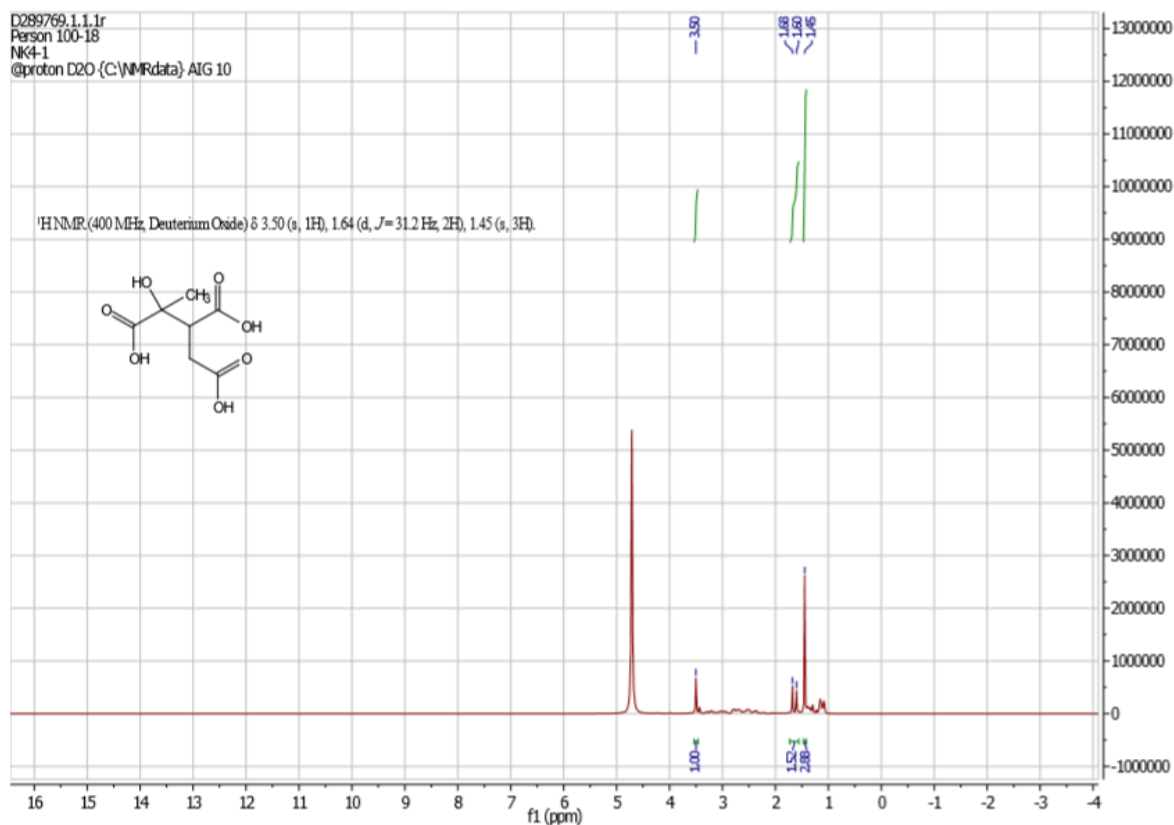


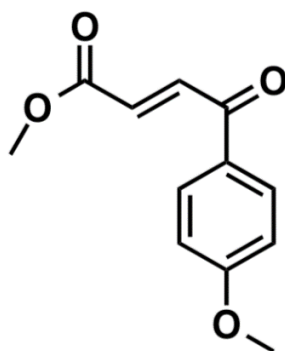
Figure 3-16: ¹H NMR of **29** in D₂O.

Synthesis of methylated compounds

Based on previous ICL inhibitors structures described above as well as other published inhibitors, compounds such as 3-(4-methoxybenzoyl)acrylic acid and 7-methoxy-4-oxo-1,4-dihydroquinoline-2-carboxylic acid, and the cinnamic acid family (3,4-dimethoxycinnamic acid, 3,4-dihydroxycinnamic acid and trans-4-hydroxy-3-methoxycinnamic acid) meets the desired structural features previously described. These candidates were tested against the isolated enzyme (Chapter 4).

The methylated analogues of 3-(4-methoxybenzoyl)acrylic acid, 3,4-dimethoxycinnamic acid, 7-methoxy-4-oxo-1,4-dihydroquinoline-2-carboxylic acid, 3,4-dihydroxycinnamic acid and trans-4-hydroxy-3-methoxycinnamic acid were synthesised.

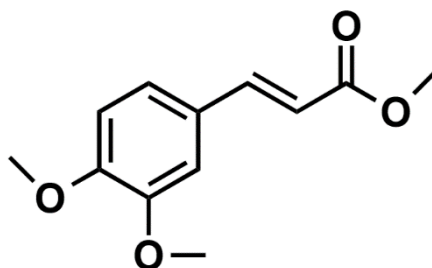
(E)-Methyl 3-(4-methoxyphenyl) acrylate (**31**)



(31)

3-(4-methoxybenzoyl)acrylic acid **30** (1 g, 2.42 mmol), potassium carbonate (1.05 g, 7.59 mmol), DMS (0.52 mL, 8.72 mmol) and 50 mL of acetone was stirred at 25 °C for 48 hours under argon. The reaction was monitored by TLC until there was no starting material left. Then, 100 mL ethyl acetate was added to the reaction mixture, and the aqueous layer was separated and concentrated to 89% yield of the desired product **31**. ¹H NMR (500 MHz, CDCl₃), δ 7.63 (d, J = 15.5 Hz, 1H), 7.48-7.46 (m, 2H), 6.91-6.89 (m, 2H), 6.33 (d, J = 15.5 Hz, 1H), 5.54 (m, 2H), 3.85 (s, 3H). The data were in good agreement with the literature value (Xu *et al.* 2017).

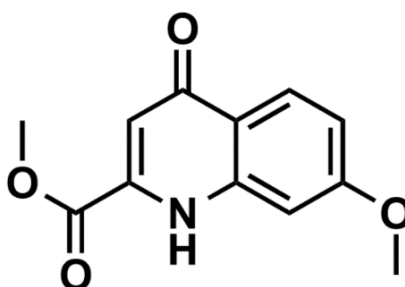
(*E*)-methyl 3-(3,4-dimethoxyphenyl)-acrylate (**33**)



(33)

3,4-dimethoxycinnamic acid **32** (1 g, 4.80 mmol), potassium carbonate (0.75 g, 5.42 mmol), DMS (0.75 mL, 5.48 mmol) and 20 mL of acetone was stirred at 25 °C for 48 hours under argon. The reaction was monitored by TLC until there was no starting material left. Then, 100 mL ethyl acetate was added to the reaction mixture, and the aqueous layer was separated and concentrated under reduced pressure to yield **33** as an oil (95%). ¹H NMR (500 MHz, CDCl₃), δ 3.78 (3H, s, -COOCH₃), 3.89 (3H, s, -OCH₃), 3.91 (3H, s, -OCH₃), 6.33 (1H, d, J = 16.0 Hz, H-8), 6.87 (1H, d, J = 8 Hz, H-5), 7.10 (2H, m, H-2 and H-6), 7.63 (1H, d, J = 16.0 Hz, H-7). The data were in good agreement with the literature value (Reta *et al.* 2012).

(*E*)-methyl 4-hydroxy-7-methoxy-2-quinolinecarboxylate (**35**)

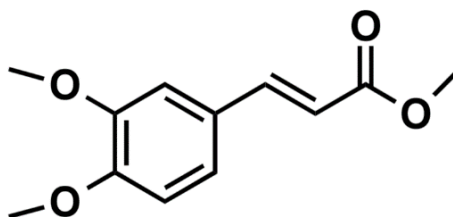


(35)

7-methoxy-4-oxo-1,4-dihydroquinoline-2-carboxylic acid **34** (0.125 g, 0.57 mmol), potassium carbonate (0.09 g, 0.65 mmol), DMS (0.14 mL, 1.47 mmol) and 15 mL of acetone was stirred at 25 °C for 48 hours under argon. The reaction was monitored

by TLC until there was no starting material left. Then, 100 mL ethyl acetate was added to the reaction mixture, and the aqueous layer was separated and concentrated with an 89% yield of the desired product **35**. ^1H NMR (500 MHz, DMSO- d_6), δ 3.96 (s, 3H), 3.71 (s, 3H), 6.60 (s, 1H), 7.41-7.62 (m, 2H), 7.97 (dd, J = 8.2, 1.3 Hz, 1H), 12.03 (s, 1H); ^{13}C NMR (500 MHz, DMSO- d_6), δ 52.0, 54.0, 112.4, 119.8, 120.2, 122.8, 130.9, 133.0, 137.4, 143.2, 162.8, 177.2; m/z (ES $^+$) 234 [(M+H) $^+$, 100%].

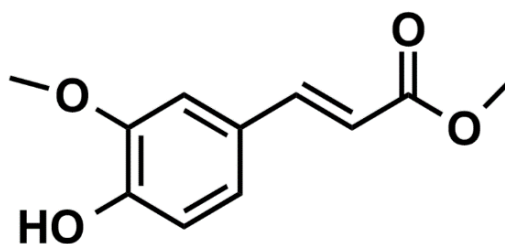
(2E)-methyl 3-(3,4-dimethoxyphenyl)acrylate (**37**)



(37)

3,4-Dihydroxycinnamic acid **36** (1 g, 5.55 mmol), potassium carbonate (3.1 g, 22.43 mmol), DMS (2.14 mL, 22.5 mmol) and 20 mL of acetone was stirred at 25 °C for 48 hours under argon. The reaction was monitored by TLC until there was no starting material left. Then, 100 mL ethyl acetate was added to the reaction mixture, and the aqueous layer was separated and concentrated to a 95% yield of the desired product **37**. δ_{H} (300 MHz, DMSO- d_6) 7.51 (1H, d, J = 16.0 Hz, 7-H), 7.30 (1H, dd, J = 8.4, 1.8 Hz, 6-H), 7.19 (1H, d, J = 1.8 Hz, 2-H), 6.96 (1H, d, J = 8.4 Hz, 5-H), 6.44 (1H, d, J = 16.0 Hz, 8-H), 3.79 (3H, s, CH $_3$), 3.78 (3H, s, CH $_3$), 3.77 (3H, s, CH $_3$).

(*E*)-methyl 3-(4-hydroxy-3-methoxyphenyl)acrylate (**39**)



(39)

trans-4-hydroxy-3-methoxycinnamic acid **38** (1 g, 5.14 mmol), potassium carbonate (1.6 g, 11.5 mmol), DMS (1.12 mL, 11.81 mmol) and 50 mL of acetone was stirred at 25 °C for 48 hours under argon. The reaction was monitored by TLC until there was no starting material left. Then, 100 mL ethylacetate was added to the reaction mixture, and the aqueous layer was separated and concentrated to give the desired product **39** in 90% yield. ¹H NMR (500 MHz, CDCl₃), δ 3.81 (3H, s, -OCH₃), 6.30 (1H, d, J = 16.0 Hz, H-8), 6.92 (1H, d, J = 6.8 Hz, H-5), 7.05 (1H, dd, J = 6.8, 1.8 Hz, H-2), 7.10 (1H, d, J = 1.8 Hz, H-6), 7.62 (1H, d, J = 16.0 Hz, H-7). The data were in good agreement with the literature value (Reta *et al.* 2012).

Discussion

A brief review of previous attempts to synthesise ICL1 inhibitors was described. Here, the main aim was to synthesise inhibitor candidates that had α,β -unsaturated carbonyl moiety and/ or aromatic/heterocyclic functionality. A 5-step reaction was done to achieve the synthesis of *DL-threo*-2-methylisocitrate. First, a reflux reaction was done to obtain an isomeric epoxide mixture. Then, methylation occurred prior to the synthesis of the lactone ring, followed by the key step, which is the opening of the lactone ring to achieve a good yield (60%) of the final molecule. This drug candidate that resembles ICL's substrate was tested *in vitro* against the isolated enzyme (Chapter 4).

The methylated analogues of 3-(4-methoxybenzoyl)acrylic acid, 3,4-dimethoxycinnamic acid, 7-methoxy-4-oxo-1,4-dihydroquinoline-2-carboxylic acid, 3,4-dihydroxycinnamic acid and trans-4-hydroxy-3-methoxycinnamic acid (**31**, **33**, **35**, **37** and **39**) were synthesised with the aim of increasing inhibitory effect against ICL.

The addition of a methyl group can provide several therapeutic benefits depending on the drug molecule and the position of the methyl group (Harrold and Zavod, 2014). These benefits include increased selectivity for one biological target over another, increased drug potency and sterically blocked metabolism, which leads to an increased duration of action of the specific drug (Harrold and Zavod, 2014). For instance, the addition of a methyl group in the drug simvastatin enhances the drug potency when compared to its un-methylated analogue, lovastatin (Harrold and Zavod, 2014). Bethanechol, a drug responsible for lowering cholesterol, has a methyl group that serves to increase selectivity to the target receptors and prevent degradation by acetylcholinesterase (Harrold and Zavod, 2014). Lastly, the addition of methyl group to methyltestosterone allows the compound to be taken orally as the methyl group can block oxidative metabolism that would otherwise be quickly metabolised (Harrold and Zavod, 2014). A limitation of the synthesised, methylated candidates (**31**, **33**, **35**, **37** and **39**) is poor solubility as they are coloured oils, which interferes with the enzyme assay. For this reason, their inhibitory property against ICL1 was not assessed. Liu *et al.* (2016) also excluded compounds with poor solubility from their screening assay as it would affect the measured results. An alternative would be to dry and crystallise the oils and break them into powder and dissolve them in either buffer or solvents, such as DMSO. However, the CL-54 drug family were identified as lead compounds with an estimated inhibition against ICL in the nanomolar range (Chapter 4). These novel inhibitors were designed by Dr Lawson as anti-malaria drugs but were repurposed as part of a collaboration. Thus, this drug family was selected for X-ray crystallography and to be tested against Mtb.

Experimental Procedures

Proton (^1H) and carbon (^{13}C) NMR spectra were recorded on a Bruker Avance 300 spectrometer operating at 300.1 MHz for ^1H , and 75.5 MHz for ^{13}C , Bruker Avance II 400 operating at 400.1 MHz for ^1H and 100 MHz for ^{13}C and Bruker Avance 500 operating at 499.90 MHz for ^1H , 125.71 MHz for ^{13}C . Chemical shifts were recorded at δ values in parts per million (ppm). Spectra were acquired in CDCl_3 , CD_3OD , DMSO-d_6 , acetone- d_6 or deuterium oxide at ambient temperature unless otherwise specified. ^1H NMR data are reported as follows: chemical shift (δ), relative integral, multiplicity

(defined as: s = singlet, d = doublet, t = triplet, q = quartet, m = multiplet, bs = broad singlet), coupling constant(s) J (Hz), assignment (Raheem, 2011).

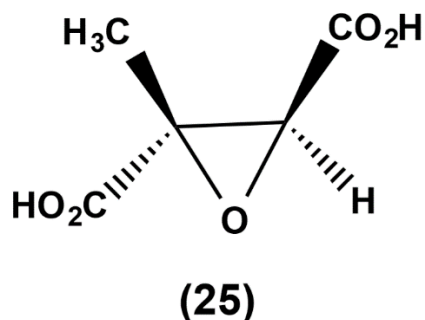
Analytical thin layer chromatography (TLC) was conducted on Merck pre-coated (25 μm) silica gel 60F₂₅₄ plates or on aluminium-backed 0.2 mm thick silica gel 60 F₂₅₄ plates (Merck), and the plates were visualized under a 254 nm UV lamp and/or by treatment with either anisaldehyde dip or alkaline potassium permanganate dip, followed by heating with a heat gun. The retention factor (R_f) quoted is rounded to the nearest 0.01. Flash chromatography was conducted using silica gel 60F₂₅₄ as the stationary phase, and the solvent indicated (Raheem, 2011).

Reagent and solvents were purified by standard means. Methanol was distilled from calcium hydride in a recycling still under nitrogen. ¹⁴³Dichloromethane (DCM), toluene, tetrahydrofuran (THF) and diethyl ether (Et₂O) were dried by passage through two columns of alumina using a MBRAUN (SPS-800) solvent purification system. Anhydrous DMF was purchased from Aldrich UK and dried by distillation from 4 Å molecular sieves under a nitrogen atmosphere. All reagents and starting materials were used as purchased from Aldrich UK, Acros UK or Alfa Aesar UK, except where otherwise stated in the experimental procedures (Raheem, 2011).

Reactions employing either air or moisture-sensitive reagents were performed under an atmosphere of nitrogen (unless otherwise specified) in flame-dried apparatus. Anhydrous reagents were handled under nitrogen using standard techniques (Raheem, 2011).

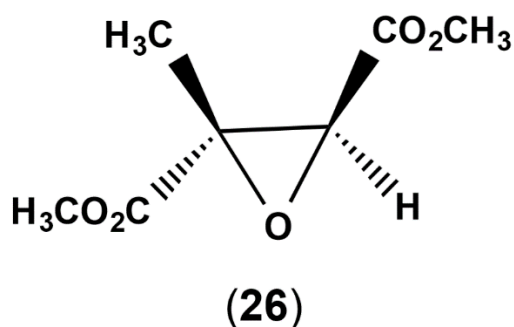
Room temperature varied between 19-25 °C. "Removed at reduced pressure" refers to the use of a rotary evaporator with the water bath temperature generally not exceeding 40 °C (Raheem, 2011).

Trans-epoxymethylsuccinic acid (**25**) (Lee *et al.*, 2018):



Mesaconate (**24**) (1.0 g, 7.88 mmol) was suspended in water (5 mL) and NaOH (0.61 g, 15.37 mmol) was added dropwise with stirring. The mixture was stirred and cooled to 0 °C and Na₂WO₄·2H₂O (76 mg, 0.23 mmol) was added, followed by dropwise addition of a 30% aqueous solution of H₂O₂ (1 mL, 8.50 mmol). After stirring at 0 °C for 1 h, the mixture was heated at 65 °C for 8 h, then cooled to RT and evaporated to dryness. The residue was partitioned between water (10 mL), ethyl acetate (20 mL) and ether (20 mL). Concentrated H₂SO₄ (1 mL) dissolved in ether (10 mL) was added, and the mixture was stirred at RT for 3h. The organic layer was separated, dried (Na₂SO₄) and evaporated to afford the epoxide **26** as a white powder in quantitative yield. ¹H NMR (400 MHz, DMSO-*d*₆) δ 13.44 (s, 2H), 3.75 (s, 1 H), 1.45 (s, 3 H).

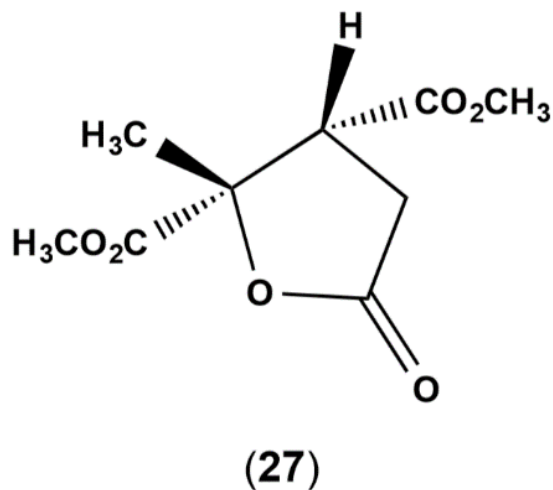
Dimethyl trans-epoxymethylsuccinate (**26**) (Lee *et al.*, 2018).



To a solution of epoxide (**26**) (1.0 g, 6.84 mmol) in anhydrous MeOH (10 mL) at 0 °C was added SO₂Cl₂ (1.1 mL, 15.0 mmol) and the resulting mixture was allowed to warm up to room temperature and stirred for 8 h. The reaction mixture was concentrated under vacuum and the residue partitioned between ether and saturated aqueous NaHCO₃. The ether layer was separated, dried and evaporated to afford the dimethyl ester **27** as a clear oil in quantitative yield and used without any further purification. ¹H

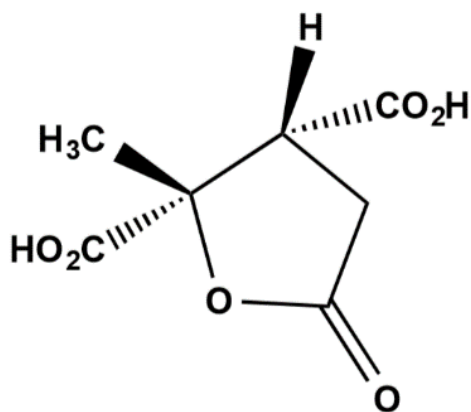
NMR (500 MHz, DMSO- d_6) δ 6.46 (d, $J = 7.2$ Hz, 1H), 6.09 (s, 1H), 4.94 (s, 1H), 4.62 (d, $J = 7.2$ Hz, 1H), 3.74 (s, 3H), 3.69 (s, 2H), 3.67 (d, $J = 4.2$ Hz, 5H), 1.71 (s, 3H), 1.44 (s, 3H).

2-Methyl-5-oxo-tetrahydro-2,3,4-tricarbomethoxytetrahydrofuran (**27**) (Lee *et al.*, 2018).



Sodium metal (0.69 g, 28.7 mmol) was added to cooled anhydrous MeOH (15 mL) under argon atmosphere at 0 °C and stirred until the metal dissolved. Dimethyl malonate (3.2 mL, 28.7 mmol) was added to the sodium methoxide thus formed, and the resulting mixture was stirred at RT until a white precipitate formed (20-30 min). Epoxide (5.0 g, 28.7 mmol) was added, and the mixture was stirred for 3 days at RT. Concentrated HCl was added, and the stirring continued for another 2 h. The solid formed (NaCl) was filtered, and the filtrate concentrated to afford crude lactone **28** as a white solid in good yield and used without further purification.

Crude lactone **(28)** (Lee *et al.*, 2018)



(28)

To the crude lactone **28** obtained above (1.5 g) 6 N HCl (50 mL) was added, and the mixture was refluxed at RT for 3 h. The reaction mixture was concentrated, and the residue was re-dissolved in water and evaporated to remove traces of HCl. The brown residue thus obtained was dissolved in water and treated with activated charcoal at 60 °C. After 30 min, the mixture was filtered, and the filtrate evaporated to afford colourless crude lactone 2-Methyl-5-oxo-tetrahydrofuran-2,3-dicarboxylic acid. To a solution of lactone **27** (1.5 g, 7.98 mmol) in H₂O (10 mL), NaOH (0.95 g, 23.9 mmol) was added, and the mixture was heated at 80 °C for 12 h, then neutralized with Amberlite H⁺ resin to pH 7.0. After solvent removal, the residue was redissolved in H₂O and treated with activated charcoal. The mixture was filtered, and the filtrate evaporated to afford DL-threo-2-methylisocitrate **29** good yield (60%).

Chapter 4 – Isocitrate lyase 1 *in vitro* assay

Introduction

Isocitrate lyase 1 (ICL1) is a key enzyme in two pathways, the glyoxylate shunt and methylcitrate cycle, which are important for the survival of latent *Mycobacterium tuberculosis* (Mtb) (Bentrup *et al.*, 1999; Muñoz-Elías and McKinney, 2005; Gengenbacher *et al.*, 2010; Eoh and Rhee, 2014). In the former pathway, ICL1 catalyses the first reaction where the substrate, isocitric acid, is converted to glyoxylate and succinate. In the latter, ICL1 catalyses the last step of the cycle, where 2-methylisocitrate is the substrate and pyruvate, and succinate are the products. To assess the inhibitory effect of drug candidates against ICL1, an enzymatic assay was employed. The assay models the glyoxylate shunt, where ICL catalyses the isocitric acid to glyoxylate and succinate. Using a spectrophotometer at 324 nm, the product formation is measured by the real-time appearance of phenylhydrazone, which is formed upon the reaction of glyoxylate and phenylhydrazine (Figure 4-1) (Dixon and Kornberg, 1959).

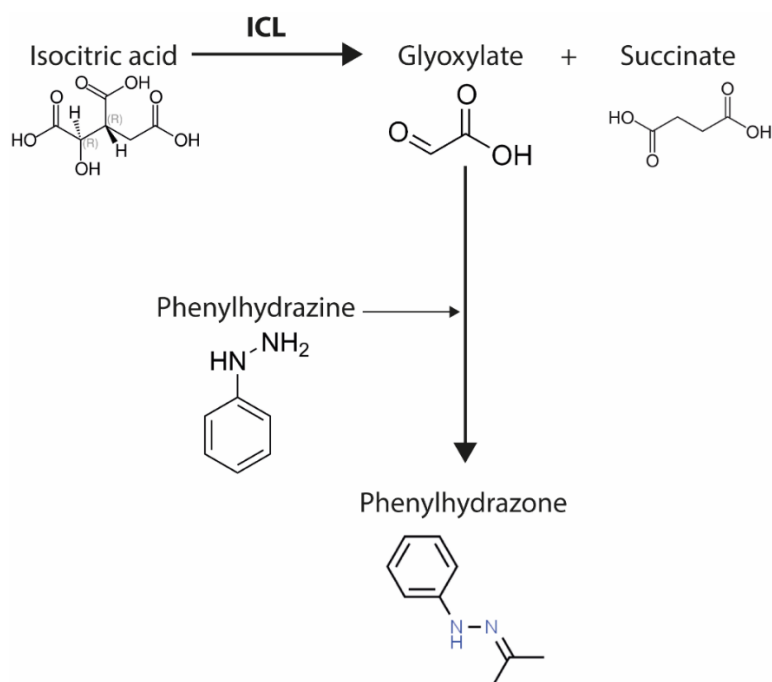


Figure 4-1: Representation of the ICL1 enzyme assay mechanism, where the substrate, isocitric acid, is converted into two products, glyoxylate and succinate, by ICL1. Glyoxylate reacts with phenylhydrazine, forming phenylhydrazone that can be detected at 324 nm.

The assay was optimised by testing different ICL1, substrate and salt concentrations. The enzyme activity was further characterised by the presence of EDTA and the effect of re-freezing and thawing. Once the assay was optimised, it was used to evaluate the activity of ten candidate ICL1 inhibitors. The most potent ICL1 inhibitors were tested against non-replicating and replication Mtb to assess their antitubercular activity (Chapter 6).

Materials and Methods

Desalting isocitrate lyase

ICL1 was expressed and purified using a nickel chromatography column prior to this work (see Chapter 2). The ICL1 was eluted in TGN (50 mM Tris.HCl pH 7.5, 10% (v/v) glycerol, 250 mM sodium chloride and 10 mM imidazole) and stored at -80 °C. Prior to the enzyme activity assay, the enzyme was buffer exchanged into 50 mM MOPS pH 7.0, 50 mM sodium chloride, 5 mM magnesium chloride buffer using a MicroSpin PD-10 desalting column (GE Healthcare) that was previously equilibrated five times with the same MOPS buffer. The enzyme was aliquoted and stored at -80 °C until further use.

Isocitrate lyase activity assay

Prior to the enzyme activity assay, the enzyme was buffer exchanged into 50 mM MOPS pH 7.0, 50 mM sodium chloride, 5 mM magnesium chloride buffer using a MicroSpin PD-10 desalting column. The reaction of isocitric acid to glyoxylic acid and succinic acid is catalysed by ICL1. Glyoxylic acid can react with phenylhydrazine to generate phenylhydrazone. The activity of ICL1 can be sensed by measuring phenylhydrazone's absorbance at 324 nm (Liu *et al.*, 2016). The enzyme assay was conducted in a 96-well UV microplate (Thermo Scientific, UK) with a 200 µL reaction volume at 37 °C in the presence of 1.27 µM recombinant ICL1, 1 mM DL-isocitric acid (Trisodium salt, Sigma, UK), 0.1% (v/v) phenylhydrazine (Sigma, UK) and 50 mM MOPS pH 7.0, 50 mM NaCl and 5 mM MgCl₂.6H₂O. The absorbance value, at 324 nm, for each reaction well was detected every ten seconds for five minutes.

ICL1 activity assay with compounds dissolved in DMSO

Unlike Garcinia acid and 2-methylisocitrate, the other 8 drugs were only soluble in DMSO (Table 3), and three of the eight compounds were coloured and absorbed light when in solution in the UV range that was used to measure the phenylhydrazine in the assay. Furthermore, the presence of DMSO in the assay caused the enzyme activity to drop by 50%, as shown in the results section (Figure 4-7). To overcome this, the drugs (2-(3-bromophenyl)-1-(2,4,6-trihydroxyphenyl)ethenone, 3,4-dihydroxycinnamic acid, 3,4-dimethoxycinnamic acid, 3-(4-methoxybenzoyl)acrylic acid, 7-methoxy-4-oxo-1,4-dihydroquinoline-2-carboxylic acid and the CL-54 family) were incubated with the enzyme for 10 minutes and then buffer exchanged with 50 mM MOPS pH 7.0 and 5 mM MgCl₂.6H₂O using a MicroSpin PD-10 desalting column (GE Healthcare) before adding to the enzyme reaction mix as described previously.

ICL1 inhibitors

Ten compounds were tested in the ICL1 activity assay to assess their inhibitory effects. Itaconate was used as a positive control (Table 3).

Table 3: Summary of the drugs tested in the ICL1 activity assay.

Drugs	Molecular weight (g/mol)	Solubility	Colour	Origin
CL-54-01	356.37	DMSO	Yellow	Synthesised by Dr Christopher Lawson*
CL-54-02	340.38	DMSO	Dark brown	Synthesised by Dr Christopher Lawson*
CL-54-04	354.40	DMSO	Dark red	Synthesised by Dr Christopher Lawson*
Garcinia acid	190.11	MOPS buffer	Colourless	Sigma, UK
Itaconate	130.099	MOPS buffer	Colourless	Sigma, UK

2-methylisocitrate	206.04	MOPS buffer	Colourless	Synthesised in-house (see Chapter 3)
2-(3-bromophenyl)-1-(2,4,6-trihydroxyphenyl)ethanone	321.9	DMSO	Colourless	Provided by Prof David Warhurst**
3,4-dihydroxycinnamic acid	180.16	DMSO	Colourless	Alfa Aesar, UK
3,4-dimethoxycinnamic acid	208.21	DMSO	Colourless	Alfa Aesar, UK
3-(4-methoxybenzoyl)acrylic acid	206.2	DMSO	Colourless	Alfa Aesar, UK
7-methoxy-4-oxo-1,4-dihydroquinoline-2-carboxylic acid	219.19	DMSO	Colourless	Activate Scientific, UK

*Dr Christopher Lawson - University of Glasgow, UK.

**Professor David Warhurst - London School of Hygiene and Tropical Medicine, UK.

Results

To observe the inhibition of ICL1 activity, the parameters for the *in vitro* assay needed to be determined. This assay was optimised by testing different ICL1 concentrations, salt gradient and substrate concentration (Figure 4-2). All enzyme assays were conducted at 37 °C.

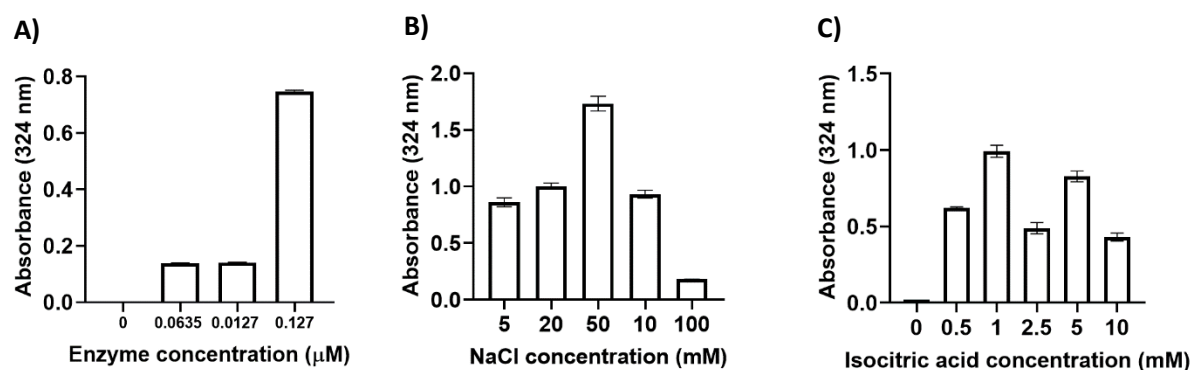


Figure 4-2: ICL1 assay optimisation with different enzyme, salt and substrate concentrations over a period of 5 minutes at 37 °C at 324 nm. **A)** Three concentrations of ICL1 were screened for assay optimisation with 1 mM of the substrate, isocitric acid. **B)** Different concentration of sodium chloride (5-100 mM), with 0.127 µM ICL1 and 1 mM substrate. **C)** Different concentrations of isocitric acid (0-10 mM) with 0.127 µM ICL1. Data represented is three biological replicates, and error bars are standard deviations.

It is clear that 0.127 μM of ICL1 yielded the highest absorbance, demonstrating that the enzyme is active, and the product formation can be detected at 324 nm (Figure 4-2A). A salt gradient (0-100 mM NaCl) was tested (Figure 4-2B), in which the ICL1 activity was found to be optimal at 50 mM NaCl, whilst completely inhibited at 100 mM NaCl. Finally, substrate (isocitric acid) inhibition was observed above 2.5 mM, whereas 1 mM, 1000-fold excess of substrate to enzyme gave robust product formation (Figure 4-2C). Therefore, 0.127 μM ICL1, 50 mM NaCl and 1 mM isocitric acid were conditions used for all assays.

It has been reported in the literature that ICL1 requires magnesium ions for activity (Cowan, 2002). Ethylenediaminetetraacetic acid (EDTA), a chelating agent that sequesters metal ions such as magnesium, was used to investigate the dependency of ICL1 on magnesium ions (Figure 4-3A). No ICL1 activity is seen in the presence of EDTA, consistent with a requirement for the metal co-factor.

The sensitivity of the enzyme to refreezing was also investigated. An ICL1 aliquot was thawed, and its enzyme activity was tested, followed by re-freezing at $-80\text{ }^{\circ}\text{C}$ and thawing again prior to testing (Figure 4-3B). The effect of re-freezing causes an approximately 50% drop in activity. As a result, aliquots of ICL1 were made such that a single aliquot was thereafter thawed for each experiment.

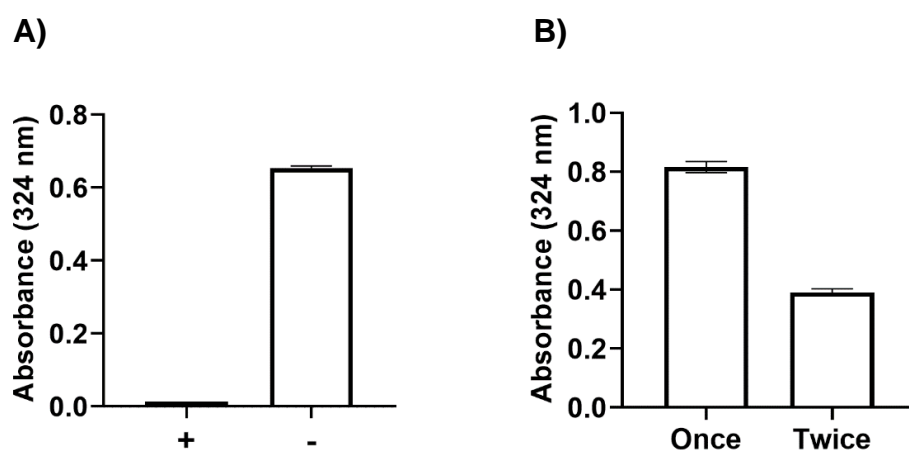


Figure 4-3: Characterisation of ICL1. **A)** The effect of 5-minute incubation of 0.127 μM ICL1 with 1 mM EDTA (+) or without EDTA (-). **B)** The effect of re-freezing to $-80\text{ }^{\circ}\text{C}$ and thawing, once or twice, in the ICL activity. All assays were measured at 324 nm over 5 minutes at $37\text{ }^{\circ}\text{C}$. Data represented is three biological replicates, and error bars are standard deviations.

After the enzyme assay characterisation, all enzyme assays were conducted with a fresh aliquot desalted enzyme in MOPS based buffer containing 50 mM NaCl, a final

enzyme concentration of 0.127 μM and 1 mM of the substrate at 37 $^{\circ}\text{C}$ for 3 minutes. In addition, itaconate, a known ICL1 inhibitor, was used as a positive control and the reaction mix without ICL1 was used as a negative control to assay putative inhibitors of ICL1.

Two compounds, Garcinia acid and 2-methylisocitrate, were the initial ICL1 inhibitors candidates due to their resemblance with the substrate, isocitric acid (Figure 4-4).

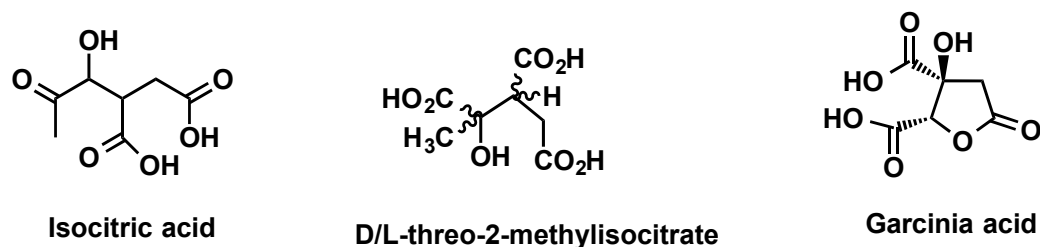


Figure 4-4: Structure of the substrate, isocitric acid, and two candidates as ICL1 inhibitors, DL-threo-2-methylisocitrate and Garcinia acid. DL-threo-2-methylisocitrate is a derivative of the substrate, 2-methylisocitrate of the methylcitrate cycle, and it was synthesised in-house (see Chapter 3), and Garcinia acid was purchased from Sigma, UK.

Garcinia acid and 2-methylisocitrate (synthesised in-house) were the first compounds to be tested in the assay (Figure 4-5). The former inhibited the enzyme at 50 mM, which is an extremely high concentration (Figure 4-5A) likely to be unachievable *in vivo*, whereas the latter caused more than 50% inhibition at 5 mM (Figure 4-5B).

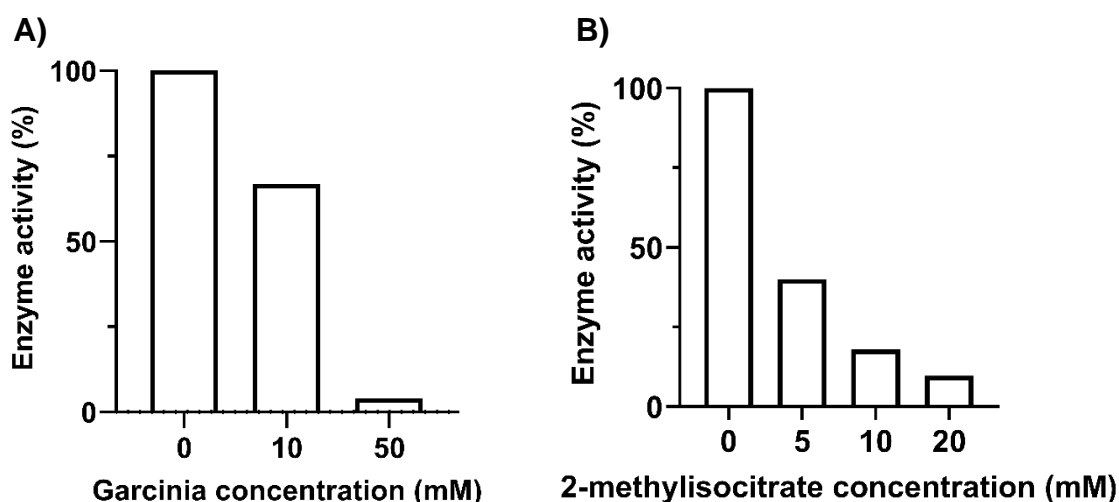


Figure 4-5: Garcinia and 2-methylisocitrate effect upon ICL1 activity. **A)** Effect of 10 and 50 mM of Garcinia acid on ICL1 activity. **B)** Effect of 5, 10 and 20 mM of 2-methylisocitrate on ICL1 activity. Values shown are one measurement and it was normalised in respect to 0 mM value, which is assigned as 100% enzyme activity.

The following compounds to be tested have the α,β -unsaturated carbonyl moiety and/or aromatic/heterocyclic features that might be responsible for occupying the enzyme pocket (Figure 4-6).

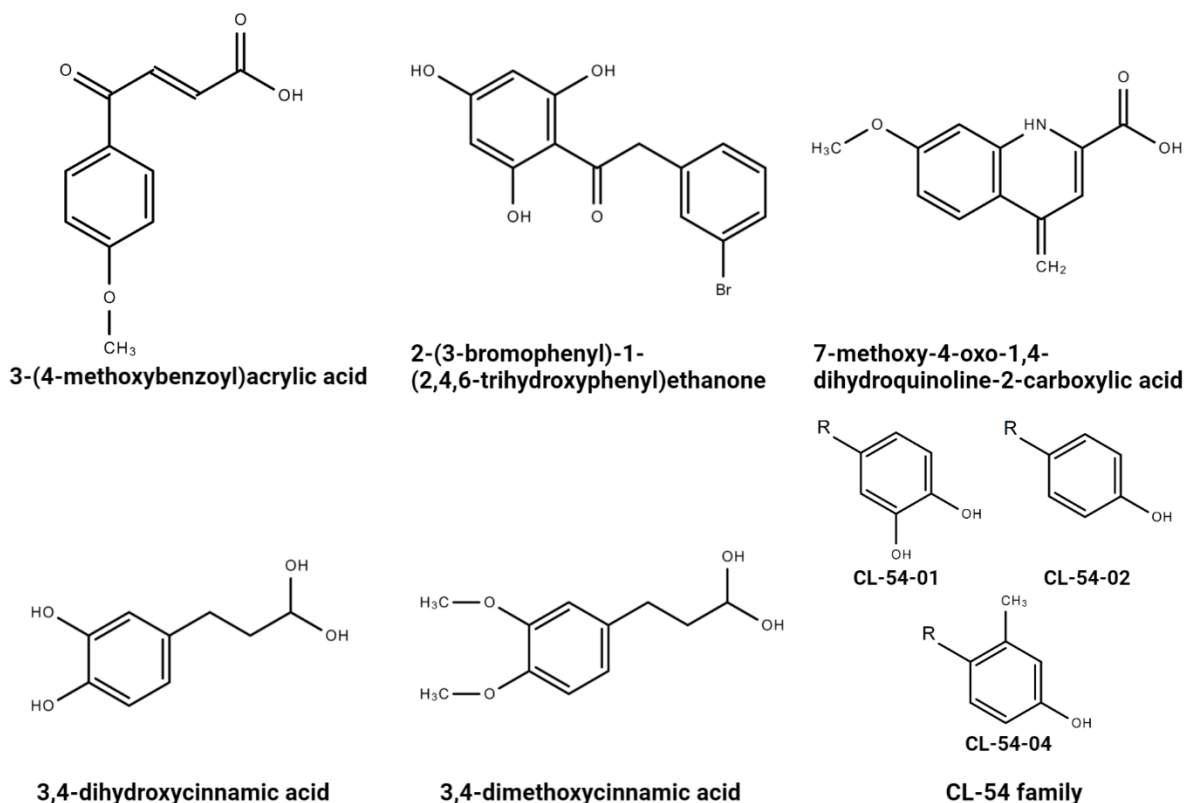


Figure 4-6: Structure of the drugs screened in the ICL1 activity assay. CL-54 drug family structures are confidential (R represents identical structure) and only the functional groups are depicted. These three analogues were chemically synthesised by Dr Lawson as an anti-malaria drug and were repurposed as part of a collaboration. See Table 3 in Materials and Methods section for more details of the drugs.

Unlike garcinia acid and 2-methylisocitrate that can be dissolved in 50 mM MOPS pH 7.0, 5 mM $MgCl_2$ buffer, these drugs were insoluble in this aqueous buffer and were dissolved in DMSO instead. Although not a permanent modification, DMSO inhibits the enzyme (Figure 4-7A). The presence of 5% (v/v) DMSO caused a 40% drop in ICL1 activity. However, the activity was retrieved when buffer was exchanged through a PD-10 MicroSpin desalting column (Figure 4-7B). It is worth pointing out that the enzyme assays do not start at zero seconds due to the delay between the introduction of the enzyme into the reaction mix and the first reading in the spectrophotometer, which takes on average 10 seconds.

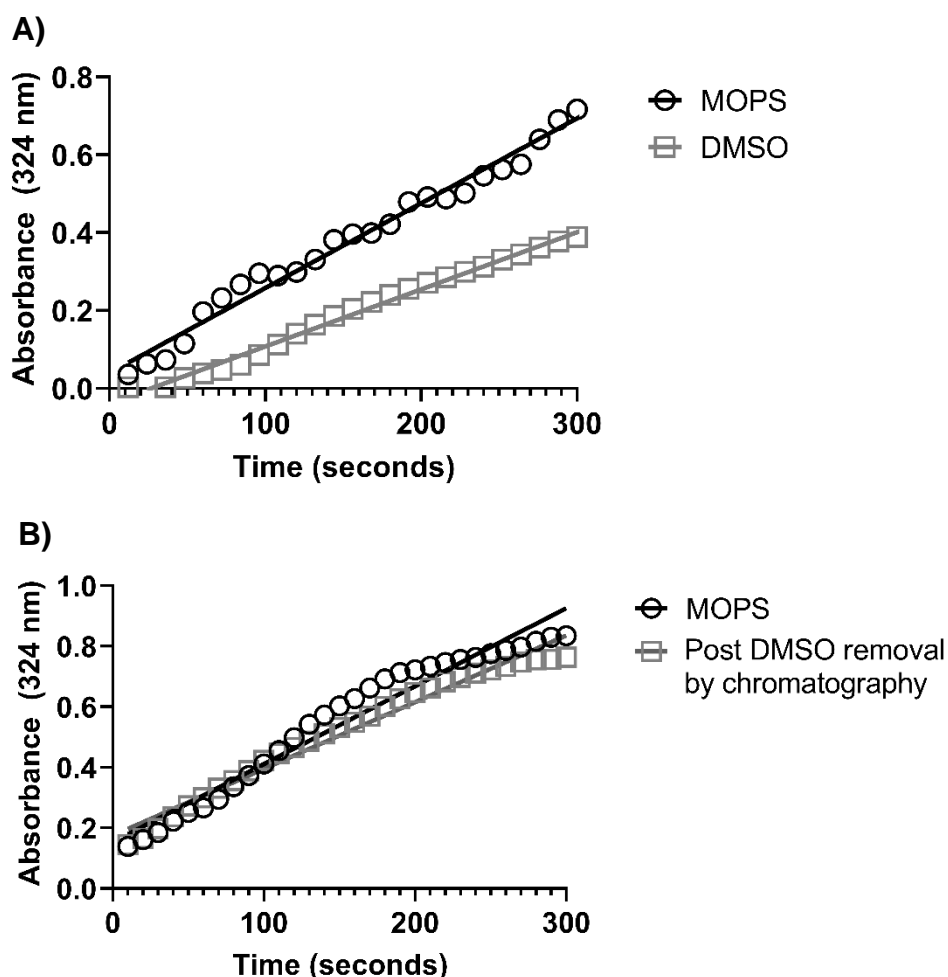


Figure 4-7: ICL1 activity assay in the presence of 5% (v/v) DMSO over 5 minutes at 324 nm at 37 °C. **A)** Activity of ICL1 with MOPS buffer (50 mM MOPS pH 7.0, 5 mM MgCl₂) or 5% (v/v) DMSO and **B)** activity of ICL1 after incubated with MOPS buffer or 5% (v/v) DMSO for 10 minutes and buffer exchanged using a MicroSpin PD-10 chromatography column.

This suggests that the DMSO interferes with the enzyme assay but does not inhibit nor modified the structure of the dimer. Thus, if the drugs dissolved in DMSO have an inhibitory effect against ICL1, the drug will be bound to the enzyme, but the DMSO will be removed in the MicroSpin column, and the impact on the activity will be possible to observe. This method was applied to assess the inhibitory effects of the putative inhibitors dissolved in DMSO and then incubated with the enzyme for 10 minutes on ice. The mixture was buffer exchanged through a PD-10 MicroSpin desalting column to remove unbound drug before testing in the assay (Figure 4-8). This adapted assay

is also useful to assess compounds, such as the CL-54 family, that have strong colours that absorb at the wavelength used in the assay (324 nm).

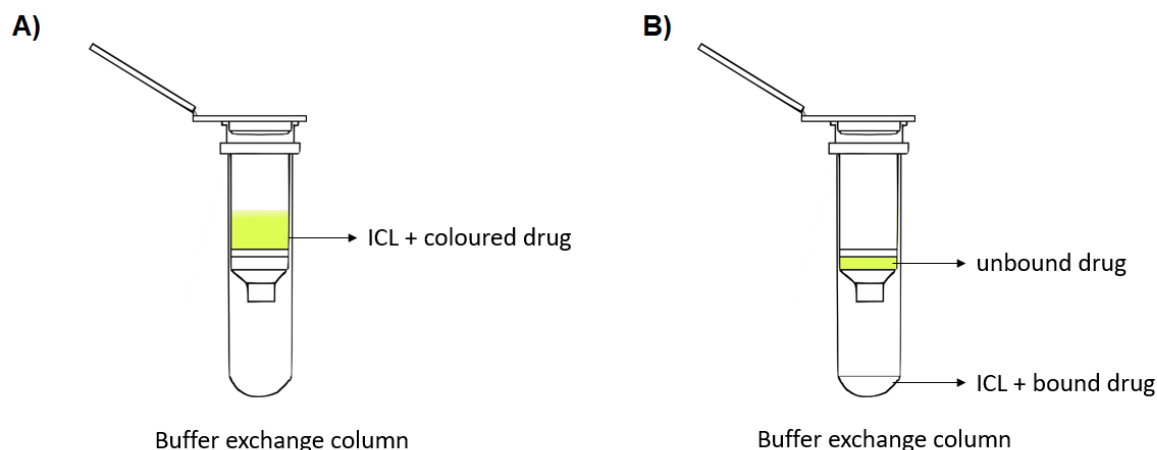


Figure 4-8: Schematic representation of the method to assess coloured inhibitors in the ICL1 activity assay. The chromatography column is equilibrated with 50 mM MOPS pH 7.0, 5 mM MgCl₂ buffer and kept on ice before adding the enzyme. **A)** After incubating the enzyme with the drug on ice for 10 minutes, the mixture was added to the chromatography column and centrifuged for 2 minutes at 800 x g. **B)** Representation of the chromatography column after centrifugation. The unbound drug is filtered by the column, and the enzyme (bound or not to the drug) is harvested and added immediately to the enzyme assay mixture for spectrophotometer analysis.

If any of the drugs demonstrate poor inhibition, it indicates that they either do not bind stably or are poor inhibitors. Still, if they remained bound during the desalting column, it shows a high affinity to the enzyme.

In the first attempt, two positive controls were employed: ICL1 in MOPS buffer and ICL1 in 1% (v/v) DMSO as in Figure 4-7 to ensure that the chromatography column is removing the DMSO, leading to a restored ICL1 activity. The first drug candidate tested using this methodology was 1 mM 7-methoxy-4-oxo-1,4-dihydroquinoline-2-carboxylic acid (labelled as '7-methoxy') and 1 mM itaconate, a known ICL1 inhibitor for comparison – Figure 4-9A.

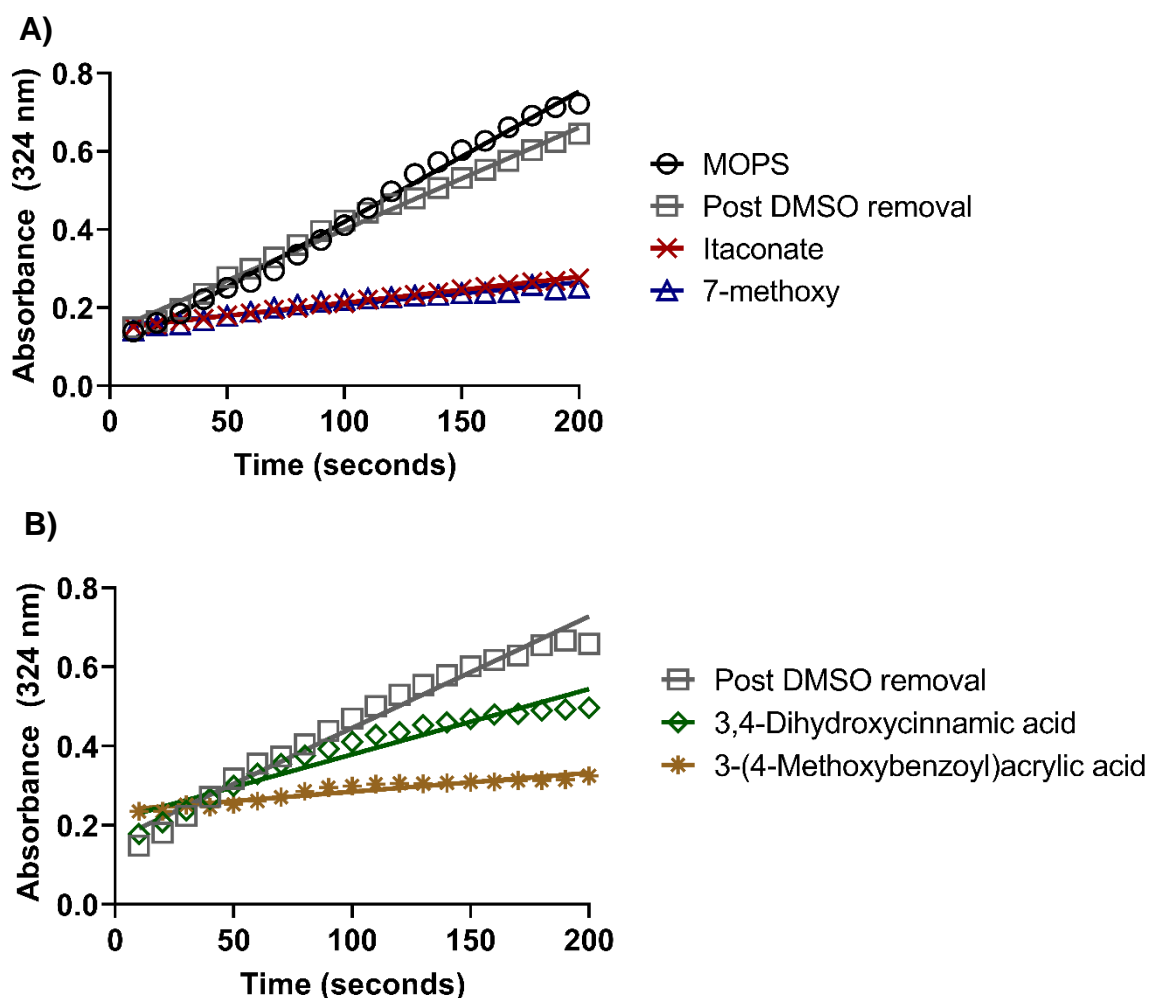


Figure 4-9: Drug effect on ICL1 activity after employing the chromatography column methodology at 324 nm for 3 minutes at 37 °C. **A)** ICL1 activity in MOPS buffer and in DMSO as positive controls, and in the initial presence of 1 mM itaconate (as a positive control) and the candidate 7-methoxy-4-oxo-1,4-dihydroquinoline-2-carboxylic acid (labelled as ‘7-methoxy’). **B)** Effect on ICL1 activity in the presence of two drugs at 1 mM (initial) 3,4-dihydroxycinnamic acid and 3-(4-methoxybenzoyl)acrylic acid. Data represents an average of three biological replicates.

The activity of ICL1 dropped by 48% in the presence of 7-methoxy-4-oxo-1,4-dihydroquinoline-2-carboxylic acid compared to DMSO alone and by 44% in the presence of 1 mM itaconate. Two other drugs, 3,4-dihydroxycinnamic acid and 3-(4-methoxybenzoyl)acrylic acid, were tested at (initial) 1 mM using the MicroSpin column method (Figure 4-9B). The former inhibited 22% of the enzyme activity, whilst the latter, 44%.

Five other drugs ((2-(3-bromophenyl)-1-(2,4,6-trihydroxyphenyl)ethanone, 3,4-dimethoxycinnamic acid, CL-54-01, CL-54-02 and CL-54-04) were tested against the enzyme at (initial) 1 mM using the chromatography column method (Figure 4-10).

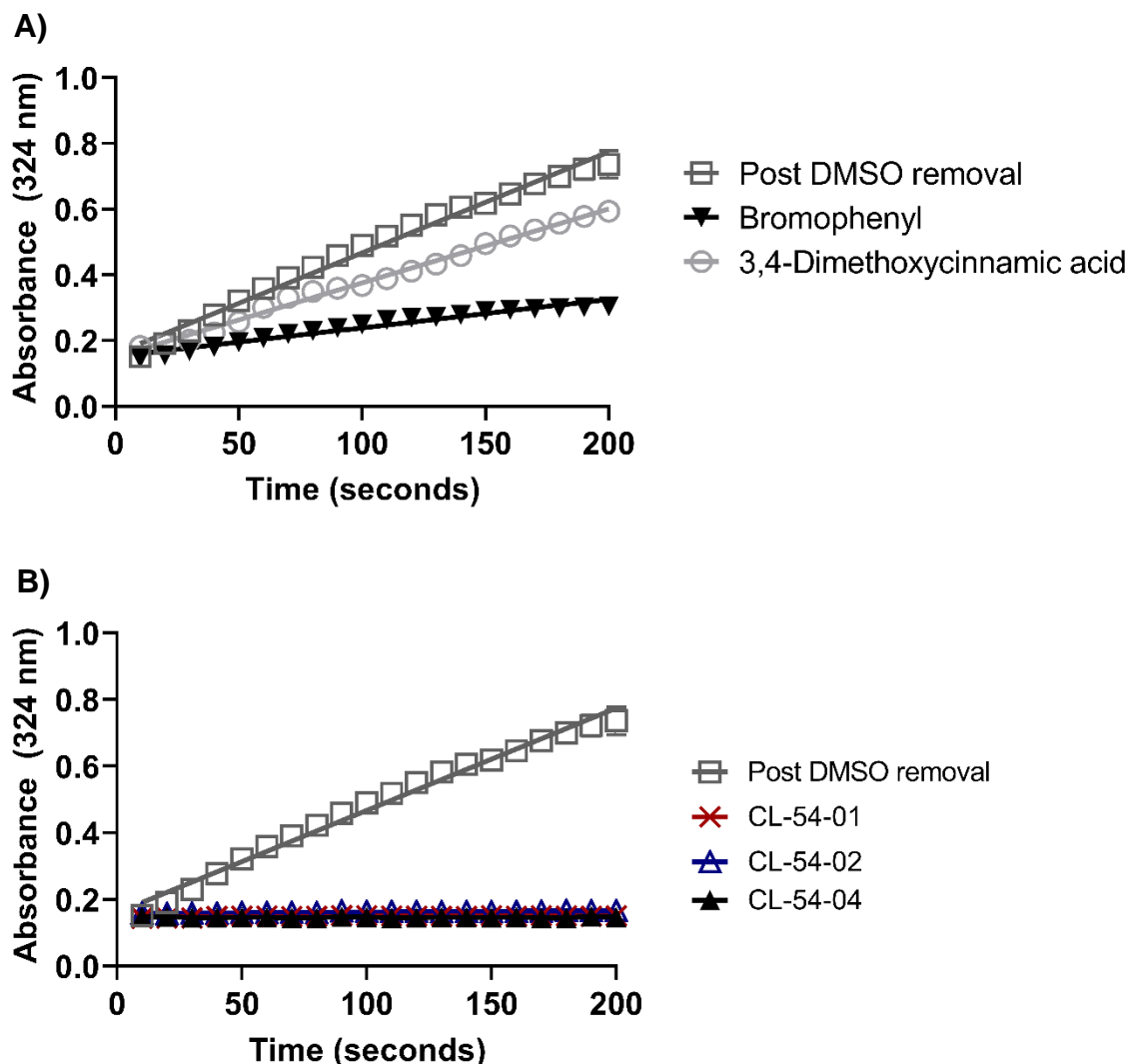


Figure 4-10: Drug effect on ICL1 activity after employing the chromatography column methodology at 324 nm for 3 minutes at 37 °C with DMSO as a negative control. **A)** Effect of 2-(3-bromophenyl)-1-(2,4,6-trihydroxyphenyl)ethanone, shown as 'bromophenyl' and 3,4-dimethoxycinnamic acid. **B)** Effect of the CL-54 drug family. Data represent an average of two biological replicates. Values represent an average of three biological replicates of one independent experiment.

There was 78% of ICL1 activity in the presence of 1 mM 3,4-dimethoxycinnamic acid when compared to DMSO alone, and a 40% of activity remaining in the presence of 2-(3-bromophenyl)-1-(2,4,6-trihydroxyphenyl)ethanone ('Bromophenyl' in Figure 4.10A), whereas all three CL-54 drugs (CL-54-01, CL-54-02 and CL-54-04) showed complete inhibition at 1 mM (Figure 4-10B).

The CL-54 family are analogues whose structures are highly similar (Figure 4-6), and therefore, one of the drugs was profiled more extensively (Figure 4-11). At 0.05 mM CL-54-01, the ICL activity is 42.5%, suggesting that the IC₅₀ is below 50 nM.

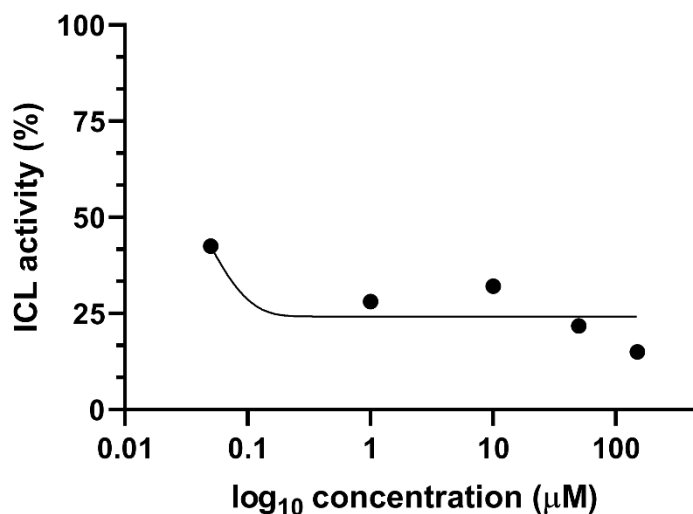


Figure 4-11: Effect of different concentrations of CL-54-01 on ICL1 activity assay. Values represent one individual reading.

This finding was reproduced by Laura Boardman-Slack at the University of Lincoln, confirming its high inhibition against ICL1. A summary of all the ICL1 inhibitors tested in this study and their estimate IC₅₀ can be found in Table 4. Given the CL-54 drug family inhibition effect, the screening of new inhibitors was concluded. The attention was focused on these lead compounds, and co-crystallisation efforts began. These drugs were also shipped to Eoh's lab (USA) to be tested against Mtb.

Table 4: Estimated IC₅₀ of the ICL inhibitors screened in this study.

Drugs	IC ₅₀
CL-54-01	Below 50 nM
CL-54-02	Predicted to be below 50 nM
CL-54-04	Predicted to be below 50 nM
Garcinia acid	20 mM
2-methylisocitrate	4 mM
2-(3-bromophenyl)-1-(2,4,6-trihydroxyphenyl)ethanone	Estimated: 800 μM
3,4-dihydroxycinnamic	Estimated: 2.5 mM
3,4-dimethoxycinnamic acid	Estimated: 1.9 mM
3-(4-methoxybenzoyl)acrylic acid	Estimated: 1.6 mM
7-methoxy-4-oxo-1,4-dihydroquinoline-2-carboxylic acid	Estimated: 800 μM

Discussion

In this chapter, the enzyme activity assay of isocitrate lyase was optimised by testing different concentrations of the enzyme, substrate and salt, and the impact of re-freezing and EDTA was also investigated. After that, 10 drugs were screened for their inhibitory properties against ICL1.

Three concentrations of ICL1 were tested, 0.127, 0.0635 and 0.0127 μM. The highest concentration (0.127 μM) showed robust, reproducible activity as reported elsewhere (Liu *et al.* 2016). In the ICL1 assay reported by Liu *et al.* (2016), the buffer used contained MOPS and MgCl₂ because ICL1 requires magnesium ions for its activity (Sharma *et al.*, 2000). When EDTA was present in the enzyme activity assay, no ICL1 activity was seen, consistent with sequestration of the essential magnesium co-factor. However, Liu *et al.* (2016) did not investigate the effect of sodium chloride on the

enzyme activity. A salt optimisation assay was done as the salt can modulate the stability of the enzyme, and changes may have profound effects on the conformational stability (Sinha and Khare, 2014). It is thought that the NaCl ions may interact directly with the polar groups, such as the amide groups (Von Hippel and Wong, 1964; Robinson and Jencks, 1965). Here, the enzyme activity is optimal at 50 mM NaCl, and the function of ICL1 was adversely affected by 100 mM NaCl. This may be as a result of the salt concentration decreasing intermolecular hydrogen bonds, which could affect solubility, binding and stability of the enzyme, potentially also increasing the hydrophobic interactions that lead to protein aggregation and precipitation (Sinha and Khare, 2014). Thus, the buffer used subsequently in drug screening assays was 50 mM MOPS pH 7.0, 50 mM NaCl and 5 mM MgCl₂. Furthermore, it has been reported the use of 50 mM Tris pH 7.5 in the ICL1 activity assay (Bhusal *et al.*, 2019); however, this is problematic as Tris reacts with glyoxylate, forming ammonium salts (Duggan *et al.*, 1964). Hence, Tris will compete with phenylhydrazine to react with the glyoxylate product, which would lead to a decrease in the detection of activity.

The optimal concentration of substrate was observed to be 1 mM which is consistent with that reported by Liu *et al.* (2016). However, it was expected that the increased substrate concentration would lead to an enzymatic response that fits a hyperbolic curve, but this was not observed. Instead, there is an increase in enzyme activity at 1 mM and 5 mM of substrate, and a decrease in enzymatic activity with 0.5 mM, 2.5 mM or 10 mM of substrate, which is unexpected. Here, it was also demonstrated that isocitrate lyase 1 is sensitive to freezing. Its activity dropped 50% on a single re-freezing and thawing cycle when the enzyme was in buffer. This could be due to the formation of ice crystals during the freeze/thaw process causing mechanical damage (Xiong, 1997). Other proteins such as trypsin, α -amylase and bile-salt-activated lipase, have been reported to be affected by freezing and thawing (Solovyev and Gisbert, 2016). Thus, a single enzyme preparation was used for all drug assays, and individual aliquots were stored at -80 °C until required.

To identify a lead compound, 10 drugs were screened in this assay against ICL1, and their estimated IC₅₀ is shown in Table 4. The first drugs tested in the ICL1 assay were Garcinia acid and 2-methylisocitrate. The former is a small compound with a lactone ring that resembles the structure of the substrate, isocitric acid. These were features to be a potential ICL1 inhibitor. However, it only inhibited the ICL1 enzyme at high

concentrations, such as 10 mM, in which approximately 30% of the enzyme activity was inhibited. This suggests the compound would not be a good candidate as a lead compound. The latter, 2-methylisocitrate, had an IC_{50} of 4 mM, which is lower than Garcinia. The activity of both 2-methylisocitrate and Garcinia acid were not considered to be in the range to be useful as a lead compound, so other potential inhibitors were trialled.

Unlike Garcinia acid and 2-methylisocitrate, the other compounds were insoluble in buffer and had to be dissolved in DMSO. However, the ICL1 activity was negatively affected by the presence of DMSO. For this reason, a desalting column was employed. ICL1 was incubated with DMSO for 10 minutes and buffer exchanged using the column, removing all the unbound DMSO. The activity of ICL1 incubated with DMSO was the same as the control with MOPS buffer. This also additionally overcame the fact that some drugs are coloured and would absorb in the wavelength used in the assay. Thus, this method was employed to estimate the inhibition of the other DMSO dissolved/coloured drug candidates. It was hypothesised that if the drug had enough affinity with the enzyme, it could remain bound during gel filtration. It is possible that some compounds could be very active but have a higher off-rate, such that the activity might be underestimated in this assay. Nonetheless, it means that this method screen compounds with the tightest affinity and low off-rate, which are desired characteristics for a lead compound.

The first attempt using this model was testing ICL1 with MOPS and ICL1 with DMSO as controls, ICL1 with itaconate as a negative control, and a drug that had not yet been tested, 7-methoxy-4-oxo-1,4-dihydroquinoline-2-carboxylic acid. This drug candidate had a similar inhibition to itaconate at 1 mM. Seven other drugs were screened using this methodology at 1 mM. The least promising drugs are 3,4-dihydroxycinnamic, 3,4-dimethoxycinnamic acid and 3-(4-methoxybenzoyl)acrylic acid, with 22%, 22% and 44% inhibition at 1 mM, respectively. The drug, 2-(3-bromophenyl)-1-(2,4,6-trihydroxyphenyl)ethanone, at 1 mM caused a 60% inhibition, which suggests that the estimated inhibition is likely to be in the micromolar (μM) scale. Nevertheless, the CL-54 drug family showed complete inhibition of ICL1 at 1 mM. The analogue, CL-54-01, was further studied, and the inhibition was estimated to be below 50 nM, by far the lowest estimated IC_{50} among the drugs tested. Any compound that has potency in the nanomolar scale is considered a lead compound (Hughes *et al.*, 2011). It is plausible

that the other two CL-54 drugs will have similar IC_{50} since they are analogues of CL-54-01. Therefore, three new lead compounds have been identified as Mtb ICL1 inhibitors. There have been attempts to develop an Mtb ICL1 inhibitor reported in the literature (see Appendix A, Table A1), with drugs documented with an IC_{50} varying between 0.1 μ M to 10 mM. The most potent ICL1 inhibitor previously identified was 3-nitropropionamide (IC_{50} of 0.1 μ M), but it caused neurotoxicity in cats (Alston *et al.*, 1977; Schloss and Cleland, 1982). The estimated IC_{50} of CL-54-01 (~50 nM) is half of the 3-nitropropionamide (100 nM), suggesting that the CL-54 drugs are the most promising ICL1 inhibitors reported to date.

Chapter 5 – Isocitrate lyase 1 co-crystallisation with inhibitors

Introduction

There are several methods, such as X-ray crystallography, NMR, neutron diffraction and electron microscopy, which allow us to characterise in detail the three-dimensional structure of proteins and their ligands (Krengel and Imberty, 2007). The former is known to be the most powerful method as it elucidates the binding pose of the ligand bound to the protein with atomic precision and because of its versatility in studying small molecules to massive protein complexes (Krengel and Imberty, 2007; Wiener-Schmidt *et al.*, 2020). Thus, X-ray crystallography is indispensable in structure-based drug design, as the information gained from the protein-ligand interaction can be used to design drug modifications that would improve such interaction (Chen *et al.*, 2018).

There are two strategies to achieve protein:ligand structures to apply X-ray beams for data collection (Hassell *et al.*, 2006; Wiener-Schmidt *et al.*, 2020) – Figure 5-1. The first is co-crystallisation, which is the process of pre-incubating the ligand/drug with the protein before setting up the crystal trials or simply including it on the crystallisation condition, aiming that the ligand is free to bind to the protein in solution prior to the formation of a crystal (Wiener-Schmidt *et al.*, 2020). The second is soaking, which is a more routinely method that uses pre-grown crystals and soaking them with the ligand (Collins *et al.*, 2017). Given the affinity and whether the binding site is available (for instance, not involved in crystal packing), the ligand can access it by diffusing through the solvent channels within the crystal lattice (Danley, 2006; Wiener-Schmidt *et al.*, 2020). This technique has become a standard technique to understand enzyme mechanisms but is now also widely used for the structure-based drug design process (Mcnae *et al.*, 2005).

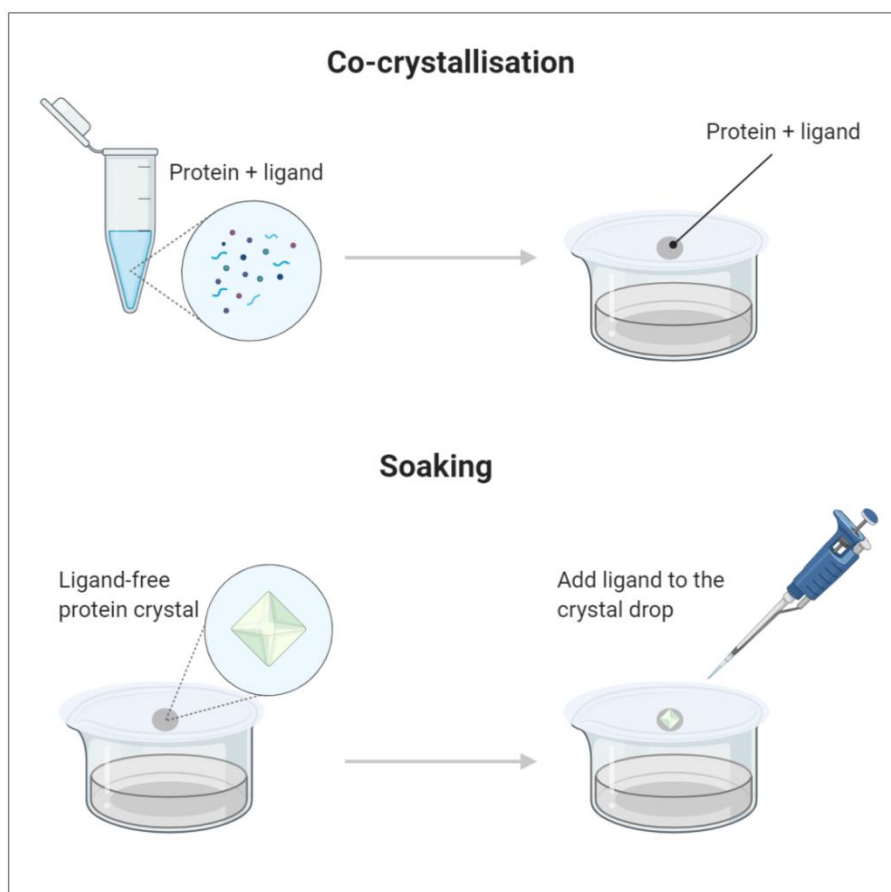


Figure 5-1: Diagrammatic representation of co-crystallisation and soaking; the two methods used in this research to obtain a crystal of ICL1 bound to the inhibitor. In the co-crystallisation method, the protein is pre-incubated with the ligand/inhibitor before the crystal trial is set up, whilst in soaking, the crystal is first obtained, and the ligand is then added to the drop prior to X-ray diffraction. Created with BioRender.com.

The former method can be trickier as new conditions must be identified for the crystallisation of the protein:ligand complex, which is often different from conditions where protein alone forms crystals. The latter can be more reliable if there is a ligand-free crystal condition identified that can be used to generate a stock of crystals to be soaked with a drug/ligand (Hassell *et al.*, 2006). The disadvantage of this approach is the low solubility of ligands in aqueous solutions, which may require organic solvents such as DMSO, which may alter the chemistry of the crystal drop and ultimately affecting the integrity of the crystal (Danley, 2006). Overall, the simplicity of soaking reduces the number of crystallisation trials, and it maximises the number of co-crystal structures per protein preparation (Müller, 2017).

The automation of crystallography through a liquid-handling robot that pipettes the conditions and the protein accordingly into a 96-well plate has improved success rate

and made initial screens much more convenient, allowing high-throughput crystallisation trials (Stewart and Mueller-Dieckmann, 2014). Besides increasing efficiency and decreasing experimental cost, this type of robot, often referred to as a mosquito robot, reduces the amount of protein required for each screen (Bard *et al.*, 2004). The instrument has adaptable hardware and software that parameters can be adjusted, including volume (in the nanolitre range), aspiration and dispensing speed, among others (Stewart and Mueller-Dieckmann, 2014). This technology was used at the University of Lincoln to set up co-crystallisation trials.

The understanding of how the inhibitor interacts with the protein is highly useful for the design of better inhibitors that can fit the active site and its interaction with each amino acid. To achieve this, hundreds of co-crystallisation trials were set up for ICL1 with itaconate (a known ICL1 inhibitor), an in-house synthesised inhibitor (2-methylisocitrate) and the most promising ICL1 inhibitor to date, CL-54-01 (see Chapter 5 for the inhibition studies against the isolated enzyme). The trials were carried out using both techniques described in Chapter 1 – the sitting (by the mosquito robot) and hanging drop vapour diffusion (following up on hits obtained from the crystal screens). As co-crystallising the enzyme with the inhibitor may not form crystals, the soaking method was also attempted simultaneously to maximise the co-crystallisation success. The ultimate aim was to confirm the binding of the inhibitor in the ICL1 active site, such that this could be used to study the mode of drug binding to refine the drug structure.

Materials and Methods

Protein crystallisation robot

The 80 μ L screening conditions (Stura MD1-02, MD1-13, MD1-20, MacroSol™ MD1-22 (Molecular Dimensions, Ltd), HR2-126, HR2-098, HR2-144 (Hampton Research)) were added to the reservoir of the 96-well MRC crystallisation plates. The Ni-NTA purified ICL1 from -80 °C stock was thawed and buffer exchanged using a PD-10 column as described previously in Chapter 1. Then, 1 mM of the drug (itaconate, 2-methylisocitrate or CL-54-04) was added to the enzyme (final concentration of 4 mg/mL) and kept on ice. The drug:enzyme mixture was loaded into the SPTLabTech mosquito® crystal instrument. The software was set up to pipette 100 nanolitres of the

enzyme and 100 or 200 nanolitres of the precipitant with reservoir precipitant solution and protein alone as controls. The plate was covered with an adhesive film (Thermo Scientific) and kept at 16 °C. Crystal growth was observed by light microscopy, and conditions that yielded crystals were recorded. The conditions that yielded crystals were expanded by adjusting the precipitant components' range to improve the quality of the crystals. The conditions were prepared and sterilised by autoclave. Trials of drug:enzyme mixture were set up using the hanging drop method as described in Chapter 1.

Soaking

The hanging drop vapour diffusion crystallisation technique was used to produce ICL1 crystals (conditions 0.2 M imidazole malate pH 7.0 and 25% (w/v) PEG 4000, 0.1 M sodium HEPES pH 7.5 and 20% PEG 10000, 0.1 M sodium cacodylate pH 6.5 and 27% (w/v) PEG 4000, and 0.2 M imidazole malate pH 6.0 and 20% (w/v) PEG 4000), as described in Chapter 1. Once the crystals were formed, 0.2 µL of 10 mM CL-54-01 was added to the 2 µL drop to a final concentration of 1 mM, and incubated for 1 hour.

X-ray diffraction and solving the crystal structure

The protein crystals generated by hanging drop vapour diffusion were sequentially dipped into cryoprotectant solutions before freezing. The crystal was removed from the drop by 'fishing' using a nylon loop before being plunged sequentially into the precipitant solution supplemented with first 10% (v/v) and then 20% (v/v) glycerol. CL-54 was also present in the cryoprotectant solution at 0.5 mM. After these brief incubations, the crystal was flash-frozen in liquid nitrogen and stored under liquid nitrogen until diffracted at Diamond Light Source (Oxford, UK). In collaboration with Professor Peter Moody (University of Leicester), the structure of ICL1 in complex with CL-54 was solved using the previously reported crystal structure of Mtb ICL1 in complex with 3-nitropropionate and glyoxylate, PDB 1F8I (Sharma *et al.*, 2000) Briefly the electron density data generated at Diamond Light Source (Oxford, UK) was utilised as an mtz file with which to search by a molecular replacement for ICL1. All but chain A was deleted from the 1F8I.pdb file and this was utilised as a search model using the program Phaser and setting the occupancy of the asymmetric unit to be two (see <https://www.ucl.ac.uk/~rmhasek/ Phaser.html>). Gel filtration data had suggested that the recombinant ICL1 was purified as a dimer. The output .pdb file was then input into

the program COOT (see <https://www.ucl.ac.uk/~rmhasek/coot.html>) together with the electron density (.mtz file). Individual amino acid side chains were then manually refined before running global refinements to better place the amino acids within the density. The output .pdb file was then manipulated in PyMOL to generate the images used within the thesis.

Results

A total of 336 conditions (STURA MD1-20, MACROSOL MD1-22, HR2-126, HR2-098, MD1-02, MD1-13, HR2-144) were tested in a ratio of 1:1 and 2:1 protein to ligand, where the ligand was 2-methylisocitrate, using the protein crystallisation robot. Of these conditions, crystals were observed in 11, where no crystal formed with ligand-free ICL1 (Appendix B, Table B2). However, these crystals did not diffract and failed to form in scale-up trials. For the co-crystallisation of itaconate and ICL1, the same screens (STURA MD1-20, MACROSOL MD1-22, HR2-126, HR2-098, MD1-02, MD1-13, HR2-144) used for 2-methylisocitrate were tested with ICL1:itaconate, with the addition of MD1-01 and HR2-122, totalling 432 conditions. Of those, 30 formed crystals that are supposedly ICL:itaconate complex structure (Appendix B, Table B2). Unfortunately, these conditions also failed to form crystals when scaling up using the hanging drop diffusion method. The same co-crystallisation effort was applied to CL-54-01, where over 700 conditions, at three temperatures, were tested. No condition was identified where crystals were formed in the presence of the drug. Thus, the soaking technique was sought by diffusing CL-54-01 into already formed crystals identified in Chapter 1 (Figure 5-2).

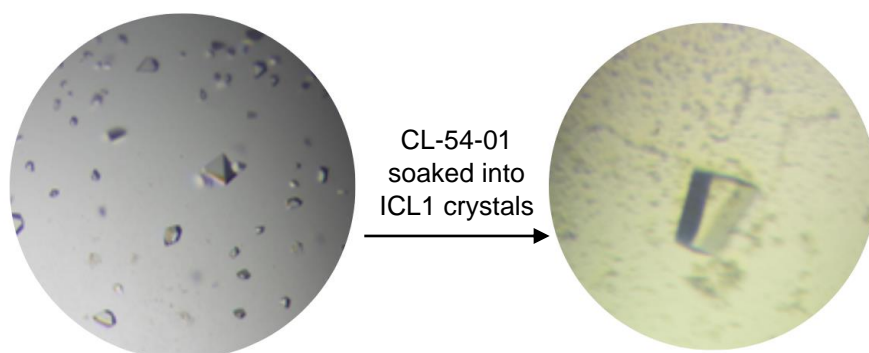


Figure 5-2: Soaking method of ICL crystals with CL-54-01. ICL1 crystals crystallised using 0.2 M imidazole malate pH 6.0 and 20% (w/v) PEG 4,000, and 1 mM (final concentration) of

CL-54-01 was added to the drop. The drug, whose colouration is yellow, can be seen faded in the drop. Pictures are courtesy of Laura Boardman-Slack from Dr Odell's lab at the University of Lincoln.

One crystal form was soaked with CL-54-01 for 60 minutes (as in Figure 5-2) and diffracted at Diamon Light Source (UK). Working with Professor Peter Moody, the structure was solved by molecular replacement. This structure was compared with ligand-free ICL1 and ICL2 by superposition (Figure 5-3). Structures were obtained from Protein Data Bank.

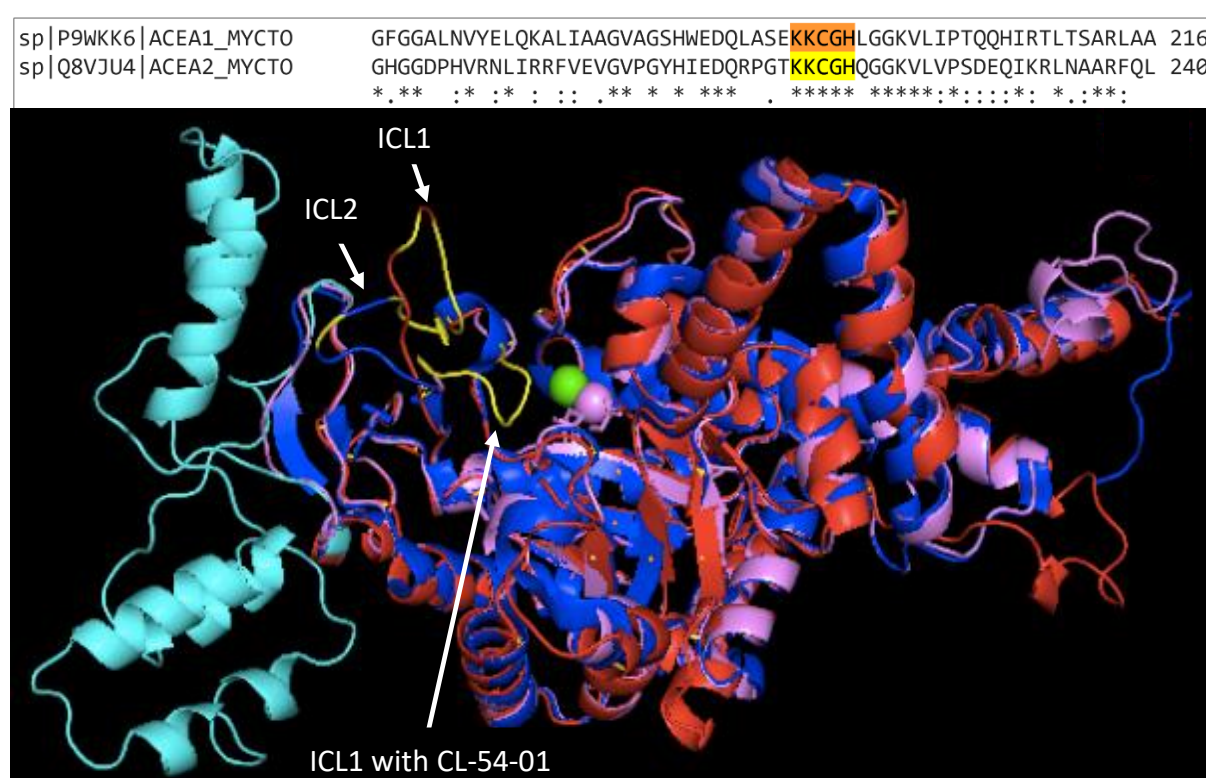


Figure 5-3: Comparison of sequence and structural alignment of CL-54-01 bound ICL with ICL1 and ICL2. The structure of ICL1 (red, PDB ID 1F61), ICL2 (blue and cyan, PDB ID 6EE1) and ICL1 bound to CL-54-01 (pink). The white arrows point at the catalytic loops containing the KKCGH motif. In the sequence alignment, ACEA1 refers to ICL1, and ACEA2 refers to ICL2.

The active sites of the untreated ICL1 and ICL2 can be seen in an open conformation, depicted in yellow/red and yellow/blue, respectively indicated by white arrows. The active site of CL-54-01-treated ICL1 can be seen in yellow. This active site shows a distinct movement of the catalytic loop KKCGH, closing over the substrate-binding pocket. The RMSD value of the two ICL1 enzymes is 0.193 Å. Taking a closer look

into the active site of CL-54-01-treated ICL1 and untreated ICL1 and ICL 2 superimposed (Figure 5-4), it is clear that the catalytic cysteine has moved considerably, by 13.8 Å when the inhibitor, CL-54-01, is bound.

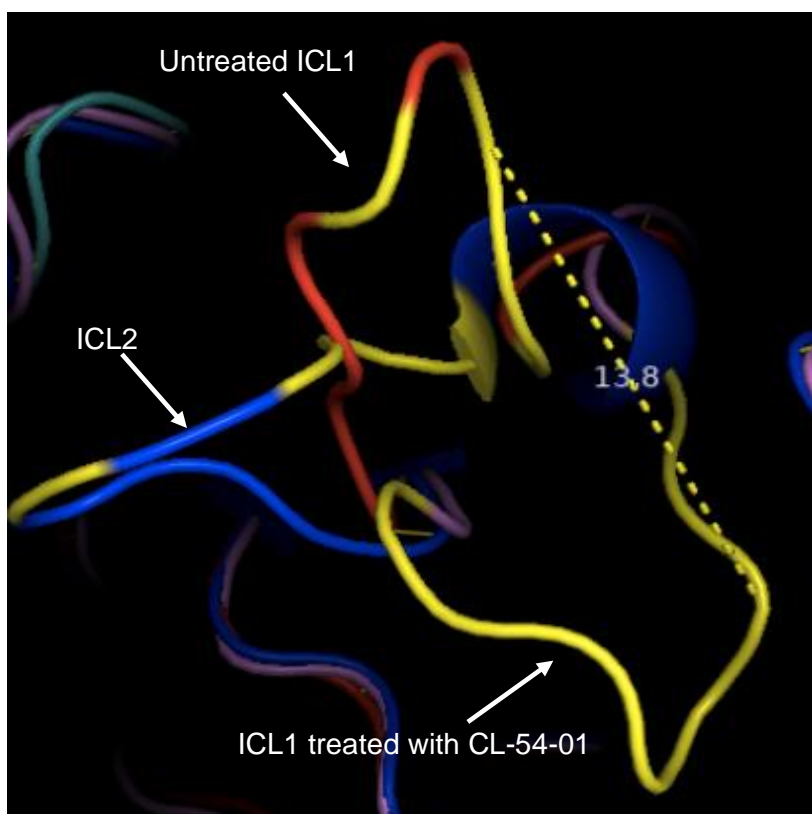


Figure 5-4: Magnified view of the catalytic loop of ICL1, ICL2 and ICL1 bound to CL-54-01, showing relative movement of the α -carbon of the active site cysteine.

The active sites of the untreated ICL1 and ICL2 can be seen in an open conformation, depicted in yellow/red and yellow/blue, respectively indicated by white arrows. This active site shows a distinct movement of the catalytic loop 'KKCGH', closing over the substrate-binding pocket.

The decision was taken to compare the presumed structure of ICL1 bound to CL-54-01 with that of ICL1 bound to the potent inhibitor, 3-nitropropionate (Figure 5-5).

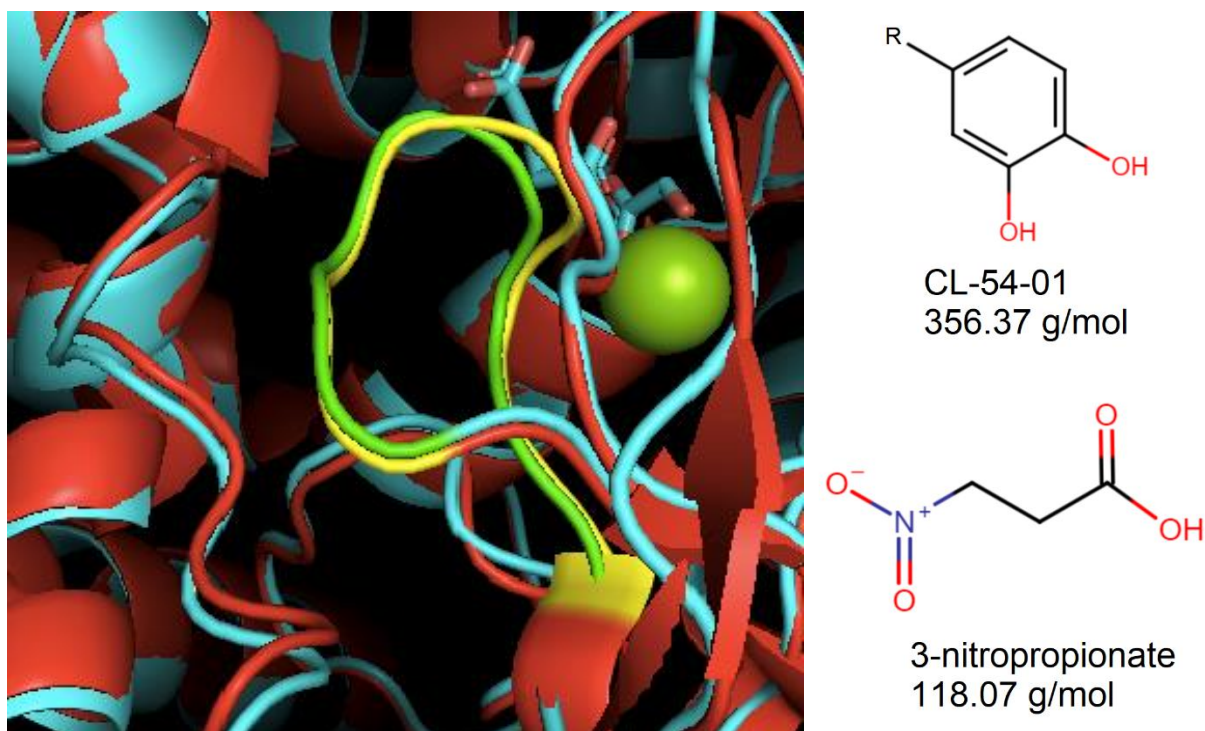


Figure 5-5: Structural alignment of ICL1 active site complexed with CL-54-01 (green) and 3-nitropropionate (yellow, PDB ID 6C4A), and their chemical structure. The green sphere is the positive magnesium ion needed for catalytic activity. For confidentiality, only the functional group of CL-54-01 is displayed, and R represents the common backbone structure that is the same for all three analogues.

The active site loops (depicted in yellow and green in Figure 5-5) are superimposable. The RMSD value of this alignment is 0.289 Å. The distance between the α -carbon of the cysteine residues in the CL-54-01-treated ICL1 active site and the 3-nitropropionate-treated ICL1, with pyruvate is only 1.0 Å. This is less than a C-C bond, showing much greater structural homology between ICL1 soaked with CL-54-01 and the 3-nitropropionate inhibitor bound than with native ICL1.

Discussion

Obtaining diffraction-quality crystals has long been a bottleneck in solving the three-dimensional structures of proteins (Hassell *et al.*, 2006). This issue was faced in Chapter 1, but new conditions that produced a diffraction-quality crystal, such as 0.2 M Imidazole malate pH 6.0 and 20% (w/v) PEG 4,000, were identified (Chapter 1) and used to obtain ICL1:inhibitor crystals.

In this study, two approaches were taken to obtain a protein:ligand structure, co-crystallisation and soaking pre-grown protein crystals with the drug. The ligands tested were 2-methylisocitrate, itaconate and CL-54-01. For each, hundreds of conditions were tested. Some conditions yielded ICL1:inhibitor crystals (Appendix B, Table B2), but only weak diffraction at best was observed 'in-house' for ICL1 with itaconate, 2-methylisocitrate or CL-54-01. Since CL-54-01 is the most promising inhibitor, the soaking efforts were focused on this compound to obtain a crystal where the inhibitor is bound to the active site.

In many cases, the ligand may be insoluble in the precipitant solution and must be dissolved in solvents such as ethanol or DMSO to achieve the required concentration (Fedarovich *et al.*, 2012). This solvent frequently damages the protein if higher than 10% (Jackson and Mantsch, 1991) and could have a detrimental effect on the crystals and result in poorer diffraction (Mcnae *et al.*, 2005). Although the CL-54-01 is dissolved in DMSO, the crystal diffraction was of good quality. The DMSO did not cause a detrimental effect on the quality of the ICL1 crystal because the CL-54-01 stock concentration was 10 mM and the final concentration was 1 mM, only 0.2 μ L of the stock was added to the 2 μ L drops.

For the visualisation of the structure, the ICL2 was also included because this isoform's structure was recently solved and published for the first time in 2019 (Bhusal *et al.*, 2019). The rationale was to understand whether the CL-54-01 could also inhibit ICL2; thus, the alignments of the ICL2 structure, ICL1 alone and ICL1 bound to CL-54-01, were generated. Both ICL1 and ICL2 active sites are conserved (Figure 5-3), suggesting that an ICL1 inhibitor can also inhibit ICL2. If we take a magnified view of the active site, ICL1 bound to CL-54-01 had a shift in the catalytic amino acids (KKCGH motif) to a close conformation (Figure 5-4). It supports the findings that suggest tighter binding – the active site loop appears to have closed over, thus, trapping the inhibitor such that it remains bound over the PD-10 column (seen in the *in vitro* studies in Chapter 4).

A structure alignment of 3-nitropropionate (a known ICL1 inhibitor) was superimposed with the solved structure of ICL1 with CL-54-01 (Figure 5-5). Both structures have an active site in close agreement (distance is 1.0 Å). This implies that this novel inhibitor binds and causes the same conformational changes as 3-nitropropionate, despite that

CL-54 family are not structurally related to 3-nitropropionate and are twice as large (e.g., 356.37 g/mol CL-54-01 vs 118.07 g/mol 3-nitropropionate). Therefore, there is strong evidence that the CL-54 drug family is the most potent ICL inhibitor to date.

Besides the concentration of the inhibitor, the soaking time is an important factor to consider. In this study, the soaking lasted 60 minutes, but the location of the drug in the active site was not well resolved, suggesting poor site occupancy. There are cases where soaking needs hours or even days to fully populate the ligand in a binding pocket of the protein (Schiebel *et al.*, 2015). This means that not only affinity but also diffusion kinetics of the inhibitor into the crystals are important for successful soaking. In the future, experiments with longer soaks are needed.

Chapter 6 – Assessing the CL-54 drug family against *Mycobacterium tuberculosis*

Introduction

After successfully screening the potential ICL inhibitors in the *in vitro* enzyme assay (Chapter 4), the most promising candidates were the CL-54 family with an estimated IC₅₀ in the nanomolar range. Although the structure of these drugs is confidential, their presumptive functional group are depicted in Figure 6-1.

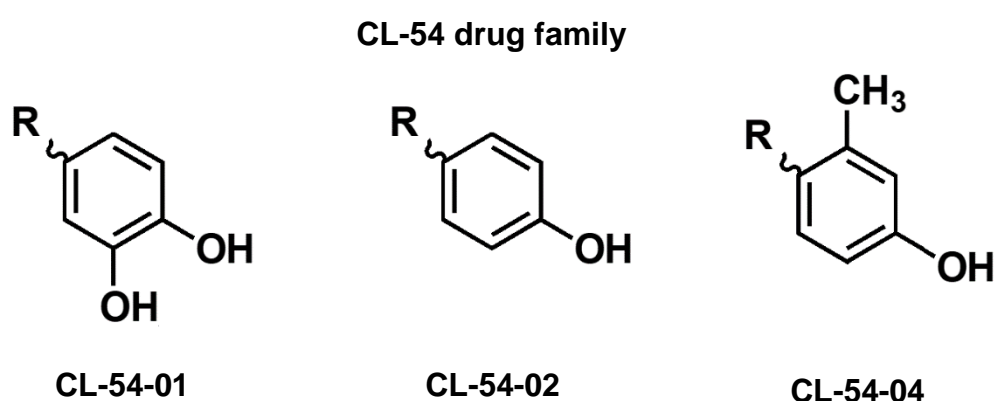


Figure 6-1: Structure of CL-54 family compounds. Only functional groups are shown as the full structure is confidential (this drug family has been synthesised by Dr Christopher Lawson at the University of Glasgow originally as anti-malaria drug but were repurposed as part of a collaboration). R represents the common backbone structure that is the same for all three analogues. Molecular weight: CL-54-01 (356.37 g/mol), CL-54-02 (340.38 g/mol), CL-54-04 (354.40 g/mol).

To treat tuberculosis, a combination of anti-mycobacterial agents are used in an effort to minimise the emergence of resistance. It has been proposed that an ICL inhibitor could be used in combination with current anti-TB drugs to decrease the treatment time as well as to minimise the emergence of resistance, as transcription levels of *icl1* are increased in Mtb in response to antibiotic treatment (Nandakumar *et al.*, 2014). Therefore, a drug combination study, by checkerboard assay, was used to assess the potency of the CL-54 drug family with currently employed anti-mycobacterial agents such as rifampicin and bedaquiline in comparison to their individual activities.

The checkerboard set up as shown in Figure 6-2, in which drug A and B is pipetted on its own and with combination with each other in a series of dilution, covering a range

of concentrations above and below the known MIC of the desired drug. The optical density at 595 nm is measured to assess growth inhibition.

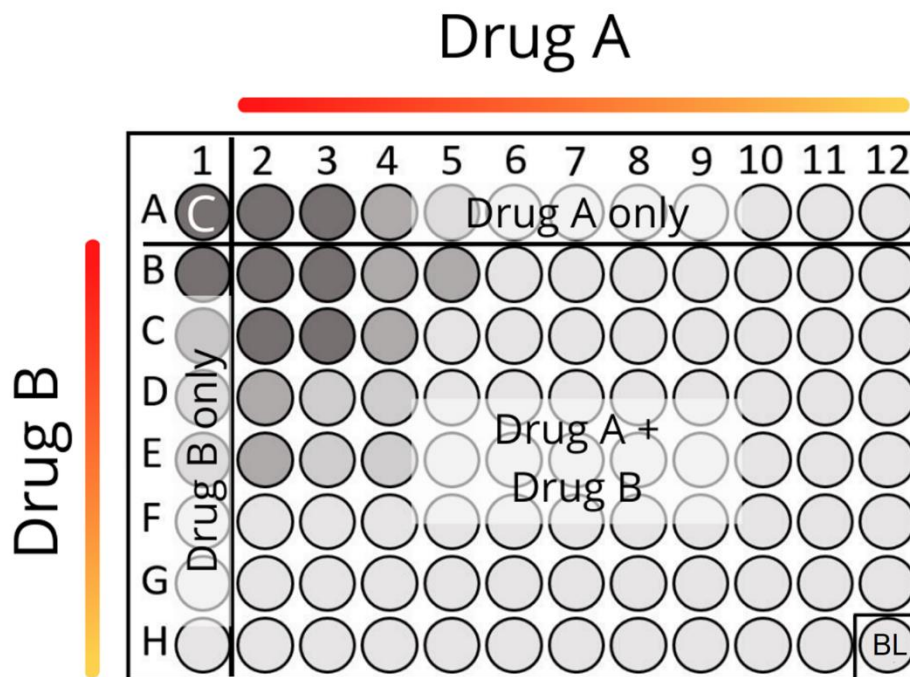


Figure 6-2: Diagrammatic representation of the checkerboard assay. A series of dilutions of Drug A is pipetted along the abscissa (the first row is drug A only to serve as a control), whilst Drug B is pipetted along the ordinate (the first column is drug B only to serve as control). Red to yellow represents the drug concentration, where red is the most concentrated and yellow the least. C stands for control, in which the mycobacteria are grown without any drug. BL stands for blank as it is only media without mycobacteria to ensure there is no contamination.

The comparison is then represented as the Fractional Inhibitory Concentration (FIC) index value. The FIC index value takes into consideration the combination of drug A + B that produces the greatest change from the individual drug's MIC. To quantify the FIC index values, the following equation is used:

$$\text{FIC index} = \frac{\text{MIC Drug A in combination}}{\text{MIC drug A alone}} + \frac{\text{MIC Drug B in combination}}{\text{MIC drug B alone}}$$

The FIC index value is used to categorise the interaction of drugs A and B as synergy, antagonism, additive or indifference – Table 5.

Table 5: Categories of Fractional Inhibitory Concentration (FIC) index

Category	FIC value
Synergy	<0.5
Additive	0.5-2
Indifference	2-4
Antagonist	>4

Synergy is when the combination of drug A and B results in an FIC value of <0.5, which means the combination increases the inhibitory activity of one or both compounds than the compound's MIC alone. The additive effect is when the combination of compounds results in an FIC value between 0.5-2, meaning the combination has no increase in inhibitory activity. Indifference (FIC value = 2-4) is the concentration used of each drug combined is no different from the MIC of each drug alone. Antagonism is when the combination of compounds (FIC value >4) increases the MIC or lower the activity of the compounds (Odds, 2003). Based on the FIC index value, the best drug combination will be selected and used to do a colony-forming unit, and metabolomics analysis to gain an understanding of the drug's effect on Mtb metabolism.

Both the glyoxylate shunt and methylcitrate cycle are metabolic pathways that are required to assimilate fatty acids (Upton and McKinney, 2007; Puckett *et al.*, 2017). To mimic this environment, carbon-defined propionate media was used for these experiments, with glycerol media as the control (main carbon source commonly used in TB research). Two strains were used, Mtb Erdman wild-type and a BSL2 version originated from Mtb H37Rv strain, mc²6206. The former is a standard virulent laboratory strain for virulence and immunisation studies (Miyoshi-Akiyama *et al.*, 2012). The former was generated as an auxotrophic strain for leucine and pantothenate and showed a lack of lethality in immunocompromised and immunocompetent mice (Vilchèze *et al.*, 2018). This strain was used to circumvent the absence of a plate reader inside the BSL3, enabling to perform the checkerboard assay.

Materials and Methods

Bacterial strains and culture conditions

Mycobacterium tuberculosis (Mtb) Erdman wild-type (Erd WT) or H37Rv $\Delta panCD \Delta leuCD$ (mc²6206) was pre-cultured in Middlebrook M7H9 broth (Difco, Detroit, MI) supplemented with 0.5% (w/v) fraction V bovine serum albumin (BSA), 0.085% (w/v) NaCl, 0.04% (v/v) tyloxapol with 0.2% (v/v) glycerol and 0.2% (w/v) dextrose. For H37Rv $\Delta panCD \Delta leuCD$ (mc²6206), the media was further supplemented with 24 mg/L L-pantothenate and 50 mg/L L-leucine. For experiments, the strains were centrifuged and resuspended in fresh M7H9 containing BSA, NaCl, tyloxapol and a carbon source were added when appropriate (0.2% (v/v) glycerol or 0.05-0.1% (w/v) propionate). For metabolomic profiling, filters were generated as previously described (de Carvalho *et al.*, 2010; Eoh and Rhee, 2013). Briefly, a Mtb culture of OD₅₉₅ 1.0 was transferred into a 22 mm 0.22 μ m nitrocellulose filter under vacuum filtration and incubated on a chemically defined agar (M7H10) at 37 °C for 5 days. The Mtb-laden filters were then transferred to an M7H10 with either 0.2% (v/v) glycerol or acetate, and with or without a combination of the drug or the drug alone (CL-54-04, bedaquiline or rifampicin). Mtb Erdman was cultured in containment of biosafety level 3 facility.

Bacterial growth curves and Colony-forming unit (CFU) assay

Bacterial growth was monitored by optical density (OD) at 595 nm using a spectrophotometer GENESYS™ 20 (Thermo Scientific). For CFU assays, mid-logarithmic phase of Mtb Erd was diluted to OD₅₉₅ 0.05 in M7H9 broth containing BSA, NaCl, tyloxapol and supplemented with 0.2% (v/v) glycerol or 0.05-0.1% (w/v) propionate and antibiotics, rifampicin (Sigma, USA), bedaquiline (AChemBlock, Burlingame, CA, USA) or CL-54 drug family, when applicable, in a 24 or 96 well plate. After 5 or 7 days of antibiotic treatment (rifampicin and bedaquiline), the cells were then serially diluted and plated on M7H10 agar with 0.5% (v/v) glycerol, 0.2% (w/v) dextrose, 0.5 g/L BSA and 0.085% (w/v) NaCl for 3 weeks at 37 °C until the colonies formed.

Drug combination analysis by checkerboard assay

H37Rv $\Delta panCD \Delta leuCD$ (mc²6206) was cultured in M7H9 containing BSA, NaCl, tyloxapol, 0.2% (v/v) glycerol and 0.2% (w/v) dextrose and supplemented with 24 mg/L L-pantothenate and 50 mg/L L-leucine until OD₅₉₅ was in mid-logarithmic phase. The culture was centrifuged and resuspended with M7H9 containing NaCl, tyloxapol, either 0.2% (v/v) glycerol or 0.05% (w/v) propionate and supplemented with 24 mg/L L-pantothenate and 50 mg/L L-leucine. The drug stocks, CL-54-04, itaconate (Sigma, USA), bedaquiline (ACChemBlock, Burlingame, CA, USA) or rifampicin (Sigma, USA) were prepared and diluted at a range of concentrations immediately prior to testing. The first drug was serially diluted along the ordinate, whilst the second drug was diluted along the abscissa (Orhan *et al.*, 2005) with a final volume of 10 μ L. The first column and the first row contained each drug alone. 50 μ L of M7H9 containing the required nutrients was distributed into each well. The culture (100 μ L) was added to each well with a final OD₅₉₅ of 0.05. Media only and media with culture were included in every plate as controls (Figure 6-2). The plate was incubated at 37 °C and 2% (v/v) CO₂. Bacterial growth was monitored by optical density at 595 nm by using a spectrophotometer GENESYS™ 20 (Thermo Scientific) after 7 days.

Metabolite extraction for LC-MS analysis

The nitrocellulose filters containing Erdman WT were incubated at 37 °C. After reaching the mid-logarithmic phase of growth (approximately 5 days), the filters were transferred to chemically identical M7H10 agar containing fresh a carbon source(s) and antibiotics when applicable and incubated for 24 hours at 37 °C. The metabolites were harvested by transferring the filters into pre-cooled -40 °C LC-MS-grade acetonitrile:methanol:water (40:40:20) solution and mechanically lysed with 0.1 mm Zirconia beads in a Precellys tissue homogeniser (Bertin Technologies, France) at 6,800 rpm for 6 minutes in dry ice. Lysates were centrifuged and filtered using 0.22 μ M Spin-X columns. Protein concentrations of metabolite extracts were measured (BCA protein assay kit; Thermo Scientific, Waltham, MA, USA) to normalise samples to cell biomass (Lee *et al.*, 2018).

Liquid Chromatography-Mass Spectrometry (LC-MS) for metabolomics profiling

LC-MS differentiation and detection of Erdman was performed with an Agilent Accurate Mass 6230 TOF coupled with an Agilent 1290 Liquid Chromatography

system using solvents and configuration as previously described (Eoh and Rhee, 2013). An isocratic pump was used for continuous infusion of a reference mass solution to allow mass axis calibration. Detected ions were classified as metabolites based on unique, accurate mass-retention time identifiers for masses showing the expected distribution of accompanying isotopologues. Metabolites were analysed using Agilent Qualitative Analysis B.07.00 and Profinder B.06.00 software (Agilent Technologies, Santa Clara, CA, USA) with a mass tolerance of <0.005 Da. Standards of authentic chemicals of known amounts were mixed with bacterial lysates and analysed to generate the standard curves used to quantify metabolite levels (Eoh and Rhee, 2013).

Results

The first experiments include testing a range of concentrations of CL-54 drugs to measure the growth inhibition of an ICL inhibitor in the Erdman wild type by optical density (OD_{595}) and colony-forming unit (CFU). The drugs were tested using the Erdman strain in two sole carbon sources (glycerol and propionate), to distinguish if the compound is active when the bacteria are replicating (glycerol condition) or slowly replicating (propionate condition) (Eoh and Rhee, 2013). The former condition is when ICL is actively required in the glyoxylate shunt and methylcitrate cycle.

CL-54-01 was the first in the drug family to be tested. Although the normal monitoring course is 21 days, CL-54-01 was tested at 200 μ M for only 9 days (Figure 6-3). This was because no immediate effect was observed in the growth by optical density at a high concentration of 200 μ M, suggesting that CL-54-01 is not effective against the whole organism.

CL-54-01

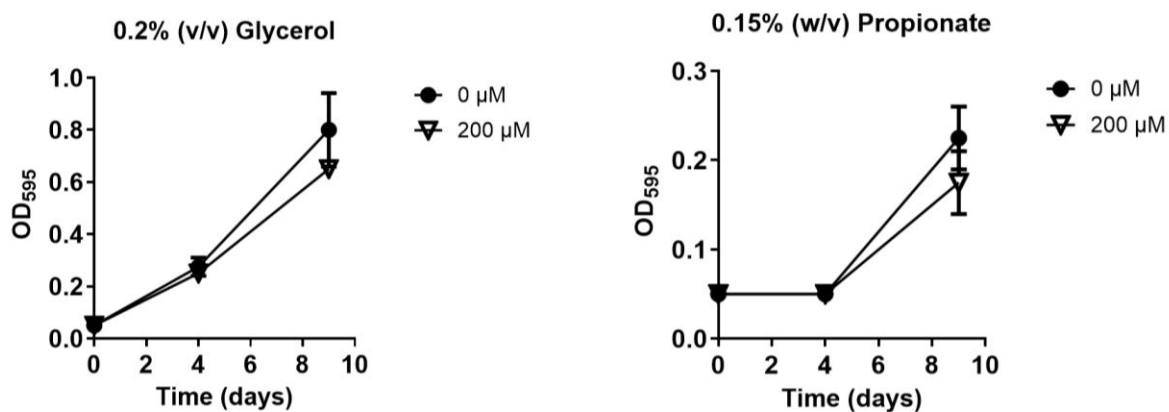
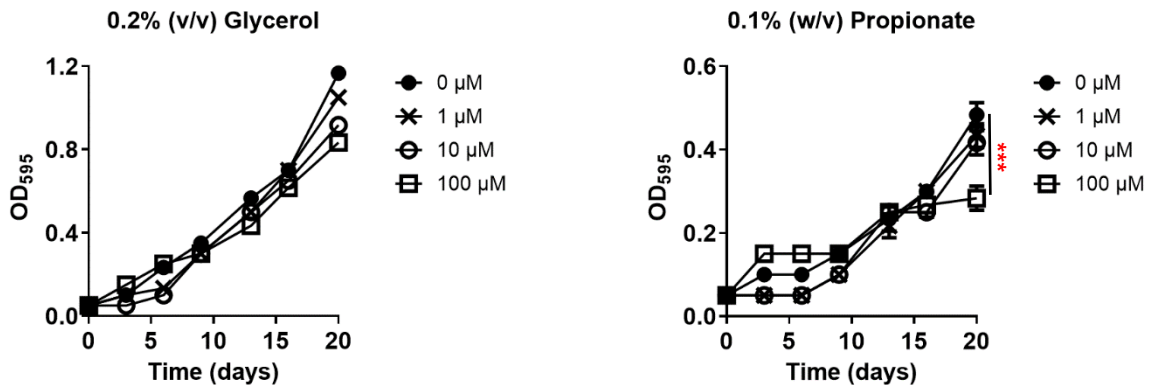


Figure 6-3: Effect of CL-54-01 in the growth of Mtb Erdman wild type in both glycerol and propionate media for 9 days. Data represent an average of three biological replicates.

The effect of the other two drugs, CL-54-02 and CL-54-04, was monitored by optical density (595 nm) over a 21-day period, using 1, 10 and 100 μM (Figure 6-4).

CL-54-02



CL-54-04

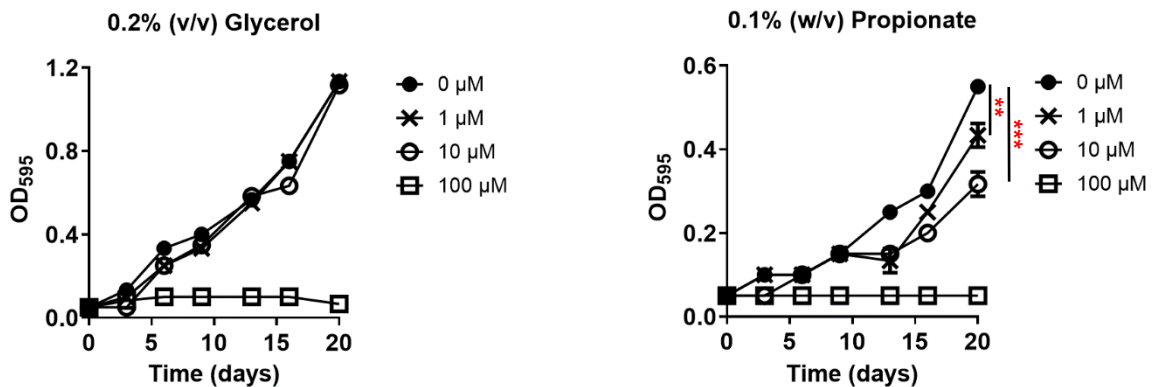
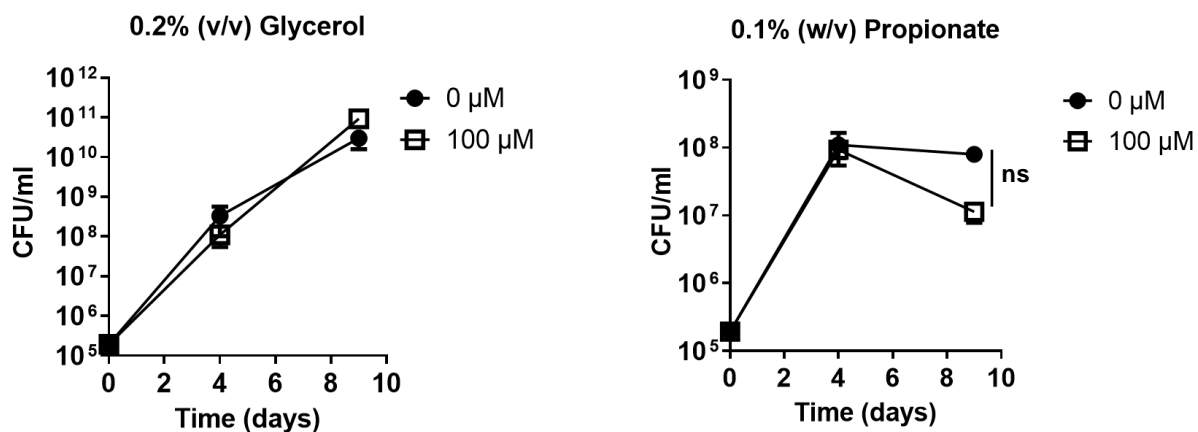


Figure 6-4: Effect of CL-54-02 and CL-54-04 in the growth of Mtb Erdman strain in both glycerol and propionate as sole carbon sources. Data represents an average of three biological replicates, and error bars are standard deviations. ***P<0.001 by two-way ANOVA.

No CL-54-02 effect was seen in glycerol media at the concentrations tested; however, the growth was slightly delayed with 100 μ M in propionate media. The effect of 1 and 10 μ M CL-54-04 had a significant growth inhibition in propionate media but no effect on glycerol media, whereas 100 μ M inhibited growth in both carbon sources.

From all three analogues, CL-54-01 was shown to be the least effective. The other two analogues were assessed by CFU experiments. After being challenged with the analogues, the bacteria were serially diluted and plated at 4 and 9 days (Figure 6-5).

CL-54-02



CL-54-04

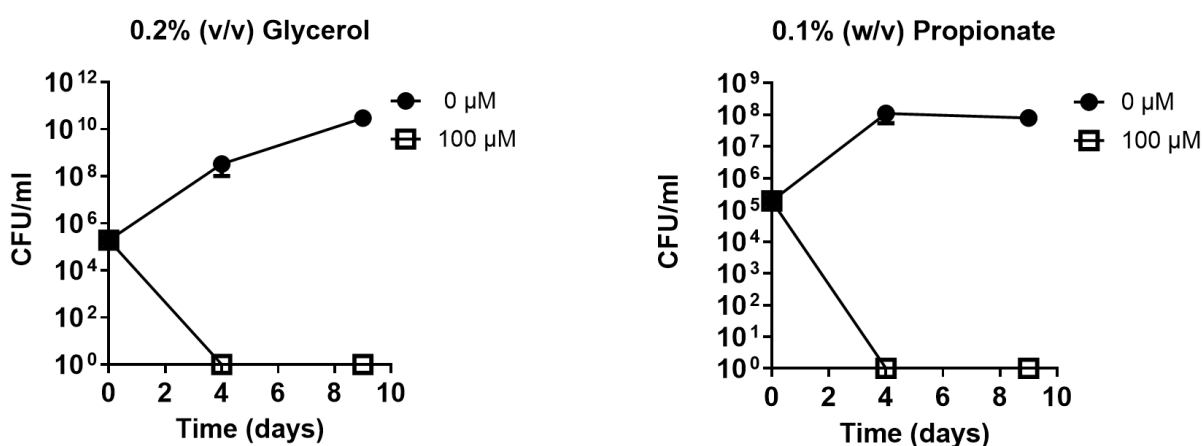


Figure 6-5: Effect of 100 μ M CL-54-02 and CL-54-04 in the growth of Mtb Erdman in glycerol and propionate media. Time points were 0, 4 and 9 days. Data represent an average of three biological replicates, and error bars are standard deviations. Ns, not significant by two-way ANOVA.

As with the growth in liquid culture, 100 μ M CL-54-02 had no effect on Mtb colony formation. CL-54-04, however, had a bactericidal effect on Mtb on both carbon sources at 100 μ M. Thus, a lower range of CL-54-04 concentrations was further tested (Figure 6-6).

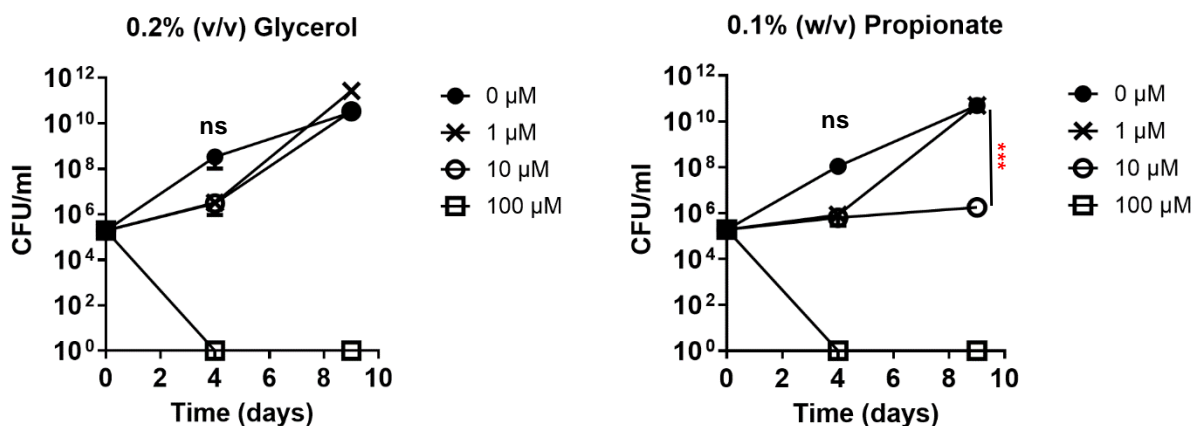


Figure 6-6: Colony-forming unit of Mtb Erdman challenged with different concentrations (1, 10 and 100 μM) of CL-54-04 in both glycerol and propionate media. Data represent an average of three biological replicates, and error bars are standard deviations. ***P<0.001; Ns, not significant by two-way ANOVA.

Although CL-54-04 had a bactericidal effect at 100 μM, a checkerboard experiment was done as an effort to identify the drug concentration needed by combining with other antimycobacterial drugs. For comparison, itaconate – a known ICL inhibitor with a high toxicity effect – was used as a control. Given the equipment limitations of the BSL3 facility, the checkerboard assay was carried out using an *M. tuberculosis* BSL2 strain, mc²6206 (H37Rv Δ*panCD* Δ*leuCD*), that is an auxotrophic attenuated version of BSL3 Mtb H37Rv (Jain *et al.*, 2014; Vilchèze *et al.*, 2018), which has only one functional ICL isoform as the *aceA* gene (encoding for ICL2) is split into two, rendering Mtb with only one copy of ICL. Thus, this strain is likely to be more sensitive to an ICL inhibitor than a strain with both functional isoforms.

First, itaconate was combined with bedaquiline using glycerol (Table 6) and propionate (Table 7) as sole carbon sources. The mycobacteria's drug sensitivity varies with the carbon source (Bald *et al.*, 2017; Kalia *et al.*, 2019); thus, the drug range used in propionate media was at a lower concentration than in glycerol. The colour scheme is used to demonstrate a range in which red represents the lowest FIC index (either synergy or additive) and green the highest (indifference or antagonistic). Given the limitation of the strain used, these experiments are representative.

Table 6: FIC index for the combination of itaconate and bedaquiline against mc²6206 with glycerol as a sole carbon source.

		Itaconate (mM)				
		1.25	2.5	5	10	20
Bedaquiline (µg/mL)	0.0375	1.7	0.9	0.6	1.0	1.2
	0.075	1.4	0.4	0.7	1.0	1.3
	0.15	0.8	0.6	1.2	1.5	2.2
	0.3	1.1	1.1	1.9	2.1	4.0
0.2% (v/v) Glycerol						

Table 7: FIC index for the combination of itaconate and bedaquiline against mc²6206 with propionate as a sole carbon source.

		Itaconate (mM)				
		0.4	0.6	0.8	1	1.2
Bedaquiline (µg/mL)	0.0035	2.2	2.2	2.3	2.3	2.2
	0.0052	2.1	2.1	2.1	2.2	1.8
	0.007	2.2	2.2	2.2	2.3	2.0
	0.011	2.0	2.0	2.0	2.0	2.0
	0.017	2.1	2.0	1.7	1.7	1.5
	0.026	1.5	1.3	1.2	1.2	1.4
0.05% (w/v) Propionate						

The combination 2.5 mM itaconate with 0.075 µg/mL bedaquiline caused a synergistic effect in glycerol media. Itaconate at all concentrations tested was additive with bedaquiline in propionate media, with the lowest concentrations of both drugs used were 0.8 mM itaconate and 0.026 µg/mL bedaquiline.

The following combination tested was itaconate with rifampicin in both carbon sources: glycerol (Table 8) and propionate (Table 9).

Table 8: FIC index for the combination of itaconate and rifampicin against mc²6206 with glycerol as a sole carbon source.

		Itaconate (mM)				
		0.625	1.25	2.5	5	10
Rifampicin ($\mu\text{g}/\text{mL}$)	0.0625	2.1	2.2	1.2	1.6	1.6
	0.125	1.9	1.8	1.0	2.1	2.0
	0.25	1.8	1.4	1.2	2.9	2.1
	0.5	1.5	1.6	1.7	2.4	2.6
	1	1.5	1.7	1.8	2.5	2.7
0.2% (v/v) Glycerol						

Table 9: FIC index for the combination of itaconate and rifampicin against mc²6206 with propionate as a sole carbon source.

		Itaconate (mM)				
		0.625	1.25	2.5	5	10
Rifampicin ($\mu\text{g}/\text{mL}$)	0.03125	2.1	2.2	1.8	1.9	1.4
	0.0625	2.0	2.0	1.6	2.0	1.7
	0.125	1.9	1.9	1.7	2.2	1.6
	0.25	1.8	1.4	1.6	2.1	1.8
	0.5	1.3	1.3	1.6	2.1	1.6
0.05% (w/v) Propionate						

The combination of rifampicin with itaconate lead to an additive effect in both carbon sources, in which 2.5 mM itaconate and 0.125 $\mu\text{g}/\text{mL}$ rifampicin was the best combination for glycerol media, and 0.625 mM itaconate and 0.5 $\mu\text{g}/\text{mL}$ rifampicin for propionate as a sole carbon source.

The same experiment was done using CL-54-04 in combination with bedaquiline in both glycerol (Table 10) and propionate (Table 11) as sole carbon sources. The rationale for decreasing the concentration of CL-54-04 in propionate media (250 – 7.81 μM as opposed to 500 – 15.62 μM in glycerol) is because Mtb depends on ICL for propionate metabolism, and therefore, a lower ICL inhibitor concentration may be required.

Table 10: FIC index for the combination of bedaquiline and CL-54-04 against mc²6206 with glycerol as a sole carbon source.

		Bedaquiline (µg/mL)				
		0.018	0.0375	0.075	0.15	0.3
CL-54-04 (µM)	15.62	2.5	2.5	2.4	2.2	0.8
	31.25	2.8	2.7	2.7	2.7	0.9
	62.5	2.9	3.0	2.9	5.2	1.0
	125	5.2	6.0	9.8	9.0	1.2
	250	11.1	10.7	12.0	6.1	1.8
	500	19.0	9.7	7.3	7.2	2.1
0.2% (v/v) Glycerol						

Table 11: FIC index for the combination of bedaquiline and CL-54-04 against mc²6206 with propionate as a sole carbon source.

		Bedaquiline (µg/mL)				
		0.052	0.007	0.011	0.017	0.026
CL-54-04 (µM)	7.81	1.9	1.8	1.8	1.8	3.6
	15.62	2.0	1.9	1.9	1.9	3.6
	31.25	2.0	1.8	1.9	1.9	3.9
	62.5	2.5	2.4	2.4	2.6	6.4
	125	3.6	3.5	3.5	3.6	9.0
	250	3.2	2.9	3.0	3.2	8.2
0.05% (w/v) Propionate						

Only an additive effect was seen when in combination with bedaquiline under both carbon sources. In glycerol media, the best combination was 0.3 µg/mL bedaquiline and 15.6 µM CL-54-04. In propionate media, the best additive effect was 0.0052 µg/mL bedaquiline and 7.8 µM CL-54-04.

The combination of CL-54-04 and rifampicin was also tested in glycerol (Table 12) and propionate (Table 13).

Table 12: FIC index for the combination of rifampicin and CL-54-04 against mc²6206 with glycerol as a sole carbon source.

		Rifampicin (µg/mL)				
		0.00781	0.01563	0.03125	0.0625	0.125
CL-54-04 (µM)	15.62	2.0	1.7	2.6	1.4	1.2
	31.25	2.2	2.1	2.4	1.7	1.3
	62.5	4.1	2.9	2.8	1.7	1.4
	125	4.9	4.0	3.0	1.7	1.6
	250	7.0	3.5	4.1	1.6	1.6
	500	12.8	9.6	6.9	3.3	3.0
0.2% (v/v) Glycerol						

Table 13: FIC index for the combination of rifampicin and CL-54-04 against mc²6206 with propionate as a sole carbon source.

		Rifampicin (µg/mL)				
		0.00391	0.00781	0.01563	0.03125	0.0625
CL-54-04 (µM)	7.81	2.3	2.2	2.2	1.8	2.9
	15.62	2.3	2.2	2.2	2.3	2.8
	31.25	2.3	2.2	2.2	2.9	3.0
	62.5	2.8	3.1	4.1	3.2	3.4
	125	5.5	5.4	4.5	3.9	4.2
	250	7.6	7.4	6.9	4.9	4.9
0.05% (w/v) Propionate						

The combination of CL-54-04 and rifampicin had an additive effect in both carbon sources at the concentrations tested. The best combination when glycerol is the sole carbon source is 0.0625 µg/mL rifampicin and 15.6 µM CL-54-04, keeping the rifampicin concentration lower than the MIC (0.125 µg/mL). In propionate media, 0.03125 µg/mL rifampicin and 7.8 µM CL-54-04 had the best additive effect. Based on the FIC index results, a colony-forming unit (CFU) assay was done using the drug combinations (bedaquiline and rifampicin with CL-54-04) under glycerol condition – Figure 6-7.

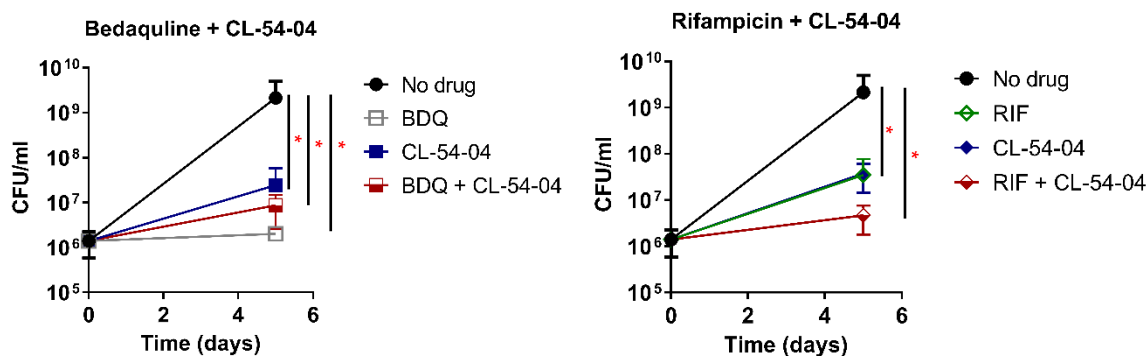


Figure 6-7: Drug combination effect of CL-54-04 with bedaquiline (BDQ) and rifampicin (RIF) against Mtb Erdman strain in 0.2% (v/v) glycerol M7H10 media. Drug concentrations were based on the FIC index: 0.3 $\mu\text{g/mL}$ bedaquiline with 15.6 μM CL-54-04 and 0.0625 $\mu\text{g/mL}$ rifampicin with 15.6 μM CL-54-04. Data represent an average of three biological replicates, and error bars are standard deviations. * $P < 0.01$ by two-way ANOVA.

There was no bactericidal effect in both drug combinations at the concentrations tested. Nonetheless, bedaquiline alone caused a bacteriostatic effect, whereas CL-54-04 alone only slowed down the growth by 100-fold. Surprisingly, the combination of CL-54-04 and bedaquiline slowed down the growth similarly to CL-54-04 alone. The effect of rifampicin with CL-54-04 slowed down the growth by 1000-fold, though it was not bacteriostatic. Both drugs alone (15 μM CL-54-04 and 0.0625 $\mu\text{g/mL}$ rifampicin) had the same effect on growth (decreased of 100-fold).

This experiment was done alongside a metabolomic analysis of the TCA cycle, MCC, and GABA shunt using the same drug combinations. Filters containing mid-logarithmic phase wild-type Erdman strain were incubated on M7H10 plates containing either glycerol or propionate and the drugs at their appropriate concentrations (Figures 6-8 and 6-9). Each plate had three filters, and the average values are depicted for each metabolite in ion count/mg.

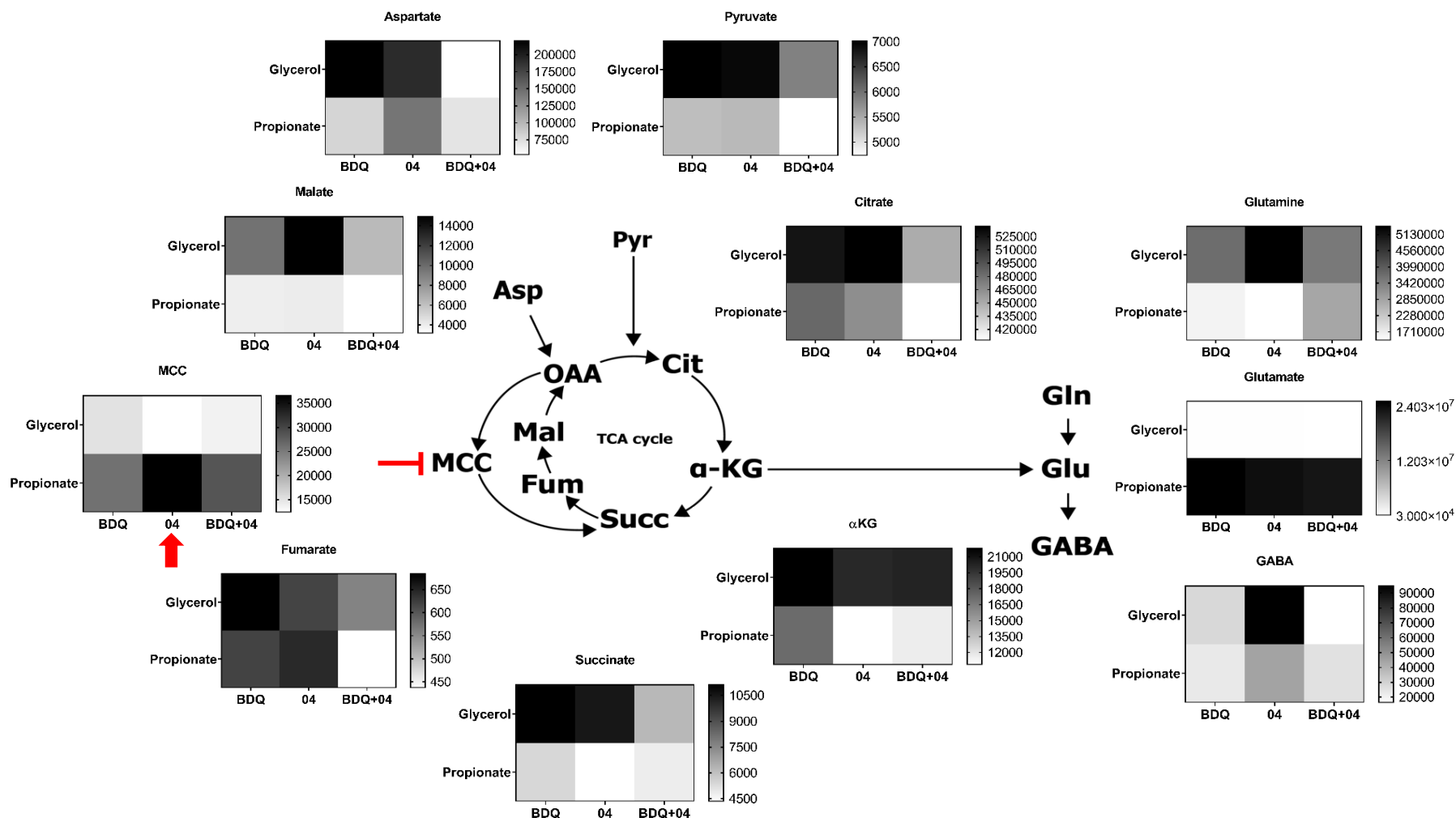


Figure 6-8: The inhibition of ICL in Erdman wild type by CL-54-04 leads to an increase in methylcitrate cycle (MCC) intermediates in propionate media. In glycerol (0.2% v/v) condition, the drug combination used was 15.62 μM CL-54-04 and 0.3 $\mu\text{g}/\text{mL}$ bedaquiline. In propionate (0.1% w/v) condition, the drug combination was 7.81 μM CL-54-04 and 0.0052 $\mu\text{g}/\text{mL}$ bedaquiline. Values depicted are ion count/mg and are an average of three biological replicates. BDQ, bedaquiline; 04, CL-54-04. MCC, 2-methyl-cis-aconitate and 2-methyl-isocitrate.

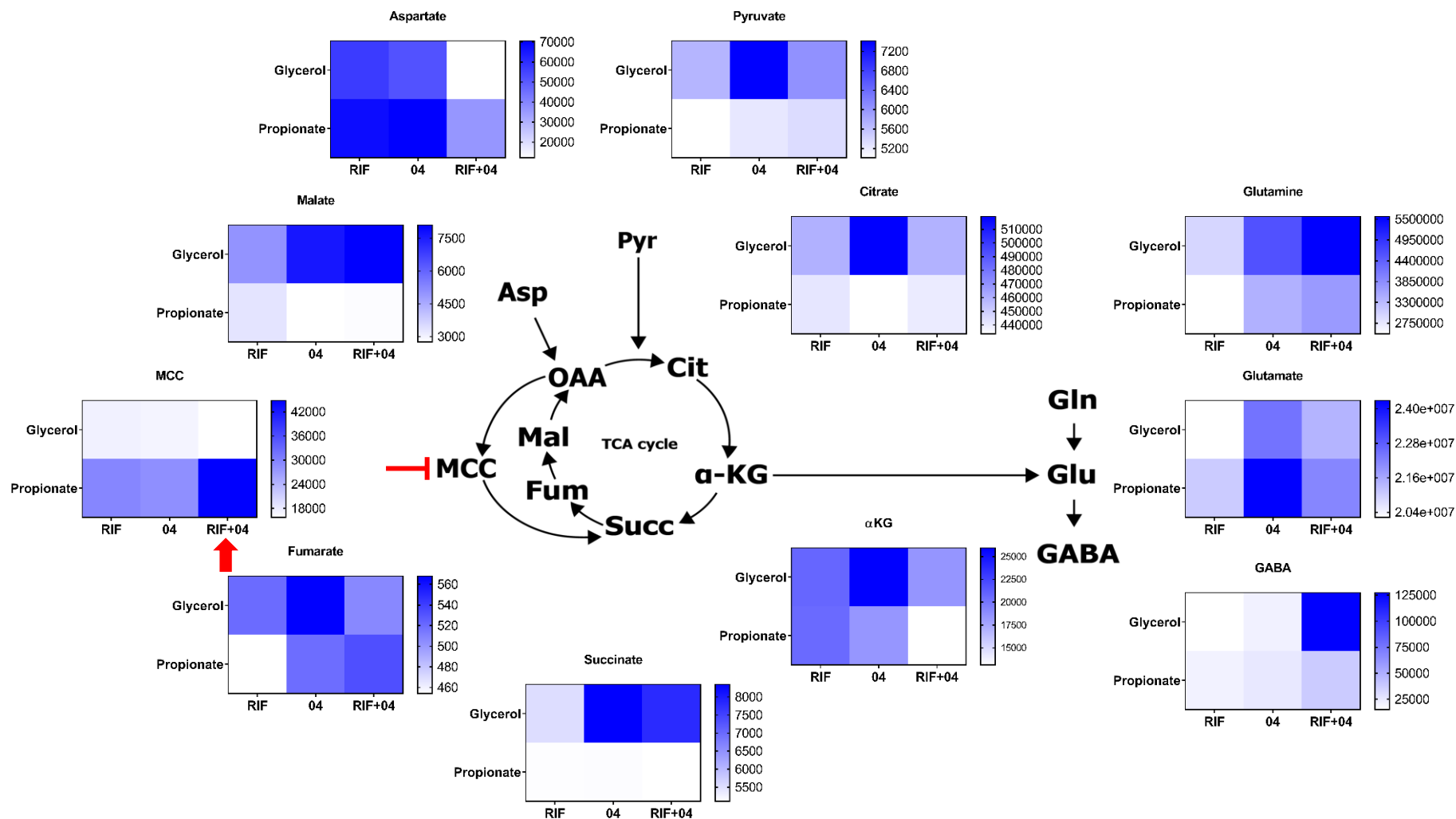


Figure 6-9: The combination of rifampicin and CL-54-04 leads to an increase in MCC metabolites in Erdman wild type in propionate media. In glycerol (0.2% v/v) condition, the drug combination used was 15.62 μM CL-54-04 and 0.0625 $\mu\text{g}/\text{mL}$ rifampicin. In propionate (0.1% w/v) condition, the drug combination was 7.81 μM CL-54-04 and 0.03125 $\mu\text{g}/\text{mL}$ rifampicin. Values depicted are ion count/mg and are an average of three biological replicates. RIF, rifampicin; 04, CL-54-04. MCC, 2-methyl-cis-aconitate and 2-methyl-isocitrate.

In glycerol condition (Figure 6-8), CL-54-04 alone has a high accumulation of TCA cycle metabolites when compared to propionate and an accumulation of both glutamine and GABA. The combination of BDQ and CL-54-04 in propionate media leads to a downregulation of pyruvate, citrate, fumarate and malate when compared to each drug individually. CL-54-04 alone in propionate media leads to a downregulation of α KG, succinate and glutamine, but upregulation of the MCC. All three conditions lead to an accumulation of glutamate in propionate media. When CL-54-04 is combined with rifampicin in glycerol media (Figure 6-9), both glutamine and GABA are accumulated, but there is a decrease in aspartate. In propionate media, the combination of CL-54-04 and rifampicin leads to an accumulation of the MCC. All three conditions lead to a decrease in succinate when propionate is the sole carbon source.

Discussion

A drug is classified as bacteriostatic or bactericidal depending on its efficiency against the bacteria. The former usually refers to an agent that prevents the growth of bacteria, such as keeping them in a stationary phase of growth, while the latter refers to an agent that kills the bacteria (Pankey and Sabath, 2004). However, the same agents considered bactericidal may exhibit bacteriostatic activity at low concentrations (Wald-Dickler *et al.*, 2018) or depending on the stage of bacterial growth (Bakker-Woudenberg *et al.*, 2005). A compound with bactericidal effects rather than bacteriostatic is usually preferred in clinical settings as this may limit the development of resistance (Stratton, 2003). Nonetheless, bacteriostatic agents can kill the bacteria; they just require a higher concentration than bactericidal agents to achieve specific thresholds of bacterial reduction (Wald-Dickler *et al.*, 2018). However, high drug concentrations are more likely to result in stronger adverse effects. A combination of one or more drugs is a standard approach to treat a series of infections to prevent resistance from arising, which is often seen with one drug alone (Fischbach, 2011; Tamma *et al.*, 2012). This is the case of TB treatment, in which two or more anti-mycobacterial drugs is given to prevent antimicrobial resistance (Sun *et al.*, 2016). Both regimens for TB and multidrug resistance TB consists of combinatory therapy, though not all anti-TB drugs are bactericidal. For instance, ethambutol (EMB) is considered bacteriostatic, but higher concentrations are used to

obtain a bactericidal effect. Its principal role has been as a companion drug to prevent resistance, such as macrolide resistance when treating *M. avium* complex (Xu *et al.*, 2018). Ethionamide and prothionamide are both bacteriostatic drugs and are used to treat MDR-TB in combination with D-cycloserine, para-aminosalicylic acid, terizidone, and thioacetazone (Onyebujoh *et al.*, 2005; WHO, 2018). Thus, a combination of bactericidal and bacteriostatic drugs is employed to treat tuberculosis.

A new family of drugs (CL-54 compounds) that had been identified as powerful ICL inhibitors (Chapter 4) and were investigated against Mtb to assess their anti-mycobacterial properties. CL-54-01 did not cause any bactericidal or bacteriostatic effect at 200 μM in both carbon sources for 9 days. However, it is unknown if a later effect would be seen if the experiment was prolonged until 21 days. This is seen with 100 μM CL-54-02, where a significant growth defect was only observed at 21 days in propionate media. Nonetheless, no effect was seen in both carbon sources with the other two concentrations (1 and 10 μM) tested. Interestingly, CL-54-04 show a bactericidal effect at 100 μM in both carbon sources and a bacteriostatic effect at 10 μM in propionate media only. This effect may be because Mtb heavily relies on the glyoxylate and methylcitrate cycles to survive in propionate media, in which ICL is a key enzyme in both pathways. Thus, 10 μM of the ICL inhibitor is enough to prevent Mtb's growth. When ICL is not essential for Mtb's survival (glycerol condition), the bacterial growth was comparable to control organisms. Evidently, the drug effect is different depending on the carbon source.

These CL-54 analogues differ in their functional groups, in which both CL-54-01 and CL-54-02 have one or two hydroxyl groups attached to the benzene ring (Figure 6-1). The former has two hydroxyl groups in meta and para positions, whilst the latter has one hydroxyl group in the para position. Similarly to CL-54-02, CL-54-04 has a hydroxyl group in the para position but an additional methyl group in the ortho position. As the rest of the structure is similar, and only CL-54-04 has bactericidal effects, it suggests that the methyl group in the ortho position is responsible for this phenotype. The methyl group might be allowing the drug to penetrate due to solvation and by increasing the affinity to cell membrane lipids, whereas CL-54-01 and CL-54-02 have one or two hydroxyl groups, without the additional methyl, making more polar which may affect their cellular uptake.

Drug combinations can reduce the treatment period, limit the development of resistance and cause milder side effects, all of which aim to increase the likelihood of treatment completion and success (Shin *et al.*, 2015). Toxic side effects associated with antimicrobial agents can be decreased when the dosage is reduced through synergistic combination therapy (Xu *et al.*, 2018). Thus, implementing an ICL inhibitor with current regimens is promising as it can shorten the treatment duration for active TB due to ICL's role in antibiotic resistance (Nandakumar *et al.*, 2014).

In this study, CL-54-04 was screened with rifampicin (RIF) and bedaquiline (BDQ) to identify a synergistic combination. The choice of the drug was based on the mode of action and clinical relevance. Both rifampicin and bedaquiline are clinically used drugs to treat TB. Rifampicin is one of the first-line drugs that inhibit the mycobacteria's RNA polymerase. The combination of an ICL inhibitor with an RNA polymerase inhibitor can be powerful as any Mtb response (such as overexpression of ICL or expression of stress response factors) would rely on a functional RNA polymerase. Bedaquiline is a second-line drug that inhibits ϵ and γ subunits of the Mtb's ATP synthase (Andries *et al.*, 2005; Koul *et al.*, 2007; Shin *et al.*, 2018). It can be hypothesised that inhibiting ICL would increase the accumulation of methylcitrate cycle metabolites, slowing down the TCA cycle and ultimately downregulating the ETC activity (Eoh and Rhee, 2014). Thus, combining bedaquiline with an ICL inhibitor could have a synergistic effect. This hypothesis was supported by the checkerboard assay done with itaconate.

Ideally, the concentrations needed of each drug in combination would require lower concentrations than the ones needed to kill or inhibit Mtb's growth on its own. Therefore, the concentrations screened in the checkerboard assay were below the minimal inhibitory concentration (MIC) of each drug. At the concentrations tested in the checkerboard assay, only an additive effect was observed when CL-54-04 and BDQ or RIF were combined in both carbon sources. The additive effect of CL-54-04 with BDQ, however, was not observed in the colony formation assay at the time point analysed, whilst in combination with RIF, there was some degree of additive effect (Figure 6-7). Neither CL-54-04 combinations had a bacteriostatic or bactericidal effect.

The disparity between the checkerboard assay and the CFU assay results may be for two reasons. The first one is the point of the growth curve of the bacteria. In the checkerboard assay, the OD₅₉₅ of 0.05 of mc²6206 is required to assess whether the drug combination prevents the mycobacterial's growth (which suggests CL-54-04 combination with either rifampicin or bedaquiline is a growth inhibitor but not bactericidal). However, in the CFU assay, an OD₅₉₅ of 0.5 was used as the start for colony-forming experiments (allowing to assess a bactericidal or bacteriostatic effect). At which point, there are not only 10-fold more bacteria than in the checkerboard assay, but they also highly diverge in their metabolic state, so the effect of the drug might be different. It has been reported that the same drug can have a bacteriostatic effect in one growth stage but be bactericidal in another (Pankey and Sabath, 2004). For instance, Mtb is less susceptible to isoniazid in the lag phase than at the later growth stages, and thus, its bactericidal activity is most notable in the log phase (Yamori *et al.*, 1992). However, it is promising that the combination of CL-54-04 with either BDQ or rifampicin is a growth inhibitor at low concentrations of CL-54-04 (7-15 µM). Anti-mycobacterial agents that have significant activity at a low growth rate are an important determinant for therapeutic efficacy given the low metabolic activity of dormant mycobacteria residing in the host's tissues (Bakker-Woudenberg *et al.*, 2005). At the site of infection, the metabolic activity intracellularly is extremely low, and thus, inhibiting the growth of the mycobacteria in this state can be an advantage (Bakker-Woudenberg *et al.*, 2005).

The second reason lies in the strains used for each assay. Due to the lack of a microplate spectrophotometer in the BSL3, an avirulent strain of *Mycobacterium tuberculosis* H37Rv (that requires leucine and vitamin B12 for growth) was used for the checkerboard experiment, whereas the colony-forming experiment was done with the *Mycobacterium tuberculosis* Erdman strain. Both H37Rv and Erdman are laboratory strains that have been widely used as standard laboratory strains for virulence and immunisation studies (Dunn and North, 1995; Miyoshi-Akiyam *et al.*, 2012). They are as virulent as the other clinical isolates, such as the NCGM2209 strain, as tested in mice (Miyoshi-Akiyama *et al.*, 2011). H37Rv genome has the *icl1* gene (Rv0467); however, unlike Erdman and other Mtb strains, the *aceA* gene (coding for ICL2) is split into two parts: *aceAa* and *aceAb* (Rv1915 and Rv1916) (Kapopoulou *et al.*, 2011). Consequently, it is more likely that Mtb

H37Rv will show more sensitivity to an ICL inhibitor compared with a strain that has both enzyme copies. In addition, the Mtb H37Rv strain used in the checkerboard assay is attenuated and reclassified as BSL2 (Vilchèze *et al.*, 2018). This auxotrophic mutation has led to an avirulent phenotype that might respond differently to drug treatment than a virulent strain. Thus, in hindsight, the effect seen in the checkerboard cannot be expected to be achieved in the CFU assay.

The metabolomic profile of Erdman wild-type strain, when treated with the drug combinations or the drugs alone, can give valuable indications of metabolic adaptations (Figures 6-8 and 6-9). For instance, succinate levels are depleted in all three treatments (RIF, CL-54-04 and RIF + CL-54-04) in propionate media, which may be due to succinate secretion as an attempt to maintain the membrane potential (Eoh and Rhee, 2013). The involvement of the reductive branch of the TCA cycle as an adaptive mechanism to hypoxia has been reported (Nandakumar *et al.*, 2014). It seems that a similar adaptation is observed in glycerol media, where there is an increased TCA cycle metabolites accumulation in CL-54-04 treated condition compared to propionate. This accumulation can be an indication of an overly active TCA cycle to cope with the drug treatment, or the drug-affected metabolism causes a downregulation of the TCA cycle enzymes, ultimately slowing down the TCA cycle.

When propionate is the sole carbon source, the accumulation of MCC metabolites observed in the CL-54-04 treatment indicates the ICL inhibition even at the low concentration tested. Interestingly, the RIF+04 combination has had a 1.6-fold increase in the accumulation of MCC metabolites (42,000 ion count/mg) compared with BDQ+04 (25,000 ion count/mg), suggesting that rifampicin may enhance the CL-54-04 effect. There seems to be an indirect correlation between aspartate levels and the MCC metabolites. The conditions with low aspartate levels are the ones with higher MCC accumulation and vice versa. The increased GABA accumulation observed in glycerol condition for CL-54-04 alone, or RIF+CL-54-04 might be a mechanism to cope with acidic and oxidative stress caused by the drugs, even in low concentrations (Tian *et al.*, 2005). GABA shunt pathway is known to remove protons at low pH, but it can also reduce the NAD⁺ by metabolising succinate semialdehyde to form succinate (Tian *et al.*, 2005),

which would explain the high levels of succinate on those same conditions. Hence, GABA participates in NAD⁺/NADH balance as an adaptation to rifampicin and the ICL1 inhibitor. The accumulation of glutamate in propionate media in all three drug conditions (BDQ, CL-54-04, CL-54-04+BDQ) can also be an adaptation to neutralise the cytoplasmic pH, as seen in propionate metabolism in BCG (Lee *et al.*, 2018). It has been observed that there are alterations of succinate and malate levels in Mtb if exposed to antibiotic-induced stress (Nandakumar *et al.*, 2014), which is also seen in the combination of CL-54-04 and bedaquiline in propionate media.

Chapter 7 – Investigating the role of fatty acids metabolism in drug tolerance in *Mycobacterium tuberculosis*

Introduction

Mtb exhibits metabolic plasticity, such as the ability to co-metabolise multiple carbon sources simultaneously (de Carvalho *et al.*, 2010). It can also adapt to a range of stress environments, such as nutrient starvation, oxygen depletion or antibiotic treatment. This occurs as a subpopulation of Mtb cells enter a reduced-growth state until conditions are favourable for them to emerge and become metabolically active again (McKinney, 2000; Torrey *et al.*, 2016). This ability to switch between replicative and non-replicative states happens through the rerouting of its metabolic flux as a response to its surrounding environment. Dormant Mtb are known to be less susceptible to anti-TB drugs (Sarathy *et al.*, 2013). This diverse metabolic versatility determines the susceptibility of Mtb to antibiotics, allowing survival even in lethal concentrations of bactericidal drugs (Gollan *et al.*, 2019; Stokes *et al.*, 2019). Furthermore, they can survive in such an environment for a prolonged period in the absence of resistance mechanisms (Gollan *et al.*, 2019). Hence, understanding the intricate metabolism during infection and dormancy (and its effect on drug tolerance) is critical in the development of new drugs.

The role of carbon-dependent metabolic changes that leads to drug tolerance in Mtb is an unexplored area. To address this, Mtb was exposed to two drugs, namely D-cycloserine (DCS) and isoniazid (INH), in carbon-defined media containing glycerol, propionate or acetate as a sole carbon source. Both acetate and propionate media are an *in vitro* model to mimic the fatty acid availability from host macrophages, whereas the glycerol media is a control condition commonly used in TB research. Using LC-MS metabolomics profiling, three Mtb strains carrying defined mutations in the central carbon metabolism were used to compare the metabolic adaptations and drug tolerance response with the wild type. Two of these mutants render Mtb viable but unable to grow

in fatty acid media (acetate or propionate). The first one is the deletion of the *pckA* gene that encodes for phosphoenolpyruvate carboxykinase (PEPCK), a metabolic enzyme in the anaplerotic node that catalyses the first committed step in gluconeogenesis. PEPCK is the sole enzyme that can convert oxaloacetate (a TCA cycle intermediate) to phosphoenolpyruvate (PEP) (Marrero *et al.*, 2010). This enzyme has been shown to be required for Mtb survival during infection (McKinney *et al.*, 2000; Muñoz-Elias and McKinney, 2005; Marrero *et al.*, 2010). PEPCK has been proposed as a potential drug target as $\Delta pckA$ strain failed to replicate during the acute phase of infection in mice, and it was cleared from the lungs by day 56. It suggests that the Mtb depends on gluconeogenic carbon substrates such as fatty acids for growth *in vivo* (Marrero *et al.*, 2010). To support the evidence that any effect seen in *pckA* mutant is due to the lack of PEPCK, a complementary strain was also used. This strain, *pckA* complementary (COM) strain, was achieved by cloning the *pckA* gene into the integrative plasmid pMV306 and transformed by electroporation in Erdman strain (Baker and Abramovitch, 2018).

The other two mutant strains lack 2-methylcitrate dehydratase (*PrpD*) or isocitrate lyase (*icl1/icl2*), the enzymes that catalyse the first and last reaction of the methylcitrate cycle (MCC), respectively. The ICL mutant is a knock-down strain that contains a tetracycline repressor-controlled expression. The presence of tetracycline leads to *icl1* gene expression, and its absence leads to a 'knock-out' phenotype where no ICL is present. This strain was constructed by inserting the expression vector containing *icl1* into the chromosome of the knockout strain Mtb Erdman $\Delta icl1 \Delta icl2$ (Blumenthal *et al.*, 2010). According to the authors, this approach was taken because fatty acids are toxic to Mtb $\Delta icl1/2$ even in the presence of carbohydrates, which would hinder the interpretation of the ICL role in mice. ICL has been identified as a promising drug target by several studies as the ICL knock-out strain failed to maintain persistence and virulence in mice and was shown to be drug-sensitive to a range of anti-TB drugs when tested in carbon-rich media (McKinney *et al.*, 2000; Nandakumar *et al.*, 2014). Although the 2-methylcitrate dehydratase is not considered a drug target, this mutant was chosen as it catalyses the first reaction in the MCC. The *PrpD* mutant phenotype will be compared to the ICL KD

strain phenotype to provide insights into MCC. Both ICL KD and $\Delta pckA$ strains are originated from the Erdman strain, whereas $\Delta prpD$ originates from CDC 1551 strain.

Fatty acids are the primary carbon source for Mtb during infections (Marrero *et al.*, 2010). From previous studies, both $\Delta pckA$ and ICL KD have exhibited a growth arrest phenotype in acetate and propionate media, respectively (Blumenthal *et al.*, 2010; Marrero *et al.*, 2010), which provides a good *in vitro* model to understand drug tolerance observed in dormant Mtb and the effect of inhibiting these two key enzymes. Therefore, in this study, glycerol and either acetate or propionate was used to understand the fatty acid metabolism and its effect on drug tolerance when treated with anti-TB drugs that are used clinically to treat both TB and MDR-TB.

Muñoz-Elias *et al.* (2006) has shown that ICL2 has minimal methylcitrate cycle activity; hence this study focused on ICL1, which is thought to have a more crucial role. However, considering recent ICL2 data that demonstrates the activation of ICL2 by acetyl-CoA (Bhusal *et al.*, 2019), the experiments may have needed the addition of acetyl-CoA to assess the ICL2 role in the MCC properly.

Materials and Methods

Bacterial strains and culture conditions

Mycobacterium tuberculosis (Mtb) Erdman wild-type (Erdman WT), Erdman $\Delta pckA$, Erdman $pckA$ complementary (COM), Erdman *icl* knock-down (ICL KD), CDC 1551 and CDC 1551 $\Delta prpD$ were pre-cultured in Middlebrook (M) 7H9 broth (Difco, Detroit, MI) supplemented with 0.5% (w/v) fraction V bovine serum albumin (BSA), 0.085% (w/v) NaCl, 0.04% (v/v) tyloxapol with 0.2% (v/v) glycerol and 0.2% (w/v) dextrose. For experiments, the strains were resuspended in fresh M7H9 containing BSA, NaCl, tyloxapol and 0.2% (v/v) glycerol, acetate or 0.05-0.1% (w/v) propionate. The antibiotics were added when necessary (0.3 $\mu\text{g}/\text{mL}$ isoniazid and 100 $\mu\text{g}/\text{mL}$ D-cycloserine). For metabolomic profiling, filters were generated as previously described (de Carvalho *et al.*, 2010; Eoh and Rhee, 2013). Mtb strains of Erdman and CDC 1551 were cultured in a

containment of biosafety level 3 facility. $\Delta prpD$ was purchased from BEI resources, and the tetracycline-regulated *icl* knock-down (ICL KD) Mtb strain and $\Delta pckA$ (with its complementary strain) were provided by Dirk Schnappinger and Sabine Ehrt.

Bacterial growth curves and colony-forming unit (CFU) assay

Bacterial growth was monitored by optical density (OD) at 595 nm by using a GENESYS™ 20 spectrophotometer (Thermo Scientific). For CFU assays, mid-logarithmic phase Mtb Erdman or CDC 1551 strains were diluted to OD₅₉₅ 0.05 in M7H9 broth containing BSA, NaCl, tyloxapol and supplemented with 0.2% (v/v) glycerol, acetate or 0.05-0.1% (w/v) propionate and antibiotics (isoniazid or D-cycloserine) when applicable, in a 24 or 96 well plate. After 5 days of antibiotic treatment (isoniazid) or 7 and 14 days for D-cycloserine, the cells were then serially diluted and plated on M7H10 agar with 0.2% (v/v) glycerol, 0.2% (w/v) dextrose, 0.5 g/L BSA and 0.085% (w/v) NaCl for three weeks at 37 °C until the colonies formed and counted. ICL KD was plated on M7H9 containing 0.5% (v/v) glycerol, 0.2% (w/v) dextrose, 0.5 g/L BSA, 0.085% (w/v) NaCl and 20 g/L agar due to its inability to grow on M7H10 media containing malachite green.

Metabolite extraction for LC-MS analysis

The filters containing Erdman or CDC 1551 strains were incubated at 37 °C. After reaching the mid-logarithmic phase of growth, the filters were transferred to chemically identical M7H10 agar containing new carbon source(s) and antibiotics and incubated for 24 hours at 37 °C. The metabolites were harvested by transferring the filters into pre-cooled -40 °C LC-MS-grade acetonitrile:methanol:water (40:40:20) solution and mechanically lysed with 0.1 mm Zirconia beads in a Precellys tissue homogenizer (Bertin Technologies, France) at 5,000 x g for 6 minutes in dry ice. The lysate was centrifuged and filtered using 0.22 µM Spin-X columns. The protein concentration of metabolite extracts was measured (BCA protein assay kit; Thermo Scientific, Waltham, MA, USA) to normalise samples to cell biomass.

Liquid Chromatography-Mass Spectrometry (LC-MS) for metabolomics profiling

LC-MS differentiation and detection of Erdman, CDC 1551 and mutant strains were performed with an Agilent Accurate Mass 6230 TOF coupled with an Agilent 1290 Liquid Chromatography system using solvents and configuration as previously described (Eoh and Rhee, 2013). An isocratic pump was used for continuous infusion of a reference mass solution to allow mass axis calibration. Detected ions were classified as metabolites based on unique, accurate mass-retention time identifiers for masses showing the expected distribution of accompanying isotopologues. Metabolites were analysed using Agilent Qualitative Analysis B.07.00 and Profinder B.06.00 software (Agilent Technologies, Santa Clara, CA, USA) with a mass tolerance of <0.005 Da. Standards of authentic chemicals of known amounts were mixed with bacterial lysates and analysed to generate the standard curves used to quantify metabolite levels.

RNA extraction for qRT-PCR

$\Delta pckA$ cells were grown in culture-filter membranes as done for metabolite extraction and exposed to glycerol or acetate as the sole carbon source for 24 hours. The total RNA was extracted using TRIzol solution (Sigma-Aldrich) and mechanical lysing with 0.1 mm zirconia beads in a Precellys tissue homogenizer. Lysates were clarified by centrifugation (10,000 x g for 5 minutes), and TRIzol supernatant was removed and used for RNA extraction. RNA was isolated using a Qiagen RNA extraction kit. Isolated RNA was treated with DNase I to remove DNA contamination (Sigma-Aldrich). RNA concentrations were determined using a Nanodrop, and qRT-PCR reactions were conducted using an iQ SYBR-Green Supermix (Bio-Rad) and C1000TM Thermal Cycler Instrument (Bio-rad). Primers used for amplification are listed in (Appendix B – Table B3). Log₁₀ were calculated using CT values that were normalized to *sigA* transcript levels.

Results

First, the phenotype of Mtb wild-type (WT), $\Delta pckA$ and *pckA* complementary (COM) strains in media containing either glycerol or acetate as a sole carbon source were characterised (Figure 7-1).

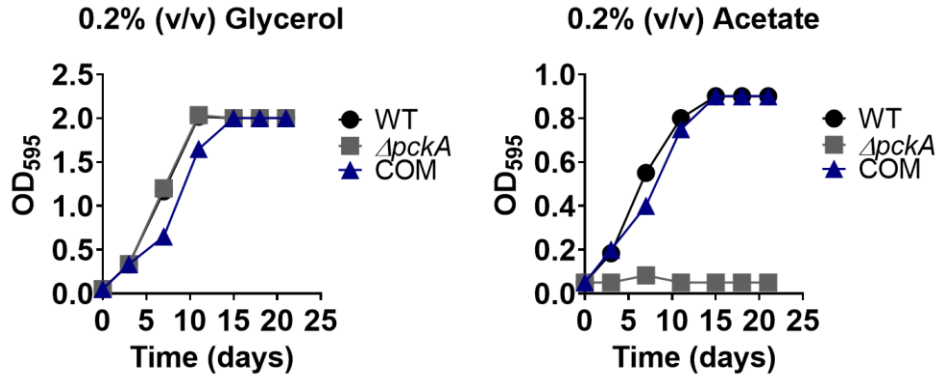
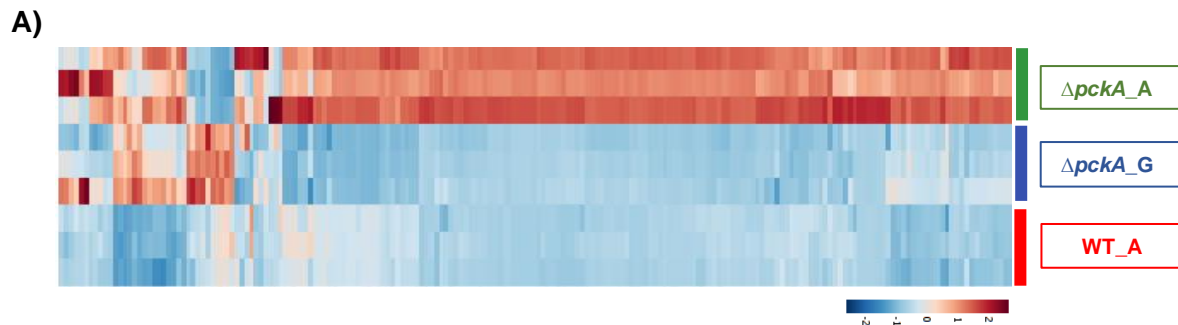


Figure 7-1: Growth curve of Erdman wild type (WT ●), Erdman $\Delta pckA$ ($\Delta pckA$ ■), and Erdman $pckA$ complementary (COM ▲) strains in glycerol and acetate media. The OD₅₉₅ was measured over a 21-day period. Data represent an average of three biological replicates.

PEPCK (the enzyme encoded by the $pckA$ gene) is essential for growth in acetate as a sole carbon source but dispensable in media containing glycerol as a sole carbon source, which was found to be close agreement with Marrero *et al.* (2010) data. Given the $\Delta pckA$ dormancy state in acetate media, its metabolic differences were investigated compared to glycerol media and wild type in acetate media (Figure 7-2). A semi-untargeted metabolic analysis between WT and $\Delta pckA$ strains was performed to see the pathways that were uniquely altered in $\Delta pckA$ strain in acetate media.



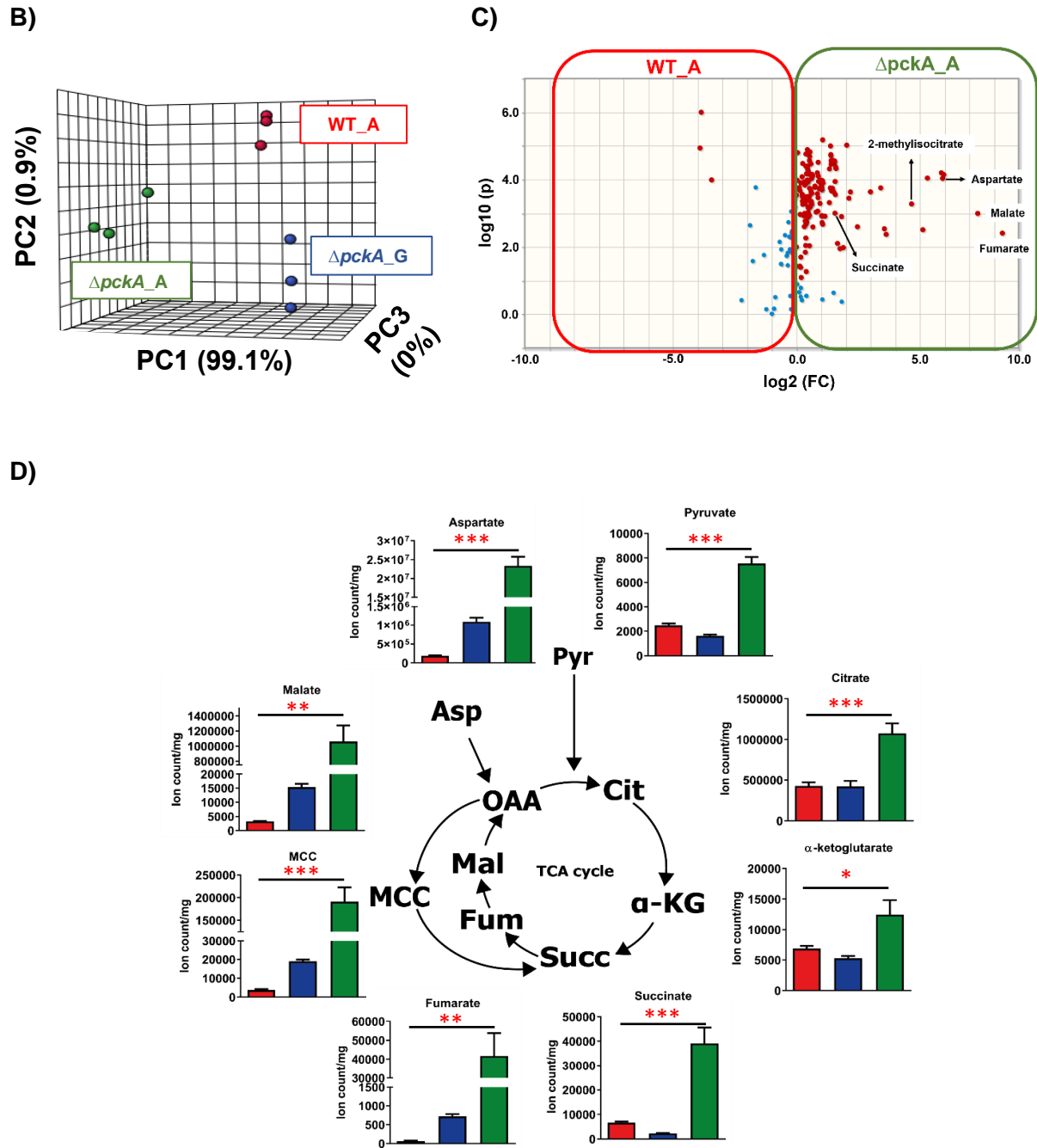


Figure 7-2: Metabolomics analysis of Erdman wild type (WT) in acetate (A) media and $\Delta pckA$ in glycerol (G) and acetate (A) media. **A)** Semi-untargeted metabolomics analysis of 231 metabolites. **B)** 3D principal component analysis (PCA). **C)** Volcano plot of up-regulated $\Delta pckA$ metabolites in acetate (A) media (green box) against up-regulated metabolites of WT in acetate (red box). **D)** TCA cycle metabolites of WT in acetate media and $\Delta pckA$ in both glycerol and acetate media. $\Delta pckA$ in acetate is depicted in green; $\Delta pckA$ in glycerol in blue; WT in acetate in red. Data represent an average of three biological replicates, and error bars are standard deviations. Cit, citrate ($p=0.001$); Pyr, pyruvate ($p=0.0001$); α -KG, α -ketoglutarate ($p=0.0159$); Succ, succinate ($p=0.001$); Fum, fumarate ($p=0.0038$); Mal, malate ($p=0.001$); MCC, 2-methyl-

Figure 7-3: Decreased mRNA expression levels (\log_{10} CT values) of the TCA cycle and MCC genes in $\Delta pckA$ strain in 0.2% (v/v) acetate (A) media compared to 0.2% glycerol (G) and Erdman wild type (WT) in both carbon sources. The diagram represents a pathway map of each gene tested and the deletion of *pckA*. Data represent an average of three biological replicates.

Overall, the RNA levels of genes coding for all enzymes in the TCA cycle were downregulated in both strains when acetate was the sole carbon source instead of glycerol. Though, RNA levels in $\Delta pckA$ were further downregulated when compared to WT. The gene expression changes could be a response to the changes in metabolite abundance and metabolic flux. Given the dormancy-like metabolic profile of $\Delta pckA$ in acetate media, the TCA cycle and MCC metabolites of the WT and COM strains were compared against the $\Delta pckA$ strain (Figure 7-4).

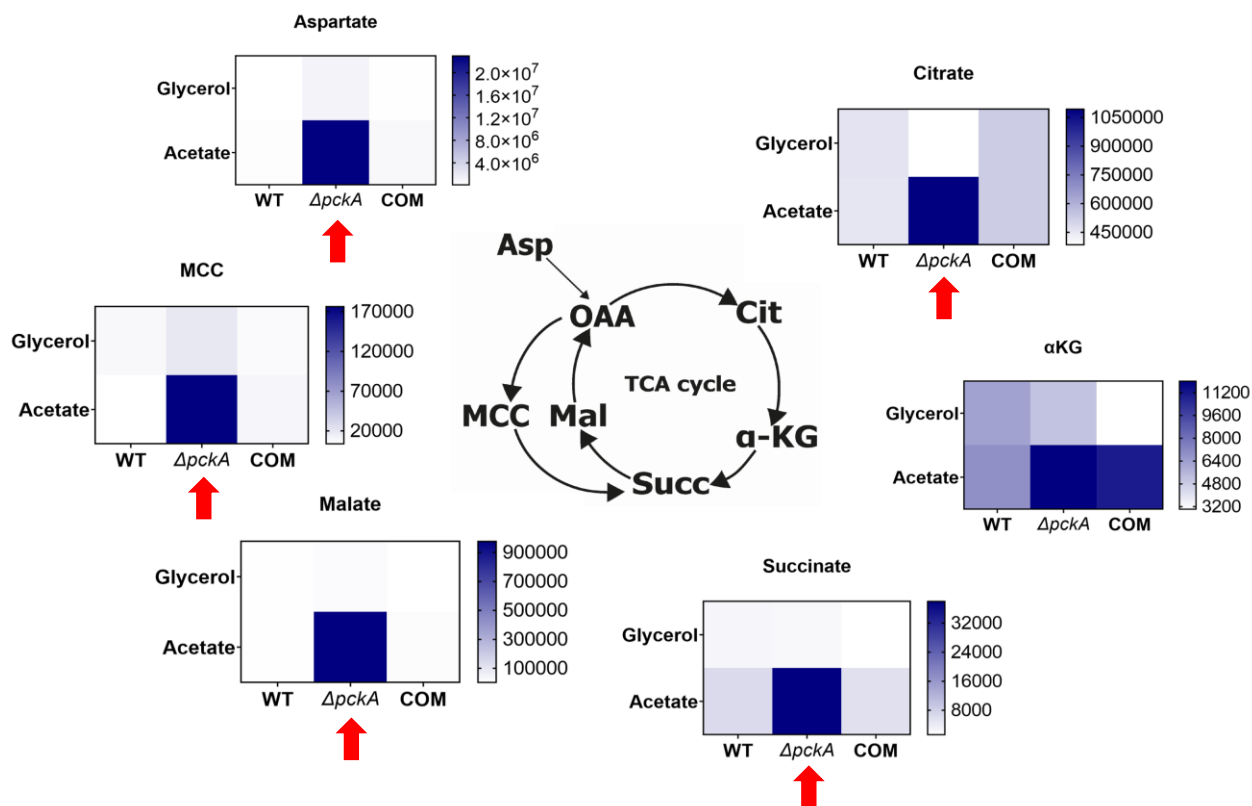


Figure 7-4: Accumulation of the TCA cycle and MCC metabolites in $\Delta pckA$ strain in 0.2% (v/v) acetate media compared to 0.2% (v/v) glycerol. Data represent an average of three biological replicates, and error bars are standard deviations. α -KG, α -ketoglutarate; Cit, Citrate; COM, complementary strain, Succ, Succinate; Fum, Fumarate; Mal, Malate; MCC, 2-methyl-cis-aconitate and 2-methyl-isocitrate, WT, wild type.

There is a higher accumulation of succinate, fumarate and malate in $\Delta pckA$ strain in acetate media compared to the other two strains. The MCC cycle is accumulated in $\Delta pckA$ in both carbon sources, but even more so in acetate media. These findings correspond to the semi-untargeted metabolomic analysis performed in $\Delta pckA$ in Figure 7-2.

PEPCK converts oxaloacetate to phosphoenolpyruvate (PEP). In $\Delta pckA$ strain, this reaction is not present, and thus, there is no PEP when acetate is the sole carbon source. However, when supplemented with uniformly ^{13}C labelled ($[\text{U-}^{13}\text{C}]$) acetate, $\Delta pckA$ strain has PEP accumulation almost as abundant as it is in WT (Figure 7-5). Interestingly, the PEP was completely unlabelled, suggesting that internal carbon sources are utilised to support glycolysis (Lee *et al.*, 2018). The majority of the PEP in WT and COM are labelled, which means it is coming from the conversion of oxaloacetate to PEP, utilising the ^{13}C labelled acetate. Nonetheless, these strains also have unlabelled PEP, which indicates that acetate as a sole carbon source forces the Mtb to utilise an internal carbon source (such as trehalose metabolism) to maintain the glycolytic pathway.

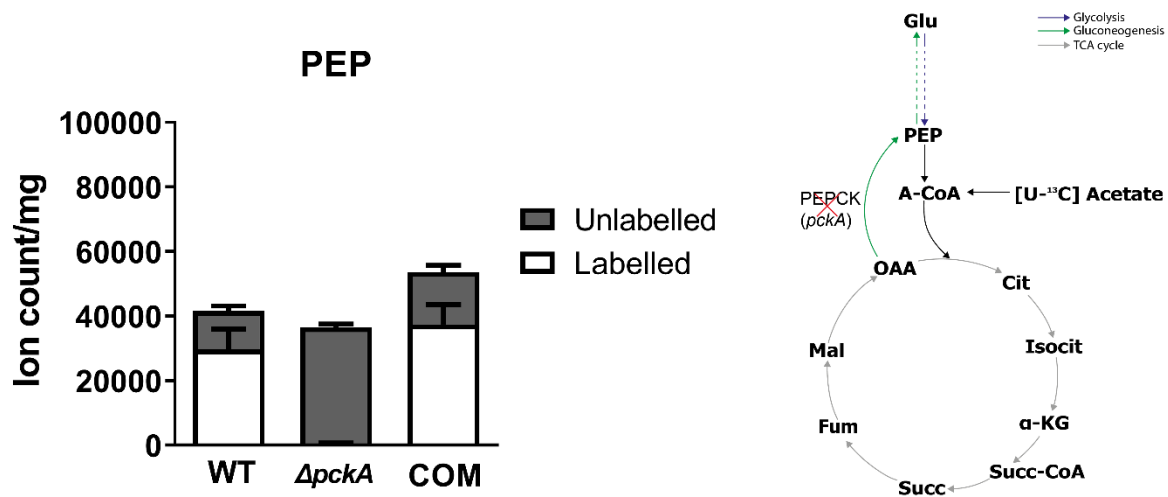


Figure 7-5: Targeted metabolomic analysis of phosphoenolpyruvate (PEP) with uniformly 0.2% (v/v) ^{13}C labelled ($[\text{U-}^{13}\text{C}]$) acetate in wild type (WT), $\Delta pckA$ and complementary (COM) strains. The diagram represents the central carbon metabolism and the $pckA$ deletion. Data represent an average of three biological replicates, and error bars are standard deviations.

As the bacteriostatic state is linked with drug tolerance, the effect of the $pckA$ deficiency mediated bacteriostatic phenotype was assessed by exposing the strains to D-

cycloserine (DCS), a second-line agent that is used to treat multi-drug resistant tuberculosis (MDR-TB). This drug inhibits cell wall biosynthesis and leads to cell lysis. The level of bacterial survival was monitored by optical density (OD) measurements or viable colony formation (CFU) (Figure 7-6).

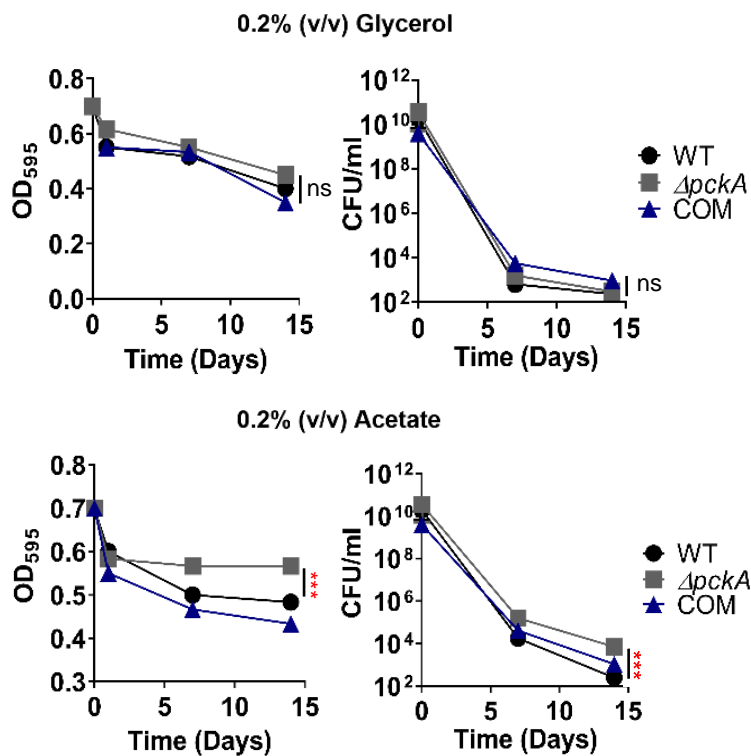


Figure 7-6: Phenotypic changes in Erdman $\Delta pckA$ ($\Delta pckA$ ■) mutant compared to Erdman wild-type (WT ●) and $pckA$ complementary (COM ▲) strains in carbon-dependent media. Viable count (CFU/mL) and optical density (OD_{595}) were used to measure the growth effect following treatment with 100 $\mu\text{g}/\text{mL}$ DCS in glycerol media and acetate media. The assay was done according to Keren *et al.* (2011). Data represent an average of three biological replicates, and error bars are standard deviations. *** $P < 0.001$, ns, not significant by two-way ANOVA. Differences of WT and $\Delta pckA$ growth in glycerol media is not statistically significant, whereas in acetate is extremely significant (***).

In glycerol media, the $\Delta pckA$ demonstrated a similar response to DCS as the other two strains. In contrast, the $\Delta pckA$ was significantly more tolerant to DCS in acetate media. To further investigate this drug tolerance phenotype in acetate, isoniazid, a first-line anti-TB drug, was assessed against these three strains in both carbon sources for five days

– Figure 7-7. The cells were serially diluted, plated on M7H10 plates, and the colonies were counted after three weeks of incubation at 37 °C and 5% (v/v) CO₂.

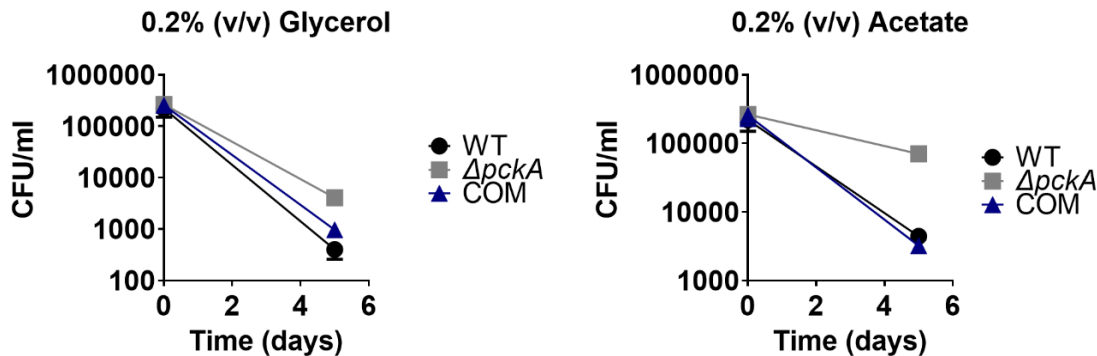


Figure 7-7: Drug tolerance against 0.3 µg/mL isoniazid (INH) of Erdman wild type (WT ●), $\Delta pckA$ (■) and *pckA* complementary (COM ▲) strains in 0.2% (v/v) glycerol and 0.2% (v/v) acetate. Data represent an average of three biological replicates, and error bars are standard deviations.

When exposed to 0.3 µg/mL of INH, $\Delta pckA$ strain demonstrated more colonies in the CFU assay than the other two strains in both carbon sources, but the difference is more prevalent in acetate media. Metabolomic analysis was used to investigate the role of metabolic changes of $\Delta pckA$ strain in fatty acid carbon source dependent drug tolerance against INH – Figure 7-8. Filters containing culture in a mid-logarithmic stage were exposed to 0.3 µg/mL of INH. After a 24-hour incubation, the cells were harvested and mechanically lysed for the LC-MS analysis.

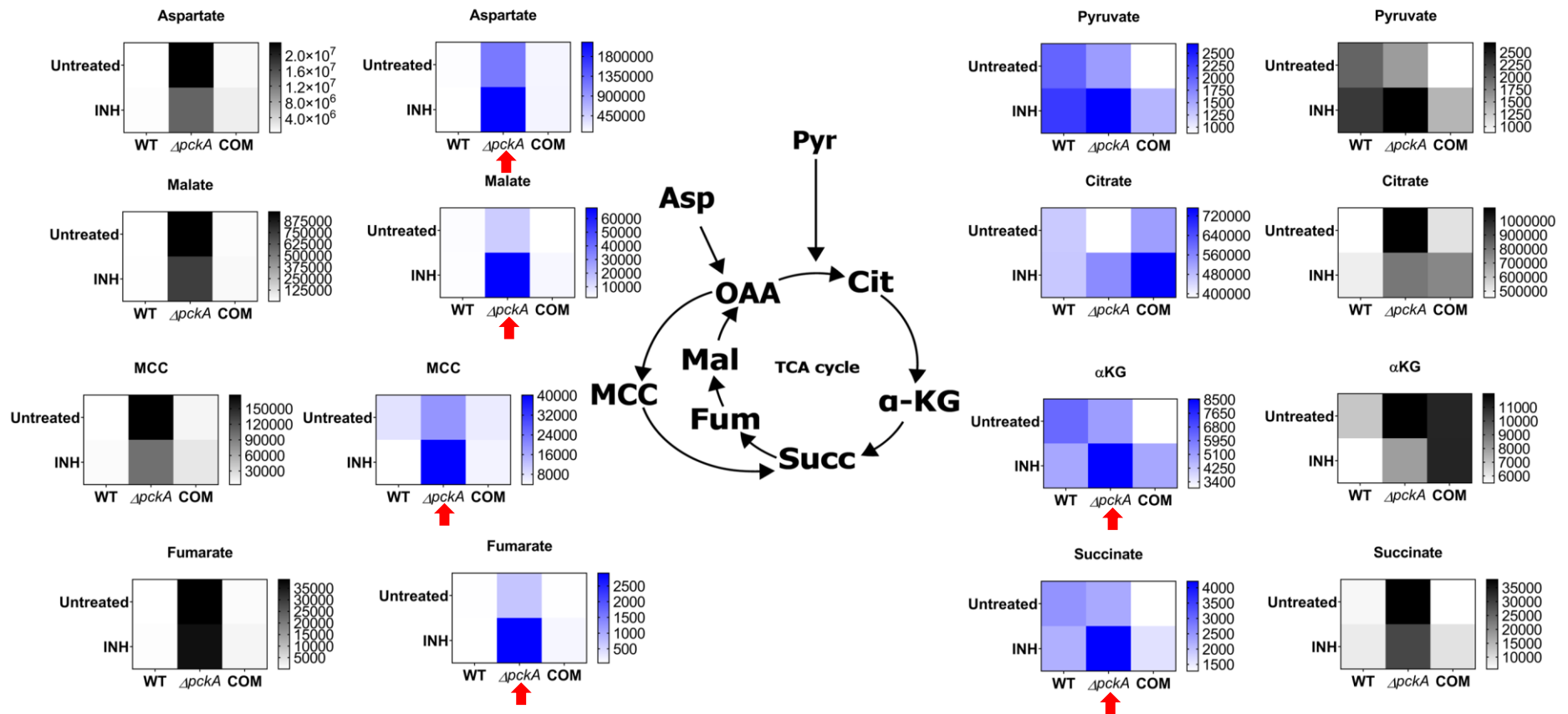


Figure 7-8: Accumulation of the TCA cycle and MCC metabolites in $\Delta pckA$ upon isoniazid treatment in acetate media. WT, $\Delta pckA$ and COM strains were cultured in 0.2% (v/v) glycerol (blue scheme) or 0.2% (v/v) acetate media (black scheme) in the presence of 3 $\mu\text{g}/\text{mL}$ isoniazid (INH). Values represent ion count/mg and are an average of three biological replicates. Asp, Aspartate; Pyr, Pyruvate; Cit, Citrate; $\alpha\text{-KG}$, α -ketoglutarate; Succ, Succinate; Fum, Fumarate; Mal, Malate; MCC, 2-methyl-cis-aconitate and 2-methyl-isocitrate.

In glycerol media, there is an accumulation of all metabolites in INH-treated $\Delta pckA$ when compared to the untreated condition. In acetate media, the opposite is observed. The accumulation of these metabolites is decreased in INH-treated $\Delta pckA$ in comparison to the untreated condition, except for fumarate that remains the same, and pyruvate that is increased.

To investigate the carbon-induced dormancy phenotype that leads to drug tolerance, two mutants in the MCC were analysed. The first mutant, ICL KD, has both *icl* genes silenced in the Erdman strain and is controlled by the presence of tetracycline (Blumenthal *et al.*, 2010). ICL catalyses the last reaction of the MCC. The silencing of ICL hinders Mtb unable to grow in propionate media (Lee *et al.*, 2018). The second mutant is Mtb CDC 1551 $\Delta prpD$ strain, a gene deletion that codes for 2-methylcitrate dehydratase, the first enzyme in the MCC. The *in vitro* growth of these two strains and their parental strains was assessed by optical density (595 nm) – Figure 7-9.

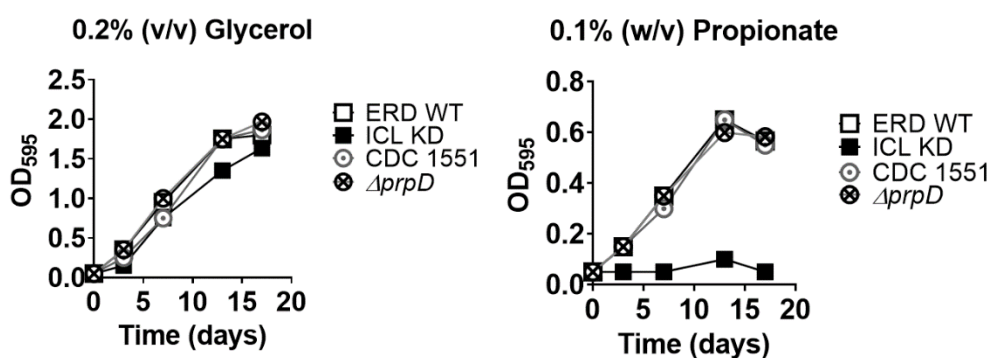


Figure 7-9: Growth curve of Erdman WT (□), ICL KD (■), CDC 1551 (○) and $\Delta prpD$ (⊗) in 0.2% (v/v) glycerol and 0.1% (w/v) propionate over 21 days.

In glycerol media, the ICL KD growth resembled the ones from the other three strains. In propionate media, $\Delta prpD$ grew normally, whereas ICL KD was unable to grow (a similar phenotype observed in $\Delta pckA$ strain in acetate media). Their metabolomic profile for these strains was investigated in both 0.2% (v/v) glycerol and 0.1% (w/v) propionate media – Figure 7-10.

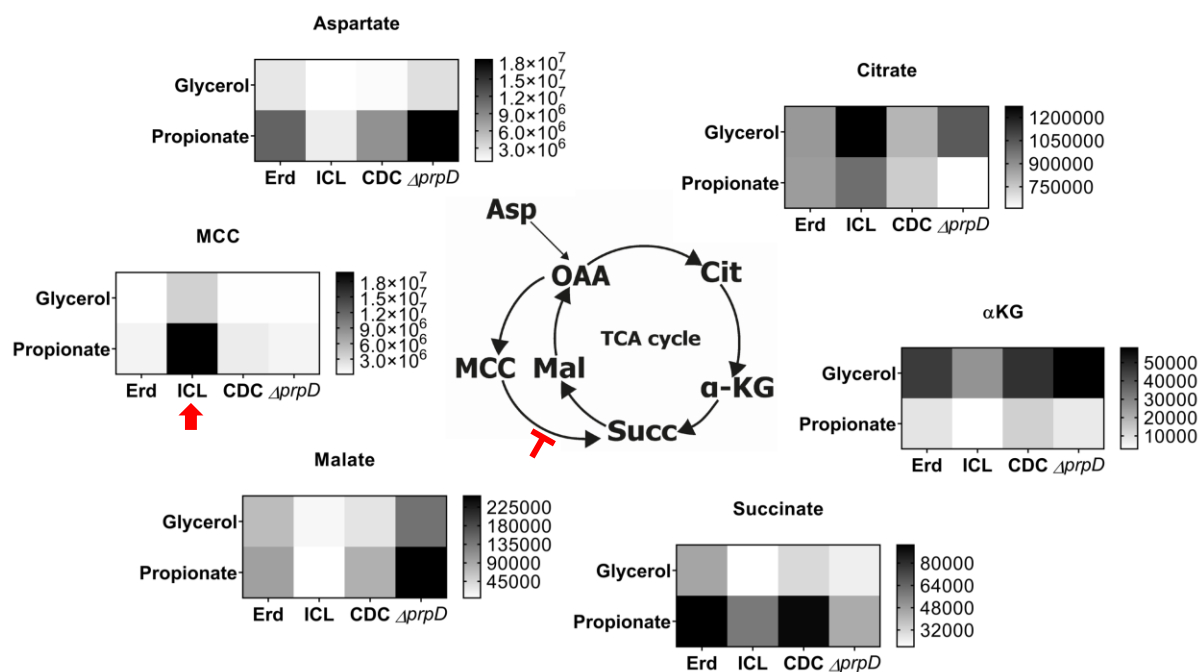


Figure 7-10: Accumulation of the MCC metabolites in ICL KD strain in 0.1% (w/v) propionate media compared to Erdmand (Erd) WT, ICL KD, CDC 1551 and $\Delta prpD$ and in 0.2% (v/v) glycerol media. Asp, Aspartate; Cit, Citrate; α -KG, α -ketoglutarate; Succ, Succinate; Mal, Malate; MCC, 2-methyl-cis-aconitate and 2-methyl-isocitrate.

The MCC accumulation was only observed in ICL KD in propionate media, whereas the other strains had no MCC metabolites accumulation. Aspartate and malate accumulation was only seen in $\Delta prpD$ strain in propionate. Unlike their parental strains, both mutants had no succinate accumulation in propionate media.

As ICL KD has a carbon-induced dormancy phenotype similar to the $\Delta pckA$ strain, the question of whether this mutant would also be tolerant to an anti-TB drug was raised. The four strains were exposed *in vitro* against isoniazid in both glycerol and propionate media for five days, and tolerance was assessed by survival (%) after comparing the CFU from day 5 relative to day 0 – Figure 7-11.

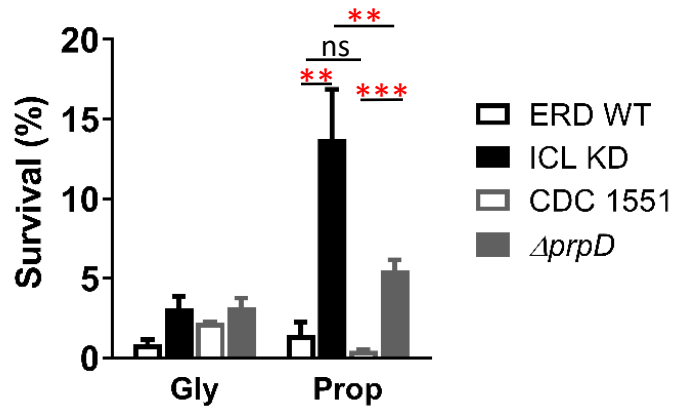
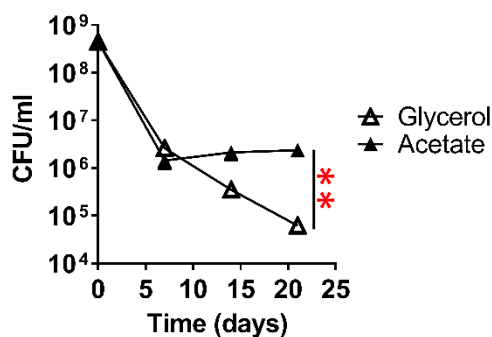


Figure 7-11: The effect of 0.3 $\mu\text{g}/\text{mL}$ isoniazid in the survival of Erdman WT, ICL KD, CDC 1551, $\Delta prpD$ in 0.2% (v/v) glycerol (Gly) and 0.1 (w/v) propionate (Prop) media after 5 days. Data represent an average of three biological replicates, and error bars show the standard deviation. *** $P < 0.001$, ** $P < 0.01$, ns, not significant by two-way ANOVA. The statistical analysis highlighted in propionate media are comparing ICL KD and $\Delta prpD$ (**), Erd WT and CDC 1551 (ns), Erd WT and ICL KD (**), and CDC 1551 and $\Delta prpD$ (***)

The ICL KD strain had a similar survival percentage as the other strains in glycerol but a higher survival percentage in propionate. The $\Delta prpD$ strain was also more tolerant in propionate than its parental strain, CDC 1551. To assess whether the carbon-induced drug tolerance is an effect only seen in the dormancy-induced state, both DCS and INH were used in Erdman wild type strain in both glycerol and acetate media – Figure 7-12.

A) D-cycloserine (DCS)



B) Isoniazid (INH)

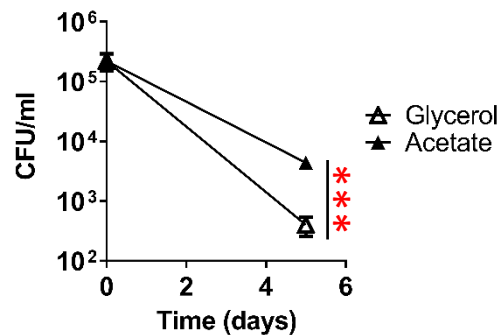


Figure 7-12: Comparison of colony formation of Erdman WT against **A)** 100 $\mu\text{g}/\text{mL}$ DCS ($p = 0.0011$) and **B)** 0.3 $\mu\text{g}/\text{mL}$ INH ($p = 0.0002$) in 0.2% (v/v) glycerol and 0.2% (v/v) acetate media. Data shown is the average of three biological replicates. *** $P < 0.001$, ** $P < 0.01$ by two-way ANOVA.

Against both drugs (DCS and INH), the Erdman wild type strain was also more tolerant in acetate media when compared to glycerol.

Discussion

Carbon metabolism is a significant determinant of Mtb ability to replicate and persist in the host (Marrero *et al.*, 2010). Fatty acid metabolism is the main carbon source available in the host's macrophages during the acute and chronic phase of Mtb infection (McKinney *et al.*, 2000; Eoh and Rhee 2013). The role of Mtb metabolic pathways to adapt to the host's carbon environment is essential to understanding pathogenicity and acting as a guide for developing new therapeutic methods.

The $\Delta pckA$ strain exhibits a growth arrest phenotype in acetate media as it is unable to assimilate acetate through gluconeogenesis. Nevertheless, this mutant remained viable. Given that dormant TB is known to be less susceptible to anti-TB drugs, understanding the $\Delta pckA$ metabolism in acetate and exposure to anti-TB drugs could reveal drug tolerance mechanisms. Therefore, the phenotype of the $\Delta pckA$ strain was explored to understand the metabolic differences between glycerol and acetate media. For instance, the accumulation of TCA cycle metabolites in $\Delta pckA$ strain in acetate media occurs due to gluconeogenic carbon flux obstruction. This accumulation, coupled with a decrease in gene expression for the TCA cycle enzymes (seen in the mRNA levels) in acetate media, demonstrates that $\Delta pckA$ is in a low metabolic status that correlates with the *in vitro* growth curve.

Another interesting finding is that the $\Delta pckA$ strain is able to remain viable in acetate media due to the consumption of the internal carbon sources, supplying the glycolytic pathway. This was seen in the ^{13}C -labelled acetate experiment, where $\Delta pckA$ strain had similar levels of PEP as the wild type; however, the PEP was unlabelled. This suggests that an internal carbon source is being used to support glycolysis. Lee *et al.* (2018) showed that trehalose metabolism, a two-glucose molecule that plays a role in cell wall synthesis, may be the primary internal source of carbon during dormancy. The $\Delta pckA$ strain has an accumulation of TCA cycle metabolites and a downregulation of the TCA cycle enzymes, which suggests a low TCA cycle activity, and hence, not

enough co-factors are generated for oxidative phosphorylation. Glycolysis generates 15x less ATP than oxidative phosphorylation but seems enough to maintain $\Delta pckA$ viable but in a dormant state. Although the majority of the PEP was labelled, both WT and COM strains also had small amounts of unlabelled PEP, which means that WT also utilises internal carbon sources in growing in acetate media.

The drug tolerance profile of the $\Delta pckA$ strain was investigated against DCS and INH. Against both drugs, the $\Delta pckA$ strain was more tolerant in acetate media than the wild type and the complementary strains. Baker and Abramovitch (2018) have also reported that $\Delta pckA$ in acid-growth arrest becomes tolerant to INH and rifampicin. In the metabolomic analysis, the opposite effect is seen in the INH-treated condition, depending on the carbon source. In glycerol, all metabolites are accumulated, whereas, in acetate condition, they are all downregulated. In acetate condition, the metabolism requires the gluconeogenesis pathway, which is defected in $\Delta pckA$ strain. The lack of gluconeogenesis explains the accumulation of both reductive and oxidative branches of the TCA cycle and the MCC accumulation in $\Delta pckA$ untreated condition. Interestingly, in INH-treated condition, there is a decrease in the accumulation of the same metabolites. As $\Delta pckA$ is tolerant to INH in acetate media, this metabolic adaptation of both the TCA cycle and MCC is likely to be beneficial for the INH tolerance.

Both ICL KD and $\Delta prpD$ strains were more tolerant to INH in propionate media than their parental strains. ICL KD is nearly three-fold more tolerant to INH than $\Delta prpD$ ($p=0.0104$); though, the statistical analysis between the mutants and their parental strains reveals that $\Delta prpD$ tolerance is highly significant ($p=0.0002$) than ICL KD and Erdman WT ($p=0.0132$). CDC 1551 is a clinical isolate that is known to be sensitive to a wide range of drugs (Fleischmann *et al.*, 2002), and therefore, the $\Delta prpD$ strain tolerance to INH is an interesting finding considering that this mutant strain has no growth arrest in propionate media. Indeed, the lack of *PrpD* enzyme should attenuate the strain's growth in propionate media as this mutant would not metabolise propionyl-CoA, a toxic by-product of propionate metabolism. Nonetheless, alternative routes for propionate oxidation have been previously suggested, such as the methylmalonyl-CoA pathway, which can be relevant for the synthesis of phthiocerol dimycocerosates; a methyl-

branched lipid highly abundant in Mtb cell wall component (Muñoz-Elías and McKinney, 2006).

The INH tolerance observed in $\Delta prpD$ strain can be due to the accumulation of malate, but specifically, aspartate. Aspartate plays a role in the biosynthesis of co-factors and peptidoglycan, which is essential for the thickening of the Mtb cell wall (a known mechanism in drug tolerance). Moreover, a recent study demonstrated that the inhibition of the aspartate pathway leads to the clearance of chronic infection (Hasenoehrl *et al.*, 2019). In INH-treated $\Delta pckA$, where tolerance was also seen, the accumulation of aspartate in acetate media (1.6×10^7 ion count/mg) is higher than in glycerol (1.8×10^5 ion count/mg). Surprisingly, the Erdman wild type strain was grown in acetate media also shows higher drug tolerance to both INH and DCS than in glycerol media. Although the WT can grow in both carbon sources, the growth is slower in acetate when compared to glycerol (Figure 7-1); in 21 days, the OD₅₉₅ in acetate media reached 1.0, whilst in glycerol media reached 2.0. This suggests further that acetate metabolism (and growth rate) is implicated in drug tolerance in Mtb. More research is needed to understand the effect of fatty acid in Mtb metabolism and drug tolerance.

Both ICL and $\Delta pckA$ strains have been proposed as drug targets due to their attenuation *in vivo* studies (Liu *et al.*, 2003; Muñoz-Elías *et al.*, 2006). Nevertheless, under these specific experimental conditions, inhibition in the gluconeogenesis or the downstream of the MCC pathway in carbon-defined media rendered Mtb more tolerant to isoniazid and D-cycloserine. If inhibiting these enzymes lead to a dormancy state in fatty acid metabolism *in vitro*, it raises questions about the applications of an ICL/ $pckA$ inhibitor. Perhaps the gene deletions cause a deleterious effect that will not be reproduced with drug inhibitors. Conversely, there are other aspects inside the macrophage that are unknown or hard to reproduce in the laboratory. The lack of this complete model may allow us to see this dormancy effect *in vitro* that would not usually happen in the host's macrophage. These questions only demonstrate the need to explore and understand the metabolism of Mtb inside the macrophage and validate whether they are indeed good drug targets. An experimental approach would test an ICL/ $pckA$ inhibitor *in vivo* to validate the proposed drug targets.

Chapter 8 – Discussion and future directions

The aim of this research was to identify novel inhibitors against ICL1 as a potent anti-tubercular agent. The core of this work depended on the availability of purified protein. To do so, the protein expression and purification protocol were optimised to increase the yields of ICL1 when using *E. coli* as a vector (Chapter 2). Simultaneously, the drug designs and synthesis were carried out (Chapter 3). The main aim was to synthesise 2-methylisocitrate, which is a substrate analogue that was tested in the enzyme assay (Chapter 4). The other five methylated drugs were synthesised, but due to their oily properties, their inhibitory effect could not be determined. With sufficient protein stocks and drug candidates selected, both enzyme assays and crystallisation were performed. In the former, a group of compounds, CL-54 family, were identified as lead ICL inhibitors, whilst in the latter, several conditions to crystallise the enzyme were determined. The co-crystallisation of ICL with itaconate (a known ICL inhibitor), 2-methylisocitrate and CL-54-01 were carried out (Chapter 5). No crystals were obtained through co-crystallisation; however, when using the soaking technique, the ICL1:CL-54-01 structure was solved. The alignment of the solved ICL1:CL-54-01 structure with ICL1 and ICL2 demonstrated that CL-54-01 caused a catalytic shift closing the active site, which is a similar effect seen with 3-nitropropionate (a known ICL inhibitor). The CL-54 drug family were tested against Mtb in a colony-forming unit assay in both glycerol and propionate (Chapter 6). The analogue, CL-54-04, caused a bacteriostatic effect at 10 μM in propionate media and a bactericidal effect at 100 μM in both carbon sources. A drug combination of CL-54-04 with rifampicin or bedaquiline was tested in a checkerboard assay, where the additive effect of the drug combinations was observed. The drug combinations were then used to test the metabolic effect using LC-MS metabolomic analysis. At the concentration of 7.81 μM , the CL-54-04 alone led to an increased accumulation of the MCC metabolites when compared to the glycerol condition (where the ICL is not required), though the combination of rifampicin with CL-54-04 led to an even greater accumulation of MCC metabolites.

Given the complexity of Mtb metabolism and its ability to adapt to a plethora of environments and go into dormancy, a series of metabolomic analyses was conducted using Mtb and mutant strains to understand better the metabolic remodelling that

occurs upon antibiotic exposure (Chapter 7). Inside the macrophage, the predominant carbon source is fatty acids. Thus, carbon-defined media with glycerol (control), acetate or propionate were tested to understand better the fatty acid metabolism and its role in drug tolerance. Surprisingly, acetate metabolism leads WT to be more tolerant to first-line, isoniazid, and second-line, D-cycloserine drugs compared to glycerol media. Further, all three mutants tested ($\Delta pckA$, ICL KD and $\Delta prpD$) exhibited higher tolerance to isoniazid than their parental strains. Targeted metabolomics was performed as an attempt to uncover the metabolic adaptations that leads to drug tolerance. Both $\Delta pckA$ and ICL KD strains have an accumulation of the MCC metabolites in fatty acid media, but this accumulation is not observed in $\Delta prpD$ strain; instead, it has a high aspartate accumulation.

For future work, further characterisation of the inhibition of the CL-54 drug family against ICL is needed. For instance, kinetic constants of ICL1 and these inhibitors could be determined. This was a challenge due to the enzyme assay. The assay is limited to colourless compounds that are soluble in a buffer. However, a number of compounds are insoluble in buffer and were dissolved in DMSO. Furthermore, the CL-54 drug family were coloured compounds that absorb at the wavelength used to measure the enzyme assay (324 nm). These limitations were circumvented by the use of a PD-10 spin column, but they also limited the feasibility of accurately determining an IC_{50} and the enzymatic kinetics. An alternative would be to measure the decrease of NADH that is oxidised when glyoxylate (formed by the isocitrate lyase cleavage of isocitric acid) is reduced to glycolate by lactate dehydrogenase (LDH) (Warren, 1970). The reaction can be stopped with 4 M urea, and 0.2 mg/mL formazan dye MTS (MTS/PMS ratio of 100:1) is added prior to the reading at 490 nm as described by Bentrup *et al.* (1999). At this wavelength, the CL-54 compounds have an absorbance of 0.1728, which would result in less background noise than the assay used in this study ($OD_{324} = 0.5790$ at the same concentration). A comparison of both assays is depicted in Figure 8-1.

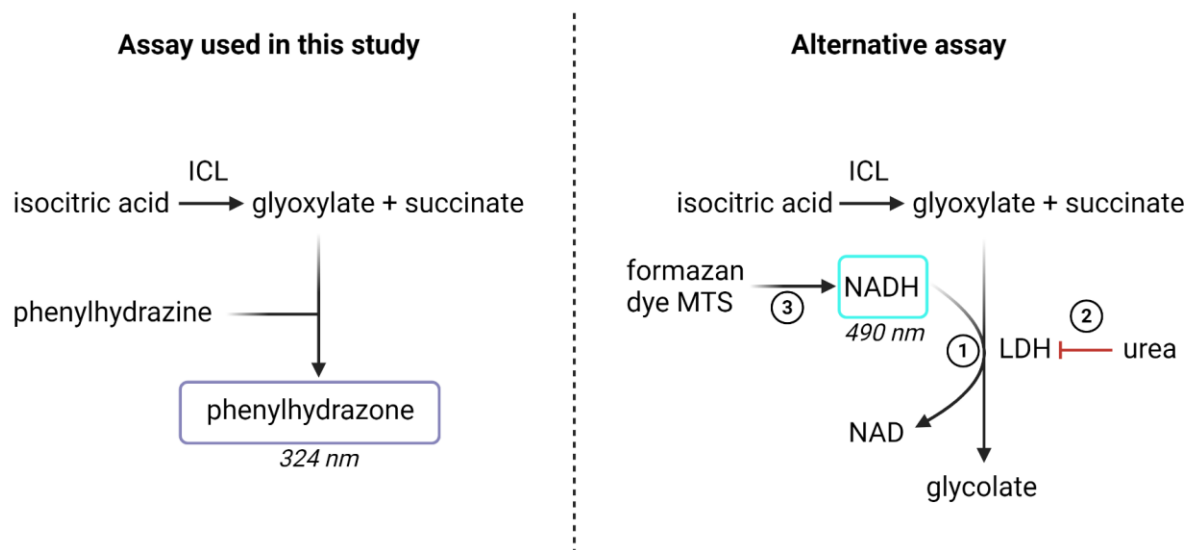


Figure 8-1: Comparison of the ICL enzymatic assay used in this study and an alternative assay. Both assays are incubated at 37 °C. Created with BioRender.com.

An advantage of the alternative assay is that the reaction can be stopped at different times by the addition of urea. A drawback of this assay is the auto-oxidation of NADH to NAD⁺, which may affect the accuracy (Chenault and Whitesides, 1989). In addition, the alternative assay will also be affected by the presence of DMSO.

To assess the thermodynamic profile of CL-54 drugs with ICL, isothermal titration calorimetry (ITC) could be used. This physical technique allows to measure the heat that is either released or absorbed during biomolecular interactions by gradually titrating the ligand (e.g., CL-54 drugs) into the sample (e.g., ICL), providing affinity constant, the stoichiometry and enthalpy and entropy (Freire *et al.*, 1990; Duff *et al.*, 2011). However, ITC requires larger quantities of both the enzyme (2.4 mg in 2 mL) and the inhibitors (1 mg in 0.3 mL) compared to other techniques (Dutta *et al.*, 2015). Although CL-54 drugs seem to bind tightly to ICL and low concentrations of these novel inhibitors will likely be required, the optimal concentration of ICL/CL-54 drugs would still need to be determined for ITC. This is a major limitation as CL-54 drugs are experimental drugs whose availability was limited to a couple of milligrams. Another consideration is that the protein and ligand buffers must be carefully matched; however, CL-54 drugs are dissolved in DMSO whereas the enzyme was in MOPS buffer (and as observed in Chapter 4, ICL1 is inhibited by DMSO, albeit reversible).

The CL-54 drug family was tested against Mtb. Interestingly, only CL-54-04 showed a bactericidal effect, whereas CL-52-02 a bacteriostatic effect and CL-54-01 seemed to have no effect at the concentration and time frame tested. This result suggested that the first two analogues (CL-54-01 and CL-54-02) may have issues penetrating Mtb cell membrane. To gain an understanding on this matter, the Mtb cell membrane can be fractionated to assess whether the drug is trapped within the membrane. Different lipid extraction methods can be used, such as AOT (dioctylsulfosuccinate sodium), to separate the inner plasma membrane, the peptidoglycan–arabinogalactan complex, and the outer membrane that is covalently linked to the arabinogalactan (Ratledge *et al.* 1982; Brennan and Nikaido, 1995). Then, each fractionate can be analysed by LC-MS to detect signals that correspond to the CL-54 drugs. Another possibility is that the drug may be secreted out of the cell by an efflux pump (Adams *et al.*, 2011). Thus, the periplasm can also be analysed to determine if drug uptake took place. A more sophisticated alternative of monitoring the drug uptake would be to synthesise radioactively labelled CL-54 drug family members. This would allow the tracking of the drug uptake but also monitor the direct effect of these ICL inhibitors on the Mtb metabolism.

The CL-54 drug family have different functional groups attached to the benzene ring. CL-54-01 have two hydroxyl groups in meta and para positions, whereas CL-54-02 have only one at the para position. In addition to the hydroxyl group at para position, CL-54-04 is the only analogue with a methyl group at the ortho position. Given the lack of effect of CL-54-01 and CL-54-02 against Mtb, but a bactericidal effect of CL-54-04, one can speculate that adding more methyl groups could lead to an even better inhibitor. Future work could look at further modifications at the six-carbon ring where the CL-54 family vary (Figure 8-2).

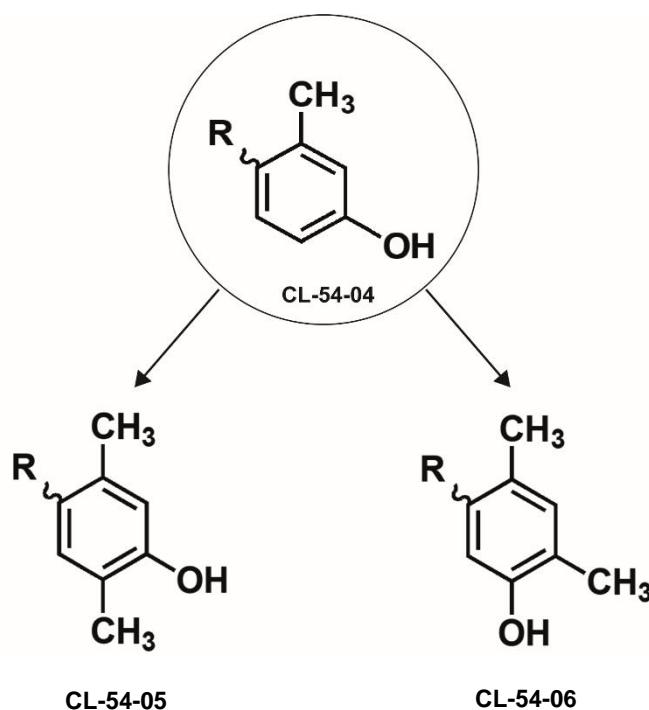


Figure 8-2: Proposed ICL inhibitors based on CL-54-04 structure. R represents the identical core structure of all CL-54 family members.

The rationale behind these two new analogues is by adding another methyl group in either meta (CL-54-05) or para position and moving the hydroxyl group to a meta position (CL-54-06). These changes may increase the drug uptake, which in turn, it would decrease the concentration required to inhibit ICL and kill Mtb. If the drug uptake is not improved, a future analogue with an ethyl group in the ortho position may have better properties. However, the ethyl group might be too bulky to bind to the active site of ICL.

The combination of CL-54-04 with rifampicin or bedaquiline was tested (Chapter 6). Neither combination led to a synergistic effect. A drug combination that could be investigated is CL-54 inhibitors with isoniazid. This first-line TB drug inhibits the mycolic acid biosynthesis, which are important lipids of the outer cell membrane composition of Mtb (Bardou *et al.*, 1998), accounting for approximately 60% of the mycobacterial cell wall (Chiaradia *et al.*, 2017). Liu *et al.* (2016) reported that the combination of an ICL inhibitor (IMBI-3) with isoniazid led to a synergetic effect, decreasing the colony-formation of *M. avium* in macrophages. Their reasoning was that the effect of isoniazid might have facilitated the penetration of IMBI-3 through the mycobacterial cell membrane. Therefore, employing CL-54 drugs with isoniazid could

be a powerful combination that could bypass the cell membrane penetration issue. For instance, the combination of CL-54-01 or CL-54-02 with isoniazid might lead to a bacteriostatic or bactericidal effect. In the case of CL-54-04, combining with isoniazid could decrease the concentration of CL-54-04 needed to cause a bactericidal effect further.

Itaconate and other ICL inhibitors never moved to clinical trials because of high toxicity in mammalian cells and animal models. Hence, future work could investigate the toxicity of the CL-54 drug family in mammalian cells by mitochondrial health in an MTT assay. The major reason behind the high toxicity of ICL inhibitors in animal models has been the inhibition of other enzymes, such as succinate dehydrogenase or 6-phosphofructo-2-kinase (Sakai *et al.*, 2004; Lampropoulou *et al.*, 2016). An approach to investigate if these drugs may inhibit other metabolic enzymes would be to test CL-54-04 against the ICL KD strain with glycerol as a sole carbon source by colony-forming unit assay. If the ICL deficient strain treated with CL-54-04 demonstrates a significant growth defect, it would mean that the inhibitor has off-target effects. An untargeted metabolomic analysis could then be done to identify the pathways being affected by the drug. This may narrow down the possible off-target candidates.

To evaluate if these novel ICL inhibitors are promising clinical trial candidates, an *ex vivo* CFU assay using TB-infected macrophages could be investigated in future work. The aim of this experiment will be to assess whether the ICL inhibitor can kill Mtb inside the macrophage. For this, monocytes could be propagated and specialised into macrophages and challenged with Mtb Erdman and ICL KD strains. A series of conditions can be tested: no drug treatment, different concentrations of CL-54 drug alone, CL-54 in combination with isoniazid, and isoniazid alone. Different time points (e.g., day 2 and day 5) can be sampled to monitor the drug effect over time. The macrophage lysate can be plated on M7H10 plates to quantify the colony-forming units after 21 days. The result from this experiment will be a crucial factor in the decision to test these inhibitors *in vivo*.

An interesting route would be to test these novel ICL inhibitors against other ICL-containing microorganisms. The first would be to try these inhibitors against different mycobacteria, such as *M. bovis* and *M. avium paratuberculosis*. Both affect animals, but the former causes TB in animals, whilst the latter is the etiologic agent of Johne's

disease-causing chronic inflammatory bowel disease (Rathnaiah *et al.*, 2017). These two agents pose a significant economic burden to beef and dairy farmers (Butler *et al.*, 2010). It is also a risk to humans as transmission can occur through ingestion of unpasteurised milk, contaminated water or foods or airborne contagion (Michel *et al.*, 2015; Buss *et al.*, 2016). Furthermore, *M. avium paratuberculosis* has also been implicated in Chron's disease in humans (McNees *et al.*, 2015; Garvey, 2018). Other pathogenic microorganisms also have ICL, such as fungi (*Candida albicans*, *Candida glabrata* and *Paracoccidioides brasiliensis*) or bacteria (*Escherichia coli* O157:H7 or *Pseudomonas aeruginosa*). A sequence alignment of the ICL from a range of organisms shows a totally conserved active site motif ('KKCGH') – Figure 8-3.

sp Q7TZA8 ACEA2_MYCBO	DTGHGGDPHVRNLI	RRFVEVGPYHIEDQRP	GT	KKCGH	QGGKVLVPSDEQIKRLNAARF	238
tr A0A0H3JR68 A0A0H3JR68_ECO57	EAGFGGVLNAFELMKAMIEAGAAVHFEDQLASV	KKCGH	MGGKVLVPTQEAIQKLVAAARL			218
sp P9WKK6 ACEA1_MYCTO	EAGFGGALNVYELQKALIAAGVAGSHWEDQLASE	KKCGH	LGGKVLIP	TQQHIRTLSARL		214
tr Q73SW2 Q73SW2_MYCPA	EAGFGGALNVFELQKAMIAAGVAGSHWEDQLASE	KKCGH	LGGKVLIP	TQQHIRTLSARL		216
sp P25248 ACEA_BRANA	DTGFGGTTATVKLCKLFVERGAAGVHIEDQSSVT	KKCGH	MAGKVLVAVSEHINRLVAARL			236
sp P28297 ACEA_ARATH	DTGFGGTTATVKLCKLFVERGAAGVHIEDQSSVT	KKCGH	MAGKVLVAVSEHINRLVAARL			236
sp Q6FPK7 ACEA_CANGA	DAGHGGLTAVFKLTKMFIERGAAGIHMEDQTSTN	KKCGH	MAGRCVIPVQEHINRLVTIRM			239
sp Q9P8Q7 ACEA_CANAX	DTGHGGITAIKLT	KMFIERGAAGIHIEDQAPGT	KKCGH	MAGKVLVVPVQEHINRLVAIRA		233
sp Q86ZF1 ACEA_LEPMC	DTGHGGLTAIMKLT	KLFIERGAAGIHIEDQAPGT	KKCGH	MAGKVLVPISEHINRLVAIRA		229
tr C1G3G7 C1G3G7_PARBD	DTGHGGLTAVMKLT	KLFIERGAAGIHIEDQAPGT	KKCGH	MAGKVLVPISEHINRLVAIRA		229
	::*.*	:* : : *	. * **	*****	.*: : : .: * . * : *	

Figure 8-3: Sequence alignment of ICL active site (motif KKCGH, highlighted in yellow) for different organisms. ACEA2_MYCBO refers to *Mycobacterium bovis*, A0A0H3JR68_ECO57 refers to *Escherichia coli* O157:H7 strain, ACEA1_MYCTO refers to *Mycobacterium tuberculosis*, Q73SW2_MYCPA refers to *Mycobacterium avium paratuberculosis*, ACEA_BRANA refers to *Brassica napus*, ACEA_ARATH refers to *Arabidopsis thaliana*, ACEA_CANGA refers to *Candida glabrata*, ACEA_CANAX refers to *Candida albicans*, ACEA_LEPMC refers to *Leptosphaeria maculans*, and C1G3G7_PARDBD refers to *Paracoccidioides brasiliensis*. All sequences were obtained from the UniProt database.

Candida albicans, for instance, is the most prevalent cause of fungal infections in humans, causing Candidiasis (Mayer *et al.*, 2013). ICL is also essential in *C. albicans* as the deletion of this enzyme rendered this opportunistic fungus avirulent in an *in vivo* mouse model, whilst reintroducing the ICL gene restored the virulence *in vivo* (Lorenz and Fink, 2001). The *C. albicans* ICL is 550 amino acid long and share a 39.29% sequence identity with Mtb ICL. The superimposition of these two ICL demonstrates that the 3D structure of their active site is also conserved – Figure 8-4.

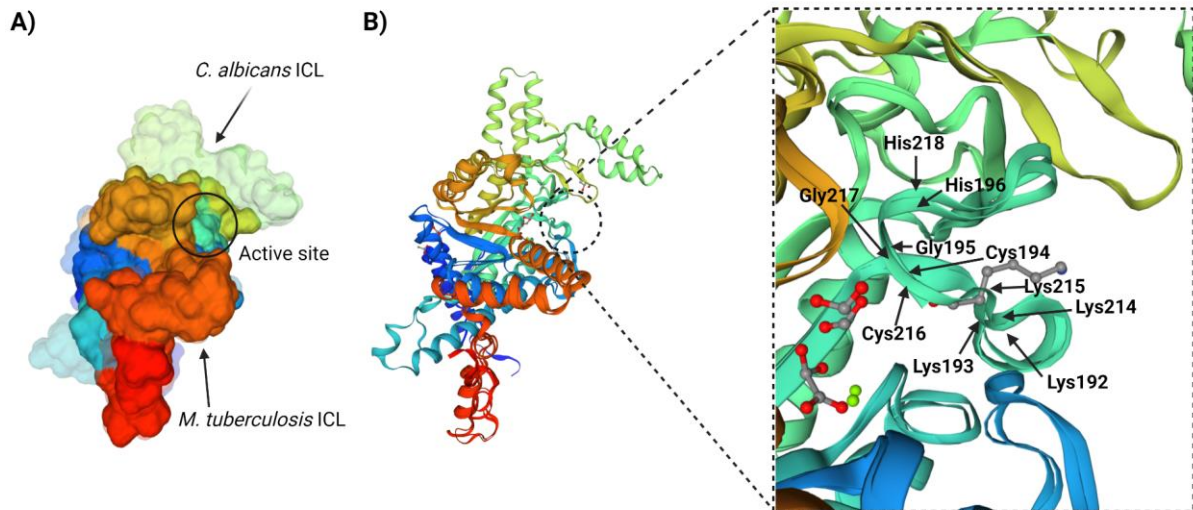


Figure 8-4: Superimposition of *C. albicans* ICL (Q9P8Q7) and Mtb ICL1 (P9WKK6). **A)** Surface model of both *C. albicans* and Mtb ICL superimposed with the active site highlighted. The faded structure refers to *C. albicans* ICL (550 amino acids), and the solid structure is Mtb ICL (428 amino acids). **B)** Ribbon representation of both ICL superimposition with a zoom in the active site. The catalytic residues ('KKCGH') are depicted, where Lys192-His196 belongs to Mtb ICL and Lys214-His218 to *C. albicans* ICL. Sequences were obtained from the UniProt database.

ICL is essential to other pathogenic fungus such as *Magnaporthe grisea* (the rice blast fungus) and bacteria such as *Pseudomonas aeruginosa* (Kretzschmar *et al.*, 2008; Chew *et al.*, 2019). In this work, it was demonstrated that the 'KKCGH' motif has a distinct movement upon CL-54 binding, closing the ICL active site in Mtb. Based on the sequence alignment, the 3D active site structure and essentiality of ICL, it is speculated that the CL-54 inhibitors could also be used against other ICL-containing bacteria and fungus. Moreover, it seems unlikely that a mutation will arise in the ICL active site, making an ICL inhibitor a potent drug candidate. An experimental approach to confirm this would be to treat an ICL-containing microorganism with sub-lethal concentrations of an ICL inhibitor for multiple generations and sequence the ICL coding gene (e.g. *icl1* and *aceA* genes for Mtb).

Chapter 9 – Conclusion

This research focused in developing and screening new inhibitors against isocitrate lyase (ICL), which is a crucial enzyme for the metabolism of the tuberculosis-causing bacteria, *Mycobacterium tuberculosis* (Mtb). The experimental aspect of this work includes the expression and purification of the ICL1 enzyme, the synthesis of inhibitor candidates and testing them against the isolated enzyme. The CL-54 family was identified as lead compounds due to their estimated half-maximal inhibitory concentration of 50 nM. New conditions to crystallise ICL were determined and used to soak with CL-54-01, whose structure was diffracted and solved. The CL-54-01 drug causes a significant conformational change of the catalytic loop, similarly to 3-nitropropionate (a known ICL1 inhibitor), but with half of the concentration needed to inhibit the enzyme *in vitro*. Although against the isolated enzyme, all three CL-54 drugs had potent inhibitory properties, only CL-54-04 had a bactericidal effect against the Mtb, suggesting that drug penetration may be the issue for CL-54-01 and CL-54-02. A drug combination screening of CL-54-04 with rifampicin or bedaquiline led to an additive effect in the checkerboard assay and a significant impact in the colony-forming unit assay. The drug combination was used to assess the drug combination effects on Mtb metabolism. Rifampicin with CL-54-04 showed a higher MCC accumulation, suggesting that rifampicin may enhance the CL-54-04 inhibitory effect against ICL. The role of fatty acid metabolism in drug tolerance was explored using three mutant strains of Mtb, $\Delta pckA$, ICL knock-down and $\Delta prpD$. All three mutants were more tolerant to isoniazid in fatty acids rich media than their parental strains. Similarly, Mtb wild type was also more tolerant to isoniazid and D-cycloserine in acetate media than in glycerol, supporting that fatty acid metabolism plays a role in drug tolerance. Future work could look at further characterising the inhibitory effect of CL-54 drug family against ICL and their specificity for ICL, testing these novel inhibitors efficacy against Mtb in macrophages, assessing their toxicity in mammalian cells, synthesising the next generation of CL-54 analogues with extra methyl groups to increase the cell wall penetration, and testing the CL-54 drugs to inhibit other ICL-containing microorganisms.

References

- Adams, K. N., Takaki, K., Connolly, L. E., Wiedenhoft, H., Winglee, K., Humbert, O., Edelstein, P. H., Cosma, C. L., and Ramakrishnan, L. (2011). Drug tolerance in replicating mycobacteria mediated by a macrophage-induced efflux mechanism. *Cell*. 145(1), pp. 39–53.
- Ahmad, S. (2011) Pathogenesis, immunology, and diagnosis of latent mycobacterium tuberculosis infection. *Clinical and Developmental Immunology*. (814943), pp. 1-17.
- Alston, T. A., Mela, L., and Bright, H. J. (1977). 3-Nitropropionate, the toxic substance of *Indigofera*, is a suicide inactivator of succinate dehydrogenase. *Proceedings of the National Academy of Sciences of the United States of America*. 74(9), pp. 3767-3771.
- Andries, K., Verhasselt, P., Guillemont, J., Göhlmann, H. W. H., Neefs, J. M., Winkler, H., Van Gestel, J., Timmerman, P., Zhu, M., Lee, E., Williams, P., De Chaffoy, D., Huitric, E., Hoffner, S., Cambau, E., Truffot-Pernot, C., Lounis, N., and Jarlier, V. (2005). A diarylquinoline drug active on the ATP synthase of *Mycobacterium tuberculosis*. *Science*, 307(5707), pp. 223–227.
- Aziz, M. A., Wright, A., Laszlo, A., De Muynck, A., Portaels, F., Van Deun, A., Wells, C., Nunn, P., Blanc, L., and Raviglione, M. (2006). Epidemiology of antituberculosis drug resistance (the Global Project on Anti-tuberculosis Drug Resistance Surveillance): an updated analysis. *Lancet*. 368(9553), pp. 2142-2154.
- Bachmann, N. L., Salamzade, R., Manson, A. L., Whittington, R., Sintchenko, V., Earl, A. M., and Marais, B. J. (2020). Key Transitions in the Evolution of Rapid and Slow Growing Mycobacteria Identified by Comparative Genomics. *Frontiers in Microbiology*, 10.
- Baer, C. E., Rubin, E. J., and Sasseti, C. M. (2015). New insights into TB physiology suggest untapped therapeutic opportunities. *Immunological Reviews*. 264(1), pp. 327-343.
- Baker, J.J. and Abramovitch, R.B. (2018). Genetic and metabolic regulation of *Mycobacterium tuberculosis* acid growth arrest. *Scientific Reports*. 8(4168), pp. 1-16.
- Bakker-Woudenberg, I. A. J. M., van Vianen, W., van Soolingen, D., Verbrugh H.A, and van Agtmael, M. A. (2005). Antimycobacterial agents differ with respect to their bacteriostatic versus bactericidal activities in relation to time of exposure, mycobacterial growth phase, and their use in combination. *Antimicrobial Agents and Chemotherapy*, 49(6), pp. 2387–2398.
- Bald, D. , Villellas, C., Lu, P., and Koul, A. (2017). Targeting energy metabolism in *Mycobacterium tuberculosis*, a new paradigm in antimycobacterial drug discovery. *mBio*. 8(2), e00272.
- Bard, J., Ercolani, K., Svenson, K., Olland, A., and Somers, W. (2004). Automated systems for protein crystallization. *Methods*, 34(3), pp. 329–347.
- Bardou, F., Raynaud, C., Ramos, C., Lanéelle, M. A., and Lanéelle, G. (1998). Mechanism of isoniazid uptake in *Mycobacterium tuberculosis*. *Microbiology*. pp.

2539-2544.

Behar, S. M., Martin, C. J., Booty, M. G., Nishimura, T., Zhao, X., Gan, H. X., Divangahi, M., and Remold, H. G. (2011). Apoptosis is an innate defense function of macrophages against *Mycobacterium tuberculosis*. *Mucosal Immunology*. 4(3), pp. 279-287.

Behr, M. A. (2013). Evolution of *Mycobacterium tuberculosis*. *Adv Exp Med Biol*, 783, pp. 81–91.

Bennett, J. E., Dolin, R., and Blaser, M. J. (2015). Mandell, Douglas, and Bennett's Principles and Practice of Infectious Diseases 5th Edn. *Journal of Antimicrobial Chemotherapy*. 46(2), p. 343.

Bentrup, K. H. Z., Miczak, A., Swenson, D. L., and Russell, D. G. (1999). Characterization of activity and expression of isocitrate lyase in *Mycobacterium avium* and *Mycobacterium tuberculosis*. *Journal of Bacteriology*. 181(23), pp. 7161-7167.

Beste, D. J. V., Espasa, M., Bonde, B., Kierzek, A. M., Stewart, G. R., and McFadden, J. (2009). The genetic requirements for fast and slow growth in mycobacteria. *PLoS ONE*, 4(4), e5349.

Bhusal, R. P., Bashiri, G., Kwai, B. X. C., Sperry, J., and Leung, I. K. H. (2017). Targeting isocitrate lyase for the treatment of latent tuberculosis. *Drug Discovery Today*. 22(7), pp. 1008-1016.

Bhusal, R., Jiao, W., Kwai, B., Reynisson, J., Collins, A., Sperry, J., Bashiri, G. and Leung, I. (2019). Acetyl-CoA-mediated activation of *Mycobacterium tuberculosis* isocitrate lyase 2. *Nature Communications*, 10(1).

Bi, J., Wang, Y., Yu, H., Qian, X., Wang, H., Liu, J., and Zhang, X. (2017). Modulation of Central Carbon Metabolism by Acetylation of Isocitrate Lyase in *Mycobacterium tuberculosis*. *Scientific Reports*. 7(44826).

Biuković, G., Basak, S., Manimekalai, M. S. S., Rishikesan, S., Roessle, M., Dick, T., Rao, S. P. S., Hunke, C., and Grüber, G. (2013). Variations of subunit ϵ of the *Mycobacterium tuberculosis* F1FO ATP synthase and a novel model for mechanism of action of the tuberculosis drug TMC207. *Antimicrobial Agents and Chemotherapy*. 57(1), pp. 168-176.

Blair, H. A., and Scott, L. J. (2015). Delamanid: a review of its use in patients with multidrug-resistant tuberculosis. *Drugs*. 75(1). pp. 91–100.

Blair, J. M. A., Webber, M. A., Baylay, A. J., Ogbolu, D. O., and Piddock, L. J. V. (2015). Molecular mechanisms of antibiotic resistance. *Nature Reviews Microbiology*. 13(1), pp 42-51.

Blomgran, R., Desvignes, L., Briken, V., and Ernst, J. D. (2012). *Mycobacterium tuberculosis* inhibits neutrophil apoptosis, leading to delayed activation of naive CD4 T cells. *Cell Host and Microbe*. 11(1), pp. 81-90.

Booth, A. N., Taylor, J., Wilson, R. H., and Deeds, F. (1952). The inhibitory effects of itaconic acid in vitro and in vivo. *The Journal of Biological Chemistry*. 195(2), pp. 697-702.

Boshtam, M., Shahreza, H. K., Feizollahzadeh, S., Rahimmanesh, I., and Asgary, S.

(2018). Expression and purification of biologically active recombinant rabbit monocyte chemoattractant protein1 in *Escherichia coli*. *FEMS Microbiology Letters*, 365(9), pp. 1–7.

Botella, H., Peyron, P., Levillain, F., Poincloux, R., Poquet, Y., Brandli, I., Wang, C., Tailleux, L., Tilleul, S., Charriere, G.M., Waddell, S.J., Foti, M., Lugo-Villarino, G., Gao, Q., Maridonneau-Parini, I., Butcher, P.D., Castagnoli, P.R., Gicquel, B., de CC, N. O. (2011). Mycobacterial p(1)-type ATPases mediate resistance to zinc poisoning in human macrophages. *Cell Host and Microbe*.10, 248–259.

Bozzano, F., Marras, F., and De Maria, A. (2014). Immunology of tuberculosis. In *Mediterranean Journal of Hematology and Infectious Diseases*. 6(1), e2014027.

Brauner, A., Fridman, O., Gefen, O., and Balaban, N. Q. (2016). Distinguishing between resistance, tolerance and persistence to antibiotic treatment. *Nature Reviews Microbiology*. 14(5), pp 320-330.

Brennan P.J. and Nikaido, H., (1995). The envelope of mycobacteria. *Annual Review of Biochemistry*. 64, pp. 29–63.

Brites, D., and Gagneux, S. (2012). Old and new selective pressures on *Mycobacterium tuberculosis*. *Infection, Genetics and Evolution*. 12(4), pp. 678-685.

Brites, D., and Gagneux, S. (2015). Co-evolution of *Mycobacterium tuberculosis* and *Homo sapiens*. *Immunological Reviews*. 264(1), pp. 6-24.

British Thoracic Association. (1975). Short-course chemotherapy in pulmonary tuberculosis. *Lancet*. 305(7899), pp. 119-124.

British Thoracic Association. (1982). A controlled trial of six months chemotherapy in pulmonary tuberculosis. Second report: results during the 24 months after the end of chemotherapy. British Thoracic Association. *The American Review of Respiratory Disease*. 126(3), pp. 460-462.

Britton, K., Langridge, S., Baker, P., Weeradechapon, K., Sedelnikova, S., De Lucas, J., Rice, D. and Turner, G. (2000). The crystal structure and active site location of isocitrate lyase from the fungus *Aspergillus nidulans*. *Structure*. 8(4), pp. 349–362.

Britton, K., Abeysinghe, I., Baker, P., Barynin, V., Diehl, P., Langridge, S., McFadden, B., Sedelnikova, S., Stillman, T., Weeradechapon, K. and Rice, D. (2001). The structure and domain organisation of *Escherichia coli* isocitrate lyase. *Acta Crystallographica Section D: Biological Crystallography*. 57(9), pp. 1209-1218.

Brzozowski, A. M. and Walton, J. (2001). Clear strategy screens for macromolecular crystallisation. *Journal of Applied Crystallography*. 34(2), pp. 97-101.

Buss, B. F., Keyser-Metobo, A., Rother, J., Holtz, L., Gall, K., Jereb, J., Murphy, C. N., Iwen, P. C., Robbe-Austerman, S., Holcomb, M. A., and Infield, P. (2016). Possible Airborne Person-to-Person Transmission of *Mycobacterium bovis* - Nebraska 2014-2015. *MMWR Morbidity Mortal Wkly Rep*. 65(8), pp.197–201.

Butler, A. J., Loble, M. and Winter, M. (2010). Economic Impact Assessment of Bovine Tuberculosis in the South West of England. *CRPR Research Reports*, University of Exeter, Centre for Rural Policy Research, 30, pp. 1-68.

Cambier, C. J., Falkow, S., and Ramakrishnan, L. (2014). Host evasion and exploitation schemes of *Mycobacterium tuberculosis*. *Cell*. 159(7), pp. 1497-1509.

Cambier, C. J., Takaki, K. K., Larson, R. P., Hernandez, R. E., Tobin, D. M., Urdahl, K. B., Cosma, C. L., and Ramakrishnan, L. (2014). *Mycobacteria* manipulate macrophage recruitment through coordinated use of membrane lipids. *Nature*. 505, pp. 218-222.

CDC. (2012). Questions and Answers About TB [Online]. Available at: https://www.cdc.gov/tb/publications/faqs/qa_introduction.htm. (Accessed: 28 April 2019).

CDC. (2014). TB Fact Sheets Treatment of Multidrug-Resistant Tuberculosis: Bedaquiline [Online]. Available at: <https://www.cdc.gov/tb/publications/factsheets/treatment/bedaquiline.htm> (Accessed 28 April 2019).

CDC. (2018). History | World TB Day | TB. Centre for Disease Control and Prevention [Online]. Available at: <https://www.cdc.gov/tb/worldtbdays/history.htm> (Accessed 28 April 2019).

Chakraborty, S., and Rhee, K. Y. (2015). Tuberculosis drug development: History and evolution of the mechanism-based paradigm. *Cold Spring Harbor Perspectives in Medicine*. 5(8), a021147.

Chan, E. D., Laurel, V., Strand, M. J., Chan, J. F., Huynh, M. L. N., Goble, M., and Iseman, M. D. (2004). Treatment and outcome analysis of 205 patients with multidrug-resistant tuberculosis. *American Journal of Respiratory and Critical Care Medicine*. 169(10), pp. 1103-1109.

Chayen, N. E. and Saridakis, E. (2008). Protein crystallisation: From purified protein to diffraction-quality crystal. *Nature Methods*. 5, pp. 147-153.

Chen, R. Y., Westfall, A. O., Mugavero, M. J., Cloud, G. A., Raper, J. L., Chatham, A. G., Acosta, E. P., Taylor, K. H., Carter, J., and Saag, M. S. (2003). Duration of Highly Active Antiretroviral Therapy Regimens. *Clinical Infectious Diseases*. 37(5), pp. 714-722.

Chen, Z., Wang, T., Liu, Z., Zhang, G., Wang, J., Feng, S., and Liang, J. (2015). Inhibition of autophagy by MiR-30A induced by *Mycobacteria tuberculosis* as a possible mechanism of immune escape in human macrophages. *Japanese Journal of Infectious Diseases*. 68(5), pp. 420-424.

Chen, E. Y., Liu, F. W., Megido, L., Diez, P., Fuentes, M., Fager, C., Olsson, E., Gessner, I. and Mathur, S. (2018). Understanding and utilizing the biomolecule/nanosystems interface. *Nanotechnologies in Preventive and Regenerative Medicine*. pp. 207-297.

Chenault, K. H. and Whitesides, G. M. (1989). Lactate dehydrogenase-catalyzed regeneration of NAD from NADH for use in enzyme-catalyzed synthesis. *Bioorganic Chemistry*. 17(4), pp. 400-409.

Chew, S.Y., Chee, W.J.Y. and Than, L.T.L. (2019). The glyoxylate cycle and alternative carbon metabolism as metabolic adaptation strategies of *Candida glabrata*:

perspectives from *Candida albicans* and *Saccharomyces cerevisiae*. *J Biomed Sci.* 26(52), pp. 1-10.

Chiaradia, L., Lefebvre, C., Parra, J., Marcoux, J., Burlet-Schiltz, O., Etienne, G., Tropis, M., and Daffé, M. (2017). Dissecting the mycobacterial cell envelope and defining the composition of the native mycomembrane. *Scientific Reports.* 7(12807).

Chitale, S., Ehrt, S., Kawamura, I., Fujimura, T., Shimono, N., Anand, N., Lu, S., Cohen-Gould, L., and Riley, L. W. (2001). Recombinant Mycobacterium tuberculosis protein associated with mammalian cell entry. *Cellular Microbiology.* 3(4), pp. 247-254.

Chokshi, A., Sifri, Z., Cennimo, D., and Horng, H. (2019). Global contributors to antibiotic resistance. *Journal of Global Infectious Diseases.* 11(1), pp. 36-42.

Cholo, M. C., Mothiba, M. T., Fourie, B., and Anderson, R. (2017). Mechanisms of action and therapeutic efficacies of the lipophilic antimycobacterial agents clofazimine and bedaquiline. *Journal of Antimicrobial Chemotherapy.* 72(2), pp. 338-353.

Collins, P. M., Ng, T. J., Talon, R., Nekrosiute, K., Krojer, T., Douanhamath, A., Neto-Brandao, J., Wright, N., Pearce, N. M. and von Delft, F. (2017). Gentle, fast and effective crystal soaking by acoustic dispensing. *Acta Crystallographica Section D: Structural Biology.* 73(3), pp. 246-255.

Cox, J. S., Chess, B., McNeil, M., and Jacobs, W. R. (1999). Complex lipid determines tissue-specific replication of Mycobacterium tuberculosis in mice. *Nature.* 4, 6757, pp. 79-83.

Daniel, T. M. (1997). Captain of death: the story of tuberculosis. *Medical History,* 43(1), pp. 149–149.

Danley, D. E. (2006). Crystallization to obtain protein-ligand complexes for structure-aided drug design. *Acta Crystallographica Section D: Biological Crystallography.* 62(6), pp. 569-575.

de Carvalho, L. P. S., Fischer, S. M., Marrero, J., Nathan, C., Ehrt, S. and Rhee, K. Y. (2010). Metabolomics of mycobacterium tuberculosis reveals compartmentalized catabolism of carbon substrates. *Chemistry and Biology.* 17(10), pp. 1122–1131.

de Martino, M., Lodi, L., Galli, L., and Chiappini, E. (2019). Immune Response to Mycobacterium tuberculosis: A Narrative Review. *Frontiers in Pediatrics.* 7(350).

Devulder, G., de Montclos, M. P., and Flandrois, J. P. (2005). A multigene approach to phylogenetic analysis using the genus Mycobacterium as a model. *International Journal of Systematic and Evolutionary Microbiology.* 55(1).

Dixon G. H. and Kornberg H. L. (1959). Assay methods for key enzymes of the glyoxylate cycle. *Proc. Biochem. Soc.*72, p. 3.

Donoghue, H. D., Lee, O. Y. C., Minnikin, D. E., Besra, G. S., Taylor, J. H., and Spigelman, M. (2010). Tuberculosis in Dr Granville's mummy: A molecular re-examination of the earliest known Egyptian mummy to be scientifically examined and given a medical diagnosis. *Proceedings of the Royal Society B: Biological Sciences.* 227(1678), pp. 51-56.

Duff, M. R., Jr, Grubbs, J. and Howell, E. E. (2011). Isothermal titration calorimetry for measuring macromolecule-ligand affinity. *Journal of visualized experiments: JoVE,*

(55), e2796.

Dunn, P. L. and North, R. J. (1995) Virulence ranking of some *Mycobacterium tuberculosis* and *Mycobacterium bovis* strains according to their ability to multiply in the lungs, induce lung pathology, and cause mortality in mice. *Infection and Immunity*, 63(9), pp. 3428–3437.

Dutta, A. K., Rösgen, J., and Rajarathnam, K. (2015). Using isothermal titration calorimetry to determine thermodynamic parameters of protein-glycosaminoglycan interactions. *Methods in molecular biology (Clifton, N.J.)*, 1229, 315–324.

Eoh, H. and Rhee, K. Y. (2013) Multifunctional essentiality of succinate metabolism in adaptation to hypoxia in *Mycobacterium tuberculosis*. *Proceedings of the National Academy of Sciences of the United States of America*, 16(110), pp. 6554–6559.

Eoh, H., and Rhee, K. Y. (2014). Methylcitrate cycle defines the bactericidal essentiality of isocitrate lyase for survival of *Mycobacterium tuberculosis* on fatty acids. *PNAS*, 13(111), pp. 4976–4981.

Eum, S. Y., Kong, J. H., Hong, M. S., Lee, Y. J., Kim, J. H., Hwang, S. H., Cho, S. N., Via, L. E., and Barry, C. E. (2010). Neutrophils are the predominant infected phagocytic cells in the airways of patients with active pulmonary TB. *Chest*. 137(1), pp. 122-128.

Evangelopoulos, D., Fonseca, J. D. da, and Waddell, S. J. (2015). Understanding anti-tuberculosis drug efficacy: Rethinking bacterial populations and how we model them. *International Journal of Infectious Diseases*. 32, pp. 76-80.

Evangelopoulos, D., Prosser, G. A., Rodgers, A., Dagg, B. M., Khatri, B., Ho, M. M., Gutierrez, M. G., Cortes, T., and de Carvalho, L. P. S. (2019). Comparative fitness analysis of D-cycloserine resistant mutants reveals both fitness-neutral and high-fitness cost genotypes. *Nature Communications*. 10, 4177.

Fedarovich, A., Djordjevic, K. A., Swanson, S. M., Peterson, Y. K., Nicholas, R. A. and Davies, C. (2012). High-Throughput Screening for Novel Inhibitors of *Neisseria gonorrhoeae* Penicillin-Binding Protein 2. *PLoS ONE*. 7(9), pp. 1-9.

Fedrizzi, T., Meehan, C. J., Grottola, A., Giacobazzi, E., Fregni Serpini, G., Tagliazucchi, S., Fabio, A., Bettua, C., Bertorelli, R., De Sanctis, V., Rumpianesi, F., Pecorari, M., Jousson, O., Tortoli, E., and Segata, N. (2017). Genomic characterization of Nontuberculous *Mycobacteria*. *Scientific Reports*. 7, 45258.

Finkelstein, M., Gold, H. and Paterno, C. (1947). Pharmacology of Itaconic acid and its sodium, magnesium, and calcium salts. *Journal of the American Pharmaceutical Association*, 36(6), 173–179.

Fischbach, M. A. (2011). Combination therapies for combating antimicrobial resistance. *Current Opinion in Microbiology*. 14(5), pp. 519–523.

Fleischmann, R.D., Alland, D., Eisen, J.A., Carpenter, L., White, O., Peterson, J., DeBoy, R., Dodson, R., Gwinn, M., Haft, D., Hickey, E., Kolonay, J.F., Nelson, W.C., Umayam, L.A., Ermolaeva, M., Salzberg, S.L., Delcher, A., Utterback, T., Weidman, J., Khouri, H., Gill, J., Mikula, A., Bishai, W., Jacobs, W.R., Jr, Venter, J.C. and Fraser,

- C.M. (2002) Whole-genome comparison of Mycobacterium tuberculosis clinical and laboratory strains. *J Bacteriol.* 184(19), pp. 5479-5490.
- Fox, W., Ellard, G. A., and Mitchison, D. A. (1999). Studies on the treatment of tuberculosis undertaken by the British Medical Research Council Tuberculosis Units, 1946-1986, with relevant subsequent publications. *International Journal of Tuberculosis and Lung Disease.* 3(10), pp.231-279.
- Freire, E., Mayorga, O. L. and Straume, M. (1990) Isothermal Titration Calorimetry. *Anal. Chem.* 62(18), pp. 950–959.
- Fry, S. H., Barnabas, S., and Cotton, M. F. (2019). Tuberculosis and HIV - An update on the “cursed duet” in children. *Frontiers in Pediatrics.* 7(159).
- Fu, L. M., and Fu-Liu, C. S. (2002). Is Mycobacterium tuberculosis a closer relative to Gram-positive or Gram-negative bacterial pathogens?. *Tuberculosis.* 82(2), pp. 85-90.
- Funatsu, G., and Wittmann, H. G. (1972). Ribosomal proteins: XXXIII. Location of amino-acid replacements in protein S12 isolated from Escherichia coli mutants resistant to streptomycin. *Journal of Molecular Biology.* 68(3), pp. 547-550.
- Furin, J., Cox, H., and Pai, M. (2019). Tuberculosis. *The Lancet.* 393(10181), pp. 1642-1656.
- Gallegos, A. M., Pamer, E. G., and Glickman, M. S. (2008). Delayed protection by ESAT-6-specific effector CD4+ T cells after airborne M. tuberculosis infection. *Journal of Experimental Medicine.* 205(10), pp. 2359-2368.
- Galloway, C. A., Sowden, M. P., and Smith, H. C. (2003). Increasing the yield of soluble recombinant protein expressed in E. coli by Induction during late log phase. *BioTechniques,* 34(3), pp. 524–530.
- Garg, A., Barnes, P. F., Porgador, A., Roy, S., Wu, S., Nanda, J. S., Griffith, D. E., Girard, W. M., Rawal, N., Shetty, S., and Vankayalapati, R. (2006). Vimentin Expressed on Mycobacterium tuberculosis -Infected Human Monocytes Is Involved in Binding to the NKp46 Receptor. *The Journal of Immunology.* 177(9), pp. 6192-6198.
- Garvey M. (2018). *Mycobacterium avium subspecies paratuberculosis*: A possible causative agent in human morbidity and risk to public health safety. *Open veterinary journal.* 8(2), pp. 172–181.
- Gawad, J., and Bonde, C. (2018). Decaprenyl-phosphoryl-ribose 2'-epimerase (DprE1): challenging target for antitubercular drug discovery. *Chemistry Central journal.* 12(1). pp 72.
- Gengenbacher, M., and Kaufmann, S. H. E. (2012). Mycobacterium tuberculosis: Success through dormancy. *FEMS Microbiology Reviews.* 36(3), pp. 514-532.
- Gengenbacher, M., Rao, S. P. S., Pethe, K., and Dick, T. (2010). Nutrient-starved, non-replicating Mycobacterium tuberculosis requires respiration, ATP synthase and isocitrate lyase for maintenance of ATP homeostasis and viability. *Microbiology.* 156(1).
- Glaziou, P., Floyd, K., and Raviglione, M. C. (2018). Global Epidemiology of Tuberculosis. *Seminars in Respiratory and Critical Care Medicine.* 39(3), pp. 271-285.

Goel, D. (2014). Bedaquiline: A novel drug to combat multiple drug-resistant tuberculosis. *Journal of Pharmacology and Pharmacotherapeutics*. 5(1), pp. 76-78.

Gollan, B., Grabe, G., Michaux, C. and Helaine, S. (2019). Bacterial persisters and infection: Past, present, and progressing. *Annu. Rev. Microbiol.* 73, 359–385.

Goude, R., Amin, A. G., Chatterjee, D., and Parish, T. (2009). The arabinosyltransferase EmbC is inhibited by ethambutol in Mycobacterium tuberculosis. *Antimicrobial Agents and Chemotherapy*. 53(10), p 4138-4146.

Gould, T. A., Van De Langemheen, H., Muñoz-Elías, E. J., McKinney, J. D., and Sacchettini, J. C. (2006). Dual role of isocitrate lyase 1 in the glyoxylate and methylcitrate cycles in Mycobacterium tuberculosis. *Molecular Microbiology*. 61(4), pp. 940-947.

Govada, L. and Chayen, N. E. (2019). Choosing the method of crystallisation to obtain optimal results. *Crystals*. 9(2), pp. 1-7.

Greene, J. G., Sheu, S. S., Gross, R. A., and Greenamyre, J. T. (1998). 3-Nitropropionic acid exacerbates N-methyl-D-aspartate toxicity in striatal culture by multiple mechanisms. *Neuroscience*. 84(2), pp. 503-510.

Grumbach, F., Rist, N., Libermann, D., Moyeux, M., Cals, S., and Clavel, S. (1956). Experimental antituberculous activity of certain isonicotinic thioamides substituted on the nucleus. *C R Hebd Seances Acad Sci*, 242(17), 2187–2189.

Guglielmetti, L., Jaspard, M., Le Dû, D., Lachâtre, M., Marigot-Outtandy, D., Bernard, C., Veziris, N., Robert, J., Yazdanpanah, Y., Caumes, E., and Fréchet-Jachym, M. (2017). Long-term outcome and safety of prolonged bedaquiline treatment for multidrug-resistant tuberculosis. *European Respiratory Journal*. 49(3).

Haagsma, A. C., Abdillahi-Ibrahim, R., Wagner, M. J., Krab, K., Vergauwen, K., Guillemont, J., Andries, K., Lill, H., Koul, A., and Bald, D. (2009). Selectivity of TMC207 towards Mycobacterial ATP synthase compared with that towards the eukaryotic homologue. *Antimicrobial Agents and Chemotherapy*. 53(3), p. 1290-1292.

Hamada, Yohei Getahun, Haileyesus Raviglione, M. (2018). Latent tuberculosis infection : updated and consolidated guidelines for programmatic management. *World Health Organization*. pp. 1-78.

Hariguchi, N., Chen, X., Hayashi, Y., Kawano, Y., Fujiwara, M., Matsuba, M., Shimizu, H., Ohba, Y., Nakamura, I., Kitamoto, R., Shinohara, T., Uematsu, Y., Ishikawa, S., Itotani, M., Haraguchi, Y., Takemura, I., and Matsumoto, M. (2020). OPC-167832, a Novel Carbostyryl Derivative with Potent Antituberculosis Activity as a DprE1 Inhibitor. *Antimicrobial agents and chemotherapy*. 64(6), e02020-19.

Harriff, M. J., Cansler, M. E., Toren, K. G., Canfield, E. T., Kwak, S., Gold, M. C., and Lewinsohn, D. M. (2014). Human lung epithelial cells contain Mycobacterium tuberculosis in a late endosomal vacuole and are efficiently recognized by CD8+ T Cells. *PLoS ONE*. 9(5).

Harrold, M. W. and Zavod, R. M. (2014) Basic Concepts in Medicinal Chemistry. *Drug Development and Industrial Pharmacy*. 40(7). pp. 1–36.

Hasenoehrl, E. J., Sajorda, D. R., Berney-Meyer, L., Johnson, S., Tufariello, J. M.,

- Fuhrer, T., Cook, G. M., Jacobs Jr., W. R. and Berney, M. (2019). Derailing the aspartate pathway of *Mycobacterium tuberculosis* to eradicate persistent infection. *Nat. Commun.* 10, pp. 1–12.
- Hassell, A., An, G., Bledsoe, R., Bynum, J., Carter, H., Deng, S., Gampe, R., Grisard, T., Madauss, K., Nolte, R., Rocque, W., Wang, L., Weaver, K., Williams, S., Wisely, G., Xu, R. and Shewchuk, L. (2006). Crystallisation of protein-ligand complexes. *Acta Crystallographica Section D: Biological Crystallography.* 63(1), pp.72-79.
- Hauptman, H. A. (1990). History of X-ray crystallography. *Structural Chemistry.* 1(6), pp. 617–620.
- Hinchey, J., Lee, S., Jeon, B. Y., Basaraba, R. J., Venkataswamy, M. M., Chen, B., Chan, J., Braunstein, M., Orme, I. M., Derrick, S. C., Morris, S. L., Jacobs, W. R., and Porcelli, S. A. (2007). Enhanced priming of adaptive immunity by a proapoptotic mutant of *Mycobacterium tuberculosis*. *Journal of Clinical Investigation.* 117(8), pp. 2279-2288.
- Honore, N., and Cole, S. T. (1994). Streptomycin resistance in mycobacteria. *Antimicrobial Agents and Chemotherapy.* 38(2), 238-242.
- Hou, H., Shi, M., Hu, S., Ahmad, F., Zhang, B., Chen, Z. and Yin, D. (2019). A systematic comparison of sitting and hanging-drop crystallisation using traditional and cross-diffusion microbatch crystallisation plates. *Journal of Crystal Growth.* 521, pp.1-8.
- Hu, Y., Coates, A. R., and Mitchison, D. A. (2006). Sterilising action of pyrazinamide in models of dormant and rifampicin-tolerant *Mycobacterium tuberculosis*. *The international journal of tuberculosis and lung disease.* 10(3), pp. 317–322.
- Jackson, M. (2014). The mycobacterial cell envelope-lipids. *Cold Spring Harbor Perspectives in Medicine,* 4(10).
- Jackson, M. and Mantsch, H. H. (1991). Beware of proteins in DMSO. *Biochimica et Biophysica Acta (BBA)/Protein Structure and Molecular,* 1078(2), pp. 231–235.
- Jain, P., Hsu, T., Arai, M., Biermann, K., Thaler, D., Nguyen, A., González, P., Tufariello, J., Kriakov, J., Chen, B., Larsen, M. and Jacobs, W. (2014). Specialized transduction designed for precise high-throughput unmarked deletions in *Mycobacterium tuberculosis*. *mBio,* 5(3).
- Jang, J., Becq, J., Gicquel, B., Deschavanne, P., and Neyrolles, O. (2008). Horizontally acquired genomic islands in the tubercle bacilli. *Trends in Microbiology.* 16(7), pp. 303-308.
- Jindani, A., Doré, C. J., and Mitchison, D. A. (2003). Bactericidal and sterilizing activities of antituberculosis drugs during the first 14 days. *American Journal of Respiratory and Critical Care Medicine.* 167(10), pp. 1348-1354.
- Joshi, S. M., Pandey, A. K., Capite, N., Fortune, S. M., Rubin, E. J., and Sasseti, C. M. (2006). Characterization of mycobacterial virulence genes through genetic interaction mapping. *Proceedings of the National Academy of Sciences of the United States of America.* 103(31), pp. 11760-11765.

- Kalia, N. P., Lee, B.S., Ab Rahman, N. B., Moraski, G. C., Miller, M. J. and Pethe, K. (2019). Carbon metabolism modulates the efficacy of drugs targeting the cytochrome bc 1 :aa 3 in Mycobacterium tuberculosis. *Scientific Reports*, 9(1), pp. 1-9.
- Kapopoulou, A., Lew, J. M. and Cole, S. T. (2011). The MycoBrowser portal: A comprehensive and manually annotated resource for mycobacterial genomes. *Tuberculosis*, 91(1), pp. 8–13.
- Kaufmann, S. H. E. (2001). How can immunology contribute to the control of tuberculosis?. *Nature Reviews Immunology*. 1, pp. 20-30.
- Keam, S.J. (2019). Pretomanid: First Approval. *Drugs*. 79, pp. 1797–1803.
- Keren, I., Minami, S., Rubin, E., and Lewis, K. (2011). Characterization and Transcriptome Analysis of Mycobacterium tuberculosis Persisters. *MBio*, 2(3), pp. 3–12.
- Kierzek, A. M. and Zielenkiewicz, P. (2001). Models of protein crystal growth. *Biophysical Chemistry*, 91(1), pp. 1–20.
- Kim, C. J., Kim, N. H., Song, K. H., Choe, P. G., Kim, E. S., Park, S. W., Kim, H. Bin, Kim, N. J., Kim, E. C., Park, W. B., and Oh, M. don. (2013). Differentiating rapid- and slow-growing mycobacteria by difference in time to growth detection in liquid media. *Diagnostic Microbiology and Infectious Disease*. 75(1), pp. 73-76.
- Khanna, V. S. and Ranganathan, N., P. (2019). Rational structure-based drug design. *Encyclopedia of Bioinformatics and Computational Biology: ABC of Bioinformatics*, 2, pp. 585–600.
- Kretzschmar, U., Khodaverdi, V., Jeoung, J. H. and Görisch, H. (2008). Function and transcriptional regulation of the isocitrate lyase in Pseudomonas aeruginosa. *Archives of Microbiology*. 190(2), pp. 151–158.
- Ko, Y. H., and McFadden, B. A. (1990). Alkylation of isocitrate lyase from Escherichia coli by 3-bromopyruvate. *Archives of Biochemistry and Biophysics*. 278(1), pp. 373-380.
- Ko, Y. H., Smith, B. L., Wang, Y., Pomper, M. G., Rini, D. A., Torbenson, M. S., Hullahen, J., and Pedersen, P. L. (2004). Advanced cancers: Eradication in all cases using 3-bromopyruvate therapy to deplete ATP. *Biochemical and Biophysical Research Communications*. 324(1), pp. 269-275.
- Koch, A., Cox, H., and Mizrahi, V. (2018). Drug-resistant tuberculosis: challenges and opportunities for diagnosis and treatment. *Current Opinion in Pharmacology*. 42(1), pp. 7-15.
- Kondrashov, F., Koonin, E., Morgunov, I., Finogenova, T. and Kondrashova, M. (2006). Evolution of glyoxylate cycle enzymes in Metazoa: Evidence of multiple horizontal transfer events and pseudogene formation. *Biology Direct*, 1(31), pp. 1–14.
- Koul, A., Dendouga, N., Vergauwen, K., Molenberghs, B., Vranckx, L., Willebrords, R., Ristic, Z., Lill, H., Dorange, I., Guillemont, J., Bald, D. and Andries, K. (2007) Diarylquinolines target subunit c of mycobacterial ATP synthase. *Nat. Chem. Biol.* 3, pp. 323–324.

Kozic, J., Novotná, E., Volková, M., Stolaříková, J., Trejtnar, F., Wsól, V. and Vinšová, J. (2012). Synthesis and in vitro antimycobacterial and isocitrate lyase inhibition properties of novel 2-methoxy-2'-hydroxybenzanilides, their thioxo analogues and benzoxazoles. *European Journal of Medicinal Chemistry*, 56, pp. 108–119.

Krengel, U. and Imberty, A. (2007) Crystallography and Lectin Structure Database. *Lectins: Analytical Technologies*, Nilsson, C. L.: Elsevier Science B.V. pp. 15-50.

Kulchavenya, E. (2014). Extrapulmonary tuberculosis: are statistical reports accurate?. *Therapeutic Advances in Infectious Diseases*, 2(2), pp. 61–70.

Kumar, R., and Bhakuni, V. (2008). Mycobacterium tuberculosis isocitrate lyase [MtbICL1]: Role of divalent cations in modulation of functional and structural properties. *Proteins: Structure, Function and Genetics*. 72(3), pp. 892-900.

Kursar, M., Koch, M., Mittrücker, H.-W., Nouailles, G., Bonhagen, K., Kamradt, T., and Kaufmann, S. H. E. (2007). Cutting Edge: Regulatory T Cells Prevent Efficient Clearance of Mycobacterium tuberculosis. *The Journal of Immunology*. 178(5), pp. 2661-2665.

Kwai, B., Collins, A., Middleditch, M., Sperry, J., Bashiri, G. and Leung, I. (2021). Itaconate is a covalent inhibitor of the Mycobacterium tuberculosis isocitrate lyase. *RSC Medicinal Chemistry*, 12 (1), pp. 57-61.

Kwon, S., Chun, H., Ha, H., Lee, S. and Park, H. (2021). Heterogeneous multimeric structure of isocitrate lyase in complex with succinate and itaconate provides novel insights into its inhibitory mechanism. *PLoS ONE*, 16 (5), e0251067.

Laemmli, U.K. (1970). Cleavage of structural proteins during assembly of the head of bacteriophage T4. *Nature*, 227, pp.680–685.

Lampropoulou, V., Sergushichev, A., Bambouskova, M., Nair, S., Vincent, E., Loginicheva, E., Cervantes-Barragan, L., Ma, X., Huang, S., Griss, T., Weinheimer, C., Khader, S., Randolph, G., Pearce, E., Jones, R., Diwan, A., Diamond, M. and Artyomov, M. (2016). Itaconate Links Inhibition of Succinate Dehydrogenase with Macrophage Metabolic Remodeling and Regulation of Inflammation. *Cell Metabolism*. 24(1), pp. 158–166.

Lee, C. Y., Huang, C. H., Lu, P. L., Ko, W. C., Chen, Y. H., and Hsueh, P. R. (2017). Role of rifampin for the treatment of bacterial infections other than mycobacteriosis. *Journal of Infection*. 75(5), pp. 395-408.

Lee, D., Yeon, D., Galera-Laporta, L., Bialecka-Fornal, M., Moon, E. C., Shen, Z., Briggs, S. P., Garcia-Ojalvo, J., and Süel, G. M. (2019). Magnesium Flux Modulates Ribosomes to Increase Bacterial Survival. *Cell*, 177(2), pp. 352-360.

Lee, J. J., Lim, J., Gao, S., Lawson, C. P., Odell, M., Raheem, S., Woo, J., Kang, S.-H., Kang, S.-S., Jeon, B.-Y. and Eoh, H. (2018). Glutamate mediated metabolic neutralization mitigates propionate toxicity in intracellular Mycobacterium tuberculosis. *Sci. Rep.* 8, pp. 1–13.

Lee, M.-R., Sheng, W.-H., Hung, C.-C., Yu, C.-J., Lee, L.-N., and Hsueh, P.-R. (2015). Mycobacterium abscessus Complex Infections in Humans. *Emerging Infectious Diseases*. 21(9), pp. 1638-1646.

- Lee, Y. V., Wahab, H. A., and Choong, Y. S. (2015). Potential inhibitors for isocitrate lyase of mycobacterium tuberculosis and Non- M. tuberculosis: A summary. *BioMed Research International*. 2015(895453), pp. 1-20.
- Lehmann, J. (1964). Twenty years afterward historical notes on the discovery of the antituberculosis effect of paraaminosalicylic acid (PAS) and the first clinical trials. *The American Review of Respiratory Disease*, 90(1), pp. 953–956.
- Lerner, T. R., Borel, S., and Gutierrez, M. G. (2015). The innate immune response in human tuberculosis. In *Cellular Microbiology*. 17(9), pp. 1277-1285.
- Levy, S. (2012). The Evolution of Tuberculosis Genetic analysis offers new insight on the spread of an ancient disease. *BioScience*. 62(7), pp. 625-629.
- Lewis, K. (2010). Persister Cells. *Annu Rev Microbiol*, 64(1), pp. 357–372.
- Lillebaek, T., Dirksen, A., Baess, I., Strunge, B., and Thomsen, V. Ø. (2002). Molecular Evidence of Endogenous Reactivation of Mycobacterium tuberculosis after 33 Years of Latent Infection. *The Journal of Infectious Diseases*, 185(1), pp. 401–404.
- Liu, C. H., Liu, H., and Ge, B. (2017). Innate immunity in tuberculosis: Host defense vs pathogen evasion. *Cellular and Molecular Immunology*. 14(1), pp. 963-975.
- Liu, K., Yu and J. Russell, D. J., (2003). *pckA*-deficient Mycobacterium bovis BCG shows attenuated virulence in mice and in macrophages. *Microbiology (Reading)*. 149(7), pp.1829-1835.
- Liu, Y., Zhou, S., Deng, Q., Li, X., Meng, J., Guan, Y., Li, C., and Xiao, C. (2016). Identification of a novel inhibitor of isocitrate lyase as a potent antitubercular agent against both active and non-replicating Mycobacterium tuberculosis. *Tuberculosis*, 97, pp. 38–46.
- Liverani, M. (2015). Globalisation and infectious diseases, Hanefeld, J. *Globalisation and health*. 2nd ed. McGraw-Hill Education. p.156.
- Li, X., Hernandez, V., Rock, F. L., Choi, W., Mak, Y., Mohan, M., Mao, W., Zhou, Y., Easom, E. E., Plattner, J. J., Zou, W., Pérez-Herrán, E., Giordano, I., Mendoza-Losana, A., Alemparte, C., Rullas, J., Angulo-Barturen, I., Crouch, S., Ortega, F., Barros, D. and Alley, M. (2017). Discovery of a Potent and Specific M. tuberculosis Leucyl-tRNA Synthetase Inhibitor: (S)-3-(Aminomethyl)-4-chloro-7-(2-hydroxyethoxy)benzo[c][1,2]oxaborol-1(3H)-ol (GSK656). *Journal of medicinal chemistry*. 60(19). pp. 8011–8026.
- Lorenz, M. C. and Fink, G.R. (2001). The glyoxylate cycle is required for fungal virulence. *Nature*. 412, pp. 83–86.
- Luft, J., Collins, R., Fehrman, N., Lauricella, A., Veatch, C. and DeTitta, G. (2003). A deliberate approach to screening for initial crystallisation conditions of biological macromolecules. *Journal of Structural Biology*. 142(1), pp.170-179.
- Luo, M., Zhou, W., Patel, H., Srivastava, A. P., Symersky, J., Bonar, M. M., Faraldo-Gomez, J. D., Liao, M. and Mueller, D. M. (2020). Bedaquiline inhibits the yeast and human mitochondrial ATP synthases. *Commun Biol*. 3(452), pp. 1-10.
- Louw, G. E., Warren, R. M., Gey Van Pittius, N. C., McEvoy, C. R. E., Van Helden, P.

- D., and Victor, T. C. (2009). A balancing act: Efflux/influx in mycobacterial drug resistance. *Antimicrobial Agents and Chemotherapy*. 53(8), pp. 3181-3189.
- Ma, Z., Lienhardt, C., McIlleron, H., Nunn, A. J., and Wang, X. (2010). Global tuberculosis drug development pipeline: the need and the reality. *The Lancet*. 375(1), 9731, pp. 2100-2109.
- Makarov, V., Manina, G., Mikusova, K., Möllmann, U., Ryabova, O., Saint-Joanis, B., Dhar, N., Pasca, M. R., Buroni, S., Lucarelli, A. P., Milano, A., De Rossi, E., Belanova, M., Bobovska, A., Dianiskova, P., Kordulakova, J., Sala, C., Fullam, E., Schneider, P., McKinney, J. D. and Cole, S. T. (2009). Benzothiazinones kill Mycobacterium tuberculosis by blocking arabinan synthesis. *Science*. 324(5928), pp. 801–804.
- Makarov, V., Neres, J., Hartkoorn, R. C., Ryabova, O. B., Kazakova, E., Šarkan, M., Huszár, S., Piton, J., Kolly, G. S., Vocat, A., Conroy, T. M., Mikušová, K., and Cole, S. T. (2015). The 8-Pyrrole-Benzothiazinones Are Noncovalent Inhibitors of DprE1 from Mycobacterium tuberculosis. *Antimicrobial agents and chemotherapy*. 59(8), pp. 4446–4452.
- Malakar, P., and Venkatesh, K. V. (2012). Effect of substrate and IPTG concentrations on the burden to growth of Escherichia coli on glycerol due to the expression of Lac proteins. *Applied Microbiology and Biotechnology*, 93(6), pp. 2543–2549.
- Malani, P. N. (2012). Harrison's Principles of Internal Medicine. *JAMA*. 308(17), pp. 1813-1814.
- Marcenaro, E., Ferranti, B., Falco, M., Moretta, L., and Moretta, A. (2008). Human NK cells directly recognize Mycobacterium bovis via TLR2 and acquire the ability to kill monocyte-derived DC. *International Immunology*. 20(9), 1155-1167.
- Marrero, J., Rhee, K. Y., Schnappinger, D., Pethe, K. and Ehrt, S. (2010). Gluconeogenic carbon flow of tricarboxylic acid cycle intermediates is critical for Mycobacterium tuberculosis to establish and maintain infection. *Proc. Natl. Acad. Sci.* 107, pp. 1–6.
- Marttila, H. J., Soini, H., Eerola, E., Vyshnevskaya, E., Vyshnevskiy, B. I., Otten, T. F., Vasilyef, A. V., and Viljanen, M. K. (1998). A Ser315Thr substitution in KatG is predominant in genetically heterogeneous multidrug-resistant Mycobacterium tuberculosis isolates originating from the St. Petersburg area in Russia. *Antimicrobial Agents and Chemotherapy*. 42(9), pp. 2443-2445.
- Mayer, F. L., Wilson, D., and Hube, B. (2013). Candida albicans pathogenicity mechanisms. *Virulence*. 4(2), pp. 119–128.
- McDermott, W. (1969). The story of INH. *Journal of Infectious Diseases*. 119(6), pp. 678-683.
- McFadden, B. A., and Purohit, S. (1977). Itaconate, an isocitrate lyase directed inhibitor in Pseudomonas indigofera. *Journal of Bacteriology*. 131(1), pp. 136-144.
- McKinney, J. D. (2000). In vivo veritas: The search for TB drug targets goes live. *Nat. Med.* 6, pp. 1330–1333.

- McKinney, J. D., Bentrup, K. H. Z., Muñoz-Elias, E. J., Miczak, A., Chen, B., Chan, W. T., Swenson, D., Sacchettini, J. C., Jacobs, W. R., and Russell, D. G. (2000). Persistence of *Mycobacterium tuberculosis* in macrophages and mice requires the glyoxylate shunt enzyme isocitrate lyase. *Nature*. 406(1), pp. 735-738.
- McNae, I., Kan, D., Kontopidis, G., Patterson, A., Taylor, P., Worrall, L. and Walkinshaw, M., 2005. Studying protein–ligand interactions using protein crystallography. *Crystallography Reviews*. 11(1), pp.61-71.
- McNees, A. L., Markesich, D., Zayyani, N. R., and Graham, D. Y. (2015). *Mycobacterium paratuberculosis* as a cause of Crohn's disease. *Expert review of gastroenterology and hepatology*. 9(12), pp. 1523–1534.
- McPherson, A. and Gavira, J. A. (2014). Introduction to protein crystallisation. *Acta Crystallographica Section F: Structural Biology Communications*. 70(1), pp. 2-20.
- Michael, C. A., Dominey-Howes, D., and Labbate, M. (2014). The antimicrobial resistance crisis: Causes, consequences, and management. In *Frontiers in Public Health*. 2(1), pp. 1-8.
- Michel, A. L., Geoghegan, C., Hlokwe, T., Raseleka, K., Getz, W. M. and Marcotty, T. (2015). Longevity of *Mycobacterium bovis* in Raw and Traditional Souring Milk as a Function of Storage Temperature and Dose. *PLoS ONE*. 10(6): e0129926
- Michelucci, A., Cordes, T., Ghelfi, J., Pailot, A., Reiling, N., Goldmann, O., Binz, T., Wegner, A., Tallam, A., Rausell, A., Buttini, M., Linster, C. L., Medina, E., Balling, R., and Hiller, K. (2013). Immune-responsive gene 1 protein links metabolism to immunity by catalyzing itaconic acid production. *Proceedings of the National Academy of Sciences of the United States of America*. 110(19), pp. 7820-7825.
- Miotto, P., Cabibbe, A. M., Mantegani, P., Borroni, E., Fattorini, L., Tortoli, E., Migliori, G. B., and Cirillo, D. M. (2012). GenoType MTBDRs/ performance on clinical samples with diverse genetic background. *European Respiratory Journal*. 40(1), pp. 690-698.
- Miyoshi-Akiyama, T., Matsumura, K., Kobayashi, N., Maeda, S. and Kirikae, T. (2011). Genome sequence of clinical isolate *Mycobacterium tuberculosis* NCGM2209, *Journal of Bacteriology*. 193(23), p. 6792.
- Miyoshi-Akiyam, T., Matsumura, K., Iwai, H., Funatogawa, K. and Kirikae, T. (2012). Complete annotated genome sequence of *Mycobacterium tuberculosis* Erdman', *Journal of Bacteriology*. 194(10), pp. 2770.
- Moazed, D., and Noller, H. F. (1987). Interaction of antibiotics with functional sites in 16S ribosomal RNA. *Nature*. 327(1), pp. 389-394.
- Moretta, A. (2002). Natural killer cells and dendritic cells: Rendezvous in abused tissues. *Nature Reviews Immunology*. 2(1), pp. 957-965.
- Moynihan, M. M., and Murkin, A. S. (2014). Cysteine is the general base that serves in catalysis by isocitrate lyase and in mechanism-based inhibition by 3-nitropropionate. *Biochemistry*. 53(1), pp. 178-187.
- Müller, I. (2017). Guidelines for the successful generation of protein-ligand complex crystals. *Acta Crystallographica Section D: Structural Biology*. 73(2), pp. 79-92.

- Muñoz-Elías, E. J. and McKinney, J. D. (2005). Mycobacterium tuberculosis isocitrate lyases 1 and 2 are jointly required for in vivo growth and virulence. *Nature Medicine*. 11(6), pp. 638-644.
- Muñoz-Elías, E. J., Upton, A. M. and Mckinney, J. D. (2006) Role of the methylcitrate cycle in Mycobacterium tuberculosis metabolism, intracellular growth, and virulence. *Mol. Microbiol.* 60. pp. 1109–1122.
- Musser, J. M. (1995). Antimicrobial agent resistance in mycobacteria: Molecular genetic insights. *Clinical Microbiology Reviews*. 8(4), pp. 496-514.
- Nandakumar, M., Nathan, C., and Rhee, K. Y. (2014). Isocitrate lyase mediates broad antibiotic tolerance in Mycobacterium tuberculosis. *Nature Communications*, 5(1), 1–10.
- Nathanson, E., Gupta, R., Huamani, P., Leimane, V., Pasechnikov, A. D., Tupasi, T. E., Vink, K., Jaramillo, E., and Espinal, M. A. (2004). Adverse events in the treatment of multidrug-resistant tuberculosis: Results from the DOTS-Plus initiative. *International Journal of Tuberculosis and Lung Disease*. 8(11), 1382-1384.
- Ndlovu, H. and Marakalala, M. J. (2016). Granulomas and Inflammation: Host-Directed Therapies for Tuberculosis. *Frontiers in Immunology*. 7(434), pp. 1-11.
- NHS. (2019). *Tuberculosis - Overview* [Online]. Available at: <https://www.nhs.uk/conditions/tuberculosis/tb/> (Accessed 29 April 2019).
- Njire, M., Tan, Y., Mugweru, J., Wang, C., Guo, J., Yew, W. W., Tan, S., and Zhang, T. (2015). Pyrazinamide resistance in Mycobacterium tuberculosis: Review and update. *Advances in Medical Sciences*. 61(1), pp. 63-71.
- Odds, F. C. (2003). Synergy, antagonism, and what the checkerboard puts between them. *Journal of Antimicrobial Chemotherapy*, 52(1).
- Oizumi, K., Kumano, N., Konno, K., and Oka, S. (1974). Mode of action of kanamycin on mycobacterium bovis, BCG. *Kekkaku(Tuberculosis)*. 49(1), pp. 9-14.
- Onyebujoh, P., Zumla, A., Ribeiro, I., Rustomjee, R., Mwaba, P. Gomes, M. and Grange, J. M. (2005). Treatment of tuberculosis: Present status and future prospects. *Bulletin of the World Health Organization*, 83(11), pp. 857–865.
- Orenstein, E. W., Basu, S., Shah, N. S., Andrews, J. R., Friedland, G. H., Moll, A. P., Gandhi, N. R., and Galvani, A. P. (2009). Treatment outcomes among patients with multidrug-resistant tuberculosis: systematic review and meta-analysis. *The Lancet Infectious Diseases*. 9(3), pp. 153-161.
- Orhan, G., Bayram, A., Zer, Y. and Balci, I. (2005). Synergy tests by E test and checkerboard methods of antimicrobial combinations against Brucella melitensis. *Journal of Clinical Microbiology*. 43(1), pp. 140–143.
- Palencia, A., Li, X., Bu, W., Choi, W., Ding, C. Z., Easom, E. E., Feng, L., Hernandez, V., Houston, P., Liu, L., Meewan, M., Mohan, M., Rock, F. L., Sexton, H., Zhang, S., Zhou, Y., Wan, B., Wang, Y., Franzblau, S. G., Woolhiser, L. and Alley, M. R. (2016). Discovery of Novel Oral Protein Synthesis Inhibitors of Mycobacterium tuberculosis That Target Leucyl-tRNA Synthetase. *Antimicrobial agents and chemotherapy*. 60(10), pp. 6271–6280.

- Palomino, J. C., and Martin, A. (2014). Drug Resistance Mechanisms in *Mycobacterium tuberculosis*. *Antibiotics (Basel, Switzerland)*, 3(3). pp. 317–340.
- Pankey, G. A. and Sabath, L. D. (2004). Clinical Relevance of Bacteriostatic versus Bactericidal Mechanisms of Action in the Treatment of Gram-Positive Bacterial Infections. *Clinical Infectious Diseases*. 38(6), pp. 864–870.
- Park, H. D., Guinn, K. M., Harrell, M. I., Liao, R., Voskuil, M. I., Tompa, M., Schoolnik, G. K., and Sherman, D. R. (2003). Rv3133c/dosR is a transcription factor that mediates the hypoxic response of *Mycobacterium tuberculosis*. *Molecular Microbiology*. 48(3), pp. 833-843.
- Park, Y., Cho, Y., Lee, Y., Lee, Y. and Rhee, S. (2016). Crystal structure and functional analysis of isocitrate lyases from *Magnaporthe oryzae* and *Fusarium graminearum*. *Journal of Structural Biology*. 194(3), pp.395-403.
- Pethe, K., Bifani, P., Jang, J. *et al.* (2013). Discovery of Q203, a potent clinical candidate for the treatment of tuberculosis. *Nat Med*. 19. pp. 1157–1160.
- Pham, T. V., Murkin, A. S., Moynihan, M. M., Harris, L., Tyler, P. C., Shetty, N., Sacchettini, J. C., Huang, H., and Meek, T. D. (2017). Mechanism-based inactivator of isocitrate lyases 1 and 2 from *Mycobacterium tuberculosis*. *Proceedings of the National Academy of Sciences*, 114(29), pp. 7617–7622.
- Pham, T. V., Mellott, D., Moghadamchargari, Z., Chen, K., Krieger, I., Laganowsky, A., Sacchettini, J. and Meek, T. (2021). Covalent Inactivation of *Mycobacterium tuberculosis* Isocitrate Lyase by cis-2,3-Epoxy-Succinic Acid. *ACS Chemical Biology*, 16 (3), pp. 463-470.
- Phillely, J. V., and Griffith, D. E. (2015). Treatment of slowly growing mycobacteria. *Clinics in Chest Medicine*. 36(1), pp. 79-90.
- Prosser, G. A., and de Carvalho, L. P. S. (2013a). Metabolomics reveal D-alanine: D-alanine ligase as the target of D-cycloserine in *Mycobacterium tuberculosis*. *ACS Medicinal Chemistry Letters*. 4(12) pp. 1233-1237.
- Prosser, G. A., and de Carvalho, L. P. S. (2013b). Reinterpreting the mechanism of inhibition of *Mycobacterium tuberculosis* d-alanine: D-alanine ligase by d-cycloserine. *Biochemistry*. 52(40), pp. 7145-7149.
- Puckett, S., Trujillo, C. Wang, Z., Eoh, H., Ioerger, T. R., Krieger, I., Sacchettini, J., Schnappinger, D. Rhee, K. Y. and Ehrt, S. (2017). Malate synthase detoxifies glyoxylate in *Mtb*. *Proceedings of the National Academy of Sciences*. 114 (11) E2225-E2232.
- Queval, C. J., Brosch, R., and Simeone, R. (2017). The macrophage: A disputed fortress in the battle against *Mycobacterium tuberculosis*. *Frontiers in Microbiology*. 8(2284), pp. 1-11.
- Quigley, J., Hughitt, V. K., Velikovskiy, C. A., Mariuzza, R. A., El-Sayed, N. M., and Briken, V. (2017). The cell wall lipid PDIM contributes to phagosomal escape and host cell exit of *Mycobacterium tuberculosis*. *MBio*. 8(2), e00148-17.
- Raheem, S. (2011). Studies on the synthesis of dicaffeoylquinic acid. PhD. University of St. Andrews.

Ramage, H. R., Connolly, L. E., and Cox, J. S. (2009). Comprehensive functional analysis of Mycobacterium tuberculosis toxin-antitoxin systems: Implications for pathogenesis, stress responses, and evolution. *PLoS Genetics*. 5(12), e1000767.

Ramaswamy, S., and Musser, J. M. (1998). Molecular genetic basis of antimicrobial agent resistance in Mycobacterium tuberculosis: 1998 update. *Tubercle and Lung Disease*. 79(1), pp. 3-29.

Rao, G. R., and McFadden, B. A. (1965). Isocitrate lyase from Pseudomonas indigofera. IV. Specificity and inhibition. *Archives of Biochemistry and Biophysics*. 112(2), pp. 294-303.

Rao, S. P. S., Alonso, S., Rand, L., Dick, T., and Pethe, K. (2008). The protonmotive force is required for maintaining ATP homeostasis and viability of hypoxic, nonreplicating Mycobacterium tuberculosis. *Proceedings of the National Academy of Sciences of the United States of America*. 105(33), pp. 11945-11950.

Rathnaiah, G., Zinniel, D. K., Bannantine, J. P., Stabel, J. R., Gröhn, Y. T., Collins, M. T., and Barletta, R. G. (2017). Pathogenesis, Molecular Genetics, and Genomics of Mycobacterium avium subsp. paratuberculosis, the Etiologic Agent of Johne's Disease. *Frontiers in Veterinary Science*. 4(187), pp 1-13.

Ratledge, C., Stanford, J., Minnikin, D.E. (1982). Lipids: Complex lipids, their chemistry, biosynthesis, and roles. *The Biology of the Mycobacteria*, eds Ratledge C, Stanford J (Academic, New York), pp. 95–184

Rawlins, M. (2012). The disputed discovery of streptomycin. *The Lancet*. 380(9838), p. 207.

Ray, S., Kreitler, D., Gulick, A. and Murkin, A. (2018). The Nitro Group as a Masked Electrophile in Covalent Enzyme Inhibition. *ACS Chemical Biology*. 13(6), pp.1470-1473

Read, A. F., and Woods, R. J. (2014). Antibiotic resistance management. *Evolution, Medicine and Public Health*. 2014(1), p. 147.

Reta, G. F., Tonn, C. E., Rios-Luci, C., Leon, L. G., Perez-Roth, E., Padron, J. M., and Donadel, O. J. (2012). Cytotoxic Bioactivity of some Phenylpropanoic Acid Derivatives. *Natural Products Communications*. 7(10), pp. 1341-1346.

Robinson, D. R. and Jencks, W. P. (1965). The Effect of Concentrated Salt Solutions on the Activity Coefficient of Acetyltetraglycine Ethyl Ester. *Journal of the American Chemical Society*. 5(87), pp. 2470–2479.

Rosano, G. L., and Ceccarelli, E. A. (2014). Recombinant protein expression in Escherichia coli: Advances and challenges. *Frontiers in Microbiology*, 5, pp. 1–17.

Rouse, D. A., Li, Z., Bai, G. H., and Morris, S. L. (1995). Characterization of the katG and inhA genes of isoniazid-resistant clinical isolates of Mycobacterium tuberculosis. *Antimicrobial Agents and Chemotherapy*. 39(11), pp. 2472-2477.

Rozwarski, D. A., Grant, G. A., Barton, D. H. R., Jacobs, W. R., and Sacchettini, J. C. (1998). Modification of the NADH of the isoniazid target (InhA) from Mycobacterium tuberculosis. *Science*. 279(5347), pp. 98-102.

- Ruiz, P., Rodríguez-Cano, F., Zerolo, F. J., and Casal, M. (2002). Investigation of the In Vitro activity of streptomycin against *Mycobacterium tuberculosis*. *Microbial Drug Resistance*. 8(2), pp. 147-149.
- Ryan, F. (1992). *The Forgotten Plague*. 1st Edition. Back Bay Books. pp. 1-488.
- Ryu, W.-S. (2017). Virus Structure. *Molecular virology of human pathogenic viruses, 1st Edition: Academic Press*. pp. 21–29.
- Sakai, A., Aki Kusumoto, B. S., Yoshinobu, K. and Furuya, E. (2004). Itaconate reduces visceral fat by inhibiting fructose 2,6-bisphosphate synthesis in rat liver. *Nutrition*. 20(11), pp. 997–1002.
- Sakula, A. (1982). Robert Koch: Centenary of the discovery of the tubercle bacillus, 1882. *Bulletin of the International Union against Tuberculosis*. 24(4), pp. 127-131.
- Sarathy, J., Dartois, V., Dick, T. and Gengenbacher, M. (2013). Reduced drug uptake in phenotypically resistant nutrient-starved nonreplicating *Mycobacterium tuberculosis*. *Antimicrob. Agents Chemother.* 57, pp. 1648–1653.
- Scardigli, A., Caminero, J. A., Sotgiu, G., Centis, R., D'Ambrosio, L., and Migliori, G. B. (2016). Efficacy and tolerability of ethionamide versus prothionamide: A systematic review. *European Respiratory Journal*. 2016(48), pp. 946-952.
- Schatz, A., Bugle, E., and Waksman, S. A. (1944). Streptomycin, a Substance Exhibiting Antibiotic Activity Against Gram-Positive and Gram-Negative Bacteria. *Proceedings of the Society for Experimental Biology and Medicine*. 55(1), pp. 66-69.
- Schloss, J. V., and Cleland, W. W. (1982). Inhibition of Isocitrate Lyase by 3-Nitropropionate, a Reaction-Intermediate Analogue. *Biochemistry*. 21(18), pp. 4420-4427.
- Schmit, J. D. and Dill, K. (2012). Growth rates of protein crystals. *Journal of the American Chemical Society*. 134(9), pp. 3934-3937.
- Schnappinger, D., Ehrh, S., Voskuil, M. I., Liu, Y., Mangan, J. A., Monahan, I. M., Dolganov, G., Efron, B., Butcher, P. D., Nathan, C., and Schoolnik, G. K. (2003). Transcriptional Adaptation of *Mycobacterium tuberculosis* within Macrophages: Insights into the Phagosomal Environment. *Journal of Experimental Medicine*. 198(5), pp. 693-704.
- Sensi, P. (1983). History of the development of rifampin. *Reviews of Infectious Diseases*. 5(3), pp. 402-406.
- Shafiani, S., Tucker-Heard, G., Kariyone, A., Takatsu, K., and Urdahl, K. B. (2010). Pathogen-specific regulatory T cells delay the arrival of effector T cells in the lung during early tuberculosis. *Journal of Experimental Medicine*. 207(7), pp. 1409-1420.
- Sharma, V., Sharma, S., Hoener, K., McKinney, J. D., Russell, D. G., Jacobs, W. R., and Sacchettini, J. C. (2000). Structure of isocitrate lyase, a persistence factor of *Mycobacterium tuberculosis*. *Nature Structural and Molecular Biology*, 7(1), pp. 663–668.
- Shepherd, R. G., Baughn, C., Cantrall, M. L., Goodstein, B., Thomas, J. P., and Wilkinson, R. G. (1966). Structure-Activity Studies Leading To Ethambutol, a New Type of Antituberculous Compound. *Annals of the New York Academy of Sciences*,

135(2), pp. 686–710.

Shin, H., Jo, S. J., Kim, D. H., Kwon, O., and Myung, S. K. (2015). Efficacy of interventions for prevention of chemotherapy-induced alopecia: a systematic review and meta-analysis. *International journal of cancer*. 136(5), pp. E442-54.

Shin, J., Ragunathan, P., Sundararaman, L., Narthey, W., Kundu, S., Manimekalai, M. S. S., Bogdanovic, N., Dick, T. and Gruber, G. (2018). The NMR solution structure of Mycobacterium tuberculosis F-ATP synthase subunit ϵ provides new insight into energy coupling inside the rotary engine. *Fed. Eur. Biochem. Soc. J.* 285, pp. 1111–1128.

Shukla, H., Kumar, V., Singh, A. K., Singh, N., Kashif, M., Siddiqi, M. I., Yasoda Krishnan, M., and Akhtar, M. S. (2015). Insight into the structural flexibility and function of Mycobacterium tuberculosis isocitrate lyase. *Biochimie*. 110(1), pp. 73-80.

Shukla, H., Shukla, R., Sonkar, A., Pandey, T., and Tripathi, T. (2017). Distant Phe345 mutation compromises the stability and activity of Mycobacterium tuberculosis isocitrate lyase by modulating its structural flexibility. *Scientific Reports*. 7(1058), pp.1-11.

Silva Miranda, M., Breiman, A., Allain, S., Deknuydt, F., and Altare, F. (2012). The tuberculous granuloma: An unsuccessful host defence mechanism providing a safety shelter for the bacteria?. *Clinical and Developmental Immunology*. 2012(139127), pp. 1-15.

Silver, L. L. (2007). Multi-targeting by monotherapeutic antibacterials. *Nature Reviews Drug Discovery*. 6(1), pp. 41-55.

Singh, J., Petter, R. C., Baillie, T. A., and Whitty, A. (2011). The resurgence of covalent drugs. *Nature Reviews Drug Discovery*. 10(1), pp. 307-317.

Sinha, R. and Khare, S. K. (2014). Protective role of salt in catalysis and maintaining structure of halophilic proteins against denaturation. *Frontiers in Microbiology*. 5(165), pp. 1-6.

Sivashanmugam, A., Murray, V., Cui, C., Zhang, Y., Wang, J., and Li, Q. (2009). Practical protocols for production of very high yields of recombinant proteins using Escherichia coli. *Protein Science*, 18(5), pp. 936–948.

Slayden, R. A., and Barry, C. E. (2000). The genetics and biochemistry of isoniazid resistance in Mycobacterium tuberculosis. *Microbes and Infection*. 2(6), pp. 659-669.

Solovyev M. and Gisbert, E. (2016). Influence of time, storage temperature and freeze/thaw cycles on the activity of digestive enzymes from gilthead sea bream (*Sparus aurata*). *Fish Physiol Biochem*. 42(5), pp. 1383–1394.

Sriram, D., Yogeewari, P., Senthilkumar, P., Dewakar, S., Rohit, N., Debjani, B., Bhat, P., Veugopal, B., Pavan, V. and Thimmappa, H. (2009). Novel Pthalazinyll Derivatives: Synthesis, Antimycobacterial Activities, and Inhibition of Mycobacterium Tuberculosis Isocitrate Lyase Enzyme. *Medicinal Chemistry*, 5(5), pp. 422–422.

Sriram, D., Yogeewari, P., Senthilkumar, P., Sangaraju, D., Nelli, R., Banerjee, D., Bhat, P. and Manjashetty, T. (2010). Synthesis and antimycobacterial evaluation of novel phthalazin-4-ylacetamides against log- and starved phase cultures: Research

article. *Chemical Biology and Drug Design*, 75(4), pp. 381–391.

Stewart, P. S. and Mueller-Dieckmann, J. (2014). Automation in biological crystallization. *Acta Crystallographica Section F: Structural Biology Communications*. 70(6), pp. 686–696.

Stokes, J. M., Lopatkin, A. J., Lobritz, M. A. and Collins, J. J. (2019). Bacterial Metabolism and Antibiotic Efficacy. *Cell Metab.* 30, pp. 251–259.

Stokes, S. S., Vermula, R. and Pucci, M. J. (2020). Advancements of GyrB Inhibitors for Treatment of Infections Caused by Mycobacterium tuberculosis and Non-tuberculous Mycobacteria. *ACS Infect. Dis.* 6(6), pp. 1323-1331

Stratton, C. W. (2003). Dead bugs don't mutate: Susceptibility issues in the emergence of bacterial resistance. *Emerging Infectious Diseases*, 9(1), pp. 10–16.

Sugimoto, M., Sakagami, H., Yokote, Y., Onuma, H., Kaneko, M., Mori, M., Sakaguchi, Y., Soga, T., and Tomita, M. (2011). Non-targeted metabolite profiling in activated macrophage secretion. *Metabolomics*. 8(1), pp. 624-633.

Sun, W., Weingarten, R. A., Xu, M., Southall, N., Dai, S., Shinn, P., Sanderson, P. E., Williamson, P. R., Frank, K. M. and Zhen, W. (2016). Rapid antimicrobial susceptibility test for identification of new therapeutics and drug combinations against multidrug-resistant bacteria. *Emerging Microbes and Infections*. 5(11), e116.

Tamma, P. D., Cosgrove, S. E. and Maragakis, L. L. (2012). Combination therapy for treatment of infections with gram-negative bacteria. *Clinical Microbiology Reviews*. 25(3), pp. 450-470.

Tangallapally, R., Yendapally, R., Lee, R., Lenaerts, A. and Lee, R. (2005). Synthesis and evaluation of cyclic secondary amine substituted phenyl and benzyl nitrofuranyl amides as novel antituberculosis agents', *Journal of Medicinal Chemistry*, 48(26), pp. 8261–8269.

TB Alliance (2020). Inadequate Treatment [Online]. Available at: <https://www.tballiance.org/why-new-tb-drugs/inadequate-treatment> (Accessed: 28 April 2019).

Tenero, D., Derimanov, G., Carlton, A., Tonkyn, J., Davies, M., Cozens, S., Gresham, S., Gaudion, A., Puri, A., Muliaditan, M., Rullas-Trincado, J., Mendoza-Losana, A., Skingsley, A., and Barros-Aguirre, D. (2019). First-Time-in-Human Study and Prediction of Early Bactericidal Activity for GSK3036656, a Potent Leucyl-tRNA Synthetase Inhibitor for Tuberculosis Treatment. *Antimicrobial agents and chemotherapy*. 63(8), e00240-19.

'The antibiotic alarm'. (2013). *Nature*. 495(1), p. 141. Available at: <https://doi.org/10.1038/495141a>

Thomas, J. P., Baughn, C. O., Wilkinson, R. G., and Sheperd, R. G. (1961). A new synthetic compound with antituberculous activity in mice: ethambutol (dextro-2,2'-(ethylenediimino)-di-l-butanol). *The American Review of Respiratory Disease*, 83, pp. 891–893.

Tian J., Bryk R., Itoh M., Suematsu M. and Nathan C. (2005). Variant tricarboxylic acid cycle in Mycobacterium tuberculosis: identification of alpha-ketoglutarate decarboxylase. *PNAS*. 102, pp. 10670–10675.

- Torres-Cerna, C. E., Alejandro Morales, J., and Hernandez-Vargas, E. A. (2019). Modeling quorum sensing dynamics and interference on *Escherichia coli*. *Frontiers in Microbiology*, 10(1835), pp. 1–20.
- Torrey, H. L., Keren, I., Via, L. E., Lee, J. S., and Lewis, K. (2016). High Persister Mutants in *Mycobacterium tuberculosis*. *PLoS ONE*, 11(5), pp. 1–28.
- Trauner, A., Loughheed, K. E. A., Bennett, M. H., Hingley-Wilson, S. M., and Williams, H. D. (2012). The dormancy regulator DosR controls ribosome stability in hypoxic mycobacteria. *Journal of Biological Chemistry*. 287(28), pp. 24053-24063.
- UniProt. (2018). *ICL1 - Isocitrate lyase - Mycobacterium tuberculosis (strain ATCC 25618 / H37Rv) - ICL1 gene and protein*. UniProt [Online]. Available at: <http://www.uniprot.org/uniprot/P9WKK7> (Accessed 29 April 2019).
- Upton, A. M. and McKinney, J. D. (2007). Role of the methylcitrate cycle in propionate metabolism and detoxification in *Mycobacterium smegmatis*. *Microbiology (Reading)*. 153(12), pp. 3973-3982.
- Vilchèze, C., Wang, F., Arai, M., Hazbón, M. H., Colangeli, R., Kremer, L., Weisbrod, T. R., Alland, D., Sacchettini, J. C., and Jacobs, W. R. (2006). Transfer of a point mutation in *Mycobacterium tuberculosis inhA* resolves the target of isoniazid. *Nature Medicine*. 12(1), pp. 1027-1029.
- Vilchèze, C., Copeland, J., Keiser, T. L., Weisbrod, T., Washington, J., Jain, P., Malek, A., Weinrick, B. and Jacobs Jr., W. R. (2018). Rational design of biosafety level 2-approved, multidrug-resistant strains of *Mycobacterium tuberculosis* through nutrient auxotrophy. *mBio*. 9(3), e00938.
- Vivier, E., Raulet, D. H., Moretta, A., Caligiuri, M. A., Zitvogel, L., Lanier, L. L., Yokoyama, W. M., and Ugolini, S. (2011). Innate or adaptive immunity? The example of natural killer cells. *Science*. 331(6013), pp. 44-49.
- Von Hippel, P. H. and Wong, K. Y. (1964). Neutral salts: The generality of their effects on the stability of macromolecular conformations. *Science*. 256(7), pp. 3394–3398.
- Wald-Dickler, N., Holtom, P. and Spellberg, B. (2018). Busting the Myth of “Static vs Cidal”: A Systemic Literature Review. *Clinical infectious diseases*. 66(9), pp. 1470–1474.
- Warner, D. F. (2015). *Mycobacterium tuberculosis* metabolism. *Cold Spring Harbor Perspectives in Medicine*. 4(5), a021121.
- Wee, W. Y., Dutta, A., and Choo, S. W. (2017). Comparative genome analyses of mycobacteria give better insights into their evolution. *PLoS ONE*. e0172831, pp. 1-13.
- Wehrli, W. (1983). Rifampin: Mechanisms of Action and Resistance. *Rev Infect Dis*, 5(3), pp. 407–411.
- Wells, C. D., Cegielski, J. P., Nelson, L. J., Laserson, K. F., Holtz, T. H., Finlay, A., Castro, K. G., and Weyer, K. (2007). HIV Infection and Multidrug-Resistant Tuberculosis—The Perfect Storm. *The Journal of Infectious Diseases*. 196(1), pp. 86-107.
- WHO. (2010). Treatment of tuberculosis Guidelines Fourth edition. *WHO library*

Cataloguing in Publication Data (WHO/HTM/TB/2009.420).
[https://doi.org/10.1016/S0011-5029\(56\)80012-6](https://doi.org/10.1016/S0011-5029(56)80012-6).

WHO. (2018). Rapid Communication : key changes to treatment of multidrug- and rifampicin-resistant tuberculosis [Online]. Available at: https://www.who.int/tb/publications/2018/rapid_communications_MDR/en/ (Accessed 29 April 2019).

WHO. (2019). Global Tuberculosis Report 2019 [Online]. Available at: https://www.who.int/tb/publications/global_report/en/ (Accessed 29 April 2019).

WHO. (2020). Global Tuberculosis Report 2020 [Online]. Available at: <https://www.who.int/publications/i/item/9789240013131> (Accessed 29 April 2019).

Wienczek, J. M. (1999). New strategies for protein crystal growth. *Annual Review of Biomedical Engineering*. 1, pp. 505–534.

Wienen-Schmidt, B., Oebbeke, M., Ngo, K., Heine, A. and Klebe, G. (2020). Two Methods, One Goal: Structural Differences between Cocrystallization and Crystal Soaking to Discover Ligand Binding Poses. *ChemMedChem*. 16(1), pp. 292–300.

Wilson, R. B., and Maloy, S. R. (1987). Isolation and characterization of Salmonella typhimurium glyoxylate shunt mutants. *Journal of Bacteriology*. 169(7), pp. 3029-3034.

Wolf, A. J., Desvignes, L., Linas, B., Banaiee, N., Tamura, T., Takatsu, K., and Ernst, J. D. (2008). Initiation of the adaptive immune response to Mycobacterium tuberculosis depends on antigen production in the local lymph node, not the lungs. *Journal of Experimental Medicine*. 205(1), pp. 105-115.

Wolf, A. J., Linas, B., Trevejo-Nuñez, G. J., Kincaid, E., Tamura, T., Takatsu, K., and Ernst, J. D. (2007). Mycobacterium tuberculosis Infects Dendritic Cells with High Frequency and Impairs Their Function In Vivo. *The Journal of Immunology*. 179(4), pp. 2509-2519.

Worley, M. V., and Estrada, S. J. (2014). Bedaquiline: A novel antitubercular agent for the treatment of multidrug-resistant tuberculosis. *Pharmacotherapy*. 34(11), pp. 1187-1197.

Xavier, A. S., and Lakshmanan, M. (2014). Delamanid: A new armor in combating drug-resistant tuberculosis. *Journal of pharmacology and pharmacotherapeutics*. 5(3), pp 222–224.

Xiong, Y.L. (1997). Protein Denaturation and Functionality Losses. In: Erickson M.C., Hung YC. (eds) *Quality in Frozen Food*. Springer, Boston, MA. https://doi.org/10.1007/978-1-4615-5975-7_8

Xu, C., Bai, X., Xu, J., Xing, Y., Li, Z., Wang, J., Shi, J., Yu, L., and Wang, Y. (2017). Substituted 4-oxo-crotonic acid derivatives as a new class of protein kinase B (PknB) inhibitors: synthesis and SAR study. *RSC Adv*. 7(8), pp. 4763-4775.

Xu, X., Xu, L., Yuan, G., Wang, Y., Qu, Y. and Zhou, M. (2018). Synergistic combination of two antimicrobial agents closing each other's mutant selection windows to prevent antimicrobial resistance. *Scientific Reports*. 8(1).

Yamori, S., Ichiyama, S., Shimokata, K., Tsukamura, M. (1992). Bacteriostatic and Bactericidal Activity of Antituberculosis Drugs against Mycobacterium tuberculosis,

Mycobacterium avium-Mycobacterium intracellulare Complex and Mycobacterium kansasii in Different Growth Phases. *Microbiology and Immunology*, 36(4), pp. 361–368.

Warren, W. A., (1970). Catalysis of both oxidation and reduction of glyoxylate by pig heart lactate dehydrogenase isozyme 1. *Journal of Biol Chem.* 245(7), pp.1675-81.

Zhang, H., Deng, J. Y., Bi, L. J., Zhou, Y. F., Zhang, Z. P., Zhang, C. G., Zhang, Y., and Zhang, X. E. (2008). Characterization of Mycobacterium tuberculosis nicotinamidase/ pyrazinamidase. *FEBS Journal.* 275(4), pp. 745-762.

Zhang, Y., Dhandayuthapani, S., and Deretic, V. (1996). Molecular basis for the exquisite sensitivity of Mycobacterium tuberculosis to isoniazid. *Proceedings of the National Academy of Sciences of the United States of America.* 93(23), pp. 13212-13216.

Zhang, Y., Heym, B., Allen, B., Young, D., and Cole, S. (1992). The catalase - Peroxidase gene and isoniazid resistance of Mycobacterium tuberculosis. *Nature.* 358(1), pp. 591-593.

Zhang, Ying, Permar, S., and Sun, Z. (2002). Conditions that may affect the results of susceptibility testing of Mycobacterium tuberculosis to pyrazinamide. *Journal of Medical Microbiology.* 51(1), pp. 42-49.

Zhang, Y., Shi, W., Zhang, W., and Mitchison, D. (2014). Mechanisms of Pyrazinamide Action and Resistance. *Microbiology spectrum*, 2(4), pp. 1-12.

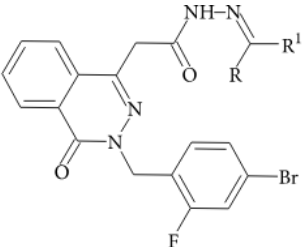
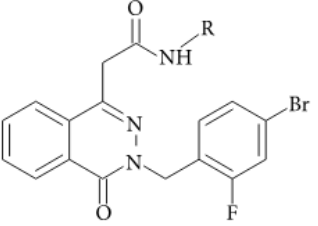
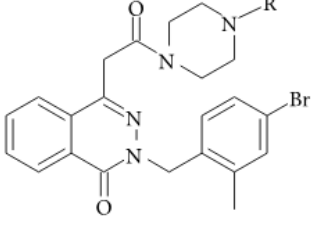
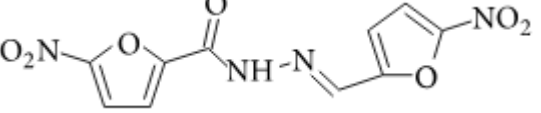
Zhang, Y., and Yew, W. W. (2015). Mechanisms of drug resistance in Mycobacterium tuberculosis: Update 2015. *International Journal of Tuberculosis and Lung Disease.* 19(11), pp. 1276-1289.

Zheng, J., Rubin, E. J., Bifani, P., Mathys, V., Lim, V., Au, M., Jang, J., Nam, J., Dick, T., Walker, J. R., Pethe, K., and Camacho, L. R. (2013). Para-aminosalicylic acid is a prodrug targeting dihydrofolate reductase in mycobacterium tuberculosis. *Journal of Biological Chemistry.* 288(32), pp. 23447-23456.

Zhou, M., Xie, L., Yang, Z., Zhou, J., and Xie, J. (2017). Lysine succinylation of Mycobacterium tuberculosis isocitrate lyase (ICL1) fine-tunes the microbial resistance to antibiotics. *Journal of Biomolecular Structure and Dynamics.* 35(5), pp. 1030-1041.

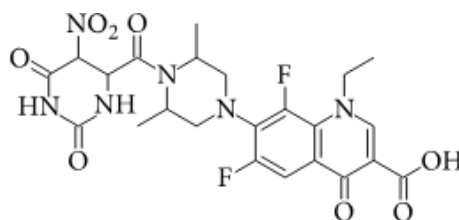
Appendix A – Literature Data

Table A1: Summary of Mtb ICL1 inhibitors and their IC₅₀ reported in the literature.

ICL1 inhibitor	Structure	IC ₅₀
Pthalazinyll derivative (Sriram <i>et al.</i> , 2009)		45–61% inhibition at 10 μM
Phthalazin-4-ylacetamides (Sriram <i>et al.</i> , 2010)		40.62–66% inhibition at 10 μM
Extract of traditional Chinese medicine (Lu <i>et al.</i> , 2010)		134 μg/mL
5-Nitro-2-furoic acid hydrazones with furan-2- carbaldehyde (Sriram <i>et al.</i> , 2010)		86.8% inhibition at 10 mM

5-Nitro-2,6-dioxohexahydro-4-pyrimidinecarboxamides

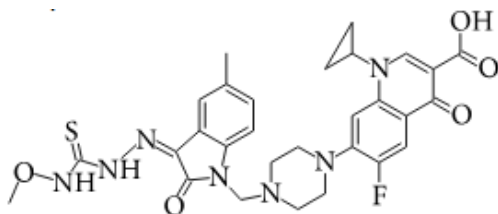
(Sriram *et al.*, 2010)



45.7% inhibition at 10 mM

Isatinyl thiosemicarbazones derivatives

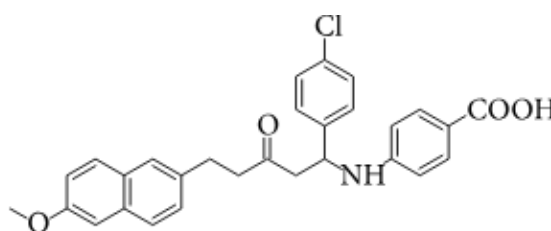
(Banerjee *et al.*, 2011)



63.44% inhibition at 10 mM

Mannich base, Ydcm67

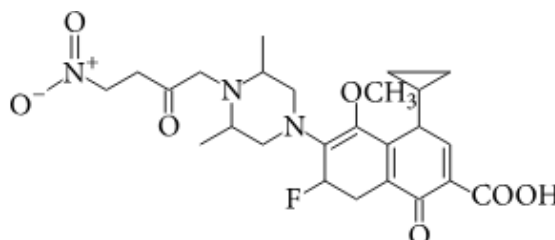
(Ji *et al.*, 2011)



57.4% inhibition at 0.05 mg/mL

3-Nitropropionamides derivatives

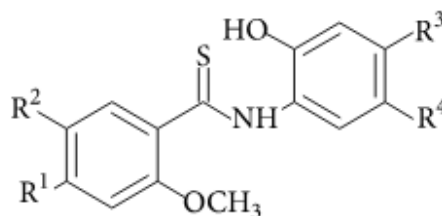
(Sriram *et al.*, 2011)



0.1 μ M

Thio benzamide

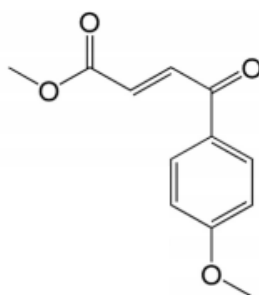
(Kozic *et al.*, 2012)



21–23% inhibition at 10 μ mol/L

IMBI-3

(Liu *et al.*, 2016)



6.80 μ g/mL (30.90 μ M)

Appendix B – Raw Data

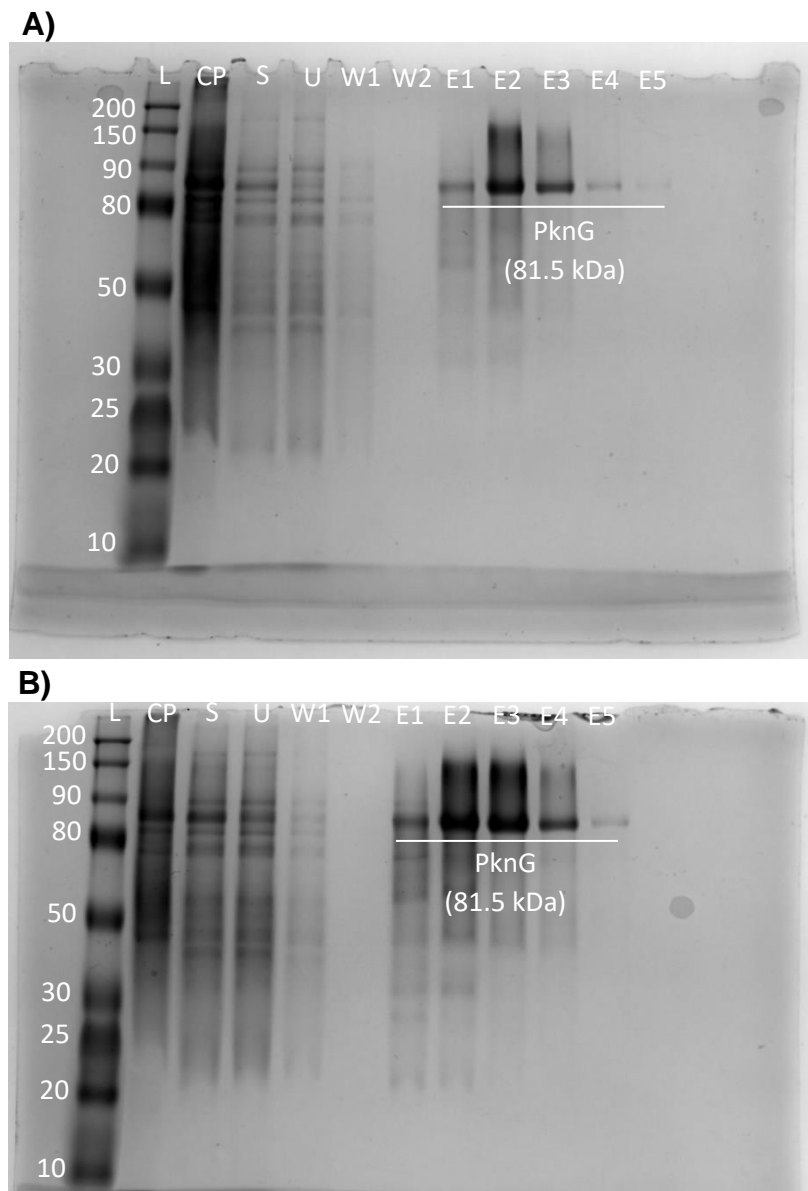


Figure B1: SDS-PAGE gel for PknG expression. **A)** Protein expression induced with IPTG at OD_{595} 0.5. **B)** Protein expression induced with IPTG at OD_{595} 0.5 after diluting with fresh media from OD_{595} 1.2. L, ladder (kDa); CP, cell pellet; S, soluble protein; U, unbound protein; W1, wash 1; W2, wash 2; E1, elution 1; E2, elution 2; E3, elution 3; E4, elution 4; E5, elution 5.

Table B2: Co-crystallisation conditions tested for ICL1 with Itaconate and 2-methylisocitrate that yielded non-diffracting crystals

Manufacturer	Condition	Inhibitor	Protein:Precipitant volume ratio (µL)	Temperature	Outcome
HR2-098	0.1 M Sodium malonate pH 7.0, 12% w/v PEG 3,350	2-methylisocitrate	02:01	16 ° C	Crystal
HR2-098	4% v/v Tacsimate TM pH 6.0, 12% w/v PEG 3,350	2-methylisocitrate	02:01	16 ° C	Crystal
HR2-126	0.2 M Sodium fluoride, 20% w/v PEG 3,350	2-methylisocitrate	01:01	16 ° C	Crystal
HR2-126	0.2 M Sodium fluoride, 20% w/v PEG 3,350	2-methylisocitrate	02:01	16 ° C	Crystal
HR2-126	0.2 M Sodium chloride, 20% w/v PEG 3,350	2-methylisocitrate	01:01	16 ° C	Crystal
HR2-126	0.2 M Zinc acetate dehydrate, 20% PEG 3350	2-methylisocitrate	01:01	16 ° C	Crystal
HR2-126	0.2 M Sodium acetate dehydrate, 20% PEG 3350	2-methylisocitrate	01:01	16 ° C	Crystal
HR2-126	0.2 M Magnesium Sulphate heptahydrate, 20% PEG 3350	2-methylisocitrate	02:01	16 ° C	Crystal
HR2-126	0.2 M Sodium phosphate monobasic monohydrate, 20% PEG 3350	2-methylisocitrate	01:01	16 ° C	Crystal
HR2-126	0.2 M Potassium phosphate monobasic, 20% PEG 3350	2-methylisocitrate	02:01	16 ° C	Crystal
HR2-126	0.2 M Potassium phosphate dibasic, 20% PEG 3350	2-methylisocitrate	02:01	16 ° C	Crystal
STURA MD1-20	0.2M Imidazole Malate pH 6.0, 8% w/v PEG 4,000	Itaconate	01:01	16 ° C	Crystal
STURA MD1-20	0.1 M Sodium Acetate pH 5.5, 14% PEG 5000 _{mme}	Itaconate	01:01	16 ° C	Crystal
STURA MD1-20	0.1 M Sodium Acetate pH 5.5, 24% PEG 5000 _{mme}	Itaconate	01:01	16 ° C	Crystal
STURA MD1-20	0.1 M Sodium Acetate pH 5.5, 24% PEG 5000 _{mme}	Itaconate	02:01	16 ° C	Crystal
MACROSOL MD1-01	0.1 M Imidazole pH 6.5, 1 M Sodium Acetate Trihydrate	Itaconate	01:01	16 ° C	Crystal
MACROSOL MD1-01	0.1 M Imidazole pH 6.5, 1M Sodium Trihydrate	Itaconate	02:01	16 ° C	Crystal
MACROSOL MD1-01	0.1 M NaHEPES pH 7.5, 1.4 M Sodium Citrate Tribasic Dihydrate	Itaconate	01:01	16 ° C	Crystal
MACROSOL MD1-01	0.1 M NaHEPES pH 7.5, 1.4 M Sodium Citrate Tribasic Dihydrate	Itaconate	01:01	16 ° C	Crystal
MACROSOL MD1-13	0.1 M NaHEPES pH 7.5, 10% v/v 2-propanol, 20% w/v PEG 4,000	Itaconate	02:01	16 ° C	Crystal
MACROSOL MD1-22	0.1 M NaHEPES pH 7.5, 2.0 M Ammonium Sulphate, 15% 2-propanol	Itaconate	01:01	16 ° C	Crystal

MACROSOL MD1-22	0.1 M NaHEPES pH 7.5, 2.0 M Ammonium Sulphate, 2% w/v PEG 400	Itaconate	01:01	16 ° C	Crystal
MACROSOL MD1-22	0.1 M NaHEPES pH 7.5, 2.0 M Ammonium Sulphate, 2% w/v PEG 400	Itaconate	02:01	16 ° C	Crystal
HR2-098	8% Tacsimate pH 4.0, 20% w/v PEG 3,350	Itaconate	02:01	16 ° C	Crystal
HR2-098	4% Tacsimate pH 5.0, 12% w/v PEG 3,350	Itaconate	01:01	16 ° C	Crystal
HR2-098	0.1 M Ammonium Citrate Tribasic pH 7.0, 12% w/v PEG 3,350	Itaconate	02:01	16 ° C	Crystal
HR2-098	0.2 M Ammonium Citrate Tribasic pH 7.0, 20% w/v PEG 3,350	Itaconate	01:01	16 ° C	Crystal
HR2-098	0.1 M HEPES pH 7.5, 2% Tacsimate pH 7.0, 20% w/v PEG 3,350	Itaconate	02:01	16 ° C	Crystal
HR2-098	0.06 M Citric Acid, 0.04 M Bis-Tris Propane pH 4.1, 16% w/v PEG 3,350	Itaconate	01:01	16 ° C	Crystal
HR2-098	0.05 M HEPES Sodium pH 7.0, 1% Tryptone, 12% w/v PEG 3,350	Itaconate	01:01	16 ° C	Crystal
HR2-112	0.1 M HEPES pH 7.5, 70% 2-methyl-2,4-pertanediol	Itaconate	01:01	16 ° C	Crystal
HR2-112	0.1 M HEPES pH 7.5, 70% 2-methyl-2,4-pertanediol	Itaconate	02:01	16 ° C	Crystal
HR2-126	0.2 M Magnesium Nitrate Hexahydrate, 20% w/v PEG 3,350	Itaconate	02:01	16 ° C	Crystal
HR2-126	0.2 M Sodium Acetate Trihydrate, 20% w/v PEG 3,350	Itaconate	02:01	16 ° C	Crystal
HR2-126	0.2 M Calcium Acetate Hydrate, 20% w/v PEG 3,350	Itaconate	02:01	16 ° C	Crystal
HR2-126	0.2 M Lithium Sulphate Monohydrate, 20% w/v PEG 3,350	Itaconate	02:01	16 ° C	Crystal
HR2-126	0.2 M Sodium Sulphate Decahydrate, 20% w/v PEG 3,350	Itaconate	02:01	16 ° C	Crystal
HR2-126	0.2 M Ammonium Sulphate, 20% w/v PEG 3,350	Itaconate	02:01	16 ° C	Crystal
HR2-126	0.2 Potassium Sulphate, 20% w/v PEG 3350	Itaconate	01:01	16 ° C	Crystal
HR2-144	0.1 M HEPES pH 7.0, 0.2 M NaCl, 25% w/v PEG 3350	Itaconate	01:01	16 ° C	Crystal
HR2-144	0.1 M Tris pH 8.5, 0.2 M NaCl, 25% PEG 3,350	Itaconate	02:01	16 ° C	Crystal
HR2-144	0.1 M BIS-Tris pH 6.5, 0.2 M Ammonium Acetate, 25% w/v PEG 3,350	Itaconate	02:01	16 ° C	Crystal
HR2-144	0.1 M HEPES pH 7.5, 0.2 M Ammonium Acetate, 25% w/v PEG 3,350	Itaconate	01:01	16 ° C	Crystal
HR2-144	0.1 M HEPES pH 7.5, 0.2 M Ammonium Acetate, 25% w/v PEG 3,350	Itaconate	02:01	16 ° C	Crystal
HR2-144	0.2 M Sodium Malonate pH 7.0, 20% w/v PEG 3,350	Itaconate	01:01	16 ° C	Crystal
HR2-144	0.2 Sodium Formate, 20% w/v PEG 3,350	Itaconate	02:01	16 ° C	Crystal
HR2-144	0.15 M DL-Malic acid pH 7.0, 20% w/v PEG 3,350	Itaconate	01:01	16 ° C	Crystal
HR2-144	0.15 M DL-Malic acid pH 7.0, 20% w/v PEG 3,350	Itaconate	02:01	16 ° C	Crystal

Table B3: Primer sets for qrt-PCR analysis.

	Forward	Reverse
<i>sdhC</i>	CGG GTC ATC TTG ATC GAT TTC T	AAC CAT CAG CAA GAG GAA GAC
<i>sdhD</i>	CCT GGG ATC TGC TGT TGT T	CAG AAT CGG GTG GTG TCT TT
<i>sdhA</i>	CTC GGG CCG CAT GTA TAA G	GGT AGG GTG AAA CTG GTG AAA
<i>sdhB</i>	GCG ATC AAA CCG TAC CTG AT	GGA TGC ACT TGG TGG TGT
<i>icd1</i>	TCC AAC GCA CCC AAG ATA AA	CTC GAT GCC CAA GTC GTA ATA G
<i>icd2</i>	ACC CAA GCA CGT CAA ACA	TGA TGC CGA TAT CCT CGA AAC
<i>fum</i>	CGT ACG GCG GCT AAT TCT T	GGA TGT CGT TGG CGA TCT T
<i>mdh</i>	GGG CTT GAT CTC CTC GTT TC	AAC TCG GCG GTT GAC TTG
<i>mgo</i>	GCG ATG CTG ACG GTA GTA TT	GAT TGA TAG CGG TTG GCA AAG
<i>acn</i>	GGT CAA GAC AAA GAC GGT AAG A	GGT GAA CAT CTC CTG GTT GAT
<i>sucC</i>	TCA AAG GAC ACA TCG TCA AGA A	CGA GCA GGA AGG ATA GGT AGT A
<i>sucD</i>	CCC AAC TGT CCT GGC ATT AT	CGA ACA TCA TCT GGT AGG TCA A
<i>icl1</i>	ATC GCC AAG TTC CAG AAG G	GCC AGA TCG AAC ATC GAG TAG
<i>prpD</i>	GCA CTG TGG CAC AAG ATT TC	TTC GTC CAC GAT CAC TTC AC
<i>prpC</i>	GCG TAC TAC CTG ATG GGA TTC	CGT GGC CTG TTC CAT GAT
<i>atpB</i>	GGT GCA GTA CAC CGA TAA ACA	TTT CGT GTT CGT CTG CTA CC
<i>atpF</i>	TCG CTG TCA TTG GCA CTT	ACA ACA AGA AGT CGG ACG AG
<i>pckA</i>	GAT GAA TGG CGT CAG GAA CT	GGG CGT CGA ACT CAT CTT T
<i>sigA</i>	ACG AAG ACC ACG AAG ACC TCG AA	GTA GGC GCG AAC CGA GTC GGC GG